Doctoral theses at NTNU, 2022:188

Per Aaslid

Optimal coordination of renewable sources and storage in energy-constrained power systems

Doctoral thesis

NTNU
Norwegian University of Science and Technology
Thesis for the Degree of
Philosophiae Doctor
Faculty of Information Technology and Electrical Engineering
Department of Electric Power Engineering

NTNU
Norwegian University of
Science and Technology

Per Aaslid

Optimal coordination of renewable sources and storage in energy-constrained power systems

Thesis for the Degree of Philosophiae Doctor

Trondheim, June 2022

Norwegian University of Science and Technology
Faculty of Information Technology and Electrical Engineering
Department of Electric Power Engineering

NTNU

Norwegian University of
Science and Technology

NTNU
Norwegian University of Science and Technology

Thesis for the Degree of Philosophiae Doctor

Faculty of Information Technology and Electrical Engineering
Department of Electric Power Engineering

ISBN 978-82-326-5308-9 (printed ver.)
ISBN 978-82-326-5536-6 (electronic ver.)
ISSN 1503-8181 (printed ver.)
ISSN 2703-8084 (online ver.)

Doctoral theses at NTNU, 2022:188

Printed by NTNU Grafisk senter

Preface

The presented research was carried out at the Department of Electric Power Engineering at the Norwegian University of Science and Technology (NTNU) and at SINTEF Energy Research, and the work started in August 2018. My main supervisor has been Professor Olav Bjarte Fosso (NTNU), and Dr Michael Martin Belsnes (SINTEF) has been my co-supervisor. Professor Magnus Korpås (NTNU) joined as co-supervisor at the end of 2019. My initial plan was to spend six months as a visiting researcher at Commonwealth Scientific and Industrial Research Organisation (CSIRO), Newcastle, Australia from January 2020, but the stay was aborted after two months due to the COVID-19 pandemic.

This project was financed as an industrial PhD through SINTEF Energy Research by the Norwegian Research Council under grant number 272398 and has also been associated with the Centre for Intelligent Electricity Distribution (CINELDI), which is one of the Centres for Environmental-Friendly Energy Research in Norway (FME).

Acknowledgements

I am grateful to my employer, SINTEF Energy Research, for their belief in me and the opportunity to pursue a PhD. I look forward to using my newly acquired knowledge in my work.

I would like to express my deepest appreciation to my main supervisor, Professor Olav Bjarte Fosso, for guiding me and sharing his extensive knowledge. I am grateful to my co-supervisor, Michael Belsnes, for his helpful contributions and fruitful discussions. I would also like to extend my deepest gratitude to Professor Magnus Korpås, who joined the supervisor team midway, for his profound belief in my abilities.

I would like to thank Julio Braslavsky for welcoming me at Commonwealth Scientific and Industrial Research Organisation (CSIRO), Newcastle, Australia. I am sorry my stay was reduced to only two months, but both me and my family enjoyed the time in Australia a lot! Many thanks to all my new research colleagues at CSIRO, especially Frederik Geth for sharing of his knowledge and ideas, which resulted in a joint publication.

I very much appreciate the discussions with my colleagues at NTNU, and thanks should also go to my colleagues at SINTEF Energy Research for your helpful advice.

The completion of this dissertation would not have been possible without the support from my family and friends. I very much appreciate the distraction from my three children, Elias, Ester, and Marie, who have helped me to divert from work. And last but not least, my wife Sigrid. Thank you for enduring my frustration and for allowing me to share the joys with you.

Summary

Integrating high levels of variable renewable energy sources (VRESs) in power systems imperils the security of supply. Energy storage systems (ESSs) contribute both to cost reduction through increased and improved utilization of VRESs, as well as to securing the supply in periods with low generation from VRESs.

The work in this thesis has considered the modeling of microgrids (MGs), small scale power systems, with a high level of VRESs and ESSs and limited dispatchable generation capacity where VRESs and ESSs contribute to the security of supply. Although the presented work focuses on MGs, the findings are also relevant for larger systems. Since these systems rely on ESSs, where the ability to deliver power depends on a sufficiently high state-of-charge (SOC), they are vulnerable to persistent low generation from VRESs. Future generation and demand should therefore be considered in operation planning models with sufficient foresight, and for a broad range of possible scenarios.

The implemented methods include:

- A detailed non-linear battery optimization model representing the battery cell voltage and the converter efficiency with spline function based on empirical battery data. The model is capable of operating closer to the operational limits of the battery compared to existing simpler optimization models.
- A linear multi-stage stochastic power system model using stochastic dual dynamic programming (SDDP) considering degradation due to cyclic and SOC dependent calendar degradation. The model can increase the expected lifetime of a battery by more than four years. The model results also show that it is advantageous to consider battery degradation in coherence with stochastic optimization.
- A stochastic power system model using SDDP considering both short-term uncertainty within weather forecast horizon and long-term uncertainty for infinite foresight. Whereas rule-based operation and deterministic optimization causes significant load shedding in critical periods, the implemented method is superior at keeping the load shedding very low while still retain-

ing low generation costs.

The solution of stochastic dynamic programming based methods also has a useful representation with respect to valuating stored energy for systems of any size dominated by VRESs. The value of stored energy changes in time due to variations in future expected generation and demand, and it also changes with the SOC for itself and all other ESSs in the system. The value of stored energy is a useful quantity for valuating the stored energy in detailed models, for real-time operation, and for bidding into competitive markets.

Contents

Preface . . . . . **iii**

Acknowledgements . . . . . **v**

Summary . . . . . **vii**

Contents . . . . . **ix**

Figures . . . . . **xiii**

Tables . . . . . **xv**

Acronyms . . . . . **xvii**

1 Introduction **1**

1.1 Background 1

1.2 Objectives 4

1.3 Contributions 5

1.4 List of publications 7

1.5 Outline of thesis 9

2 Power system operation **11**

2.1 Power balance 11

2.1.1 Organization 12

2.2 Power-constrained systems 14

2.3 Energy-constrained systems 15

2.3.1 Storage marginal value 16

2.4 Transmission and distribution 17
2.5 Uncertainty 17
2.6 Complexity 18
2.7 The microgrid perspective 19
2.7.1 Rye microgrid 20
3 Modeling of flexible energy resources 21
3.1 Electric energy storage 21
3.1.1 Electrochemical batteries 22
3.1.2 Generic storage model 24
3.1.3 Operating costs 25
3.2 Variable renewable energy sources 26
3.2.1 Solar power 26
3.2.2 Wind power 27
3.3 Demand side response 27
3.4 Grid modeling 28
3.4.1 Bus power injections 28
3.4.2 Power flow 28
4 Stochastic programming for power systems with energy storage . . . 31
4.1 Modeling uncertainty 32
4.1.1 Rolling horizon optimization 32
4.1.2 Modeling horizon and expected future value 33
4.1.3 Stochastic programming 34
4.1.4 Storage marginal value 37
4.2 Scenario generation 39
4.2.1 Auto-regressive models 39

4.2.2 Markov model 40

4.2.3 Stage length 41

5 Results and discussion 43

5.1 Operational limits of energy storage systems 43

5.2 Degradation of energy storage systems 45

5.3 Stochastic operation of energy-constrained systems 47

5.4 Pricing and valuation of stored energy 50

6 Conclusion and recommendations for future work 53

6.1 Future work 56

6.1.1 Modeling of flexible resources 56

6.1.2 Stochastic modeling of energy systems 57

6.1.3 Cost recovery of energy storage systems in markets 57

Bibliography 59

Paper I 69

Paper II 77

Paper III 91

Paper IV 107

Paper V 121

Figures

1.1 Overview of papers and objectives. 7

2.1 Optimal price and quantity are given where the supply and demand curves cross. The gray areas indicate the total surplus that can be divided into consumer and producer surplus for competitive markets. 12

2.2 Load duration curve showing the optimal duration and the respective optimal capacities for three generation technologies ordered from highest to lowest operating costs. 15

2.3 Classification of power system uncertainties [39] 18

2.4 Conceptual topology of Rye microgrid. 20

3.1 Organization of cells in series and parallel in a battery and conversion between DC and AC. 23

3.2 Battery capacity as a function of cycle depth. 25

3.3 Ratio between wind speed and power generation for a Vestas V27 wind turbine [70]. 27

3.4 Illustration of convex relaxation (blue) compared to approximation (red) of a non-convex space (gray) (redrawn based on [76, p.4]). . 29

4.1 Illustration of rolling horizon optimization. 33

4.2 Approximation of the storage end value function bounded by linear cuts (illustrated with red lines). 37

4.3 Energy storage systems act as both supply and demand in the market clearing problem. The figures illustrate how the market price can be set by either the charge value (Equation (4.7)) for high storage marginal value (left) or the discharge value (Equation (4.8)) for low storage marginal value (right). 38

4.4 Example of possible Markov model to describe how the weather develops. 40

5.1 Topology of grid connected system with battery, solar photovoltaic and converter (figure adopted from Paper II [28]). 43

5.2 Battery and VSC efficiencies (figure adopted from Paper II [28]). . . 44

5.3 Expected battery lifetime for operation with different optimization methods. Text in parentheses indicates which type of degradation costs that has been included in the optimization model: depth-of-discharge (DOD)/cyclic degradation and state-of-charge (SOC)/calendar degradation. 46

5.4 Four-day average SOC for co-operation of hydrogen and battery (based on case 1 from Paper V [31]). 47

5.5 Comparison of operating costs for Rye microgrid using rule-based operation, deterministic optimization, and SDDP both with respect to short- and long-term operation. The results includes the following variations of the case: large diesel generator (75 kW), small diesel generator (15 kW), and weak grid connection (15 kW). . . . 49

5.6 Topology of small grid with variable solar power and battery (figure adopted from Paper III [29]). 50

5.7 Multiple simulations of case with only solar PV generation and EES (figure adopted from Paper II [28]). 51

Tables

5.1 Methods used for the operation of the microgrid presented in Paper IV. 48

Acronyms

AR auto-regressive. 6, 57

ARMA auto-regressive moving average. 34, 37, 39

CCGT combined cycle gas turbine. 14

CI clearness index. 26

DER distributed energy resource. 9, 11, 19

DHI diffuse horizontal irradiance. 26

DNI direct normal irradiance. 26

DSR demand side response. 2, 16, 19, 21, 27, 47, 56

ESS energy storage system. 1–9, 14–17, 21, 22, 24, 25, 28, 31, 33, 34, 37, 38, 45, 47, 50–57

EV electric vehicle. 2, 19, 27, 39, 56

IEA International Energy Agency. 1

IRENA International Renewable Energy Agency. 1

LMP locational marginal price. 8, 51

MG microgrid. 3, 5, 7–9, 11, 19, 20, 25, 26, 32, 46–48, 53, 54, 56

MPC model predictive control. 32

MSSP multi-stage stochastic programming. 5, 7, 34, 35

PV photovoltaic. 22, 26, 45, 46

SDDP stochastic dual dynamic programming. 5, 7, 9, 16, 25, 26, 35–37, 39, 48, 54

SDP stochastic dynamic programming. 8, 16, 35–37, 50

SEV storage end value. 8, 36, 48, 50, 52, 54, 55

SMV storage marginal value. 16, 36–38, 50–52, 55

SOC state-of-charge. 2, 5, 6, 8, 9, 17, 22–26, 33, 34, 38, 44–46, 50, 53–55

TSO transmission system operator. 13

VOLL value of lost load. 50, 51, 54, 55

VRES variable renewable energy source. 1–6, 8, 9, 15, 17, 19, 21, 22, 25–27, 31, 32, 39, 47, 48, 50, 51, 53–57

Chapter 1

Introduction

1.1 Background

The goal of the Paris agreement is to limit the global temperature rise [1], and the EU intends to make Europe emission neutral, as stated in the European Green Deal [2], by 2050. Roadmaps toward net zero emissions by 2050 have been presented by both the International Energy Agency (IEA) and International Renewable Energy Agency (IRENA), and require electrification of industry, transportation, and buildings [3, 4].

Both the growth in the electricity sector and the phase-out of fossil generation sources must to a great extent be met by variable renewable energy sources (VRESs). Around 63% of the energy and 74% of the power capacity in the electricity sector are expected to originate from solar and wind power by 2050 [4]. The large scale integration of VRESs also increases the demand for flexible resources, such as different types of energy storage systems (ESSs), to maximize the utilization of VRESs [5].

Besides not producing CO_2 nor other harmful exhaust gases, generation from VRESs differs from conventional dispatchable generators in the following ways [6]:

1. The output is variable.
2. The output is uncertain due to the characteristics of the primary resource.
3. They are modular and relatively small.
4. They are bounded to specific locations due to the availability of the natural resource.
5. They are mostly non-synchronous.
6. The short-run marginal operating costs are low.

These fundamental differences impose significant changes with respect to how these systems are analyzed and operated.

Grid scale ESSs, in particular lithium-ion batteries, have seen tremendous growth during the past decade [7] partly driven by decreasing costs [8]. The increasing level of electric vehicles (EVs) also has great potential for offering flexibility to the grid [9]. Operation of ESSs does not incur direct costs, but both efficiency losses as well as degradation costs [10] should be considered.

System adequacy is the ability to provide electricity, both power and energy. Generation from VRESs does not contribute to power capacity adequacy in the same way as dispatchable generators due to their output variability [11]. Meeting the demand in periods with low wind and solar power production necessitates either sufficient dispatchable generation capacity or other types of flexibility, both ESSs and demand side response (DSR). ESS technologies enable shifting surplus generation to periods with lacking generation from VRESs, and contribute to improved power capacity adequacy. However, ESSs are only capable of providing power capacity if the state-of-charge (SOC) is sufficiently high, and these systems are therefore energy-constrained as opposed to power systems dominated by dispatchable (thermal) generators that are power-constrained. The ESSs must be large enough to tackle the variations in demand and generation. VRESs are subject to significant uncertainty, which mandates a probabilistic approach to supply adequacy. Whereas the most prominent risk in power-constrained systems is power capacity inadequacy, systems with a high share of VRESs and ESSs are vulnerable to energy inadequacy.

The marginal cost pricing principle is widely deployed in competitive energy markets through day-ahead auctions and real-time markets [12]. The producers and consumers place their bids based on their marginal operating cost and marginal utility at the different production/consumption volumes. The generators' marginal costs are dependent on the fuel price and efficiency. Since VRESs have marginal operating costs close to zero, they will produce at maximum unless the price is close to zero or negative. ESSs exposed to short-term energy markets gain their profit on arbitrage, and their marginal value will therefore be some place between the least and most expensive unit in the system. Initial studies of the cost recovery and marginal cost of ESSs has been reported in Korpås and Botterud [13]. Moreover, the marginal operating value of ESSs will also be influenced by their degradation with respect to power charge and discharge in conjunction with its replacement cost [10].

The emerging electricity systems with high VRES penetration have interesting similarities with hydropower dominated systems. Both systems are dependent on limited energy storage capacities, and they both must manage variable and uncertain energy inflows. The utilization of stored hydropower has been studied for decades where the focus has been on minimizing the operation costs from thermal power

generation while keeping the risk of scarcity low under uncertain inflow to the hydro power reservoirs [14, 15]. Pumped hydro is also efficient for managing daily and weekly variations, and is experiencing a renewed interest due to the rapid increase in VRES [16]. A limiting factor for ESS technologies in general are their strict limitations on the amount of energy that can be stored, and their ability to deliver capacity will, of course, depend on sufficient stored energy. It is therefore crucial that the ESS operation is planned with sufficient foresight, in particular for systems where the ESS capacity contributes to securing the supply and the consequence of empty ESS is scarcity. Therefore, supply adequacy not only concerns having sufficient generation capacity to meet the demand but will also require secure operation of ESS over time to avoid situations with energy shortage.

Power systems have traditionally been organized hierarchically with power flow from large centralized generation units through the transmission system down to the distribution systems. The interaction between the different levels has been very limited. In 2005, the European Commission Research Directorate established the *Technology Platform for the Electricity Networks of the Future*, where the objective was to increase the efficiency, safety and reliability of both electricity transmission and distribution in Europe, and to facilitate large-scale integration of distributed renewable sources [17]. The large increase in VRESs urges the need for flexibility, and distributed flexibility is one of several contributors [18]. The increasing share of distributed flexibility also influences the security of supply, and Sperstad *et al.* [19] summarizes some of the implications:

- The distribution systems are becoming more equal to the transmission systems.
- There will be more interaction between the transmission and distribution systems.
- There will be greater interplay between different aspects of security of supply.

Recent trends also impose that microgrids (MGs), small scale power systems that can operate both connected and disconnected from the utility grid, provide a viable option for how to operate distributed flexibility [20–22].

Considering the major transition toward a decarbonized energy system, it is evident that proper tools for planning, operation, and control of the emerging VRESs and ESSs in the power system are crucial for a secure, cost efficient, and sustainable power system.

1.2 Objectives

The goal of this thesis is to study how high levels of VRESs and ESSs influence the power system operation strategy and the electricity price. This thesis develops power system modeling techniques to manage both VRESs and ESSs with a sufficient level of detail, and manage the uncertainty concerning both generation and demand in energy-constrained systems with sufficient foresight as described in more detail in the following objectives:

Develop optimization models for ESS, generation and demand: ESSs are key enablers for integrating a high level of VRESs in power systems while keeping the need for dispatchable generation capacity low. Different ESS technologies have distinctive characteristics such as energy rating, power rating, efficiency, operating limits, and operating costs that must be addressed properly. Since the energy storage links power dispatch over time, they must be planned and operated with sufficient foresight to maximize the utilization of VRESs while keeping the risk of scarcity low. For example, batteries are capable of delivering and absorbing high power at very high efficiency, but only for a very limited time due to energy constraints. On the other hand, large amounts of energy can be stored as hydrogen at a relatively low cost while the charge and discharge capacity is expensive to scale up and the efficiency is intermediate. The modeling objectives can be summarized as:

- The operational limits and efficiency should be represented sufficiently accurately for the model purpose.
- The models should account for marginal operating costs due to degradation and fuel consumption.

Develop stochastic optimization methods for operating VRESs and ESSs considering both short- and long-term uncertainties: Managing uncertainty is essential in energy-constrained power systems where the level of VRESs is high, and the ESSs must contribute to the security of supply due to low dispatchable generation capacity. Therefore, stochastic models are important for operating the systems such that the costs are minimized while keeping the risk of scarcity low. The main objectives with the stochastic optimization models are:

- Implement methods for operating multiple ESSs in energy-constrained power systems considering both short- and long-term uncertainty in demand and generation from VRESs.
- Study the marginal value of the stored energy based on the solution of the optimization methods.

- Study the electricity price formation in coherence with the marginal value of the stored energy.
- Study the role of storage devices in periods with energy scarcity.

1.3 Contributions

The main contributions of this thesis are:

Non-linear battery model expressed in the current and voltage variable space (Paper II). The implemented model optimizes the operation of a lithium-ion battery using charge, current, and voltage as variables. These variables are closer to the battery chemistry compared to a classical model with power and energy variables, and enable a more detailed representation of the operational limits. The battery voltage and the converter efficiency are given by cubic spline functions. The overall model formulation can be solved with interior-point based non-linear solvers, and the spline technique can also be adapted to other storage types.

Linear approximation of SOC dependent battery calendar aging (Paper V). The proposed formulation approximates the SOC dependent battery calendar aging with piece-wise linear segments and requires a convex calendar aging function. Battery degradation models are often non-linear and dependent on multiple variables. However, stochastic programming methods often utilize the structure of linear programs for decomposition and computation time reduction. The formulation has been implemented and tested in combination with a linear cyclic degradation model [10] in a multi-stage stochastic programming (MSSP) energy management model that has been solved with stochastic dual dynamic programming (SDDP).

Multi-stage stochastic energy management models considering battery degradation, both cyclic and calendar aging, and an analysis studying the implications with respect to operation costs and battery lifetime (Papers I and V). This thesis studies the consequence of considering battery degradation in optimization, both stochastic and deterministic, for long-term operation of a MG with a high level of generation from VRESs, and both hydrogen and battery ESSs. Batteries have relatively high investment costs and limited lifetime, but the battery lifetime can be prolonged by properly accounting for the degradation in the operation strategy.

Methods for considering uncertainties associated with wind and solar power forecast uncertainties (Papers I and IV). Solar and wind power are expected to be the two most important sources of renewable energy. Both are highly uncertain, and it is therefore important to investigate how they can be embedded into stochastic energy management models, and how their statistical properties can be utilized to improve the model performance. The implemented methods include auto-regressive (AR) models as well as Markov chains to account for the VRES generation auto-correlation.

Comparison of stochastic, deterministic, and rule-based methods for managing high levels of VRESs and ESSs in microgrids (Paper IV). This thesis studies the value of using stochastic methods as opposed to deterministic and rule-based methods to coordinate operation of ESSs in systems with high penetration from VRESs. Energy-constrained systems, where the dispatchable generation capacity is low, have been the main focus. The gap between rule-based operation strategies and stochastic optimization is bridged by showing how the ESS marginal values can be translated into operating rules.

Implementation of linear distribution power flow formulation in PowerModels.jl PowerModels.jl is an open source tool developed through the *Los Alamos National Laboratory's Advanced Network Science Initiative* by Coffrin *et al.* [23]. The purpose of PowerModels.jl is to study and compare different power flow formulations in a unified framework, and the framework has attracted high attention in research communities. As a contribution to the completeness of this framework, the author of this thesis has implemented the linear distribution flow [24, 25] described in Section 3.4.2. Unlike the purely linear formulation, the implemented formulation also includes second order cone flow bounds.

Price formation in systems with high VRES and ESS levels (Paper III). The electricity price in energy-contrained systems is highly influenced by the expected future generation from VRES as well as the SOC of the ESSs. The marginal value of stored energy has been studied, as well as corresponding electricity price formation.

Market clearing with VRES and ESS: an open-source tool for visualizing the market clearing in systems where ESS bid their marginal value [26]. This is an educational tool for visualizing how ESSs, bidding their marginal value, influence the merit order and market clearing in competitive markets. The tool visualizes supply and demand curves, where the ESSs appear on both curves, and shows the cleared volume and price for the given combination. The user can modify the

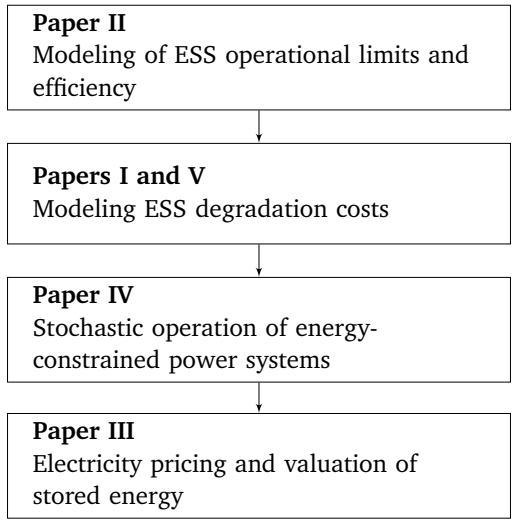

Figure 1.1: Overview of papers and objectives.

capacity, value, and efficiency for all units while the market clearing illustration updates dynamically.

1.4 List of publications

Figure 1.1 shows how the papers in this thesis relate to the objectives presented in Section 1.2. The papers and short summaries are presented below:

Paper I P. Aaslid, M. M. Belsnes, and O. B. Fosso, "Optimal microgrid operation considering battery degradation using stochastic dual dynamic programming," in *SEST 2019 - 2nd International Conference on Smart Energy Systems and Technologies*, Institute of Electrical and Electronics Engineers (IEEE), Sep. 2019, pp. 1–6, ISBN: 9781728111568. DOI: 10.1109/SEST.2019.8849150

This paper considers the operation of a MG exposed to a variable market price through a weak grid connection. The objective is to minimize battery degradation, diesel generation, and power purchase costs under wind and demand uncertainty. The implemented model uses SDDP to solve the MSSP model. The wind power generation and the demand are subject to uncertainty, where the forecast error auto-correlation is represented with an order one auto-regressive model. Battery degradation is implemented with a piece-wise linear approximation to represent quadratic cyclic degradation. The analysis investigates the effect of including battery degradation costs both for a stochastic model and a deterministic model. The results show that the stochastic model avoids operating close to the battery upper

bound to prevent unnecessary battery cycling compared to the corresponding deterministic model and the model without degradation costs. Moreover, the model considering battery degradation also requires a greater price differences for arbitrage.

Paper II P. Aaslid, F. Geth, M. Korpås, M. M. Belsnes, and O. B. Fosso, "Non-linear charge-based battery storage optimization model with bi-variate cubic spline constraints," *Journal of Energy Storage*, vol. 32, p. 101 979, Dec. 2020, ISSN: 2352152X. DOI: 10.1016/j.est.2020.101979

This paper implements a non-linear battery optimization model in the variable space of voltage $[V]$, current $[A]$, and charge $[Ah]$, referred to as the IVQ-model, that is compared with a more traditional model formulation in the variable space of power $[W]$ and energy $[Wh]$, referred to as the PE-model. The IVQ-model is closer to the battery chemistry than the PE-model and enforces operating limits with respect to current, voltage, and charge. This model enables operation closer to the battery capabilities and more accurate estimation of the battery SOC. The battery voltage characteristics and converter efficiency are given by cubic spline functions based on empirical data.

Paper III P. Aaslid, M. Korpås, M. M. Belsnes, and O. B. Fosso, "Pricing electricity in constrained networks dominated by stochastic renewable generation and electric energy storage," *Electric Power Systems Research*, vol. 197, p. 107 169, Aug. 2021, ISSN: 03787796. DOI: 10.1016/j.epsr.2021.107169

This paper describes the electricity price formation process for energy-constrained systems where ESSs must contribute to the security of supply. The implemented method uses stochastic dynamic programming (SDP) to analyze the operating strategy, and the stage-wise optimization problems are connected with storage end value (SEV) functions using cubic splines. The results present locational marginal prices (LMPs) and ESS marginal values to show how electricity prices are influenced by the probability of scarcity. The prices, which increase with increasing probability of scarcity, incite flexible units to respond as a precautionary action against scarcity.

Paper IV P. Aaslid, M. Korpas, M. M. Belsnes, and O. Fosso, "Stochastic Optimization of Microgrid Operation With Renewable Generation and Energy Storages," *IEEE Transactions on Sustainable Energy*, pp. 1–1, 2022, ISSN: 1949-3029. DOI: 10.1109/TSTE.2022.3156069. [Online]. Available: https://ieeexplore.ieee.org/document/9727092/

This paper considers the optimal operation of a real MG where the demand is met with generation from VRESs, both wind and solar power as well as a diesel generator serving as backup. A lithium-ion battery and a hydrogen ESS balance the supply and demand. The model is divided into a short-term model for the interval

covered by the weather forecast, and a long-term model for the period beyond the weather forecast horizon. SDDP, deterministic, and rule-based methods are tested in six different combinations of short- and long-term models and compared with each other using rolling horizon simulation over almost a full year for real observations and real meteorological forecasts for the MG. The proposed method is tested for three different variations of the MG: *a)* large diesel generator, *b)* small diesel generator, and *c)* weakly grid connected. The results show that stochastic optimization, especially for the long-term perspective, outperforms the rule-based and deterministic approaches for the energy-constrained cases where the diesel generator is too small or the grid connection is too weak to meet the peak demand in case of empty ESSs. Whereas the deterministic and rule-based approaches incur significant operating costs due to load shedding, the SDDP-based approaches keep the load shedding low while still retaining low diesel generating costs. The paper also explains how the cutting hyperplanes from SDDP can be interpreted as adaptive time and state dependent priorities for the flexible resources.

Paper V P. Aaslid, M. Korpås, M. M. Belsnes, and O. B. Fosso, *Stochastic Operation of Energy Constrained Microgrids Considering Battery Degradation*, 2021. [Online]. Available: `https://arxiv.org/abs/2111.03313`

This paper considers the optimal operation of the MG from Paper IV, and investigates how battery degradation influences the operational pattern and costs. The paper proposes a piece-wise linear approximation of the SOC dependent degradation and combines it with a cycling dependent degradation model. The results indicate that the battery lifetime can be extended by around four years by including both degradation types in the operation costs for the analyzed system.

1.5 Outline of thesis

Chapter 2 gives a fundamental introduction to power system operation, and the distinct characteristics of power-constrained and energy-constrained systems. We also explain the role of the transmission and distribution systems in coherence with the emerging distributed energy resources (DERs), and how new types of complexity can be managed.

The two main topics of the thesis are covered in Chapters 3 and 4. Chapter 3 presents modeling techniques for DERs, both ESSs and VRESs as well as grid. Chapter 4 presents methods for combining the modeling techniques presented in Chapter 3 into stochastic models capable of solving models with several states across several stages under uncertainty. A summary of the results is presented and discussed in Chapter 5, and the conclusions and recommendations for future work are presented in Chapter 6.

Chapter 2

Power system operation

This chapter provides background information about power system operation. Section 2.1 introduces fundamental concepts like supply, demand, power balance, and the difference between centralized and market-based organization. Sections 2.2 and 2.3 explain the characteristics of power-constrained systems compared to energy-constrained systems. Section 2.4 considers the DERs as opposed to centralized resources with respect to managing grid limitations, and Section 2.5 describes the role of uncertainty in energy-constrained systems. Section 2.6 considers how complexity in several dimensions adds up, and Section 2.7 considers the MG perspective as a part of the solution for how to operate the future power system.

Electricity is a commodity that can be purchased and sold in competitive markets, but it is also a service that is critical for most parts of modern society. Residential, industrial, and commercial appliances as well as transportation and public services are strongly dependent on a secure and reliable power supply. The objectives of power system operation are therefore to ensure that the supply and demand balances in a reliable, safe, and cost effective way [32].

2.1 Power balance

Compared to many other commodities, electricity cannot be stored directly but must be delivered at the time of generation. In other words, supply and demand must be balanced at all times. The power systems comprise large networks, from high to low voltage, for distributing the produced electricity to the consumers. The operation of a power system is a complex sequence of decisions that respect the technical limitations of both the network as well as the producers and consumers. The decisions must be cost effective while ensuring reliable and secure system

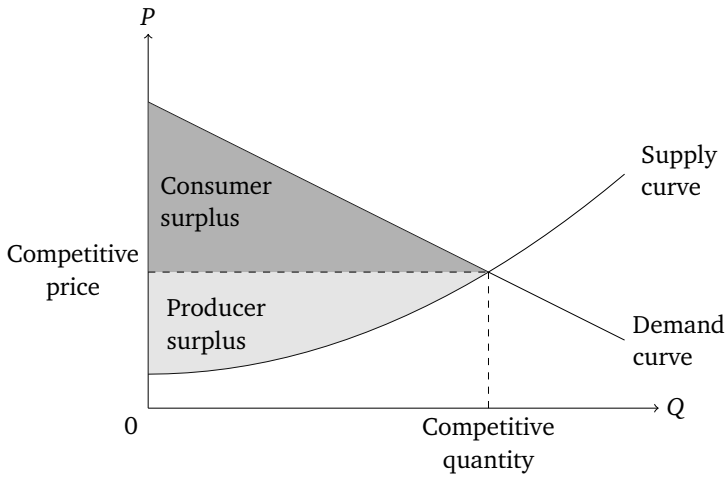

Figure 2.1: Optimal price and quantity are given where the supply and demand curves cross. The gray areas indicate the total surplus that can be divided into consumer and producer surplus for competitive markets.

operation.

A power system comprises multiple producers and consumers. From an economic perspective, the objective is to maximize the total surplus, the sum of consumer and producer surplus, as illustrated in Figure 2.1. The supply curve shows the suppliers' willingness to produce and indicates their marginal production cost. Likewise, the demand curve indicates how much the consumers are willing to pay, their marginal utility [12]. The optimal solution is to operate where the supply and demand curves cross, and the competitive price is given by the marginal producing or consuming unit.

The power system operation does not directly consider the optimal sizing of the production, consumption, or corresponding investment costs, only the marginal operating cost and utility.

2.1.1 Organization

Power systems are either organized through centralized control, competitive markets, or hybrid markets. Centralized control means that the total production and consumption are decided by a centralized operator based on operating costs of the production and the value of supplying the consumers. This was the dominant way of operating power systems until the first power markets emerged in the 1980s. Competitive markets have multiple individual producers and consumers that each seek to maximize their surplus. A fundamental requirement for efficient markets

is perfect competition where some of the requirements are [12]:

1. The agents are acting on the market price without exercising market power.
2. The agents have well behaved costs that increase with output.
3. Market prices are publicly known.

These requirements are valid to a lesser extent for distribution systems, which are typically organized as regulated monopolies.

Given perfect competition, both centralized control and competitive power markets will, from a theoretical perspective, maximize the total surplus. The price in a competitive market is set where supply and demand intersect as shown in Figure 2.1, and the distribution of the surplus between producers and consumers is given by the market price. A high market price will therefore allocate a higher share of the total surplus to the producers while the consumers will benefit from low prices. Both organizations have pros and cons and cause many practical challenges that will not be discussed further in this thesis. For further reading about power markets, the reader is referred to Stoft [12].

The Norwegian power system is a part of joint power market with the Nordic countries (except Iceland) and the Baltic countries organized by Nord Pool [33], and is also connected to the UK, Germany, and the Netherlands. Nord Pool currently divides the market into 15 price zones, five of them in Norway, where the producers and consumers place their bids daily for their willingness to produce or consume in the day-ahead market. Nord Pool clears the market for each zone based on the bids and the exchange capacities for connected zones the day before implementation, and each participant is allocated a volume to produce or consume for each hour at the cleared price. The participants are also allowed to adjust their volumes after the market clearing before activation by trading in the intra-day market.

The transmission system operator (TSO), in Norway Statnett [34], is responsible for the real-time operation of the power system. The system is continuously monitored and adjusted to keep the system frequency stable without violating other operational constraints like voltage limits, thermal capacity limits as well as reliability measures. The scope of this thesis is system operation with respect to energy management, primarily hourly, but the presented methods are also adequate for shorter time steps.

2.2 Power-constrained systems

Power systems dominated by thermal dispatchable generators have well-defined operating costs. Characteristics like ramping capabilities and minimum load should be considered, especially for coal and combined cycle gas turbine (CCGT) power plants [35], but their marginal generation costs are principally given by the fuel costs. Except for ramping restrictions and unit-commitment, their generation and the corresponding cost at one step is independent from the generation at other time steps.

Given well-defined operating costs, the optimal operation of a power system (with unlimited and lossless transmission) can be found using the merit order, where the supply is ranked with ascending marginal costs and the demand with descending marginal utility. The activation order is given by the merit order, and more supply is activated to meet the demand until the remaining supply has higher marginal cost than the marginal utility of the remaining demand as illustrated in Figure 2.1.

Due to the relatively weak coupling in time compared to systems with ESSs, the optimal generation capacities of these systems are often analysed based on the load duration curve as shown in Figure 2.2. The load duration curve indicates the system demand ordered by power magnitude instead of chronologically and shows the duration (x-axis) of the different power levels (y-axis) through a year. For known generation capacity investment costs and marginal operating costs, the optimal durations and capacities, denoted t_i and p_i in Figure 2.2, can be found [12]. The optimal capacities based on load duration curves have also been derived for ESSs under the assumption of limited power capacity and infinite energy capacity [13]. The optimal capacities ensure the demand is met with a mix of generation technologies that minimizes the long-term operating costs, and that the suppliers recover their investment cost through the generator's lifetime.

These systems are considered power-constrained, given the fuel availability at the given price is not a limiting factor, since the total available power capacity is the main limiting factor to meet meet the demand in a cost effective way at all times. As illustrated in Figure 2.2, the highest demand has a very short duration. It is therefore extremely expensive to provide the peak capacity since it is rarely used. Moreover, since the price is set by the marginal producing unit, each unit will only be profitable in the periods where an even more expensive unit sets the price. Therefore, the optimal solution in a competitive market involves some scarcity to enable the most expensive generators to recover their investment costs.

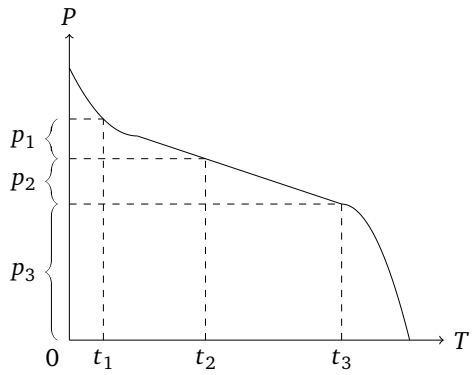

Figure 2.2: Load duration curve showing the optimal duration and the respective optimal capacities for three generation technologies ordered from highest to lowest operating costs.

2.3 Energy-constrained systems

Power systems dominated by VRESs and ESSs, for example hydro-power dominated systems, are fundamentally different from power-constrained systems in the following ways:

- A high share of the energy inflow is variable and uncertain with a marginal cost close to zero.
- Energy spent from ESSs influenced their capability of delivering and absorbing energy later. The operation strategy is therefore strongly coupled in time.
- The systems often have high installed power capacity, but they are limited by the available stored energy.

Unlike power-constrained systems, where the marginal cost of most units are well-defined through the fuel costs, energy-constrained systems have a high share of variable units with marginal cost close to zero. Moreover, ESSs act as both supply and demand by shifting energy in time without adding energy to the system. Although the ESSs' net energy delivery is less than zero due to losses, they add value to the system by maximizing the utilization of VRESs with close to zero marginal cost and minimizing expensive dispatchable generation and load shedding. Therefore, their marginal cost/value are mainly given by the costs of all the other units in the system.

However, energy-constrained systems can still use the marginal cost/value principle for operating the system in a safe and cost effective way like in the Norwegian case [36]. Whereas power-constrained systems are dominated by dispatchable

generators with well-defined costs that are independent from previous decisions, the costs in energy-constrained systems are given by the marginal value of the ESSs. ESSs comprise hydro-power reservoirs, batteries, and hydrogen storage systems as well as other resources that permit shifting energy in time and can also include some types of DSR.

The hourly decisions for ESSs cannot be taken independently from decisions in other time steps due to the strong time coupling. The optimal decisions from a price taker perspective will therefore require price forecasts. Price forecasts are derived based on analysis from a system perspective, hence the system analysis still has a relevance for competitive markets. Both price taker and system optimization perspectives are therefore considered in this thesis: Papers I and II take a price taker perspective, Paper III considers the price formation seen from a system perspective, while Papers IV and V consider small subsystems that act as price takers in a larger system.

2.3.1 Storage marginal value

The marginal value of ESSs can be considered as the future opportunity cost of the stored energy. How valuable is the stored energy compared to other resources? How much power should be charged or discharged now? Unlike thermal resources, ESSs have a very strong coupling in time. The storage marginal value (SMV) is therefore obtained through optimization considering:

- Variability and uncertainty in both generation and demand.
- All future decisions are not taken at once, but updated stage-wise as time elapses and uncertainty is revealed.
- The modeling horizon is in reality undefined.

Methods for complying with the uncertainty, stage-wise decisions and undefined horizon are presented in Section 4.1, and the interpretation of the SMV is discussed in Section 4.1.4.

Valuation of stored energy, primarily in hydro-power reservoirs, has been extensively studied in hydro-power dominated areas such as Norway, Sweden, Brazil, New Zealand, and Canada for decades. The process of deriving the marginal operating value for hydro-power reservoirs for a stage-wise process under uncertainty, commonly known as the *water value* [37], is closely related to SDP and has also driven the development of SDDP [38].

This thesis will extend the marginal value principle to other ESS types, such as batteries and hydrogen storage with fuel cell and electrolyzer, as well as other uncertainties like wind and solar power generation.

2.4 Transmission and distribution

The transmission system is the backbone of the power system enabling transmission of power over large geographical distances between large-scale producers, consumers, and distribution networks. The transmission system operates at high voltage to minimize the losses, and typically has a meshed structure for high security in case of outages. The distribution systems are regional medium and low voltage networks, typically with a radial structure, that distribute the power from the transmission system all the way down to the consumers. Whereas the transmission system is operated actively to stay within its physical operating limits, the distribution systems have been operated more passively by ensuring the network capacity is sufficient to handle the maximum load at all times [19]. Moreover, the transmission system can experience alternating power flow directions, while the distribution systems have typically had a well-defined power flow direction from the transmission system connection point to the consumers.

The emerging distributed resources, including production, flexible demand, and ESSs, reveal new challenges and opportunities for how the distribution system is operated and utilized. The flexibility enables operation of the distribution system in a similar manner as the transmission system [19], and can both manage challenges on the distribution level as well as interact with the markets on the transmission level.

The increasing share of VRESs also imposes new challenges with respect to managing geographical imbalances. For example, areas with a high level of solar power will often experience contrary production compared to areas with a high level of wind power. Temporary local energy shortages can be avoided by transmitting power from areas with surplus. However, grid limitations necessitate planning of power exchange upfront to ensure a sufficiently high SOC of the ESSs in areas with energy deficit.

2.5 Uncertainty

Power systems are exposed to uncertainties, which can be classified into technical and economical, as illustrated in Figure 2.3 [39].

This thesis considers the uncertainty in power delivered from VRESs and power absorbed by consumers, which can be classified as a technical operational uncertainty. Whereas the power-constrained systems dominated by thermal generators must mainly manage the demand uncertainty, the energy-constrained systems with a high share of VRESs must also manage uncertainties in both wind and solar power. Lasting low generation from VRESs can potentially empty ESSs and

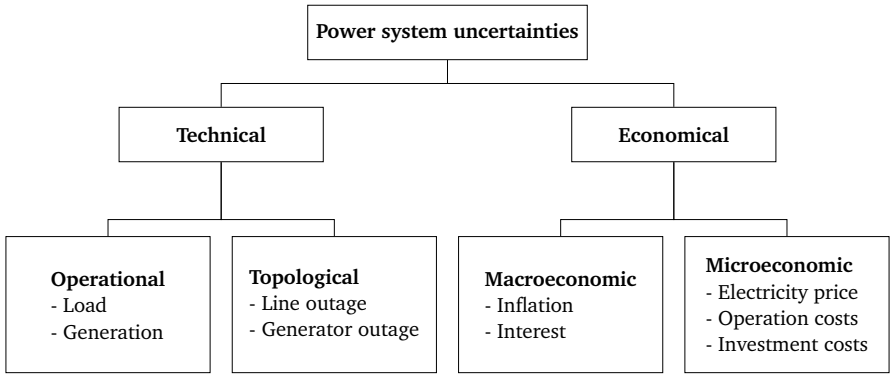

Figure 2.3: Classification of power system uncertainties [39]

cause energy deficit. Hence, operational efficiency and security of supply must be carefully balanced under adequate uncertainty management.

2.6 Complexity

The operation of energy-constrained systems should consider:

- The system's technical characteristics.
- A broad range of possible scenarios.
- Long time horizons.
- Large geographical areas.

However, the temporal and spatial level as well as the scenarios will each increase the size of any system model linearly. Formulating detailed optimization models in a straightforward manner while accounting for complexity in multiple dimensions yields intractable models that are difficult to solve within moderate computation time.

Aggregation and decomposition techniques are widely deployed in hydro-power scheduling. The models are often decomposed into a sequence of models where the first covers all the three aspects above, but with an aggregated representation of the power system. The following levels use the previous model results as input, and have an increasing level of detail but decreasing time horizon and/or geographical extension [40]. By doing so, detailed technical modeling can be included while still accounting for large-scale phenomena like long-term energy adequacy and transmission between distant geographical areas.

2.7 The microgrid perspective

The US Department of Energy define a MG in the following way [41]:

> *A microgrid is a group of interconnected loads and distributed energy resources within clearly defined electrical boundaries that acts as a single controllable entity with respect to the grid. A microgrid can connect and disconnect from the grid to enable it to operate in both grid-connected or island-mode.*

This definition includes the following requirements [42]:

- The boundaries of a MG are clearly defined.
- The MG resources are controlled with respect to each other rather than the grid.
- The MG can also operate disconnected from the grid.

MGs have recently attracted increasing attention for several reasons:

- Whereas the traditional distribution systems are vulnerable to failures at any point of a radial, MGs provide increased security of supply by allowing disconnected operation for limited periods or permanently [43].
- Electrification of and expansion of remote areas is costly due to the geographical distances, and sometimes few consumers to pay for the costs. In some situations, MGs can be a viable alternative to expensive grid expansions [44].
- The market price signals does not necessary capture local scarcity or surplus of supply. MGs facilitate local energy trading and local harvesting of profit [45].
- A high number of DERs can become intractable to manage for system operators. MGs enable efficient integration of distributed generation from VRESs [22] and utilization of distributed flexibility, such as DSR [21] and EVs [46]. MGs can serve as an aggregation layer to simplify the interaction between DERs and the grid operator [47].

The points above can be summarized into three main drivers for MG deployment: 1) energy security, 2) economic benefits, and 3) clean energy integration [42].

All papers in this thesis take a MG perspective, where the operation considers a set of resources with clearly-defined boundaries. The contributions and main findings are therefore mostly seen from the body of MG research. However, several of the results are also valid for large-scale systems and will be further discussed in Chapter 5.

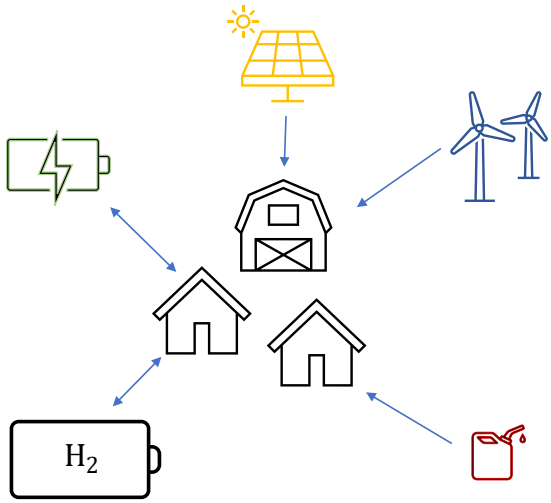

Figure 2.4: Conceptual topology of Rye microgrid.

2.7.1 Rye microgrid

Rye microgrid is located near Trondheim in Central Norway. As illustrated in Figure 2.4, the MG comprises a farm and a few households, which are supplied by solar and wind power. Supply and demand are balanced with a lithium-ion battery and a hydrogen unit with electrolyzer and fuel cell, and a diesel generator serves as backup [48]. Papers IV and V have used different variations of Rye to study the optimal operation strategies.

Chapter 3

Modeling of flexible energy resources

This chapter considers basic modeling principles for ESSs, wind and solar power as well as the grid. Section 3.1 presents detailed modeling principles for batteries and under which assumptions they can be simplified to a representation in the power and energy variable space. Common operating costs due to degradation are also outlined. Section 3.2 presents common modeling principles for wind and solar power. Section 3.3 briefly explains how DSR can be considered as a combination of a ESS and flexible load. Section 3.4 presents basic grid modeling and some common linear approximations.

Flexibility comprises DSR, ESSs, and flexible generation [49]. The mathematical description of the flexible resources are the main building block of power system models. The description should be accurate enough to represent the technical properties and limitations, yet simple enough to integrate into larger power system models. As opposed to traditional power systems with large centralized flexible generators, the emerging flexibility is often distributed and uncertain. Grid limitations must also be accounted for at a more detailed level to enable high utilization of the distribution systems.

3.1 Electric energy storage

ESSs in power systems has previously mainly included stored hydropower designed for managing seasonal variations, and pumped hydro for managing daily and intra-day variations. With the increasing amount of installed VRESs, the interest in pumped hydro has been renewed, resulting in both new plants and re-

habilitation of existing plants [16, 50].

However, hydropower is only possible in areas where the geographical conditions are right. Therefore, alternative ESS technologies have gained significant attention to increase the utilization of generation from VRESs. One of the most salient ESS technologies are lithium-ion batteries. The 150 MW/193.5 MWh Tesla battery in Hornsdale, South Australia has been successful in balancing a power system with an increasing share of generation from VRESs [51], and even larger batteries are under construction such as the 300 MW/1200 MWh battery at the Moss Landing Power plant, California [52]. Batteries are also widely deployed on distribution level where their applications range from short-term power quality improvement to energy management to increased the utilization of VRESs [53]. Residential scale batteries are also pointed out as an important factor for efficient solar photovoltaic (PV) integration [54].

Although lithium-ion batteries can increase the utilization of VRESs, they suffer from a relatively short duration (typically 1-4 hours) and high energy capacity costs. Reaching 50-80% generation from VRESs require ESSs with a duration of up to 10 hours, while 70-90% VRESs requires ESSs with a duration of up to 100 hours [55]. Hydrogen is a possible long-duration storage alternative due to its relatively low energy capacity cost [56]. The cost of scaling up batteries with respect to energy storage capacity is relatively high, and they also suffer from self discharge. In contrast, hydrogen tanks are relatively inexpensive and hydrogen can be stored for long periods without worrying about self discharge. On the other hand, they have poor round-trip efficiency, typically below 40% [57], and despite decades of research, they still struggle to compete commercially due to high fuel cell and electrolyzer costs and limited lifetime [58]. However, hydrogen can connect electricity and gas markets, increasing the overall system flexibility. Providing sufficient flexibility into the energy system with variability at both short and long timescales will require a wide range of flexible resources with high efficiency, high power capabilities, and a long duration.

3.1.1 Electrochemical batteries

Electrochemical batteries comprise multiple interconnected cells, both in series and parallel, as shown in Figure 3.1. They deliver energy by converting a high energy reactant to lower energy products, where this process is reversible for chargeable batteries. Battery models for economic dispatch often consider batteries in the variable space of power and energy, while more detailed battery models consider the current, voltage, and electric charge variable space [59, 60]. The cell voltage $v_{cell}(i_{cell}, q_{cell})$ depends on both the current i and the SOC q.

By assuming identical cells, and that the voltage and SOC always will be equal

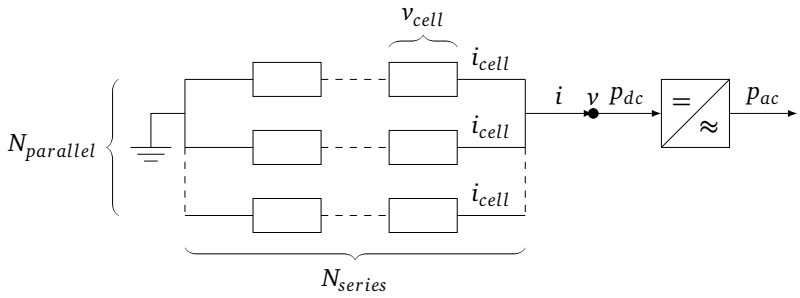

Figure 3.1: Organization of cells in series and parallel in a battery and conversion between DC and AC.

for all cells, the battery voltage is given by the cell voltage times number of cells in series as shown in Equation (3.1a) and the current by the cell current times number of cells in parallel given by Equation (3.1b). The power equals the product of current and voltage as shown in Equation (3.1c), and Equation (3.1d) shows how the converter losses depends on the power charge/discharge. The change in SOC is given by the injected current as shown in Equation (3.1e). Voltage, current, and charge are limited by the properties and capabilities of the cells as shown in Equations (3.1f) to (3.1h).

$$v = v_{cell}(i_{cell}, q_{cell}) \cdot N_{series} \tag{3.1a}$$
$$i = i_{cell} \cdot N_{parallel} \tag{3.1b}$$
$$p_{dc} = i \cdot v \tag{3.1c}$$
$$p_{ac} = p_{dc} - p_{loss}(p_{ac}) \tag{3.1d}$$
$$q_{cell,t} = \int_0^t (-i_{cell,t})dt \tag{3.1e}$$

$$V^{min} \leq v \leq V^{max} \tag{3.1f}$$
$$-I^{max} \leq i \leq I^{max} \tag{3.1g}$$
$$Q^{min} \leq q \leq Q^{max} \tag{3.1h}$$

This battery model formulation has been implemented as a non-linear optimization model in Paper II where the relation between cell voltage, current, and charge and the converter loss has been represented using spline functions based on empirical data. Equation (3.1e) is reformulated using numerical integration, where forward Euler is the most common method. However, the discharge power depends on the voltage as shown in Equation (3.1c), which is a function of both current and charge as shown in Equation (3.1a). The numerical integration method

and the step length will therefore influence the optimization results, which have been studied and discussed in Paper II.

3.1.2 Generic storage model

The voltage profile for lithium-ion batteries is relatively flat compared to other battery technologies, and is commonly assumed to be constant in battery modeling for economic dispatch. By also assuming the losses are proportional with the power, the proposed formulation reduces to the generic storage model in Equation (3.2), where the ESS is represented in the power and energy variable space. The losses are given by the efficiency coefficients η_c, η_d for charging and discharging, respectively.

$$e_t = \int_0^t p_t dt \tag{3.2a}$$

$$p_t = \eta_c sc_t - \frac{sd_t}{\eta_d} \tag{3.2b}$$

$$E^{min} \leq e_t \leq E^{max} \tag{3.2c}$$

$$0 \leq sc_t \leq SC^{max} \tag{3.2d}$$

$$0 \leq sd_t \leq SD^{max} \tag{3.2e}$$

This simplification ignores the dependency between charge power and SOC, hence the choice of numerical integration method does not influence the results such that Equation (3.2a) can be written as Equation (3.3) when using the forward Euler method.

$$e_t = e_{t-1} + \Delta T_t \left(\eta_c sc_t - \frac{sd_t}{\eta_d} \right) \tag{3.3}$$

Many formulations also include restrictions preventing simultaneous charging and discharging. It can either be formulated as a non-linear constraint as shown in Equation (3.4), or with a binary variable δ as shown in Equation (3.5) [61].

$$sc_t \cdot sd_t = 0 \tag{3.4}$$

$$\begin{aligned} &0 \leq sc_t \leq SC^{max} \cdot \delta_t \\ &0 \leq sd_t \leq SD^{max} \cdot (1 - \delta_t) \\ &\delta \in \{0, 1\} \end{aligned} \tag{3.5}$$

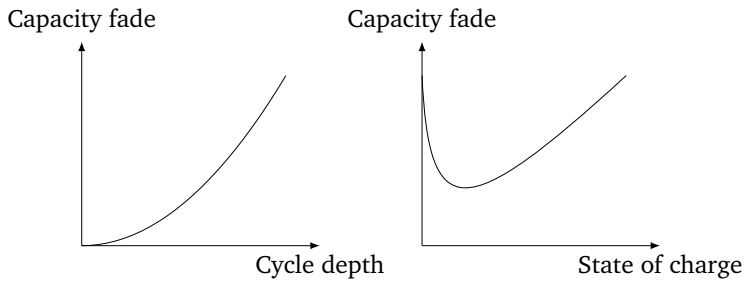

Figure 3.2: Battery capacity as a function of cycle depth.

However, simultaneous charging and discharging is, in reality, a way for the optimization model to discard energy due to rigorous constraints, for example, thermal generators ramping constraints or non-dispatchable generation from VRESs [62]. This effect can be reduced by making the generation from VRESs dispatchable as shown in Papers I to V, and include discharge costs for ESS dispatch as shown in Papers I and V. Moreover, Paper II avoids simultaneous charge and discharge by representing the charge/discharge in the voltage and current variable space where the current variable can be both positive and negative, but this formulation is non-linear.

Although a more detailed mathematical formulation imposes a more complex optimization problem, the solution time will not necessarily increase correspondingly. An optimization problem with an overly simplified storage model will in many situation have a flat optimum (multiple equally good solutions). By adding more details to the modeling, more curvature is added to the solution space, yielding a smaller or a unique optimum that, in turn, might contribute to reduce the solution time.

3.1.3 Operating costs

Whereas thermal generator operating costs are highly dependent on fuel consumption and emission costs, an ESS only shifts energy in time. However, the operational pattern may influence the degradation rate. For example, electrochemical batteries like lithium-ion batteries degrade with time (calendar aging), temperature, ampere throughput, charge/discharge power, and cycling depth [63].

Figure 3.2 illustrates how the battery degradation increases with increasing cycling depth and how the degradation changes with SOC. These degradation effects are operationally dependent, and Paper I studies the implications of cyclic degradation in coherence with wind uncertainty in a MG using SDDP. Moreover, Paper V studies the optimal operation of both battery and hydrogen storage considering

both cycling and calendar aging under solar PV, wind, and demand uncertainty over a full year for the Rye MG [48, 64].

Non-linear degradation effects can be linearized using piece-wise linear segments both for cyclic degradation as described in Xu *et al.* [10] and SOC dependent degradation as shown in Paper V. By using linear formulations, these degradation effects can be combined with powerful stochastic optimization methods like SDDP.

3.2 Variable renewable energy sources

The deployment of VRESs world-wide is dominated by solar and wind power [3]. The maximum power production from these sources are solely given by the weather, but they can often be controlled freely below the maximum power production. Curtailment has traditionally been considered as a last resort measure, but supply shaping and proactive curtailment are necessary for optimal and safe operation of the energy system when the levels of VRESs are high [65].

3.2.1 Solar power

Solar power production depends mainly on the solar-zenith angle and the cloud cover. The solar-zenith angle is a predictable quantity given by the geographical location of the PV array, and the time of day and year. The relation between the power production and the solar radiation, often expressed as direct normal irradiance (DNI) and diffuse horizontal irradiance (DHI), are well described in the literature [66]. From a stochastic programming perspective, it is advantageous to divide the solar power production into a deterministic and a stochastic part as shown in Equation (3.6) where PF_t^{max} is the theoretical maximum production at time t with clear sky and ci_t is the clearness index (CI).

$$p_t = PF_t^{max} \cdot ci_t \tag{3.6}$$

The CI is a value between zero and one, where one represents clear sky. The CI is strongly connected to the *cloud fraction*, which represent the fraction of an area that is covered with clouds based on satellite images [67] and is a common quantity for meteorological forecasts [68]. The CI is more suitable to represent as a stochastic process than the power directly since the CI varies between zero and one and has a weaker coupling to time of day and year than the actual production. Papers II, IV and V consider solar power uncertainty representing uncertainty through the CI.

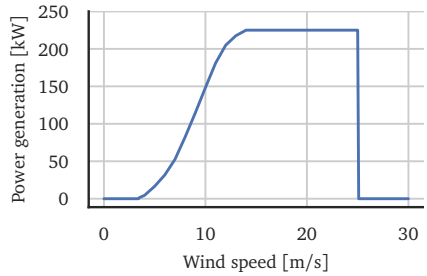

Figure 3.3: Ratio between wind speed and power generation for a Vestas V27 wind turbine [70].

3.2.2 Wind power

The maximum power production from a wind turbine is primarily given by the wind speed as shown in Figure 3.3. The ratio is non-linear, and at intermediate wind speeds even small variations can cause significant change in production. This curve is therefore important for the variance of the wind power production, which will depend on the wind speed. The wind turbine will not produce power at all below the lower threshold, the cut-in speed. Moreover, wind speeds above the upper threshold, the cut-off speed, will either cause a controlled shut-down or a gradual ramp down to avoid excessive loading of the equipment [69]. In the range between the cut-in and cut-off speed, the production can be adjusted freely below the maximum production by adjusting the blade tilt angle. Different turbine types have a distinct generation curve as well as cut-in and cut-off speeds.

3.3 Demand side response

DSR is expected to be an increasingly important balancing tool as more VRESs are connected to the grid. Potential flexibility is available in different sectors, for example, large-scale industry, heating of buildings [71], EV charging [72], and household appliances [73]. These types of flexibility can be considered as either changing or shifting the load, or a combination of both. Whereas changing the load involves either shedding or increasing the load without any future obligations, load shifting means the load reduction/increase has to be compensated for later and can be represented as a virtual battery [74].

This thesis only considers demand flexibility through load shedding, which is an essential instrument in energy-constrained systems. Systems with low dispatchable generation capacity will possibly yield infeasible optimization problems in periods with low generation from VRESs unless load shedding is permitted. Moreover, Section 2.2 emphasizes that the theoretical optimal solution from a system

perspective involves some load shedding [12].

3.4 Grid modeling

The networks connecting generation, consumption, and ESSs, both transmission and distribution, are represented through the power flow equations. The power flow follows the physical laws, and they describe the relation between voltage magnitude $|v|$, voltage angle θ, active power p, and reactive power q at each bus or line in the system. The power system must be operated within its technical limits, such as thermal rating of lines and voltage limits, and the power flow equations enable us to operate generation, demands, and ESSs within these limits.

3.4.1 Bus power injections

The total bus power injections, both active power and reactive power, balance the power transmitted to other buses at each individual bus. The power injections p_i/q_i at bus i in Equation (3.7) are the sum of generated power p_g/q_g and power discharged from ESSs p_e/q_e minus the consumption p_d/q_d, where the sets of of generators, ESSs, and demands at bus i are denoted as $\mathcal{G}_i, \mathcal{E}_i, \mathcal{D}_i$ respectively.

$$p_{i,t} = \sum_{g \in \mathcal{G}_i} p_{g,t} + \sum_{e \in \mathcal{E}_i} p_{e,t} - \sum_{d \in \mathcal{D}_i} p_{d,t} \tag{3.7a}$$

$$q_{i,t} = \sum_{g \in \mathcal{G}_i} q_{g,t} + \sum_{e \in \mathcal{E}_i} q_{e,t} - \sum_{d \in \mathcal{D}_i} q_{d,t} \tag{3.7b}$$

$$\forall i \in \mathcal{B}, \forall t \in \mathcal{T}$$

3.4.2 Power flow

The power flow between the buses is given by the power flow in Equation (3.8) where $|v_{i,t}|/|v_{j,t}|$ are the bus voltage magnitudes, $\theta_{i,t}/\theta_{j,t}$ are the voltage angles, and $Y_{ij} = G_{ij} + jB_{ij}$ where Y_{ij} is element ij of the system admittance matrix.

$$p_{i,t} = |v_{i,t}| \sum_{j=1}^{n} |v_{j,t}| (G_{ij} \cos(\theta_{i,t} - \theta_{j,t}) + B_{ij} \sin(\theta_{i,t} - \theta_{j,t})) \tag{3.8a}$$

$$q_{i,t} = |v_{i,t}| \sum_{j=1}^{n} |v_{j,t}| (G_{ij} \sin(\theta_{i,t} - \theta_{j,t}) - B_{ij} \cos(\theta_{i,t} - \theta_{j,t})) \tag{3.8b}$$

$$\forall i \in \mathcal{B}, \forall t \in \mathcal{T}$$

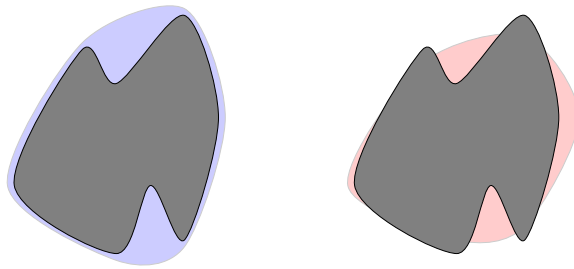

Figure 3.4: Illustration of convex relaxation (blue) compared to approximation (red) of a non-convex space (gray) (redrawn based on [76, p.4]).

The power flow equations are key constraints for power system optimization models when network limits are considered. The full power flow equations are both non-linear and non-convex, and computationally difficult to solve [75]. It is also difficult to guarantee whether an optimal solution is globally or locally optimal. However, there are a wide range of alternative formulations, both convex relaxation and approximations, as illustrated in Figure 3.4, that reduce the complexity at the sacrifice of precision. The convex relaxations encloses the whole non-convex feasible space of Equations (3.8a) and (3.8b) and guarantees a global optimum. However, the solution is not guaranteed to be a feasible solution of the power flow equations. Approximations can neither guarantee that the solution is a feasible solution of the power flow equations nor global optimality, but they are often satisfactorily accurate yet simple enough. The reader is referred to Molzahn and Hiskens [76] for further reading about power flow formulations.

DC power flow

A simple yet very common linear approximation is the DC power flow. As summarized by Stott *et al.* [77], there are many variations of the DC power flow. However, the main assumptions are:

- The voltage is high such that $R \ll X$ (resistance is small compared to reactance.
- The difference in voltage angle between buses is small such that $\sin(\theta_i - \theta_j) \approx \theta_i - \theta_j$ and $\cos(\theta_i - \theta_j) \approx 1$.
- The voltage magnitudes are close to unity $|v_i| \approx 1$.

The DC power flow approximation has been used in Papers I and III. Due to the DC power flow's limitations with respect to modeling medium- and low-voltage

grids accurately, alternative formulations has been addressed as future work in Section 6.1.

Distribution power flow (DistFlow)

The distribution power flow (DistFlow) [24, 25] is an exact solution of the AC power flow for radial systems and is therefore commonly used for distribution systems. Instead of expressing the power flow equations using bus power injections and bus voltages, DistFlow considers line powers p_{ij}/q_{ij} and current i_{ij}. Moreover, the voltage and current variables are expressed using the squared magnitudes $|v_i|^2$ and $|i_{ij}|^2$. The line resistance and reactance are denoted by R_{ij} and X_{ij}, respectively. The branch connections between buses j and k are denoted $j \to k$ where k is located below j seen from the substation. The resulting set of equations defined for each line ij in the network are shown in Equation (3.9) [76].

$$p_{ij} = R_{ij}|i_{ij}|^2 - p_j + \sum_{k \in j \to k} p_{jk} \tag{3.9a}$$

$$q_{ij} = X_{ij}|i_{ij}|^2 - q_j + \sum_{k \in j \to k} q_{jk} \tag{3.9b}$$

$$|v_j|^2 = |v_i|^2 - 2(R_{ij}p_{ij} + X_{ij}q_{ij}) + (R_{ij}^2 + X_{ij}^2)|i_{ij}|^2 \tag{3.9c}$$

$$|i_{ij}|^2|v_i|^2 = p_{ij}^2 + q_{ij}^2 \tag{3.9d}$$

The linear DistFlow assumes the active and reactive power losses are small compared to the power flows and ignores the losses associated with the squared current in Equation (3.9). The equation reduces to Equation (3.10), which is linear if the squared voltage magnitudes $|v_i|^2$ and $|v_j|^2$ are used as variables.

$$p_{ij} = -p_j + \sum_{k \in j \to k} p_{jk} \tag{3.10a}$$

$$q_{ij} = -q_j + \sum_{k \in j \to k} q_{jk} \tag{3.10b}$$

$$|v_j|^2 = |v_i|^2 - 2(R_{ij}p_{ij} + X_{ij}q_{ij}) \tag{3.10c}$$

Chapter 4

Stochastic programming for power systems with energy storage

This chapter presents stochastic optimization methods for power system operation. Section 4.1 describes how to account for uncertainty using rolling horizon and stochastic dynamic programming, and how stage-wise decomposition provides a useful method for deriving the value of stored energy as a function of time and state. Section 4.2 presents techniques for modeling uncertainty.

Power systems are exposed to both technical and economical uncertainties as emphasized in Section 2.5. This thesis focuses on the technical operational uncertainties associated with generation from VRESs and demand. Power generation from VRESs is highly uncertain due to forecast discrepancies, and the demand side is also uncertain due to variations in the individual consumption both for residential, commercial, and industrial consumers.

Power systems with high energy storage capabilities can store surplus energy from VRESs to maximize their utilization, and they can withdraw energy from ESSs to minimize load shedding and thermal generation. However, the current operation of ESSs is connected to the future capability of delivering and absorbing energy.

Energy-constrained systems, where the dispatchable generation capacity depends on support from VRESs and ESSs to meet the peak demand, must consider the operation of ESSs carefully since the current decisions are connected to the future security of supply. Likewise, demand and generation discrepancies caused by uncertainty also influences the future security of supply.

Section 4.1 considers different modeling techniques to manage uncertainty associated with generation and demand discrepancies in power system operation, both rolling horizon modeling, value-based storage management as well as multi-stage stochastic programming.

Energy-constrained systems are particularly vulnerable to generation and demand uncertainties. Weather dependent uncertainties, like wind and cloud cover, are often strongly auto-correlated. Low wind at one time step increases the probability of low wind at the next time step, and forecast errors are also correlated. The auto-correlation can therefore increase the risk of scarcity if not properly accounted for. Modeling of correlations both in time and between different resources can contribute to an increased utilization of VRESs without compromising the security of supply. Selected methods for modeling uncertainties are presented in Section 4.2.

4.1 Modeling uncertainty

The result of an optimization model for operation is a proposal for how to operate a system's flexible resources from an initial condition and for a limited time forward. The proposed solution is only optimal for the conditions defined by the model, and due to modeling inaccuracies and uncertainties, the control may not be optimal or feasible for the real-time control of the system.

4.1.1 Rolling horizon optimization

Rolling horizon involves finding the optimal decisions within a prediction horizon as illustrated in Figure 4.1, where the decisions within the *roll horizon* are implemented. When the roll horizon has elapsed, the initial states and the forecasts are updated, and the system is re-optimized for the new prediction horizon.

By repeating the procedure, the optimal strategy is corrected stage-wise through the updated forecasts and initial states. This procedure is often associated with model predictive control (MPC) [78]. The rolling horizon approach is tractable since it ensures the state of the system and the optimization model are synchronized regularly, reducing the risk of infeasible operating strategies.

Rolling horizon optimization has been used to optimize the operation of the Rye MG in combination with both deterministic and stochastic models in Papers IV and V.

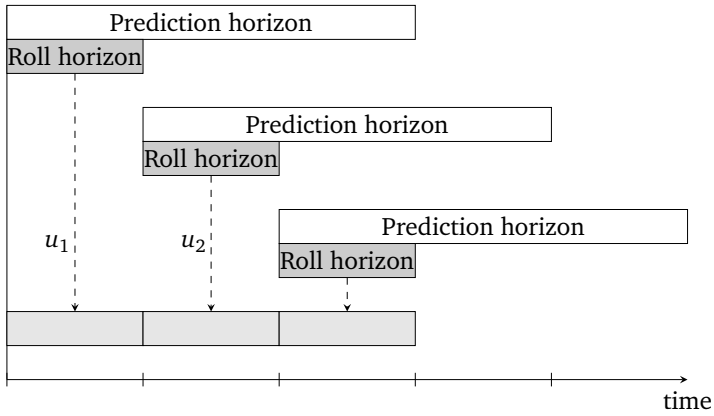

Figure 4.1: Illustration of rolling horizon optimization.

4.1.2 Modeling horizon and expected future value

Although generation and demand forecasts have limited look-ahead, in reality, power system operation models have an undefined time horizon. Unless the stored energy is properly valued beyond the time horizon of the operational optimization models, the ESSs tend to be emptied. This can be avoided by simply enforcing a fixed lower bound for the SOC at the end. However, in many situations this approach will be unnecessary rigorous and will be further discussed in Section 5.3.

A more sophisticated method is to determine the value of the stored energy as a function of SOC, an idea which is widely deployed in hydro-power scheduling. Papers III and IV demonstrate how to determine the value of stored energy in ESSs, both batteries and hydrogen, in systems with high penetration from solar and wind power.

Let $V_s(x_s)$ represent the cost of the system state x_s, typically the SOC of all ESSs as well as other systems states. $V_s(x_s)$ is the expected future cost of the system states if the system is operated perfectly in the future for the given states.

ESSs balances the operation between the extremes: generation curtailment and load shedding. High SOC is associated with high risk of generation curtailment, hence adding more energy to an almost full ESS has low value. Low SOC is associated with high risk of scarcity, hence adding more energy can contribute to prevent load shedding and will therefore have a high incremental value.

4.1.3 Stochastic programming

This section uses the terminology from Dowson [79] to describe the MSSP formulation in general terms:

- A *stage* s is a discrete moment in time where uncertainty is revealed and a control is chosen.
- The *state* variable x_s is a vector that encapsulates all necessary information to model the system from stage s and onward.
- The *control* variable vector u_s represents all decisions, both explicit and implicit, taken at stage s. The control must be within the set of admissible controls $U_s(x_s, \omega_s)$.
- The *random* variable vector ω_s represents the uncertainty revealed at stage s.
- The *stage-objective* function $C_s(x_s, u_s, \omega_s)$ represents the cost accrued at stage s given the initial state x_s, the uncertainty ω_s, and the control action u_s.
- The *state-transition* function $T_s(x_s, u_s, \omega_s)$ maps the incoming state x_s to the outgoing state for the given control action u_s and uncertainty ω_s.

From a power system operation perspective, the state variable vector typically includes all variables that are coupled in time such as the SOC of ESSs, and may also include auto-regressive moving average (ARMA)-model variables (see Section 4.2.1). The control variable vector includes all decisions, where the explicit decisions include how the generators and ESSs are dispatched, while the implicit decisions include variables like power flow and voltage levels that are connected to the decisions but cannot be controlled directly. All these variables must stay within the set of admissible controls defining the technical limitations of the system. The random variable vector typically includes the demand and generation uncertainty. The stage-objective function represents the operating costs from, for example, thermal generators, load shedding, and degradation. The state-transition function describes how the state evolves between stages, for example, how the SOC of the ESSs changes for the given initial state, control, and random variable vectors.

The classical two-stage stochastic model [80] is a decision process where the agent first makes a decision under uncertainty before the uncertainty is revealed and a corrective action can be taken. This decision process is given by Equation (4.1).

$$\begin{aligned} \min_{u_1} \quad & C_1(x_1, u_1, \omega_1) + \mathop{\mathbb{E}}_{\omega_2 \in \Omega_2} \left[\min_{u_2} C_2(x_2, u_2, \omega_2) \right] \\ \text{subject to} \quad & x_2 = T_1(x_1, u_1, \omega_1) \\ & u_1 \in U_1(x_1, \omega_1) \\ & u_2 \in U_2(x_2, \omega_2) \end{aligned} \tag{4.1}$$

The objective is to find the optimal control of the first stage that minimizes the

operating costs for both stages, when the future is partly uncertain. The second term in the objective function is actually the expectation of an optimization problem, hence we assume the future decisions are taken optimally. This formulation is very useful for power system operation since the decision process, in reality, is a sequence of decisions that can be corrected stage-wise as uncertainty becomes known.

A key advantage with a stochastic model compared to a deterministic model is that it considers the possibility of discrepancies between generation and demand forecast and actual values. For example, a deterministic model will not take any precautionary actions against scarcity before it is expected to occur. For a stochastic model, it is sufficient that one of the scenarios indicates the possibility of scarcity such that precautionary actions can be taken to keep the probability of scarcity low.

The two-stage stochastic model can be generalized to the MSSP formulation [80] as shown in Equation (4.2).

$$\begin{aligned} \min_{u_1} \quad & C_1(x_1,u_1,\omega_1) + \mathop{\mathbb{E}}_{\omega_2|\omega_1}\Big[\min_{u_2} C_2(x_2,u_2,\omega_2) + \dots \\ & \qquad + \mathop{\mathbb{E}}_{\omega_S|\omega_{S-1},\dots,\omega_1}\Big[\min_{u_S} C_S(x_S,u_S,\omega_S)\Big]\Big] \\ \text{subject to} \quad & x_{s+1} = T_s(x_s,u_s,\omega_s) \\ & u_s \in U_s(x_s,\omega_s) \\ & \qquad\qquad\qquad\qquad s \in \{1,\dots,S\} \end{aligned} \tag{4.2}$$

Besides considering the expectation value of multiple nested optimization problems, the stage-wise uncertainty is also dependent on the noise of all previous stages. Due to its complexity, the MSSP formulation in extended form is normally intractable to solve for large-scale problems and various techniques have been proposed to reduce the complexity. This thesis considers dynamic programming techniques, both SDP [81] and SDDP [38]. The formulation in Equation (4.2) is tractable to reformulate as a recursive problem as shown in Equation (4.3), given stage-wise independent uncertainty, and is known as the Bellman equation [81].

$$\begin{aligned} Q_s(x_s,\omega_s) = \min_{u_s} \quad & C_s(x_s,u_s,\omega_s) + V_{s+1}(x_{s+1}) \\ & V_s(x_s) = \mathop{\mathbb{E}}_{\omega_s}[Q_s(x_s,\omega_s)] \\ \text{subject to} \quad & x_{s+1} = T_s(x_s,u_s,\omega_s) \\ & u_s \in U_s(x_s,\omega_s) \\ & \qquad\qquad s \in \{1,\dots,S\} \end{aligned} \tag{4.3}$$

As emphasized in Paper III, the recursive problem comprises two terms with the following interpretations: The first term $C_s(x_s,u_s,\omega_s)$ represents the operating

costs of the current stage s, while the second term $V_{s+1}(x_{s+1})$ represents the future cost for the state x_{s+1} given optimal future operation. The negative future cost is denoted as the storage end value (SEV) in Equation (4.4), where the storage marginal value (SMV) for each individual element in the state variable vector is given by the gradient of the SEV-function with respect to the state x_s as shown in Equation (4.5).

$$SEV_s(x_s) = -V_s(x_s) \tag{4.4}$$

$$SMV_s(x_s) = \nabla SEV_s(x_s) \tag{4.5}$$

The SMV represent the marginal value of the stored energy and is referred to as the *water value* [37] in hydropower scheduling. The interpretation of SMV is further discussed in Section 4.1.4.

Stochastic dynamic programming

SDP is a classical approach for solving the stochastic recursive problem in Equation (4.3) given the stage-wise independency, where the state space x_s is divided into a finite number of discrete states. The problem is solved for each discrete state starting at the final stage S. The solution of the problem at each discrete state constructs a SEV-function for the previous stage. Using backward recursion, the whole problem can be solved yielding an optimal operating strategy for all combinations of stages and states. Unfortunately, the problem size grows exponentially with number of state variables due to the discretization, also known as *the curse of dimensionality* [81]. The variation proposed in Paper III uses splines to generate the SEV-functions, and the method requires fewer discrete points for each state than the classical linear approach [82].

Stochastic dual dynamic programming

Convex models can be solved without discretizing the state space using SDDP [38]. The SEV-function is approximated with linear cutting planes using a sampling-based forward-backward sweeping algorithm. The forward pass samples and optimizes a sequence of random scenarios from either historical scenarios or a statistical distribution. The backward pass refines the approximation of the SEV-function by adding new cuts as illustrated in Figure 4.2. The stage-wise mathematical formulation is shown in Equation (4.6) where θ_s represents the negative SEV-function (expressed as a cost), and α_s^k and β_s^k are cut coefficients obtained by the algorithm in iteration k. Detailed algorithms are presented by Pereira and Pinto

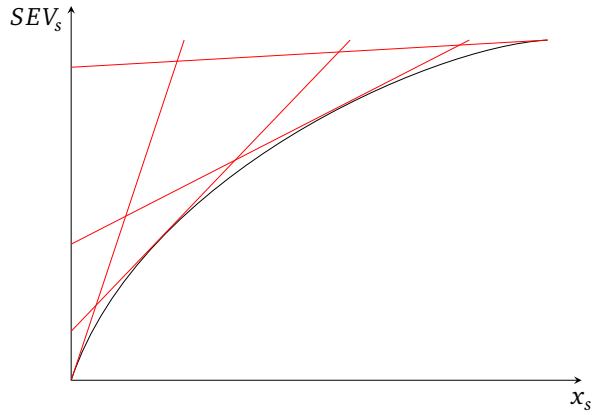

Figure 4.2: Approximation of the storage end value function bounded by linear cuts (illustrated with red lines).

[38] and Dowson [79].

$$\begin{aligned} \min_{u_s} \quad & C_s(x_s, u_s, \omega_s) + \theta_s \\ \text{subject to} \quad & x_{s+1} = T_s(x_s, u_s, \omega_s) \\ & u_s \in U_s(x_s, \omega_s) \\ & \theta_s \geq \alpha_s^k + \beta_s^k x_{s+1}, \quad k \in \{1, 2, ..., K\} \\ & \qquad\qquad\qquad\qquad\qquad\qquad s \in \{1, \ldots, S\} \end{aligned} \tag{4.6}$$

Whereas SDP typically reaches its computational limit for only a few state variables due to the curse of dimensionality [81], SDDP has been used to handle hundreds of state variables [83].

The original SDDP algorithm [38] requires stage-wise independent noise. However, stage-wise dependencies in noise can be managed by modeling the dependent noise as a part of the state using ARMA-models [84, 85] as demonstrated in Paper I, and will be further explained in Section 4.2. The combination of SDP and SDDP can also handle non-linear stage-wise dependencies through Markov models [79, 86]. The proposed approach was originally used to model stage-wise dependent price uncertainty [86], but Paper IV shows that the method can also capture the non-linear auto-correlation in wind power forecasts.

4.1.4 Storage marginal value

The SMV represents the marginal value of charging or discharging stored energy, where both cause efficiency losses. Let $CS_s^c(x_s)$ denote the marginal value of charging energy to an ESS, and $CS_s^d(x_s)$ the marginal cost of discharging energy.

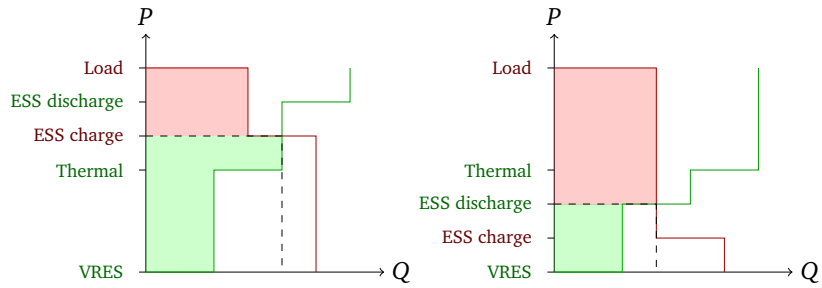

Figure 4.3: Energy storage systems act as both supply and demand in the market clearing problem. The figures illustrate how the market price can be set by either the charge value (Equation (4.7)) for high storage marginal value (left) or the discharge value (Equation (4.8)) for low storage marginal value (right).

The charge value and discharge cost for an ESS with fixed efficiencies as shown in Equation (3.2b) are then given by Equations (4.7) and (4.8).

$$CS_s^c(x_s) = \eta^c \cdot SMV_s(x_s) \tag{4.7}$$

$$CS_s^d(x_s) = \frac{1}{\eta^d} \cdot SMV_s(x_s) \tag{4.8}$$

The charge value indicates how much value is added to the system by charging one unit to the ESS, and its value compared to other demands and charge values in the system. Likewise, the discharge cost indicates the cost of discharging one unit from the ESS and how it should be prioritized compared to other supplies. These values change in time and as a function of all states in the system. For example, in systems with both battery and hydrogen as described in Papers III and IV, the battery SMV depends on the SOC for both the battery and hydrogen system.

The priorities based on SMVs can be visualized, as a snapshot, using supply and demand curves where the ESSs act as both producers and consumers as shown in Figure 4.3. In case of high SMV (left figure), the thermal generation will be used to charge the ESS and the charging becomes the marginal unit that sets the competitive price. In case of low SMV (right figure), the ESS is cheaper than the thermal generation, hence ESS discharging becomes the marginal unit that sets the competitive price.

The tool *Market clearing with VRES and ESS* [26], one of the contributions of this thesis, visualizes how different supply and demand capacities and values in combination with ESS power capacity, efficiency, and marginal value influence the market clearing with respect to volume and price. The user can adjust the parameters of the individual parameters while the visualization of the market clearing updates dynamically.

Since the future cost $V_s(x_s)$ is only a function of the state x_s, it can also be used to valuate the stored energy at the end of the optimization period in more detailed power system models like the non-linear model proposed in Paper II. This approach is commonly applied in hydropower scheduling [40].

4.2 Scenario generation

Stochastic programming methods rely on realistic scenarios spanning the sample space adequately. Generation from VRESs is primarily weather dependent, hence meteorological weather forecasts are essential to generate accurate generation scenarios. Demand is also weather dependent through heating and cooling needs, but will also, for example, follow known patterns through the day and week based on habits associated with heating, cooking, washing, EV charging, and so on.

4.2.1 Auto-regressive models

Dynamic programming assumes stage-wise independence to decompose the problem into a sequence of decisions. It is therefore useful to represent uncertainty using auto-regressive models capturing the correlations both in time and between variables in a way that can be effectively implemented into SDDP as demonstrated in Paper I.

A standard ARMA-model is shown in Equation (4.9) where X_t represents the predicted variable at time t, ϵ_t is a white noise variable, α_i and θ_j are the model parameters, and c is a constant. As seen from the structure, the predicted variable depends on its value and the noise from previous time steps. Since weather phenomena often tend to persist, auto-regressive models are commonly used to model VRES uncertainties.

$$X_t = c + \sum_{i=1}^{p} \alpha_i X_{t-i} + \epsilon_t + \sum_{j=1}^{q} \theta_j \epsilon_{t-j} \tag{4.9}$$

Forecast error

Instead of modeling the power p_t directly using ARMA-models, it may be beneficial to model the forecast error Δp_t as shown in Equation (4.10) where PF_t is the forecast.

$$\begin{aligned} \Delta p_t &= c + \sum_{i=1}^{p} \alpha_i \Delta p_{t-i} + \epsilon_t + \sum_{j=1}^{q} \theta_j \epsilon_{t-j} \\ p_t &= PF_t + \Delta p_t \end{aligned} \tag{4.10}$$

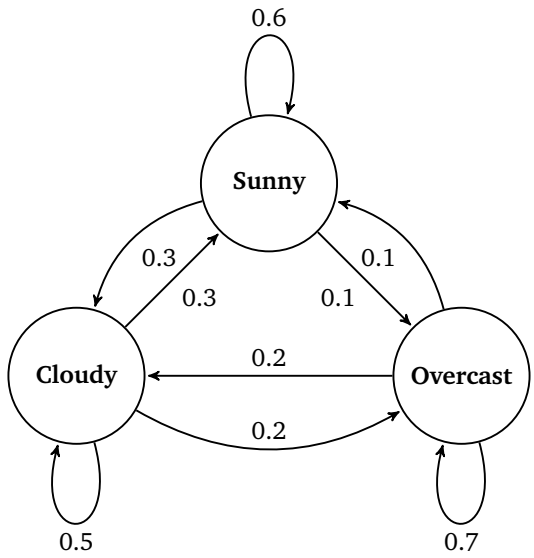

Figure 4.4: Example of possible Markov model to describe how the weather develops.

A limitation with this representation is that the generation can become negative, especially when the forecast PF_t is low. Moreover, it also assumes constant variance. However, wind power variance tends to increase for increasing wind power. An alternative representation is to use a multiplicative model as shown in Equation (4.11), which both eliminates the negative production and makes the variance proportional with the forecast power [85].

$$\begin{aligned} \Delta p_t &= \left(c + \sum_{t=1}^{p} \Delta p_{t-i} \right) \epsilon_t \\ p_t &= PF_t \cdot \Delta p_t \end{aligned} \tag{4.11}$$

4.2.2 Markov model

A Markov model is a stochastic model where future state only depends on the current state. For example, Figure 4.4 shows a very simple example for how the weather tomorrow depends on the weather today. If the weather is sunny today, the probability of sunny weather tomorrow is higher than the probability of cloudy or overcast weather.

A benefit of Markov models is that the probabilities can be chosen freely and do not need to follow any probability distribution, and they can easily incorporate nonlinearities. A clear disadvantage is that it is discrete, hence optimization models

must explore all different states to find an exact solution.

4.2.3 Stage length

Correlations in time and between variables can also be captured by using representative scenarios. For example, historical scenarios are commonly used for long-term hydropower scheduling in the Nordic system [87] since correlations both in time and space are difficult to preserve in stochastic models such that the risk of prolonged dry or wet periods are underestimated [83].

A limitation with historical scenarios is that the model does not capture the possibility to correct the operation strategy as new uncertainty becomes known. Power system operation is in reality a sequence of decisions in time that are updated each time new information is available, such as new observations and updated forecasts. Moreover, the historical scenarios are only appropriate to use for long-term scheduling beyond the horizon of the forecasts.

Chapter 5

Results and discussion

This chapter discusses the main results of the presented papers in coherence with the objectives in Section 1.2. Section 5.1 concerns findings related to detailed battery modeling in Paper II, and Section 5.2 presents results from the modeling of battery degradation in Papers I and V. Stochastic operation of energy-constrained systems as presented in Paper IV is considered in Section 5.3, and electricity pricing and the valuation of stored energy from Paper IV are discussed in Section 5.4.

5.1 Operational limits of energy storage systems

The non-linear battery operation optimization model that was implemented in Paper II illustrated by Figure 5.1 uses the current, voltage, and charge variable space for the battery instead of power and energy. Some of the benefits of this formulation compared to a simpler model using the power and energy variable

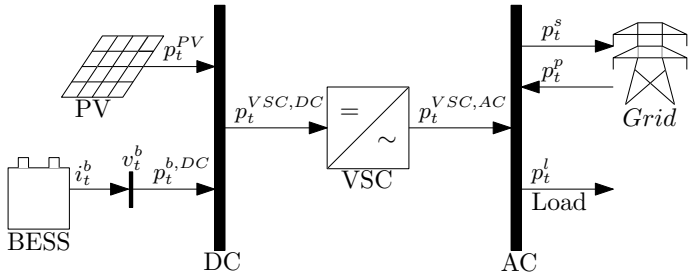

Figure 5.1: Topology of grid connected system with battery, solar photovoltaic and converter (figure adopted from Paper II [28]).

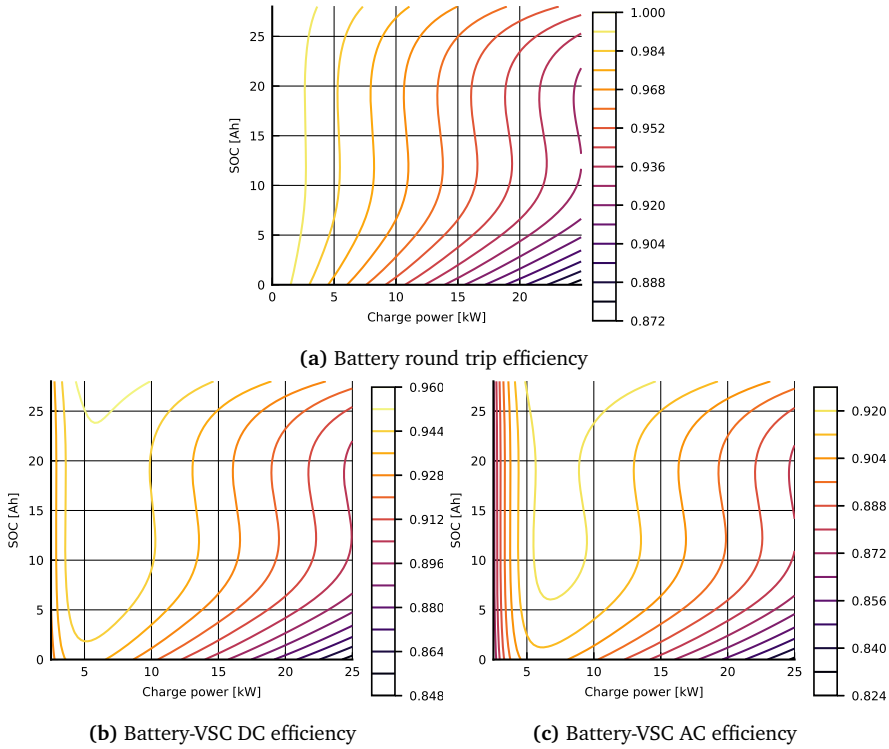

(a) Battery round trip efficiency

(b) Battery-VSC DC efficiency

(c) Battery-VSC AC efficiency

Figure 5.2: Battery and VSC efficiencies (figure adopted from Paper II [28]).

space and fixed efficiencies are:

- The voltage and current limits are enforced directly instead of through the power. This representation is closer to the physical properties of the battery and enables operation closer to the battery capabilities.
- The current variable can be both positive and negative allowing bi-directional power flow without separate charge/discharge variables. The typical non-linear or binary complementarity constraints to avoid simultaneous charging and discharging are therefore avoided.
- The SOC limits are enforced through the charge (Ampere hours) instead of energy. This is considered a more accurate way of estimating the battery SOC.
- Empirical data is used to represent the battery voltage and converter efficiency, ensuring the model is accurate, and it captures the efficiency losses in both battery and converter.

The results show that the implemented model enables operating closer to the operational limits of the battery. The efficiency is also represented more accurately, and

Figure 5.2a illustrates how the battery round-trip efficiency depends on both SOC and charge/discharge power. The converter efficiency also influences the overall efficiency, depending on whether the energy has to pass the AC/DC converter once (consumption of stored energy that originates from solar PV) or twice (consumption of stored energy that originates from grid) as shown in Figures 5.2b and 5.2c. As a consequence, the estimation of SOC is more accurate compared to simpler models. However, lithium-ion batteries have a relatively flat voltage curve and low losses, and the differences between the simple and detailed model are relatively small.

However, the principle of using variable space close to the physical representation of the ESS and estimating physical relations with spline functions are still applicable for other ESS types, such as flow batteries, hydropower plants as well as hydrogen electrolyzers and fuel cells.

For real-time operation, it is highly important that the proposed schedule does not violate the technical limitations such as power, current, and voltage limits. From a daily and weekly perspective, it is important that the ESSs are scheduled with sufficient foresight considering generation and demand uncertainties to prevent energy deficit. The long-term perspective might sacrifice technical details and time resolution granularity, to increase the foresight and the number of scenarios.

Both the short- and long-term requirements can be met by dividing the model into a sequence of models as suggested in Section 4.1.4. The optimization results from coarse aggregated models with a long modeling horizon over large geographical areas can be used as boundary conditions for more detailed models with shorter time perspectives.

5.2 Degradation of energy storage systems

Battery degradation partly depends on the operation. Papers I and V implemented cyclic degradation costs and Paper V also implemented SOC dependent degradation as piece-wise linear approximations. The capacity fade associated with the operation dependent variables was converted to a cost reflecting the battery investment cost and expected end of life.

Paper I shows that the cyclic operating costs make the stochastic operating strategy more precautionary against operating close to maximum SOC to keep the risk of generation curtailment low and prevent unnecessary charging and discharging of the battery. Moreover, the price difference threshold for arbitrage is also increased by the cyclic degradation costs.

Paper V considers cyclic degradation (also referred to as DOD degradation) in

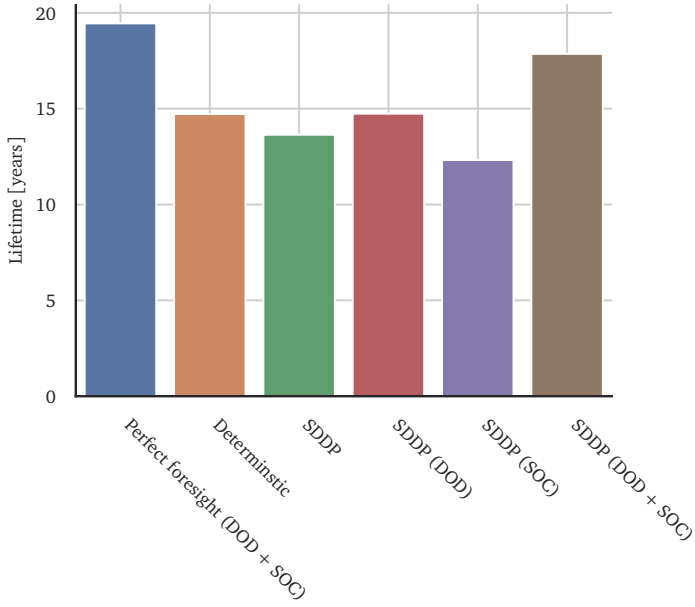

Figure 5.3: Expected battery lifetime for operation with different optimization methods. Text in parentheses indicates which type of degradation costs that has been included in the optimization model: depth-of-discharge (DOD)/cyclic degradation and state-of-charge (SOC)/calendar degradation.

combination with SOC dependent calendar aging. The comparison of the expected lifetime for the operation of a 1MW battery in Rye MG in Figure 5.3 shows that the implemented method (SDDP (DOD + SOC)) is capable of increasing the expected battery lifetime with more than four years compared to the plain stochastic model (SDDP), and that the cost reduction associated with battery degradation exceeded the increase in other operating costs. The results also demonstrate that the operational pattern adapts to seasonal variations. For example, the summer has high stable PV power production and scarcity occurs less frequently than during winter. It is therefore beneficial to lower the SOC in this period to reduce the calendar aging as shown in Figure 5.4.

However, SOC dependent degradation can also potentially provoke non-physical energy dumping through simultaneous charging and discharging since there is actually an increasing cost associated with storing energy. This undesirable effect is effectively reduced when implemented in combination with cyclic degradation where the discharging is penalized.

When considering co-operation of battery and hydrogen, the annual energy throughput for hydrogen nearly doubles when battery degradation is considered. There-

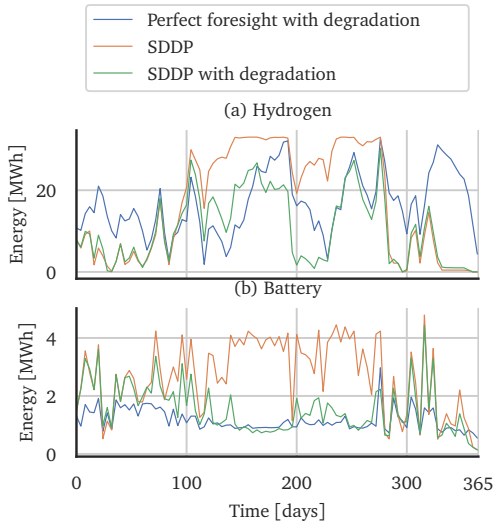

Figure 5.4: Four-day average SOC for co-operation of hydrogen and battery (based on case 1 from Paper V [31]).

fore, it is important to consistently model degradation for all involved units to prevent the burden being moved from one unit to another. Degradation costs associated with rapid change in power for hydrogen electrolyzers and fuel cells should therefore be studied more in depth.

The costs and prices in traditional power systems dominated by large thermal power plants are principally set by the global gas, coal, and oil price as well as the CO_2 price. However, the marginal operating cost of VRESs is close to zero while the value of energy delivered by ESSs depends on the ability to reduce the use of expensive units by shifting generation and consumption temporally. The future power system costs and prices will therefore depend less on fuel costs and more on technology costs. The technology costs influence the prices both directly through the degradation costs, and indirectly through the mixture of generation technologies, DSR, and ESS driven by the market investments.

5.3 Stochastic operation of energy-constrained systems

The stochastic operation of a MG with high level of VRESs and ESSs has been studied in Paper I, and with particular emphasis on energy-constrained systems in Papers IV and V. Paper IV performs a comparison of state-of-the-art methods for MG operation based on rule-based approaches and deterministic rolling hori-

zon optimization, both with respect to short- and long-term perspectives for Rye MG. The MG has generation from wind and solar power, as well as a diesel generator as backup, and balances the generation and demand with a battery and a hydrogen system with fuel cell and electrolyzer. The paper shows how the short- and long-term perspectives can be optimized individually and connected through the SEV expressed as linear hyperplanes using SDDP. The short-term model considers the period where the generation can be predicted through meteorological forecasts, and the long-term model considers typical seasonal conditions for the present month. Six different combinations of short- and long-term methods as well as perfect foresight, as shown in Table 5.1, have been simulated using rolling horizon for almost a full year with rolling horizon for the following three different variations of the MG:

a) Large diesel generator (75 kW).
b) Small diesel generator (15 kW).
c) Weak grid connection (15 kW).

The results presented in Figure 5.5 show that the SDDP short-term model in methods 2-4 reduces the operating costs compared to rule-based and deterministic operation strategies, and that the difference is more pronounced for energy-constrained systems. Cases b) and c) also show that the stochastic short-term model contributes to a significant reduction in load shedding compared to the other methods.

Moreover, the SDDP long-term model in methods 5-7 causes an even more significant cost reduction, in particular with respect to load shedding in cases b) and c). Energy-constrained systems are vulnerable to persistent low generation from VRESs. Due to the limited dispatchable generation capacity, it is decisive to have sufficient stored energy upfront for situations with high demand and low generation from VRESs to prevent scarcity.

A key assumption for the model is that the load can be freely curtailed at a high

Table 5.1: Methods used for the operation of the microgrid presented in Paper IV.

Method	Short-term model	Long-term model
1	Prefect foresight	
2	None	Rule-based
3	Deterministic	Rule-based
4	SDDP	Rule-based
5	None	SDDP
6	Deterministic	SDDP
7	SDDP	SDDP

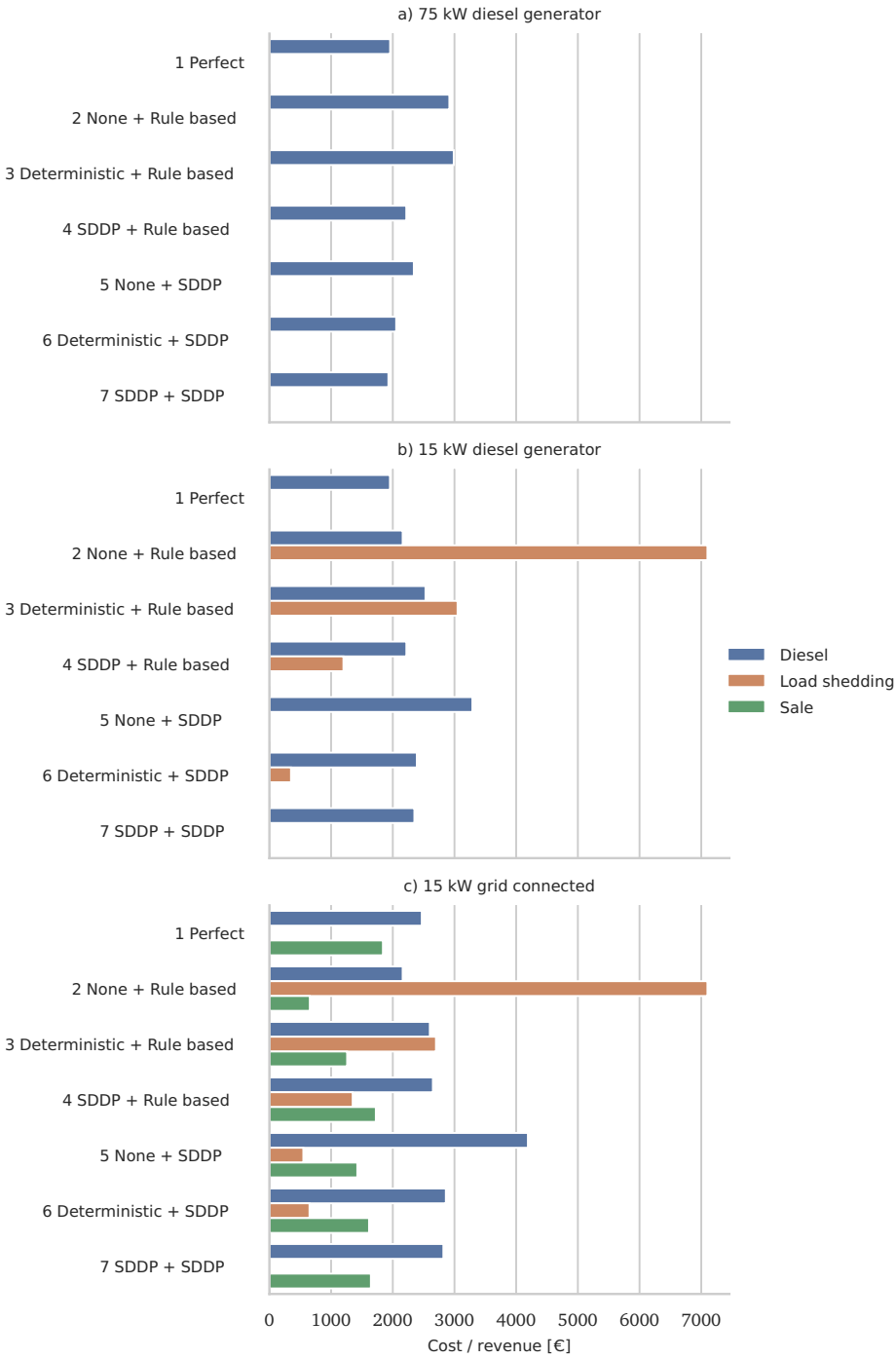

Figure 5.5: Comparison of operating costs for Rye microgrid using rule-based operation, deterministic optimization, and SDDP both with respect to short- and long-term operation. The results includes the following variations of the case: large diesel generator (75 kW), small diesel generator (15 kW), and weak grid connection (15 kW).

cost defined by the value of lost load (VOLL). In other words, the stochastic optimization method performs well in minimizing the thermal generation costs while considering the risk of extreme prices. The VOLL is a way of quantifying the power system reliability, and the system reliability is dependent on the quantity of the VOLL. This approach is similar to how the water-value in the Norwegian hydropower system also encapsulates the system's reliability through the risk of scarcity that influences the system price.

Stochastic optimization methods are computationally intensive. The number of scenarios and stages must be chosen carefully such that the sample space is explored sufficiently, to capture both the risk of scarcity as well as the probability of generation curtailment accurately, while keeping the computational burden low.

To prevent the ESSs from being emptied at the end of the optimization horizon, the implemented methods in Papers III to V consider an infinite horizon, either through the iterative SDP approach suggested in Paper III or through cyclic Markov chains as shown in Papers IV and V. Whereas a fixed final SOC is commonly used in many studies, this thesis uses value-based criteria for the final SOC. Fixed final SOC promotes the worst sides of optimization by forcing imbalances, both surplus and deficit, to be resolved within the optimization period. Value-based termination criteria, through the SEV, is more flexible by permitting utilization of the ESS flexibility beyond the optimization horizon.

5.4 Pricing and valuation of stored energy

The electricity price formation in systems with a high level of VRESs and ESSs has been studied in Paper III using an SDP model. Figure 5.7a shows the expected future SMV for a full week as a function of SOC for the system illustrated in Figure 5.6 when fully supplied by VRESs where the SMV is influenced by the VOLL. The optimal operation has been simulated for 100 random scenarios, and Figure 5.7b shows the quantiles for how the resulting SOC develops, and Figures 5.7c

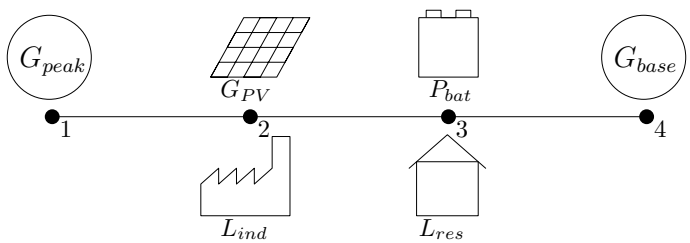

Figure 5.6: Topology of small grid with variable solar power and battery (figure adopted from Paper III [29]).

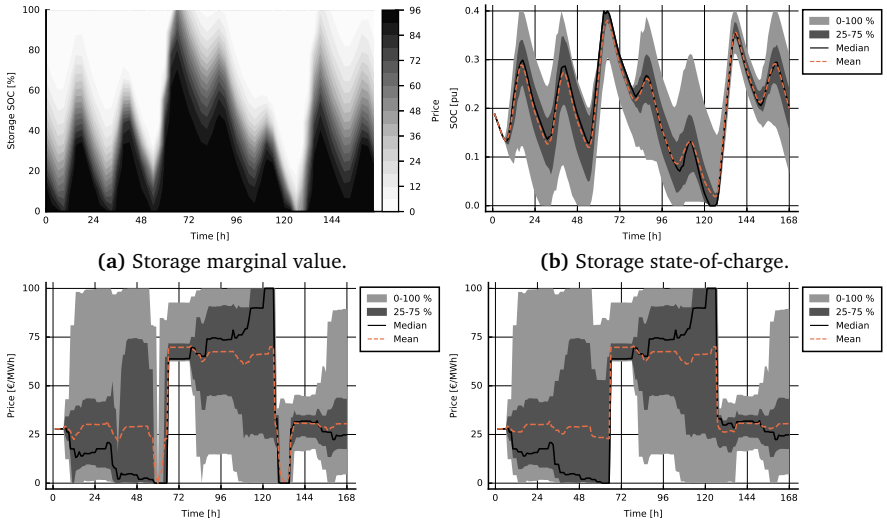

(a) Storage marginal value.

(b) Storage state-of-charge.

(c) LMP at industrial bus.

(d) LMP at residential bus.

Figure 5.7: Multiple simulations of case with only solar PV generation and EES (figure adopted from Paper II [28]).

and 5.7d display how the corresponding LMP develops at the respective buses.

The electricity price in competitive markets is set by the marginal value of the marginal unit as explained in Section 4.1.4. An ESS will in many situations be the marginal unit, either as a consumer or a producer, and set the price. The marginal value of ESSs, referred to as the SMV, can be considered as the opportunity cost of the stored energy given perfect future operation. The SMV is influenced by the value of all the other units in the system. In situations where load shedding is a possible outcome, load shedding can become the marginal unit and the ESS operation can be considered as an arbitrage against scarcity. In these situations, the VOLL gradually becomes effective when the probability of load shedding increases as a precautionary signal against scarcity before it eventually occurs.

Whereas high prices in power-constrained systems are driven by high power, high prices in energy-constrained systems are driven by lasting low generation from VRESs and high demand. The prices in energy-constrained systems can therefore vary between zero and the VOLL. Lasting periods with low wind power can therefore cause lasting periods with a high price, and lasting periods with high wind power can also cause lasting periods with a low price. These variations will incite more flexibility, both supply and demand, that responds to the extreme prices as well as ESSs that gain their profit from arbitrage. Even ESSs with poor efficiency become profitable if the price variations are high enough, while the required energy capacity is connected with the frequency of the price variations. Low frequency in the price variations imposes larger energy capacity.

The SMV is an important quantity for valuating the ESS operation as opposed to other units in the system. Paper IV shows how the SMV can be interpreted as a set of adaptive decision rules that changes over time. Figure 5 in Paper IV also shows how these decision rules are state dependent.

The SMV is an important quantity for bidding ESSs into competitive energy markets, and has been extensively studied regarding hydropower [88]. Moreover, the optimal bidding value of ancillary services like frequency reserves is also related to the SMV as shown in Gebrekiros *et al.* [89].

The valuation of stored energy can also be combined with more detailed models, such as the detailed model proposed in Paper II. The SEV function from the stochastic models can be used as a boundary value condition for more detailed models. By doing so, the potential future value of saving stored energy for later can be encapsulated in a detailed model with short foresight.

Chapter 6

Conclusion and recommendations for future work

This thesis has made new contributions with respect to modeling MGs with high levels of VRESs and ESSs. The contributions include both detailed ESS modeling as well as modeling of grids with multiple ESS technologies under uncertainty with long foresight.

The operation of lithium-ion batteries can be more accurately optimized by using the current, voltage, and charge variable space compared to the power and energy variable space. The current, voltage, and charge variable space has previously mainly been considered for simulation but to a lesser extent for optimization. The non-linear optimization model presented in Paper II uses cubic spline functions to express the battery voltage and the converter efficiency based on empirical data, and has the following advantages compared to traditional models in the power and energy variable space:

- The operational limits are represented in both current and voltage, which are closer to the actual physical limits compared to simpler models. The SOC is expressed as charge (in ampere hours) instead of energy (in Watt hours). This enables operation to be close to the physical limits of the battery and more accurate estimation of SOC.
- The model considers efficiency due to both voltage variations and converter characteristics instead of assuming a fixed efficiency. Therefore, the losses are approximated more accurately and can increase the overall performance.
- The use of spline functions based on empirical data is generic and can also be adapted for other ESS technologies such as flow batteries, hydrogen (with

electrolyzer and fuel cell), and hydropower.

The use of the SEV function to valuate stored energy is a useful way to connect models with different time perspectives. The stage-wise SEV functions can be extracted from the results of the optimization models presented in Papers I and III to V and inserted in the objective of the detailed battery model presented in Paper II. This method enables the combination of detailed component modeling with long-term strategic considerations.

The operating costs of systems with high levels of VRESs and ESSs have a high degree of generation with a marginal cost close to zero. They are therefore less dependent on fuel costs, and the operating costs are to a greater extent set by the technology costs through degradation properties and the risk of extreme prices due to expensive generators and scarcity. The implemented models considers degradation due to cycling and SOC dependent calendar aging, and based on the results from Papers I and III, the following conclusions are drawn:

- ESS degradation costs influence the optimal operation strategy, especially under uncertainty. Correcting a sub-optimal SOC caused by uncertainty has a significant cost.
- Proper valuation of degradation during operation can prolong the expected lifetime of ESSs.
- Battery degradation costs also influence the operation of other flexible resources and the degradation costs should be represented consistently for all flexible units in the system.

Stochastic optimization is important for both the short- and long-term operation of systems with high levels of VRESs and ESSs, especially for energy-constrained systems where the dispatchable generation capacity is a limiting factor. The MG in Paper IV considers the operation of both battery and hydrogen ESSs under uncertainty from demand as well as solar and wind power generation. Whereas the battery has high power capacity and high efficiency but low energy capacity, the hydrogen storage has low power capacity and low efficiency but high energy capacity. The main conclusions from this paper are:

- The coordination of short- and long-duration ESSs in energy-constrained power systems must balance operating cost minimization against the risk of scarcity quantified through the VOLL. The ESS operation, in particular the long-duration hydrogen storage, must consider sufficient foresight to manage potential periods with lasting low generation from VRESs.
- Stochastic optimization, in this thesis SDDP, reduces the operating costs compared to rule-based operation and deterministic optimization. The differences are most significant for energy-constrained systems, where SDDP shows a superior ability to minimize operating costs without compromising

the security of supply.

As emphasized in the research literature, long-duration storage is a potential solution for VRES intermittency [56]. Balancing the advantages of highly efficient short-duration ESS against less efficient long-duration ESS require stochastic models with sufficient foresight. The security of supply is not only connected to sizing the system's units properly but also operating ESSs such that they have sufficient high SOC upfront periods with potential low generation from VRESs. The operation of ESSs is a combination of generation cost minimization and minimizing the risk of extreme costs associated with scarcity.

A high level of ESSs also influences the formation of electricity prices. Whereas the marginal production cost of thermal and renewable generators is relatively well defined, the marginal production cost and consumption value for ESSs is both time and state dependent, as such:

- ESSs act as both supply and demand in competitive markets. Both the ESS discharge cost and the charge value are related to the SMV (as decirbed in Section 4.1.4), and set the market price when they are the marginal producing unit.
- The marginal value of stored energy (SMV) is the marginal future value of the stored energy assuming it is operated optimally. The SMV is influenced by the marginal cost/value of all other units in the system, including scarcity through the VOLL, and considers future generation and demand under uncertainty. The SMV value is both time and state dependent.

The ESS marginal cost/value can be extracted from the solution of the methods implemented in Papers I and III to V through the SEV function. Whereas high prices are driven by high power in power-constrained systems, the high prices in energy-constrained systems are driven by the risk of expensive generation or scarcity caused by energy deficit. The price signals provide incentives for all units in the system to operate in a cost optimal way that minimizes the risk of scarcity.

Safe and efficient coordination of VRESs and ESSs, both at the spatial and temporal level, is a key factor to reach net zero emissions. Both VRESs and ESSs have complementary properties that should be carefully utilized. The winters are typically windy, while the summers are sunny, while batteries have high efficiency and power capacity, and hydrogen has high energy capacity. An optimal utilization of the complementary properties of the diverse generation and storage technologies requires coordination at the right spatial and temporal level. Decomposition is a an efficient instrument for breaking down complexity, and an alternative to solving detailed large-scale models is to formulate a sequence of models with decreasing temporal and spatial level and increasing level of detail. Valuation of energy, both through SMVs and electricity prices, mandates safe and efficient coordina-

tion of both conventional dispatchable resources as well as the emerging VRESs and ESSs.

6.1 Future work

The operation of the future power systems, both MGs and large-scale systems, includes a wide range of flexible units: dispatchable and variable generators, short- and long-duration ESSs, as well as small- and large-scale DSRs. The flexibility can be both centralized and distributed. This thesis has only considered batteries and hydrogen ESSs in combination with solar and wind power, with a particular emphasis on the detailed battery modeling. Several research areas need further investigation both with respect to modeling different types of flexible units as well as further development of the stochastic system models.

6.1.1 Modeling of flexible resources

Different storage technologies have distinct characteristics that must be treated carefully. Hydrogen electrolyzers should avoid frequent start and stop, and they must be operated above a predefined minimum limit. This challenge is similar to the thermal unit commitment problem. Both electrolyzers and fuel cells have variable efficiency depending on how they are operated, and they also have their own degradation characteristics that should be considered. The wide range of energy storage technologies all have distinct properties that must be considered with respect to how they influence the power system operation.

The internet-of-things makes unused DSR accessible. For example, charging of EVs and heating appliances have a great potential for managing daily variations. However, the operation of DSR must be done carefully to prevent inconveniences for the consumer who offers the flexibility. Further research is needed to better understand and model the potential in DSR such that it can be fully utilized.

Grid limitations should also be more carefully analysed at a detailed level, both with respect to voltage and thermal limits, due the increasing share of distributed flexibility. The power flow equations are non-linear and non-convex, but a wide range of alternative formulations, both convex and linear, have been presented in the research literature. Several of these aim for good performance for medium- and low voltage grids, such as the linear DistFlow [24, 25] described in Section 3.4, and are promising candidates to combine with stochastic optimization methods.

6.1.2 Stochastic modeling of energy systems

This thesis has proposed representing auto-correlation in demand and wind power through AR-models in Paper I and in wind power with Markov chains in Paper IV. Both solar and wind power as well as demand are weather dependent. Wind and solar power are often complementary. The wind speed is low on sunny days and vice versa. The weather also influences the cooling and heating of buildings through temperature, wind, and solar radiation. The weather is also a naturally slow process and has a strong auto-correlation. Representing both the correlations between the different generation sources and the demand as well as the auto-correlation can reduce the operating costs and the risk of scarcity for these systems, and should be addressed in future research.

Subsystems are often modeled individually to reduce the system complexity, and the prices for exchanging power with adjacent systems are typically given exogenously. Surplus generation can be exported and power deficit can be imported. However, if all systems are weather dependent, they may experience surplus or deficit simultaneously. An energy deficit in a subsystem is therefore often correlated with a high price in the adjacent subsystems, hence correlation in power exchange price and generation from VRESs can be an important factor to consider.

6.1.3 Cost recovery of energy storage systems in markets

Cost recovery conditions for power-constrained systems have been extensively studied based on load duration curves, see, e.g., Stoft [12]. Moreover, Korpås and Botterud [13] derived cost recovery conditions for VRESs and ESSs based on load duration curves. However, these approaches assume power-constrained systems where the ESS energy capacity is unlimited. The methods presented in this thesis can analyze the expected annual income associated with optimal operation of VRESs and ESSs. Moreover, by introducing the sizes of the VRESs and ESSs as decision variables, the optimal sizes can be optimized in a way that accounts for the energy-constrained nature of these systems.

Bibliography

[1] United Nations Framework Convention on Climate Change, *Paris Agreement*, Paris, 2015. [Online]. Available: https://unfccc.int/sites/default/files/english_paris_agreement.pdf.

[2] European Commission, *Communication from the commission to the European Parliament, the European Council, the council, the European economic and social committee and the committee of the regions - The European Green Deal*, 2019. [Online]. Available: https://eur-lex.europa.eu/legal-content/EN/TXT/?qid=1576150542719&uri=COM%3A2019%3A640%3AFIN.

[3] International Energy Agency, *Net Zero by 2050 A Roadmap for the Global Energy Sector*, Paris, 2021. [Online]. Available: https://www.iea.org/reports/net-zero-by-2050.

[4] International Renewable Energy Agency, *WORLD ENERGY TRANSITIONS OUTLOOK 1.5° C PATHWAY*. 2021, ISBN: 978-92-9260-334-2.

[5] International Energy Agency, "Status of Power System Transformation 2019," International Energy Agency, Paris, Tech. Rep. [Online]. Available: https://www.iea.org/reports/status-of-power-system-transformation-2019.

[6] International Energy Agency, *The Power of Transformation - Wind, Sun and the Economics of Flexible Power Systems*. OECD, Feb. 2014. DOI: 10.1787/9789264208032-EN.

[7] IEA, "Energy Storage," International Energy Agency, Paris, Tech. Rep., 2020. [Online]. Available: https://www.iea.org/reports/energy-storage.

[8] W. Cole and A. Frazier, "Cost Projections for Utility-Scale Battery Storage: 2020 Update," National Renewable Energy Laboratory (NREL), Golden, CO (United States), Tech. Rep., Jun. 2020. DOI: 10.2172/1665769. [Online]. Available: https://www.osti.gov/servlets/purl/1665769/.

[9] K. M. Tan, V. K. Ramachandaramurthy, and J. Y. Yong, "Integration of electric vehicles in smart grid: A review on vehicle to grid technologies and optimization techniques," *Renewable and Sustainable Energy Reviews*, vol. 53, pp. 720–732, Jan. 2016, ISSN: 1364-0321. DOI: 10.1016/J.RSER.2015.09.012.

[10] B. Xu, J. Zhao, T. Zheng, E. Litvinov, and D. S. Kirschen, "Factoring the Cycle Aging Cost of Batteries Participating in Electricity Markets," *IEEE Transactions on Power Systems*, vol. 33, no. 2, pp. 2248–2259, Mar. 2018, ISSN: 08858950. DOI: 10.1109/TPWRS.2017.2733339.

[11] M. Milligan, B. A. Frew, A. Bloom, E. Ela, A. Botterud, A. Townsend, and T. Levin, "Wholesale electricity market design with increasing levels of renewable generation: Revenue sufficiency and long-term reliability," *The Electricity Journal*, vol. 29, no. 2, pp. 26–38, Mar. 2016, ISSN: 1040-6190. DOI: 10.1016/J.TEJ.2016.02.005.

[12] S. Stoft, *Power System Economics: Designing Markets for Electricity*. IEEE Press, 2002, p. 496, ISBN: 9780470545584. DOI: 10.1109/MPAE.2003.1180363.

[13] M. Korpås and A. Botterud, "Optimality Conditions and Cost Recovery in Electricity Markets with Variable Renewable Energy and Energy Storage," 2020, [Online]. Available: http://ceepr.mit.edu/files/papers/2020-005.pdf.

[14] O. B. Fosso, A. Gjelsvik, A. Haugstad, B. Mo, and I. Wangensteen, "Generation scheduling in a deregulated system. the norwegian case," *IEEE Transactions on Power Systems*, vol. 14, no. 1, pp. 75–80, 1999, ISSN: 08858950. DOI: 10.1109/59.744487.

[15] M. V. Pereira and L. M. Pinto, "Stochastic Optimization of a Multireservoir Hydroelectric System: A Decomposition Approach," *Water Resources Research*, vol. 21, no. 6, pp. 779–792, Jun. 1985, ISSN: 19447973. DOI: 10.1029/WR021i006p00779.

[16] S. Rehman, L. M. Al-Hadhrami, and M. M. Alam, "Pumped hydro energy storage system: A technological review," *Renewable and Sustainable Energy Reviews*, vol. 44, pp. 586–598, Apr. 2015, ISSN: 1364-0321. DOI: 10.1016/J.RSER.2014.12.040.

[17] C. Sasse, "Electricity networks of the future," *2006 IEEE Power Engineering Society General Meeting, PES*, 2006. DOI: 10.1109/PES.2006.1709058.

[18] P. D. Lund, J. Lindgren, J. Mikkola, and J. Salpakari, "Review of energy system flexibility measures to enable high levels of variable renewable electricity," *Renewable and Sustainable Energy Reviews*, vol. 45, pp. 785–807, May 2015, ISSN: 1364-0321. DOI: 10.1016/J.RSER.2015.01.057.

[19] I. B. Sperstad, M. Z. Degefa, and G. Kjølle, "The impact of flexible resources in distribution systems on the security of electricity supply: A literature review," *Electric Power Systems Research*, vol. 188, p. 106 532, Nov. 2020, ISSN: 0378-7796. DOI: 10.1016/J.EPSR.2020.106532.

[20] M. Yan, M. Shahidehpour, A. Paaso, L. Zhang, A. Alabdulwahab, and A. Abusorrah, "Distribution Network-Constrained Optimization of Peer-to-Peer Transactive Energy Trading among Multi-Microgrids," *IEEE Transactions on Smart Grid*, vol. 12, no. 2, pp. 1033–1047, Mar. 2021, ISSN: 19493061. DOI: 10.1109/TSG.2020.3032889.

[21] H. Karimi and S. Jadid, "Optimal energy management for multi-microgrid considering demand response programs: A stochastic multi-objective framework," *Energy*, vol. 195, p. 116 992, Mar. 2020, ISSN: 03605442. DOI: 10.1016/j.energy.2020.116992.

[22] A. Hasankhani and S. M. Hakimi, "Stochastic energy management of smart microgrid with intermittent renewable energy resources in electricity market," *Energy*, vol. 219, p. 119 668, Mar. 2021, ISSN: 03605442. DOI: 10.1016/j.energy.2020.119668.

[23] C. Coffrin, R. Bent, K. Sundar, Y. Ng, and M. Lubin, "PowerModels.jl: An Open-source framework for exploring power flow formulations," in *20th Power Systems Computation Conference, PSCC 2018*, Institute of Electrical and Electronics Engineers Inc., Aug. 2018, pp. 1–8, ISBN: 9781910963104. DOI: 10.23919/PSCC.2018.8442948.

[24] M. E. Baran and F. F. Wu, "Optimal capacitor placement on radial distribution systems," *IEEE Transactions on Power Delivery*, vol. 4, no. 1, pp. 725–734, 1989, ISSN: 19374208. DOI: 10.1109/61.19265.

[25] M. E. Baran and F. F. Wu, "Optimal sizing of capacitors placed on a radial distribution system," *IEEE Transactions on Power Delivery*, vol. 4, no. 1, pp. 735–743, 1989, ISSN: 19374208. DOI: 10.1109/61.19266.

[26] P. Aaslid, *Market clearing with VRES and ESS*, 2021. DOI: 10.5281/zenodo.5704377. [Online]. Available: https://peraaslid.github.io.

[27] P. Aaslid, M. M. Belsnes, and O. B. Fosso, "Optimal microgrid operation considering battery degradation using stochastic dual dynamic programming," in *SEST 2019 - 2nd International Conference on Smart Energy Systems and Technologies*, Institute of Electrical and Electronics Engineers (IEEE), Sep. 2019, pp. 1–6, ISBN: 9781728111568. DOI: 10.1109/SEST.2019.8849150.

[28] P. Aaslid, F. Geth, M. Korpås, M. M. Belsnes, and O. B. Fosso, "Non-linear charge-based battery storage optimization model with bi-variate cubic spline constraints," *Journal of Energy Storage*, vol. 32, p. 101 979, Dec. 2020, ISSN: 2352152X. DOI: 10.1016/j.est.2020.101979.

[29] P. Aaslid, M. Korpås, M. M. Belsnes, and O. B. Fosso, "Pricing electricity in constrained networks dominated by stochastic renewable generation and electric energy storage," *Electric Power Systems Research*, vol. 197, p. 107 169, Aug. 2021, ISSN: 03787796. DOI: 10.1016/j.epsr.2021.107169.

[30] P. Aaslid, M. Korpas, M. M. Belsnes, and O. Fosso, "Stochastic Optimization of Microgrid Operation With Renewable Generation and Energy Storages," *IEEE Transactions on Sustainable Energy*, pp. 1–1, 2022, ISSN: 1949-3029. DOI: 10.1109/TSTE.2022.3156069. [Online]. Available: https://ieeexplore.ieee.org/document/9727092/.

[31] P. Aaslid, M. Korpås, M. M. Belsnes, and O. B. Fosso, *Stochastic Operation of Energy Constrained Microgrids Considering Battery Degradation*, 2021. [Online]. Available: https://arxiv.org/abs/2111.03313.

[32] E. Vaahedi, "Practical Power System Operation," *Practical Power System Operation*, vol. 9781118394, pp. 1–226, Apr. 2014. DOI: 10.1002/9781118915110.

[33] *Nord Pool*, 2021. [Online]. Available: https://www.nordpoolgroup.com/.

[34] *Statnett*, 2021. [Online]. Available: https://www.statnett.no/.

[35] International Renewable Energy Agency, "Innovation landscape brief: Flexibility in conventional power plants," Tech. Rep., 2019. [Online]. Available: www.irena.org.

[36] O. Wolfgang, A. Haugstad, B. Mo, A. Gjelsvik, I. Wangensteen, and G. Doorman, "Hydro reservoir handling in Norway before and after deregulation," *Energy*, vol. 34, no. 10, pp. 1642–1651, Oct. 2009, ISSN: 03605442. DOI: 10.1016/j.energy.2009.07.025.

[37] S. Stage and Y. Larsson, "Incremental Cost of Water Power," *Transactions of the American Institute of Electrical Engineers. Part III: Power Apparatus and Systems*, vol. 80, no. 3, pp. 361–364, 1961, ISSN: 00972460. DOI: 10.1109/AIEEPAS.1961.4501045.

[38] M. V. F. Pereira and L. M. V. G. Pinto, "Multi-stage stochastic optimization applied to energy planning," *Mathematical Programming*, vol. 52, no. 1-3, pp. 359–375, May 1991, ISSN: 00255610. DOI: 10.1007/BF01582895.

[39] A. Soroudi and T. Amraee, "Decision making under uncertainty in energy systems: State of the art," *Renewable and Sustainable Energy Reviews*, vol. 28, pp. 376–384, Dec. 2013, ISSN: 1364-0321. DOI: 10.1016/J.RSER.2013.08.039.

[40] A. Helseth, A. Cordeiro, and G. De Melo, *Scheduling Toolchains in Hydro-Dominated Systems Evolution, Current Status and Future Challenges for Norway and Brazil*. 2020, ISBN: 9788214065787.

[41] "DOE Microgrid Workshop Report," US Department of Energy, Tech. Rep., 2011, p. 32. [Online]. Available: https://www.energy.gov/sites/prod/files/Microgrid%20Workshop%20Report%20August%202011.pdf.

[42] A. Hirsch, Y. Parag, and J. Guerrero, "Microgrids: A review of technologies, key drivers, and outstanding issues," *Renewable and Sustainable Energy Reviews*, vol. 90, pp. 402–411, Jul. 2018, ISSN: 1364-0321. DOI: 10.1016/J.RSER.2018.03.040.

[43] A. Hussain, V. H. Bui, and H. M. Kim, "Microgrids as a resilience resource and strategies used by microgrids for enhancing resilience," *Applied Energy*, vol. 240, pp. 56–72, Apr. 2019, ISSN: 0306-2619. DOI: 10.1016/J.APENERGY.2019.02.055.

[44] P. Asmus and M. Lawrence, "Emerging Microgrid Business Models," Tech. Rep., 2016. [Online]. Available: http://www.g20ys.org/upload/auto/abf2f0a71ea657d34c551214a4ff7045515582eb.pdf.

[45] E. Mengelkamp, J. Gärttner, K. Rock, S. Kessler, L. Orsini, and C. Weinhardt, "Designing microgrid energy markets: A case study: The Brooklyn Microgrid," *Applied Energy*, vol. 210, pp. 870–880, Jan. 2018, ISSN: 03062619. DOI: 10.1016/j.apenergy.2017.06.054.

[46] M. Zhang and J. Chen, "The Energy Management and Optimized Operation of Electric Vehicles Based on Microgrid," *IEEE Transactions on Power Delivery*, vol. 29, no. 3, pp. 1427–1435, 2014. DOI: 10.1109/TPWRD.2014.2303492.

[47] J. T. Reilly, "From microgrids to aggregators of distributed energy resources. The microgrid controller and distributed energy management systems," *The Electricity Journal*, vol. 32, no. 5, pp. 30–34, Jun. 2019, ISSN: 1040-6190. DOI: 10.1016/J.TEJ.2019.05.007.

[48] P. Marocco, D. Ferrero, M. Gandiglio, and M. Santarelli, *Remote area Energy supply with Multiple Options for integrated hydrogen-based TEchnologies - Deliverable number 2.2*, 2018. [Online]. Available: https://www.remote-euproject.eu/remote18/rem18-cont/uploads/2019/03/REMOTE-D2.2.pdf.

[49] O. M. Babatunde, J. L. Munda, and Y. Hamam, "Power system flexibility: A review," *Energy Reports*, vol. 6, pp. 101–106, Feb. 2020, ISSN: 2352-4847. DOI: 10.1016/J.EGYR.2019.11.048.

[50] J. P. Deane, B. P. Ó Gallachóir, and E. J. McKeogh, "Techno-economic review of existing and new pumped hydro energy storage plant," *Renewable and Sustainable Energy Reviews*, vol. 14, no. 4, pp. 1293–1302, May 2010, ISSN: 1364-0321. DOI: 10.1016/J.RSER.2009.11.015.

[51] *Hornsdale Power Reserve | South Australia's Big Battery*. [Online]. Available: https://hornsdalepowerreserve.com.au/.

[52] *Moss Landing Battery Storage Project, California, US*. [Online]. Available: https://www.nsenergybusiness.com/projects/moss-landing/.

[53] M. Stecca, L. Ramirez Elizondo, T. Batista Soeiro, P. Bauer, and P. Palensky, "A Comprehensive Review of the Integration of Battery Energy Storage Systems into Distribution Networks," *IEEE Open Journal of the Industrial Electronics Society*, pp. 1–1, Mar. 2020. DOI: 10.1109/OJIES.2020.2981832.

[54] S. Agnew and P. Dargusch, "Effect of residential solar and storage on centralized electricity supply systems," *Nature Climate Change 2015 5:4*, vol. 5, no. 4, pp. 315–318, Mar. 2015, ISSN: 1758-6798. DOI: 10.1038/nclimate2523.

[55] P. Albertus, J. S. Manser, and S. Litzelman, "Long-Duration Electricity Storage Applications, Economics, and Technologies," *Joule*, vol. 4, no. 1, pp. 21–32, Jan. 2020, ISSN: 2542-4351. DOI: 10.1016/J.JOULE.2019.11.009.

[56] N. A. Sepulveda, J. D. Jenkins, A. Edington, D. S. Mallapragada, and R. K. Lester, "The design space for long-duration energy storage in decarbonized power systems," *Nature Energy 2021 6:5*, vol. 6, no. 5, pp. 506–516, Mar. 2021, ISSN: 2058-7546. DOI: 10.1038/s41560-021-00796-8.

[57] M. A. Pellow, C. J. Emmott, C. J. Barnhart, and S. M. Benson, "Hydrogen or batteries for grid storage? A net energy analysis," *Energy and Environmental Science*, vol. 8, no. 7, pp. 1938–1952, Jul. 2015, ISSN: 17545706. DOI: 10.1039/c4ee04041d.

[58] L. Gracia, P. Casero, C. Bourasseau, and A. Chabert, "Use of Hydrogen in Off-Grid Locations, a Techno-Economic Assessment," *Energies 2018, Vol. 11, Page 3141*, vol. 11, no. 11, p. 3141, Nov. 2018, ISSN: 19961073. DOI: 10.3390/EN11113141.

[59] O. Tremblay, L.-A. Dessaint, and A.-I. Dekkiche, "A Generic Battery Model for the Dynamic Simulation of Hybrid Electric Vehicles," in *2007 IEEE Vehicle Power and Propulsion Conference*, IEEE, 2007, pp. 284–289, ISBN: 978-0-7803-9760-6. DOI: 10.1109/VPPC.2007.4544139.

[60] S. M. Mousavi G. and M. Nikdel, "Various battery models for various simulation studies and applications," *Renewable and Sustainable Energy Reviews*, vol. 32, pp. 477–485, Apr. 2014, ISSN: 13640321. DOI: 10.1016/j.rser.2014.01.048.

[61] F. Geth, C. Coffrin, and D. M. Fobes, "A Flexible Storage Model for Power Network Optimization," *e-Energy 2020 - Proceedings of the 11th ACM International Conference on Future Energy Systems*, pp. 503–508, Apr. 2020. [Online]. Available: http://arxiv.org/abs/2004.14768.

[62] K. Garifi, K. Baker, D. Christensen, and B. Touri, "Convex Relaxation of Grid-Connected Energy Storage System Models With Complementarity Constraints in DC OPF," *IEEE Transactions on Smart Grid*, vol. 11, no. 5, pp. 4070–4079, 2020. DOI: 10.1109/TSG.2020.2987785.

[63] O. Tremblay and L.-A. Dessaint, "Experimental Validation of a Battery Dynamic Model for EV Applications," *World Electric Vehicle Journal*, vol. 3, no. 2, pp. 289–298, Jun. 2009, ISSN: 2032-6653. DOI: 10.3390/wevj3020289.

[64] *Remote EU project*, 2021. [Online]. Available: https://www.remote-euproject.eu/remote-project/.

[65] M. Perez, R. Perez, K. R. Rábago, and M. Putnam, "Overbuilding & curtailment: The cost-effective enablers of firm PV generation," *Solar Energy*, vol. 180, pp. 412–422, Mar. 2019, ISSN: 0038-092X. DOI: 10.1016/J.SOLENER.2018.12.074.

[66] J. Kleissl, "Solar Energy Forecasting and Resource Assessment," *Solar Energy Forecasting and Resource Assessment*, pp. 1–416, 2013. DOI: 10.1016/C2011-0-07022-9.

[67] *NASA earth observatory: Cloud Fraction*. [Online]. Available: https://earthobservatory.nasa.gov/global-maps/MODAL2_M_CLD_FR.

[68] *Meteorologisk Institutt*, 2021. [Online]. Available: https://met.no.

[69] V. Petrović and C. L. Bottasso, "Wind turbine optimal control during storms," *Journal of Physics: Conference Series*, vol. 524, no. 1, p. 012 052, Jun. 2014, ISSN: 1742-6596. DOI: 10.1088/1742-6596/524/1/012052.

[70] *Vestas V27*. [Online]. Available: https://en.wind-turbine-models.com/turbines/9-vestas-v27.

[71] C. Finck, R. Li, R. Kramer, and W. Zeiler, "Quantifying demand flexibility of power-to-heat and thermal energy storage in the control of building heating systems," *Applied Energy*, vol. 209, pp. 409–425, Jan. 2018, ISSN: 0306-2619. DOI: 10.1016/J.APENERGY.2017.11.036.

[72] L. Gan, U. Topcu, and S. H. Low, "Optimal decentralized protocol for electric vehicle charging," *IEEE Transactions on Power Systems*, vol. 28, no. 2, pp. 940–951, 2013. DOI: 10.1109/TPWRS.2012.2210288.

[73] M. Z. Degefa, H. Sale, I. Petersen, and P. Ahcin, "Data-driven Household Load Flexibility Modelling: Shiftable Atomic Load," in *2018 IEEE PES Innovative Smart Grid Technologies Conference Europe (ISGT-Europe)*, IEEE, Oct. 2018, pp. 1–6, ISBN: 978-1-5386-4505-5. DOI: 10.1109/ISGTEurope.2018.8571836.

[74] J. T. Hughes, A. D. Domínguez-García, and K. Poolla, "Identification of Virtual Battery Models for Flexible Loads," *IEEE Transactions on Power Systems*, vol. 31, no. 6, pp. 4660–4669, Nov. 2016. DOI: 10.1109/TPWRS.2015.2505645.

[75] S. Zaferanlouei, H. Farahmand, V. V. Vadlamudi, and M. Korpas, "BATTPOWER Toolbox: Memory-Efficient and High-Performance Multi-Period AC Optimal Power Flow Solver," *IEEE Transactions on Power Systems*, vol. 36, no. 5, pp. 3921–3937, Sep. 2021, ISSN: 15580679. DOI: 10.1109/TPWRS.2021.3055429.

[76] D. K. Molzahn and I. A. Hiskens, *A survey of relaxations and approximations of the power flow equations*. Now Publishers, 2019.

[77] B. Stott, J. Jardim, and O. Alsaç, "DC power flow revisited," *IEEE Transactions on Power Systems*, vol. 24, no. 3, pp. 1290–1300, 2009, ISSN: 08858950. DOI: 10.1109/TPWRS.2009.2021235.

[78] J. M. Maciejowski, *Predictive Control with Constraints*. Pearson education, 2002, ISBN: 0-201-39823-0.

[79] O. Dowson, "The policy graph decomposition of multistage stochastic optimization problems," *Networks*, vol. 76, no. 1, pp. 3–23, 2020. DOI: 10.1002/net.21932.

[80] J. R. Birge and F. Louveaux, *Introduction to Stochastic Programming*, 2nd, ser. Springer Series in Operations Research and Financial Engineering. New York, NY: Springer New York, 2011, p. 512, ISBN: 978-1-4614-0236-7. DOI: 10.1007/978-1-4614-0237-4.

[81] R. Bellman, *Dynamic Programming*, 1st ed. Princeton University Press, 1957. [Online]. Available: http://books.google.com/books?id=fyVtp3EMxasC&pg=PR5&dq=dynamic+programming+richard+e+bellman&client=firefox-a#v=onepage&q=dynamic%20programming%20richard%20e%20bellman&f=false.

[82] S. A. Johnson, J. R. Stedinger, C. A. Shoemaker, Y. Li, and J. A. Tejada-Guibert, "Numerical solution of continuous-state dynamic programs using linear and spline interpolation," *Operations Research*, vol. 41, no. 3, pp. 484–500, Jun. 1993, ISSN: 0030364X. DOI: 10.1287/opre.41.3.484.

[83] K. S. Gjerden, A. Helseth, B. Mo, and G. Warland, "Hydrothermal scheduling in Norway using stochastic dual dynamic programming; a large-scale case study," in *2015 IEEE Eindhoven PowerTech*, IEEE, Jun. 2015, pp. 1–6, ISBN: 978-1-4799-7693-5. DOI: 10.1109/PTC.2015.7232278.

[84] A. Shapiro, W. Tekaya, J. P. da Costa, and M. P. Soares, "Risk neutral and risk averse Stochastic Dual Dynamic Programming method," *European Journal of Operational Research*, vol. 224, no. 2, pp. 375–391, Jan. 2013, ISSN: 0377-2217. DOI: 10.1016/J.EJOR.2012.08.022.

[85] A. Papavasiliou, Y. Mou, L. Cambier, and D. Scieur, "Application of Stochastic Dual Dynamic Programming to the Real-Time Dispatch of Storage under Renewable Supply Uncertainty," *IEEE Transactions on Sustainable Energy*, vol. 9, no. 2, pp. 547–558, Apr. 2018, ISSN: 19493029. DOI: 10.1109/TSTE.2017.2748463.

[86] A. Gjelsvik, M. M. Belsnes, and A. Haugstad, "An algorithm for stochastic medium-term hydrothermal scheduling under spot price uncertainty," in *Proc. 13th Power System Computation Conference*, Trondheim, Norway, 1999, pp. 1079–1085.

[87] A. Helseth, B. Mo, A. Lote Henden, and G. Warland, "Detailed long-term hydro-thermal scheduling for expansion planning in the Nordic power system," *IET Generation, Transmission and Distribution*, vol. 12, no. 2, pp. 441–447, 2017, ISSN: 1751-8687. DOI: 10.1049/iet-gtd.2017.0903.

[88] E. Krohn Aasgård, ·. Christian, Ø. Naversen, ·. M. Fodstad, ·. Hans, and I. Skjelbred, "Optimizing day-ahead bid curves in hydropower production," *Energy Systems*, vol. 9, pp. 257–275, 2018. DOI: 10.1007/s12667-017-0234-z.

[89] Y. Gebrekiros, G. Doorman, S. Jaehnert, and H. Farahmand, "Reserve procurement and transmission capacity reservation in the Northern European power market," *International Journal of Electrical Power and Energy Systems*, vol. 67, pp. 546–559, 2015, ISSN: 01420615. DOI: 10.1016/j.ijepes.2014.12.042.

Paper I

The paper *"Optimal microgrid operation considering battery degradation using stochastic dual dynamic programming"* is published by *IEEE* in the conference proceedings of the *2019 International Conference on Smart Energy Systems and Technologies (SEST)*. The accepted version of the paper is reprinted here with the permission from the authors and publisher,

Cite as:

> P. Aaslid, M. M. Belsnes, and O. B. Fosso, "Optimal microgrid operation considering battery degradation using stochastic dual dynamic programming," in *SEST 2019 - 2nd International Conference on Smart Energy Systems and Technologies*, Institute of Electrical and Electronics Engineers (IEEE), Sep. 2019, pp. 1–6, ISBN: 9781728111568. DOI: 10.1109/SEST.2019.8849150

Optimal microgrid operation considering battery degradation using stochastic dual dynamic programming

Per Aaslid*†, Michael M Belsnes* and Olav B Fosso†
Email: per.aaslid@sintef.no, michael.m.belsnes@sintef.no, olav.fosso@ntnu.no
*Department of Energy Systems, SINTEF Energy Research, Trondheim, Norway
†Department of Electrical Power Engineering, Norwegian University of Science and Technology, Trondheim, Norway

***Abstract*—Intermittent energy sources demand temporal storages to balance generation and load, and batteries stand out as an alternative. However, the lifetime is limited, and cycling depth affects the battery degradation rate. Current stochastic multi-stage methods lack proper representation of battery degradation. This paper proposes a stochastic multi-stage model for optimizing battery operation in a microgrid considering battery degradation with a piece-wise linear cost function with uncertain wind power production and load. The model is solved using Stochastic Dual Dynamic Programming (SDDP) and is demonstrated on a 4-bus test case with limited import and export capacity to illustrate the battery degradation cost's impacts on the battery cycling strategy. The results show that the importance of a stochastic method is more pronounced when battery degradation is modelled.**

***Index Terms*—stochastic dual dynamic programming, battery degradation, microgrid, arbitrage**

I. Introduction

A. Motivation and background

The increasing share of energy conversion from intermittent sources such as photovoltaics (PV) and wind energy conversion systems (WECS) increase the demand for balancing services in the power system. Coordination of energy storages in distribution grids and microgrids are important for reliability of supply as well as optimal economic dispatch [1].

Energy conversion from PV and WECS are uncertain by nature, and smaller energy systems yields larger variation both in generation and load. Optimal operation of storage in a deterministic model will typically provide an overly aggressive utilization of the storage capacity by frequently cycling between maximum and minimum. Unfortunately, this strategy does not account for forecast error, which may cause load shedding or production curtailment. Therefore, the forecast error may increase the operation cost, but also accelerate aging of battery storage [2]. Stochastic methods are effective for balancing cost minimization and risk, and applicable both for planning, operation and control of microgrids [3].

B. Relevant literature

A commonly used stochastic formulation is the two-stage stochastic problem. Reference [4] suggests a two-stage stochastic formulation for minimizing the operational costs including the grid power losses of a microgrid. Similar two-stage formulations are shown in [5]–[7].

A limitation of the two-stage stochastic formulation is the assumption that all uncertainty is revealed at once. For a multi-stage formulation, the uncertainty is revealed stage-wise and the control of the system is updated stage-wise as the uncertainty is revealed. This formulation is widely used in hydropower scheduling [8], and stochastic dual dynamic programming is an efficient technique for solving large scale multi-stage stochastic problems [9].

There are a few proposed methods for managing storages in microgrids based on SDDP in the literature. Reference [10] suggests a microgrid model minimizing procurement cost under uncertain wind generation where load is balanced in terms of purchase and sale to the utility grid, by using load shifting and micro generators. Reference [11] has a similar formulation also including power loss minimization and uncertain price. In [12], the cost is minimized for a private household with battery storage and uncertain PV generation. Reference [13] balances uncertain wind generation with conventional generation and battery storage including a cost associated with varying the battery level.

C. Contributions and organization

Batteries degrade from several factor, among others state-of-charge (SoC), depth-of-discharge (DoD) and operating temperature. A shortcoming among the aforementioned papers are lack of more sophisticated modelling of degradation due to DoD. Batteries will typically have an increasing degradation rate with increasing cycling depth, and [14] shows how to represent this with a piece-wise linear model.

The contributions of this paper can be summarized as follows: i) The microgrid storage coordination problem has been formulated as a multi-stage stochastic problem. Battery degradation has been modelled as a piece-wise linear cost function to assess cycling costs. ii) The proposed method has been applied on a 4-bus test case to demonstrate the impact of battery degradation both for stochastic and deterministic model formulations. The problem has been solved using the SDDP algorithm.

The remainder of this paper is organized as follows. Section II formulates the multi-stage stochastic formulation of the microgrid storage dispatch problem, section III presents a test case including numerical values, and discusses the impact

This is the accepted version of an article published in 2019 International Conference on Smart Energy Systems and Technologies - SEST
DOI: 10.1109/SEST.2019.8849150

TABLE I
NOMENCLATURE

Sets	
T	Time steps
N	Buses
S	Battery segments
Parameters	
η_k^c	Charge efficiency for battery at bus k
η_k^d	Discharge efficiency for battery at bus k
R	Storage replacement cost €$/MWh$
$c_{k,t}^m$	Power price at bus k, time t
$c_{k,s}^b$	Marginal storage aging cost of cycle depth at bus k, segment s
$\bar{e}_{k,s}$	Maximum energy stored in bus k, segment s
WP_k	Wind scale factor at bus k
LP_k	Load scale factor at bus k
$\hat{p}_{k,t}^w$	Normalized wind power forecast at bus k, time t
$\hat{p}_{k,t}^l$	Normalized load forecast at bus k, time t
ϕ^w	Auto-correlation wind forecast error
ϕ^l	Auto-correlation load forecast error
E_k^{max}	Maximum energy storage in battery at bus k
E_k^{min}	Minimum energy storage in battery at bus k
B_k^c	Maximum charge power to battery at bus k
B_k^d	Maximum discharge power from battery at bus k
P_k^s	Maximum sale power to market at bus k
P_k^b	Maximum purchase power from market at bus k
P_k^w	Maximum wind power generation at bus k
Variables	
Δt	Time step length
$e_{k,t,s}$	Energy stored at bus k, time t, segment s
$b_{k,t,s}^c$	Storage charge power bus k, time t, segment s
$b_{k,t,s}^d$	Storage discharge power bus k, time t, segment s
$p_{k,t}^b$	Power purchase in wholesale market at bus k, time t
$p_{k,t}^s$	Power sale in wholesale market at bus k, time t
$p_{k,t}^w$	Wind power generation at bus k, time t
$p_{k,t}^l$	Load at bus k, time t
$\hat{p}_t^w$	Normalized wind power generation at time t
$\hat{p}_t^l$	Normalized load at time t
$\Delta\hat{p}_{k,t}^w$	Normalized wind forecast error at bus k, time t
$\Delta\hat{p}_{k,t}^l$	Normalized load forecast error at bus k, time t
ε_t^w	Normalized wind forecast error noise at time t
ε_t^l	Normalized load forecast error noise at time t
Φ	Battery cycle stress cost
δ	Battery cycle depth

of modelling the battery degradation costs. The algorithm convergence properties are also presented. Conclusions are drawn in section IV.

II. MODEL DESCRIPTION

This section presents a mathematical formulation of the optimal purchase, sale, storage and generation dispatch in a microgrid with uncertain wind power generation and load. The objective is to minimize utility grid power exchange costs, diesel generation costs, and battery cycling degradation costs. Diesel generation is considered as a purchase opportunity with fixed price. Symbols used in the mathematical formulations are shown in the nomenclature in table I.

A. Problem definition

Each stage in the multi-stage problem is given by a linear problem formulation and linear objective terms. Each time step t represents a stage in this formulation, but the formulation may be generalized such that each stage can have multiple time steps. A state variable represents the required information to model the system from present time and onward. A stage problem may contain both current and previous state variables. A control variable is an internal stage variable and represents an action or decision, either implicit or explicit. A noise is a stage-wise independent random variable [15], [16].

In this paper, the state variables are given by the battery level, wind generation forecast error and load forecast error. The battery level must be a state variable since the current level depends on the previous, while the wind generation and load forecast errors are state variables since they are modelled with auto-regressive models. The system noise is the noise terms in the AR-models describing generation and load error. The remaining variables are control variables.

The objective is to minimize purchase costs from the utility grid and minimize battery degradation costs as shown in (1) under exogenous power price.

$$\min \sum_{t\in T}\sum_{k\in N}\left(c_{k,t}^m(p_{k,t}^b - p_{k,t}^s) + \sum_{s\in S} c_{k,s}^b b_{k,t,s}^d\right)\Delta t \quad (1)$$

B. Battery degradation

Some of the factors causing battery degradation are depth-of-discharge (DoD), state-of-charge (SoC) and operating temperature. This paper only considers degradation due to DoD. The cycle depth stress function describes how much the battery degrades as a percentage of its expected lifetime, and is approximated using a quadratic stress function based on the results from [17]. The cycle depth stress function in (2), where δ is the cycle depth percentage, has been used in this paper. It permits 10 000 cycles at 50% DoD before battery must be replaced.

$$\Phi(\delta) = 4 \cdot 10^{-4}\ \delta^2 \quad (2)$$

The battery cycling cost is implemented as a piece-wise linear model as described in [14]. The battery is divided into segments, where the discharge cost is increasing for increasing segment number. This method demands segmentation of the energy storage state variable, and the charge and discharge variables since SDDP is not capable of handling non-linear states. This is a potential drawback with this method as increased accuracy for the cycling cost function demands additional state variables, which again increase the computation time.

To avoid simultaneous charging and discharging of battery one must ensure that loosing power never is profitable. In this case generation curtailment is free, and the power exchange price is always non-negative. Simultaneous charging and discharging may also be avoided by using binary variables, but that is not supported by standard SDDP. The objective function (1) has an individual cost associated with discharging each segment. The low-cost segments will always be charged and discharged first, while deeper cycles also demand use of the

This is the accepted version of an article published in 2019 International Conference on Smart Energy Systems and Technologies - SEST
DOI: 10.1109/SEST.2019.8849150

high-cost segments. The marginal cost of the segment is given by (3) where $\bar{s}$ is the number of segments.

$$c^b_{k,s} = \frac{R}{\eta^d_k}\ \bar{s}\left[\Phi\left(\frac{s}{\bar{s}}\right) - \Phi\left(\frac{s-1}{\bar{s}}\right)\right], s \in 1,\ldots,\bar{s} \quad (3)$$

C. Battery and energy balance

The battery energy balance is given by the charge/discharge and efficiency as shown in (4). Moreover, the charge/discharge is given by the sum of the segment variables as shown in (5). The battery segments are enforced by (7), and the segments have equal size for each storage in our model. The charge/discharge is enforced by (6) limiting maximum battery charge and discharge. The total energy stored at a bus is limited by the battery maximum and minimum limits as shown in (8), and the purchase and sale with the utility grid is limited as shown in (9). The power must balance at every bus in the network, thus the net injection must be zero (10).

$$e_{k,t,s} - e_{k,t-1,s} = \left(b^c_{k,t,s}\eta^c_k - b^d_{k,t,s}\frac{1}{\eta^d_k}\right)\Delta t \quad (4)$$

$$b^c_{k,t} = \sum_{s\in S} b^c_{k,t,s}, \quad b^d_{k,t} = \sum_{s\in S} b^d_{k,t,s} \quad (5)$$

$$0 \le b^c_{k,t} \le B^c_k, \quad 0 \le b^d_{k,t} \le B^d_k \quad (6)$$

$$e_{k,t,s} \le \bar{e}_{k,s} \quad (7)$$

$$E^{min}_k \le \sum_{s\in S} e_{k,t,s} \le E^{max}_k \quad (8)$$

$$0 \le p^s_{k,t} \le P^s_k, \quad 0 \le p^b_{k,t} \le P^b_k \quad (9)$$

$$\sum_{k\in N}\left(b^c_{k,t} - b^d_{k,t} + p^s_{k,t} - p^b_{k,t} + p^l_{k,t} - p^w_{k,t}\right) = 0 \quad (10)$$

D. Load and generation uncertainty

The SDDP algorithm is only capable of solving stochastic problems with stage-wise independent uncertainty. However, the uncertainty is introduced as a state variable and modelled as a first order auto regressive model, and the uncertainty is decomposed into a dependent and an independent term [18] as shown in (11).

$$\Delta\hat{p}^w_t = \phi^w\ \Delta\hat{p}^w_{t-1} + \varepsilon^w_t \quad (11)$$

Generation and load are correlated series. However, the uncertainty in this model is not the generation and load but the generation and load forecast error. Since most of the correlation between generation and load is captured by the forecast, the weak correlation between the forecast errors is neglected.

The expression for wind power generation at a specific node is given by (12) and (13) where WP_k is the maximum generation at node k, $\hat{p}^k_t$ the normalized wind generation forecast and $\Delta\hat{p}^w_t$ the normalized forecast error. The normalized forecast is computed by dividing the forecast on the historical maximum from the three previous years. To avoid negative production, a slack variable is introduced to capture negative values.

$$p^w_{k,t} - p^{w,slack}_{k,t} = WP_k(\hat{p}^w_t + \Delta\hat{p}^w_t) \quad (12)$$

$$p^w_{k,t},\ p^{w,slack}_{k,t} \ge 0 \quad (13)$$

The wind forecast error is modelled as an auto-regressive model of first order (11), which holds under the assumption that the process is weak stationary. This is a common assumption for wind forecasting, for details see [19].

The slack variable may also be used to generate power, hence the cost for using it must be greater than the highest generation cost in the system.

Similar representation is used for load forecast error but with no cost on the slack variable, which implies that load may be added at no cost.

E. Storage end value

If the end value is not included in the objective, the algorithm tends to always empty the storage in the end since there are no incentives for saving the energy for later. In this model, the value of the stored energy in the last stage is set equal to the value of selling all stored energy in the market after the last stage.

F. Stochastic dual dynamic programming (SDDP)

The model has been solved with SDDP, which is a decomposition technique for solving linear multistage stochastic programs. The SDDP algorithm approximates the expected cost-to-go function with piece-wise linear bounds obtained from the dual solutions of the optimization problem at each stage. The SDDP algorithm has two main phases: forward simulation where scenarios are sampled based on the probability distribution of the random variables, and backward recursion where each stage is optimized backwards along the trajectory from the forward simulation. This procedure is repeated until a convergence criteria is reached [9].

The model has been implemented in Julia with SDDP.jl [20] using CPLEX 12.8.0.

III. Case study

This section presents the results from a case study of a 4-bus test system with storage, generation and load, where both generation and load are subject to uncertainty. The maximum purchase and sale for the system is limited. Figure 1 shows the topology of the test system where the utility grid connection is limited such that the battery and the emergency generator must balance the load and wind power generation.

A. Case numerical data

This case study uses historical time series from ENTSO-E Transparency Platform [21]. The price series is day-ahead for Denmark (DK-2) between 2018-12-15 and 2018-12-18. The corresponding series are used for load and onshore wind generation. The load and wind series has been normalized as described in section II. The AR(1) model parameters are calculated based on normalized historical generation and forecast values from the given time with regression analysis. The historical forecasts are day-ahead forecasts. The shift between old and new forecast at midnight has therefore been removed when doing the regression analysis. The calculated auto-correlation for the normalized series was 0.90 and 0.65

This is the accepted version of an article published in 2019 International Conference on Smart Energy Systems and Technologies - SEST
DOI: 10.1109/SEST.2019.8849150

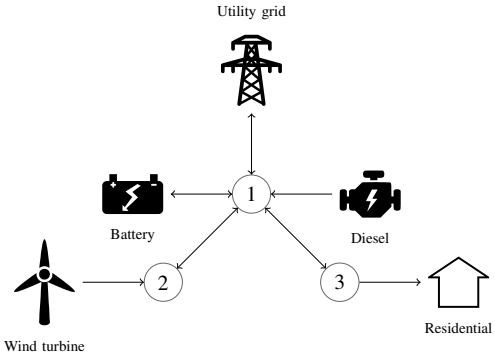

Fig. 1. Test system

TABLE II
CASE PARAMETERS

Utility grid	
Maximum purchase	1 MW
Maximum sale	1 MW
Max purchase/sale violation penalty	600 €/MWh
Storage	
Size	3 MWh
Maximum charge/discharge	1 MW
Efficiency charge/discharge	95%
Replacement cost	100,000 €/MWh
Diesel	
Maximum generation	1 MW
Cost	500 €/MWh
Wind generation	
Maximum generation	2 MW
Forecast error auto-correlation	0.90
Forecast error standard deviation	0.05
Slack variable cost	600 €/MWh
Load	
Maximum load	2 MW
Forecast error auto-correlation	0.65
Forecast error standard deviation	0.05

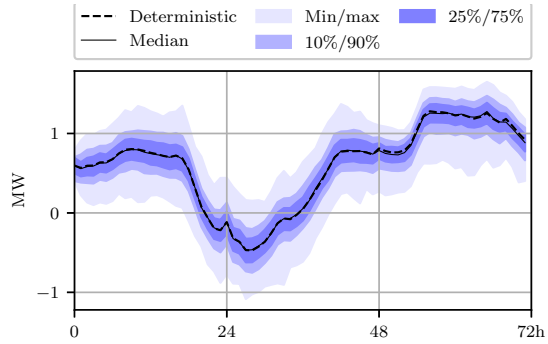

(a) Net load: Difference between load and generation

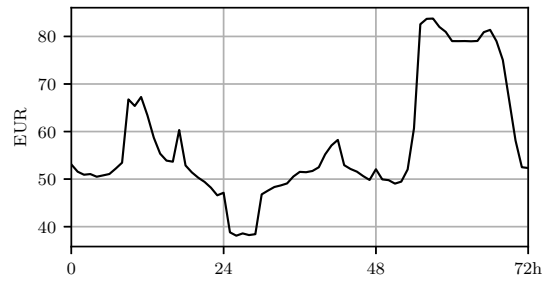

(b) Price.

Fig. 2. Sampled load, wind power generation and price.

TABLE III
BATTERY CYCLING MARGINAL COST

Segment	Marginal cost
0-20%	24
20-40%	72
40-60%	120
60-80%	168
80-100%	216

for wind and load respectively, and the standard deviation was 0.02 and 0.0065. Note that these are the statistical properties of the forecast errors. In this case, the standard deviation is increased to 0.05 for both generation and load to demonstrate the capabilities of the method, and to reflect that a smaller population yields greater standard deviation. Each noise variable is sampled into three evenly spaced quantiles such that the number of discrete outcomes for each stage is nine. Other parameters are presented in table II, while net load and price profiles are shown in figure 2. The storage cycling cost function is divided into five segments of equal size, and the segment marginal costs for this particular case is shown in table III.

B. Results and discussion

The presented stochastic solution shows the percentiles of 500 simulations of 72 stages where each hour represents a stage. The results show that the primary objective is to avoid expensive generation from diesel by ensuring high battery level when reaching the period with high net load as seen from around hour 54 where the net load in figure 2a exceeds the maximum purchase limit, and the battery level is 100% in both figure 3a and 3b. Figure 3c and 3d shows that there is no sale for at least 90% of the scenarios despite the very high price, since all the stored energy is used to avoid generation from diesel. Nevertheless, diesel generation is unavoidable in 25-50% of the scenarios as shown in figure 3e and 3f.

The secondary objective, given that the diesel cost always is higher than the price difference, is using battery for arbitrage. The battery level without degradation cost in figure 3a shows arbitrage between hour 0 and 54. This is also shown in figure 3c where there are frequent changes between purchase and sale. However, when including battery degradation costs as shown in figure 3b, there is no sign of arbitrage, and the purchase/sale profile in figure 3d is much more stable. The lowest prices are found between hour 24 and 30 causing two spikes in the deterministic solution in figure 3d to fully charge

This is the accepted version of an article published in 2019 International Conference on Smart Energy Systems and Technologies - SEST
DOI: 10.1109/SEST.2019.8849150

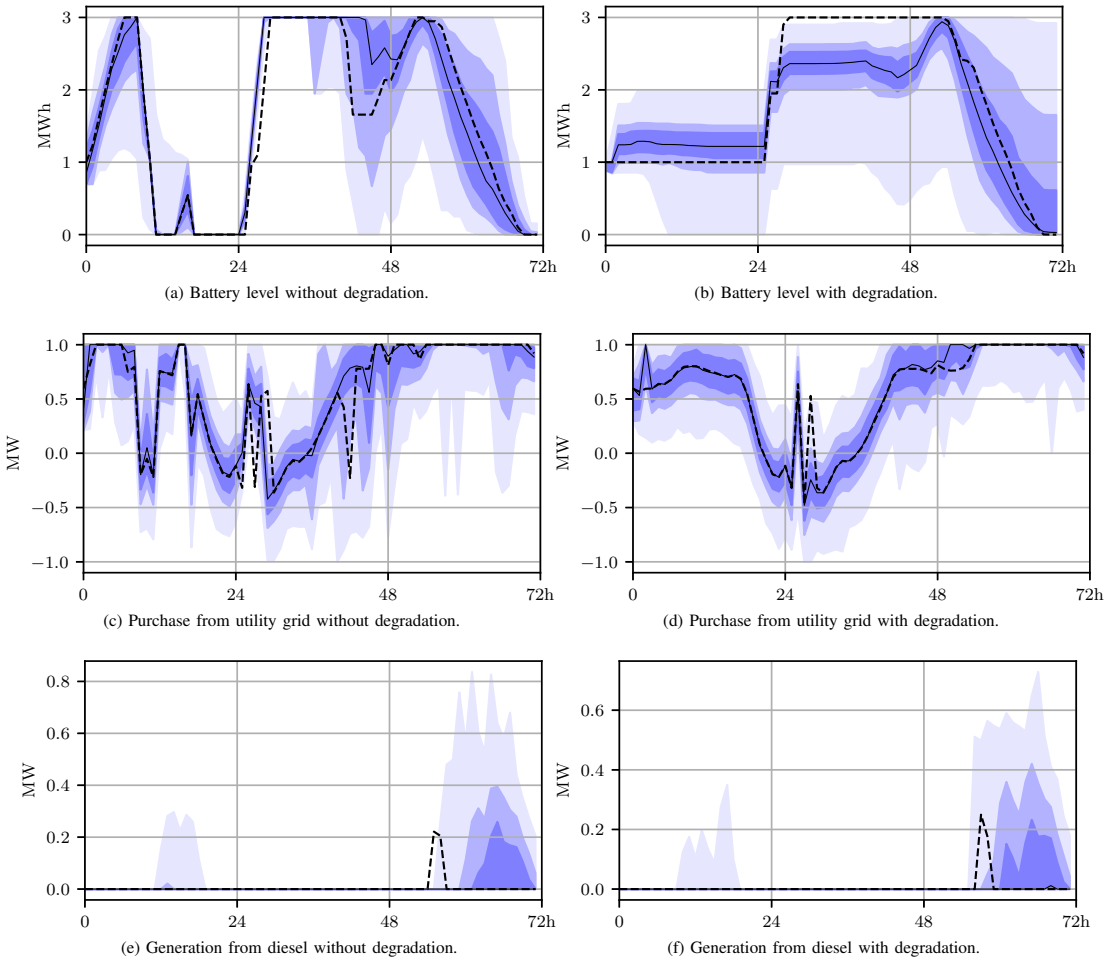

(a) Battery level without degradation.

(b) Battery level with degradation.

(c) Purchase from utility grid without degradation.

(d) Purchase from utility grid with degradation.

(e) Generation from diesel without degradation.

(f) Generation from diesel with degradation.

Fig. 3. Comparison of optimization without and with battery degradation costs.

the battery in advance to the high load from hour 54.

The difference between the deterministic and stochastic solution is more pronounced when battery degradation costs are included. With no degradation cost, figure 3a shows that the deterministic and the stochastic median solutions have almost overlapping solutions much of the time. In contrast, the solution including battery degradation costs has a more risk averse strategy for the stochastic solution. Instead of charging the battery immediately as the deterministic solution, the storage level is kept below maximum to avoid production curtailment in case the net load should exceed the export limit.

Calculating the value of the stochastic solution is a computationally hard task. Nevertheless, an interesting property with the solution of a SDDP problem is the interpretation of the cuts added by SDDP. For a minimization problem, the cuts are lower bounds for the future cost functions of the problem state variables. These cuts may also be used as boundary conditions for an optimization model with shorter time horizon and possibly different solving methodology.

Note that these analysis has been carried out on a limited case for the purpose of demonstrating the concept. To verify the scalability of the method, it should be tested on a larger case.

C. Algorithm convergence

To check if the algorithm has converged, the lower bound is compared with and upper bound confidence interval as described by [9]. The 95% confidence interval for the upper bound is computed regularly with 200 Monte Carlo simulations, and figure 4 shows how the confidence interval and

This is the accepted version of an article published in 2019 International Conference on Smart Energy Systems and Technologies - SEST
DOI: 10.1109/SEST.2019.8849150

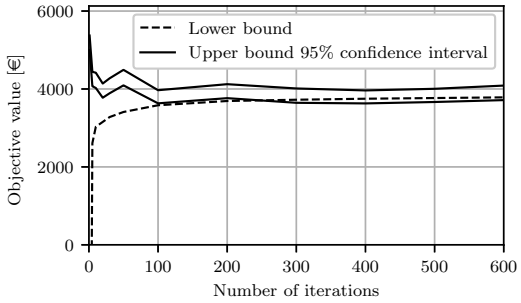

Fig. 4. Algorithm convergence

lower bound develops for the case with degradation costs. The results show that a high number of iterations are required to satisfy the convergence criteria. Testing also shows that if the diesel generation and penalty costs had been closer to the day-ahead price, the algorithm would have converged faster.

IV. Conclusions

The importance of stochastic methods in the microgrid storage coordination problem is more pronounced when including degradation costs incurred by battery cycling. A naive model permits correction of a sub-optimal battery level by charging and discharging at no other cost than the energy price. For a model including battery degradation costs, the stochastic strategy will attempt to avoid correction of a sub-optimal battery level caused by uncertainty by operating farther away from the battery limits than a deterministic solution.

The battery price and cycling cost used in this case also shows that high price differences are necessary to profit on arbitrage with batteries. Since the net demand is correlated with price, the battery is already occupied with load shifting in the hours with the highest arbitrage potential.

Battery degradation has significant impact on the optimal strategy, hence it will be instructive to extend the degradation model to also include SoC in future work. Moreover, it will also be instructive to embed different types of end-user flexibility to compare how they can provide an alternative or supplement to battery storage. Finally, recent developments in SDDP has provided new methods for handling correlated uncertainty in price [22] and integer problems [23] enabling more precise formulations of multi-stage stochastic programs.

References

[1] L. Meng, E. R. Sanseverino, A. Luna, T. Dragicevic, J. C. Vasquez, and J. M. Guerrero, "Microgrid supervisory controllers and energy management systems: A literature review," *Renewable and Sustainable Energy Reviews*, vol. 60, pp. 1263–1273, 7 2016.

[2] Y. Chen, C. Deng, W. Yao, N. Liang, P. Xia, P. Cao, Y. Dong, Y.-a. Zhang, Z. Liu, D. Li, M. Chen, and P. Peng, "Impacts of stochastic forecast errors of renewable energy generation and load demands on microgrid operation," *Renewable Energy*, vol. 133, pp. 442–461, 4 2019.

[3] H. Liang and W. Zhuang, "Stochastic modeling and optimization in a microgrid: A survey," *Energies*, 2014.

[4] W. Su, J. Wang, and J. Roh, "Stochastic energy scheduling in microgrids with intermittent renewable energy resources," *IEEE Transactions on Smart Grid*, vol. 5, pp. 1876–1883, 7 2014.

[5] G. Martinez, N. Gatsis, and G. B. Giannakis, "Stochastic programming for energy planning in microgrids with renewables," in *2013 5th IEEE International Workshop on Computational Advances in Multi-Sensor Adaptive Processing, CAMSAP 2013*, pp. 472–475, 2013.

[6] A. Gholami, T. Shekari, F. Aminifar, and M. Shahidehpour, "Microgrid Scheduling With Uncertainty: The Quest for Resilience," *IEEE Transactions on Smart Grid*, vol. 7, pp. 2849–2858, 11 2016.

[7] G. Cardoso, M. Stadler, A. Siddiqui, C. Marnay, N. DeForest, A. Barbosa-Póvoa, and P. Ferrão, "Microgrid reliability modeling and battery scheduling using stochastic linear programming," *Electric Power Systems Research*, vol. 103, pp. 61–69, 10 2013.

[8] M. V. Pereira and L. M. Pinto, "Stochastic Optimization of a Multireservoir Hydroelectric System: A Decomposition Approach," *Water Resources Research*, vol. 21, pp. 779–792, 6 1985.

[9] M. V. F. Pereira and L. M. V. G. Pinto, "Multi-stage stochastic optimization applied to energy planning," *Mathematical Programming*, vol. 52, pp. 359–375, 5 1991.

[10] P. Fatouros, I. Konstantelos, D. Papadaskalopoulos, and G. Strbac, "A stochastic dual dynamic programming approach for optimal operation of der aggregators," in *2017 IEEE Manchester PowerTech, Powertech 2017*, pp. 1–6, IEEE, 6 2017.

[11] A. Bhattacharya, J. P. Kharoufeh, and B. Zeng, "Managing energy storage in microgrids: A multistage stochastic programming approach," *IEEE Transactions on Smart Grid*, vol. 9, pp. 483–496, 1 2018.

[12] F. Hafiz, A. R. De Queiroz, and I. Husain, "Multi-stage stochastic optimization for a PV-storage hybrid unit in a household," in *2017 IEEE Industry Applications Society Annual Meeting, IAS 2017*, vol. 2017-Janua, pp. 1–7, IEEE, 10 2017.

[13] L. Zéphyr and C. L. Anderson, "Stochastic dynamic programming approach to managing power system uncertainty with distributed storage," *Computational Management Science*, vol. 15, pp. 87–110, 1 2018.

[14] B. Xu, J. Zhao, T. Zheng, E. Litvinov, and D. S. Kirschen, "Factoring the Cycle Aging Cost of Batteries Participating in Electricity Markets," *IEEE Transactions on Power Systems*, vol. 33, pp. 2248–2259, 3 2018.

[15] O. Dowson, "The policy graph decomposition of multistage stochastic optimization problems," *Optimization Online*, 2018.

[16] W. B. Powell, "A Unified Framework for Optimization Under Uncertainty," in *Optimization Challenges in Complex, Networked and Risky Systems*, pp. 45–83, INFORMS, 10 2016.

[17] I. Laresgoiti, S. Käbitz, M. Ecker, and D. U. Sauer, "Modeling mechanical degradation in lithium ion batteries during cycling: Solid electrolyte interphase fracture," *Journal of Power Sources*, vol. 300, pp. 112–122, 12 2015.

[18] A. Shapiro, "Analysis of stochastic dual dynamic programming method," *European Journal of Operational Research*, 2011.

[19] D. Barbosa de Alencar, C. de Mattos Affonso, R. Limão de Oliveira, J. Moya Rodríguez, J. Leite, J. Reston Filho, D. Barbosa de Alencar, C. De Mattos Affonso, R. C. Limão de Oliveira, J. L. Moya Rodríguez, J. C. Leite, and J. C. Reston Filho, "Different Models for Forecasting Wind Power Generation: Case Study," *Energies*, vol. 10, p. 1976, 11 2017.

[20] O. Dowson and L. Kapelevich, "SDDP.jl: a Julia package for Stochastic Dual Dynamic Programming," *Optimization Online*, 2017.

[21] "ENTSO-E Transparency Platform." https://transparency.entsoe.eu/, 2019.

[22] A. Downward, O. Dowson, and R. Baucke, "Stochastic dual dynamic programming with stagewise dependent objective uncertainty," *Optimization Online*, 2018.

[23] J. Zou, S. Ahmed, and X. A. Sun, "Stochastic dual dynamic integer programming," *Mathematical Programming*, pp. 1–42, 3 2018.

This is the accepted version of an article published in 2019 International Conference on Smart Energy Systems and Technologies - SEST
DOI: 10.1109/SEST.2019.8849150

Paper II

The paper *"Non-linear charge-based battery storage optimization model with bi-variate cubic spline constraints"* is published by *Elsevier* in the *Journal of Energy Storage*. The final published paper is reprinted here without changes in compliance with the CC-BY 4.0 license [1] it is published under.

Cite as:

> P. Aaslid, F. Geth, M. Korpås, M. M. Belsnes, and O. B. Fosso, "Non-linear charge-based battery storage optimization model with bi-variate cubic spline constraints," *Journal of Energy Storage*, vol. 32, p. 101 979, Dec. 2020, ISSN: 2352152X. DOI: 10.1016/j.est.2020.101979

[1] For license details, see: https://creativecommons.org/licenses/by/4.0/

Journal of Energy Storage 32 (2020) 101979

Contents lists available at ScienceDirect

Journal of Energy Storage

journal homepage: www.elsevier.com/locate/est

Non-linear charge-based battery storage optimization model with bi-variate cubic spline constraints

Per Aaslid [*,a,b], Frederik Geth [c], Magnus Korpås [b], Michael M Belsnes [a], Olav B Fosso [b]

[a] SINTEF Energy Research, Trondheim, Norway
[b] Norwegian University of Science and Technology, Department of Electric Power Engineering, Trondheim, Norway
[c] CSIRO Energy Centre, Newcastle NSW, Australia

ARTICLE INFO

Keywords:
Non-linear optimization
Battery operation
Distributed storage
Voltage source converter
Splines

ABSTRACT

Variable renewable generation demands increasing amount of flexible resources to balance the electric power system, and batteries stand out as a promising alternative. Battery models for optimization typically represent the battery with power and energy variables, while the voltage, current, charge variable space is used for simulation models. This paper proposes a non-linear battery storage optimization model in the voltage, current, charge variable space. The battery voltage is conceived as an empirical function of both state-of-charge and charge current and represented through bi-variate cubic splines. The voltage source converter losses are also approximated with a cubic spline function. Compared to energy-based storage models, the results show that this approach enables safe operation closer to the battery voltage and current limits. Furthermore, it prefers operating around high state-of-charge due to the higher efficiency in that region.

1. Introduction

1.1. Motivation and background

The increasing amount of variable renewable energy in the electric power system increases the demand of flexible resources and energy storage. Battery energy storage systems (BESS) are capable of delivering and consuming high power almost instantaneously, and BESS costs are decreasing rapidly. BESS is expected to play an important role in ensuring efficient and reliable operation of the electric power system. They are also easy to install and goes hand in hand with distributed power generation.

BESS installed in low voltage grids also have positive effects in medium and high-voltage grids [1]. Different applications of BESS systems are described in reference [2–4], such as energy trade, ancillary services and grid support, and customer energy management. The optimal strategy for BESS operation depend on the application, but the overall goal is to balance load and generation both in the time domain and geographically. Customer energy management is demonstrated in [5] where load is shifted due to grid tariff design in combination with PV. Energy trade is shown in [6] where the price differences over time is utilized for arbitrage, and a grid support application is shown in [7] where battery is applied for voltage control. Several applications are often combined, such as simultaneous operation in day-ahead market (energy trade) and frequency reserve market (ancillary service) [8,9].

Batteries can be modelled both in the current, voltage, electric charge variable space, and in the power, energy variable space, hereby referred to as IVQ-model and PE-model respectively. The IVQ-model represents the battery state by counting charge in coulomb or ampere-hours, while the battery state for the PE-model is represented as energy in joule or watt-hours. The IVQ-model treats voltage and current as individual variables, while the PE-model is a special case of the IVQ-model with constant battery voltage. Since the battery voltage depends on both state of charge (SOC) and discharge current, the battery efficiency will also depend on those.

Existing battery simulation models span from simple models based on basic electric circuits to generic models with controlled voltage source [10]. One of the most common generic models is the Shepherd model [11], which has been further developed in [12,13]. All these models describe the battery behaviour in a more detailed and accurate way than the PE-models, and they provide insight into the battery voltage characteristics. However, an accurate model demands a complex model structure with many parameters, whereas a simpler model with fewer parameters will be less accurate.

Techno-economic BESS optimization models are dominated by PE-models [2,5,6,8,9]. In [14], an optimization model considering variations in efficiency for changing battery states is presented. Reference

* Corresponding author.
E-mail address: per.aaslid@sintef.no (P. Aaslid).

https://doi.org/10.1016/j.est.2020.101979
Received 4 June 2020; Received in revised form 10 September 2020; Accepted 11 October 2020
Available online 22 October 2020

Nomenclature

Sets and indices

t	Time step index
n / m	Degree of x / y in spline function
i / j	Spline function indices along x / y axis
x_i / y_j	Spline function control point at index i /j
tx_i / ty_j	Spline knot at index i / j

Parameters

ΔT_t	Step length at time t (h)
η^c / η^d	Battery charge/discharge efficiency
$\widehat{p}_t^{\,l}$	Load forecast at time t (kW)
$\widehat{p}_t^{\,PV}$	PV generation forecast at time t (kW)
c_t^p /c_t^s	Power purchase/sale price at time t (€ /kWh)
$E^{\min}$/ $E^{\max}$	Battery min/max storage energy (kWh)
$I^{b,ch}$ / $I^{b,dch}$	Battery max charge/discharge current (A)
$MC^{b,max}$	BESS marginal end-value at empty storage (€ /kWh)
N_{par}^b	Number of battery cells in parallel
N_{ser}^b	Number of battery cells in series
$P^{b,ch}$ / $P^{b,dch}$	Battery max charge/discharge power (kW)
$P^{p,max}$/$P^{s,max}$	Maximum purchase/sale (kW)
$P^{VSC,max}$	VSC maximum AC conversion power (kW)
$P_0^{VSC,loss}$/$P_2^{VSC,loss}$	VSC loss constant/quadratic term
$Q^{\min}$/ $Q^{\max}$	Battery min/max storage charge (Ah)
$V^{b,\ avg}$	Battery average voltage (V)
$V^{b,min}$ / $V^{b,max}$	Battery min/max operating voltage (V)

Variables and functions

$C_e(e)$	BESS energy end value function (€)
$C_q(q)$	BESS charge end value function (€)
e_t	BESS SOC (energy) at time t (kWh)
$f_v^b(q_t, i_t^b)$	Battery voltage function (V)
$f_{loss}^{VSC}(p_t^{VSC,AC})$	VSC loss function (kW)
i_t^b	Battery discharge current at time t (A)
$p_t^{b,ch}$/ $p_t^{b,ch}$	BESS charge/discharge power at time t (kW)
$p_t^{b,DC}$	DC discharge power from battery at time t (kW)
p_t^c/p_t^d	BESS PE-model charge/discharge power at time t (kW)
p_t^{PV}/ $p_t^{PV,curt}$	PV generation and curtailment at time t (kW)
p_t^p/p_t^s	Power purchase/sale at time t (kW)
$p_t^{VSC,AC}$	Power from VSC to AC bus at time t (kW)
$p_t^{VSC,DC}$	Power to VSC from DC bus at time t (kW)
$p_t^{VSC,loss}$	VSC power loss at time t (kW)
q_t	BESS SOC (electric charge) at time t (Ah)
v_t^b	Battery voltage at time t (V)

[15] compares battery operation optimization including degradation with a PE-model, an equivalent circuit model and a single particle model, where the equivalent circuit- and the single particle model are IVQ-models. The single particle model combines detailed modelling, optimal operation and degradation well, but it requires a very detailed parametric description of the BESS.

Optimal BESS operation also relies on a accurate representation of power electronics. Many optimization models consider the battery and the voltage source converter (VSC) as a joint unit with a fixed charge and discharge efficiency. However, the VSC efficiency both depends on current and voltage. Reference [16] suggests the modelling of the VSC losses for optimization as a second order polynomial of current. The small scale VSC in [17] is provided with efficiency curves as a function of AC side power and DC side voltage. Detailed simulation of battery and power electronics is conducted in [18] showing that round-trip efficiency both depends on charge/discharge power and SOC, which is not accounted for in the PE-models.

1.2. Contributions and organization

The contribution of this paper is a non-linear IVQ-model for battery storage optimization. The battery voltage and the VSC power loss is embedded with cubic splines generated from empirical data of the battery voltage and the VSC efficiency. The cubic splines are implemented directly into the non-linear optimization problem. The model accounts for voltage and efficiency variations due to SOC and charge/discharge power, and efficiency variations in VSC. The battery voltage splines also encapsulate the battery series resistance. Moreover, since battery operation limitations are defined by voltage and current individually instead of power, this model enables safer operation close to the battery boundaries. Since the battery voltage is described by empirical data, it could also be updated based on measurement data as the battery degrades. Finally, the modelling method can easily be adapted to other battery types as well as other storage technologies such as hydrogen and hydro-power.

The remainder of this paper is organized as follows: Section 2 presents mathematical model of BESS, VSC, load, market and solar PV, Section 3 presents numerical values used in this model, Section 4 presents results from numerical examples demonstrating the model capabilities, and Section 5 draws the conclusions and suggests further work.

2. Model description

This section presents an IVQ-model for a BESS, VSC, load and grid connection as shown in Fig. 1, where the objective is to minimize operation costs. Symbols used for the mathematical modelling are described in the nomenclature. A corresponding PE-model is also presented as a comparison to investigate the differences between the IVQ- and the PE-model.

2.1. Battery energy storage system

BESS are assembled by multiple chemical cells connected in series or parallel. This section will outline a non-linear IVQ-model, and a simple quadratic PE-model.

2.1.1. Assumptions

This paper studies battery operation for daily market optimization, typically 24–48 hours ahead. Therefore, self discharge and change in voltage characteristics due to degradation are neglected. Faster transients, which are more pronounced at high SOC [13], demanding time resolution down to a few seconds are also neglected. Wiring losses

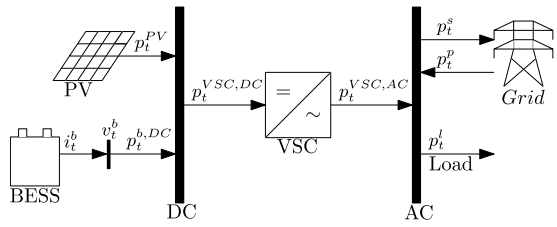

Fig. 1. Test system topology.

internal in battery and between VSC are much lower than other inefficiencies and will not be accounted for.

2.1.2. PE-Model

A basic BESS optimization model is shown in (1), (2), (3), (4), (5), (6). The model assumes that the charge and discharge efficiencies are fixed. Numerical examples will later show the limitations of this assumption. This formulation often includes a charge/discharge complementarity constraint to prevent simultaneous charging and discharging. Since the system in this paper allows curtailing generation at no cost, this constraint has been excluded to avoid mixed integer variables.

$$e_t = \int_0^t \left(\eta_c p_t^c - \frac{1}{\eta_d} p_t^d\right) dt \tag{1}$$

$$P^{b,ch} = I^{b,ch} V^{b,avg} \tag{2}$$

$$P^{b,dch} = I^{b,dch} V^{b,avg} \tag{3}$$

$$E^{min} \le e_t \le E^{max} \tag{4}$$

$$0 \le p_t^c \le P^{b,ch} \tag{5}$$

$$0 \le p_t^d \le P^{b,dch} \tag{6}$$

2.1.3. IVQ-Model

A representation closer to the battery chemistry is considering the SOC in terms of charge q in ampere hours (7), and the voltage as a function of SOC and discharge current (8). Both values are given for an individual battery cell under the assumption that all battery cells will have identical SOC at all times. Equation (9), (10), (11) show the bounds for SOC, current and voltage respectively.

$$q_t = \int_0^t \left(-i_t^b\right) dt \tag{7}$$

$$v_t^b = f_v^b\left(q_t, i_t^b\right) \tag{8}$$

$$Q^{min} \le q_t \le Q^{max} \tag{9}$$

$$-I^{b,ch} \le i_t^b \le I^{b,dch} \tag{10}$$

$$V^{b,min} \le v_t^b \le V^{b,max} \tag{11}$$

2.1.4. Battery package

Let N_{ser}^brepresent the number of cells in series and $N_{par}^b$the number of cells in parallel, hence the total number of cells is $N_{ser}^b \cdot N_{par}^b$. The battery discharge power is given by (12). The *DC*superscript is used to distinguish power on DC and AC side of the VSC.

$$p_t^{b,DC} = v_t^b \cdot N_{ser}^b \cdot i_t^b \cdot N_{par}^b \tag{12}$$

2.2. Voltage source converter

The voltage source converter (VSC) converts between DC and AC power in both directions. Typical DC sources and loads are battery storages and solar PV generations, but other DC loads and sources can also occur. The VSC is also subject to losses, and [16] suggests to model the losses with constant, linear and quadratic terms of the AC side current. For the PE-model, a convex relaxation with a constant and a quadratic term will be used to model VSC losses. For the IVQ-model, the losses are approximated with a cubic spline function.

2.2.1. Assumptions

The AC side is often part of a large utility grid with relatively stable voltage, hence the effects of voltage variation on this side are neglected. Moreover, the efficiency variations due to DC side voltage in [dataset] [17] are relatively small, hence they are neglected. Therefore, the losses will solely depend on the DC side power.

2.2.2. Model

The VSC efficiency is undefined when $p_t^{VSC,AC} = 0$yielding a discontinuous function. Therefore, the power loss is expressed as the absolute power loss instead. The conversion from efficiency to absolute power loss is explained in Section 3.3. The IVQ-model uses a cubic spline function (13). The properties of cubic spline functions are discussed more in detail in Section 2.6, but the function shape will typically be close to quadratic. The PE-model uses a convex relaxation of a polynomial function (14). The VSC AC and DC power and losses for both models are tied together as shown in (15) where the losses always are positive.

$$p_t^{VSC,loss} = f_{loss}^{VSC}\left(p_t^{VSC,AC}\right) \tag{13}$$

$$p_t^{VSC,loss} \ge P_0^{VSC,loss} + P_2^{VSC,loss}\left(p_t^{VSC,AC}\right)^2 \tag{14}$$

$$p_t^{VSC,DC} = p_t^{VSC,AC} + p_t^{VSC,loss} \tag{15}$$

2.3. Load, generation and utility grid

The solar PV generation and load are given by separate forecasts. Generation curtailment and import from the power grid are decision variables.

2.3.1. Assumptions

To keep computational burden modest, uncertainties in forecasts are not accounted for. Generation can be curtailed, and power can be purchased from or sold to the utility grid at a fixed or variable exogenous positive price. In one of the examples, the effect of only being able to change the purchase/sale volume hourly will be studied. This aligns well with typical market structures where the energy is traded hourly either in the day-ahead or intra-day market. If forecast data has fewer data points than the optimization problem, data is re-sampled with linear interpolation.

2.3.2. Model

The relation between solar PV generation, forecast and curtailment is shown in (16).

$$\begin{aligned} p_t^{PV} &= \widehat{p}_t^{PV} - p_t^{PV,curt} \\ p_t^{PV} &\ge 0 \end{aligned} \tag{16}$$

The PV generation is injected on the DC side, while the power exchanged with the utility grid is injected on the AC side. The PV and the BESS share a common VSC. Storing energy from utility grid yields larger losses than PV generation since power injected on the AC side must pass the VSC before being stored in the battery.

Utility grid imports and exports are permitted within certain limits as shown in (17).

$$\begin{aligned} 0 &\le p_t^p \le P^{p,max} \\ 0 &\le p_t^s \le P^{s,max} \end{aligned} \tag{17}$$

The resulting DC and AC bus power balances are shown in (18) and (19) respectively.

$$p_t^{VSC,DC} = p_t^{PV} + p_t^{b,DC} \tag{18}$$

$$\widehat{p}_t^{l} = p_t^{VSC,AC} + p_t^{p,AC} - p_t^{s,AC} \tag{19}$$

2.4. Objective function

The objective function is given by the integral of the power exchange costs minus the BESS end storage value (20), which is described in Section 2.7.

$$\min \int_0^T \left(c_t^p p_t^p - c_t^s p_t^s\right) dt - C_q(q) \tag{20}$$

2.5. Integration rule

The integrals of (1), (7) and (20) can be discretized and solved numerically using methods for solving ordinary differential equations (ODE). Some of the simplest methods for solving the initial value problem in (21) are forward Euler (22), backward Euler (23) and the trapezoidal method (24).

$$y'(t) = f(t, y(t)),\ \ y(t_0) = y_0 \tag{21}$$

$$y_{n+1} = y_n + h{\cdot}f(t_n, y_n) \tag{22}$$

$$y_{n+1} = y_n + h{\cdot}f(t_{n+1}, y_{n+1}) \tag{23}$$

$$y_{n+1} = y_n + \frac{h}{2}\left(f(t_n, y_n) + f(t_{n+1}, y_{n+1})\right) \tag{24}$$

The choice of method is of minor importance for the PE-model in (1) since the charging and discharging are independent of SOC. This paper has used forward Euler integration as shown in (25).

$$\begin{aligned} e_{t+1} &= e_t + \Delta T_t \left(\eta_c p_t^c - \frac{1}{\eta_d} p_t^d\right) \\ e_1 &= e_{init} \\ e_{end} &= e_T + \Delta T_T \left(\eta_c p_T^c - \frac{1}{\eta_d} p_T^d\right) \end{aligned} \tag{25}$$

However, in the IVQ-model the discharge power is function of voltage, while the voltage is a function both SOC and charge/discharge current. Hence, the choice of integration method will affect the results. Moreover, the choice of step length will also be more critical with respect to both the precision and the numerical stability.

The IVQ-model in (7) can be written recursively (26). Applying the different integration methods on (26) yields sets of sparse difference equations: the storage balance for forward Euler (27), backward Euler (28) and trapezoidal (29).

$$q_{t+1} = q_t + \int_t^{t+1} \left(-i_t^b\right) dt \tag{26}$$

Forward Euler:

$$\begin{aligned} q_{t+1} &= q_t - \Delta T_t i_t \\ q_1 &= q_{init} \\ q_{end} &= q_T - \Delta T_T i_T \end{aligned} \tag{27}$$

Backward Euler:

$$\begin{aligned} q_{t+1} &= q_t - \Delta T_t i_{t+1} \\ q_1 &= q_{init} - \Delta T_1 i_1 \\ q_{end} &= q_T \end{aligned} \tag{28}$$

Trapezoidal method:

$$\begin{aligned} q_{t+1} &= q_t - \frac{\Delta T_t}{2}(i_t + i_{t+1}) \\ q_1 &= q_{init} - \frac{\Delta T_1}{2} i_1 \\ q_{end} &= q_T - \frac{\Delta T_T i_T}{2} \end{aligned} \tag{29}$$

Forward integration rewards discharge using high power since the high voltage at high SOC yields higher power per charge unit, and the SOC update is delayed due to forward integration. Likewise, it will also reward charging using high power, as less power is demanded per ampere hour stored compared to low voltage charging. On the other hand, backward Euler gives incentive to discharge with lower power as the SOC is changed in advance. For these reasons, the trapezoidal method yields the most accurate integration for continuous operation, but will also build a slightly denser system of equations as the storage balance equations contain two discharge variables instead of one. The objective function is integrated in the same manner as the storage.

Overall, the presented approaches convert the ODE-constraints into a set of sparse difference equations (algebraic) of the same variables, which are only defined at a pre-determined set of time steps. These final sets of algebraic equations are used in the implementation of the optimization model, enabled by the use of non-linear programming solvers. Implementation and solution method are presented in Section 4.1.

2.6. Cubic splines

The constraints (8) and (13) will be modelled with cubic splines as these are compatible with non-linear programming, and possible to implement in interior point solvers. Interior point solvers are also relatively efficient at solving large-scale non-linear dynamic problems [19].

A spline function is a piece-wise polynomial function. A k degree spline function has continuous derivatives up to order $k-1$, hence a spline function with degree 3 is guaranteed to have continuous derivatives up to order two. This is a necessary property for non-linear optimization tools requiring twice continuously differentiable functions. Spline functions are composed of multiple Bezier curves shown in (30). The Bezier curves are linear combinations of the Bernstein basis polynomials shown in (31) where n is the degree, and β_ν are known as Bernstein or Bezier coefficients.

$$BZ_n(x) = \sum_{\nu=0}^{n} = \beta_\nu be_{\nu,n}(x) \tag{30}$$

$$\begin{aligned} be_{\nu,n}(x) &= \binom{n}{\nu} x^\nu (1-x)^{n-\nu}, \\ &\nu = 0, \cdots, n,\ \ x = [0, 1] \end{aligned} \tag{31}$$

A property of the Bezier curve is that the start and the end value of the function is a linear combination of the Bezier coefficients, and the same applies for the start and the end values for the derivatives of the curve. This makes them well suited for building piece-wise polynomial functions with continuous derivatives.

A spline function can be uniquely described as a linear combination of basis functions as shown in (32), and this representation is known as B-splines. The spline function parameters are the control points x_i and knots t_i. The knots represent the distance between the control points. A k degree spline with $n+1$control points will consist of $n-k+1$polynomial segments. The basis function is constructed in a recursive manner using the Cox-de Boor formula (33)[20]. The derivatives are also defined as a linear combination of the basis functions.

$$S_{n,t}(x) = \sum_i \alpha_i B_{i,n}(x) \tag{32}$$

$$\begin{aligned} B_{i,0} &= \begin{cases} 1 \text{ if } t_i \le x \le t_{i+1} \\ 0 \text{ otherwise} \end{cases} \\ B_{i,k}(x) &= \frac{x - t_i}{t_{i+k} - t_i} B_{i,k-1}(x) + \frac{t_{i+k+1} - x}{t_{i+k+1} - t_{i+1}} B_{i+1,k-1}(x) \end{aligned} \tag{33}$$

Moreover, the bi-variate spline function is given by (34) where n and m are the spline degrees of the two dimensions x and y respectively. The bivariate spline describes a smooth surface given by a mesh of control points α_{ij} where the corresponding knots are tx_i, ty_i.

$$S_{n,m,tx,ty}(x,y) = \sum_i \sum_j \alpha_{ij} B_{i,n}(x) B_{j,m}(y) \tag{34}$$

Alternatively, the splines can also be described as a matrix of polynomials. This description is more extensive than the combination of basis splines, but the resulting function is differentiable in Julia/JuMP. Surface (*i, j*) of the bi-variate spline function on polynomial form is shown in (35).

$$\begin{aligned} S_{i,j,n,m,tx,ty}(x,y) &= \sum_{km=0}^{n} \sum_{km=0}^{m} \beta_{i,j,kn,km}\ \Delta x_i^{kn}\ \Delta y_j^{km} \\ \Delta x_i &= x - x_i \\ \Delta y_i &= y - y_i \end{aligned} \tag{35}$$

Each polynomial surface is defined by $(n+1)\cdot(m+1)$coefficients, for cubic splines in both x and y yields a 4 by 4 matrix with coefficients for each polynomial surface. These coefficients are obtained by evaluating (34) and its derivatives at the corners of the respective surfaces.

The splines have been generated using the Python Scipy [21] functions *bisplrep* and *splrep*, which are based on [20].

2.7. Battery energy storage system end value

In energy storage optimization, the storage tends to be emptied at the end of the optimization period, unless the end value is bounded by constraints, or the stored energy at the end is valuated in the objective function. A possible approach is to keep the end value fixed, for example to the initial value. However, the conversion between SOC in terms of charge and energy is not uniquely defined since the battery voltage depends on both SOC and charge/discharge current. Instead of keeping the end value fixed, an end value function is defined in this model. This enables comparison of the objective function through simulation of different cases even though the end point values are different. The valuation of end storage is a well established concept from hydro power scheduling [22,23], and [24] gives a general description also including PV generation.

When the SOC is 100%, it is unable to receive more power, hence the energy marginal value is zero. On the other hand, an empty storage is not capable of supplying energy, hence it has a high marginal value $MC^b_{\max}$. For simplicity, the marginal value of the end storage is set to vary linearly between these to points. The marginal value function for a PE-model is shown in (36). The corresponding storage end value function is the integral of (36)as shown in (37). The value function is converted from energy in the PE variable space *(kWh)* to charge in the IVQ variable space *(Ah)* through a conversion (38) under the assumption that the BESS is charged/discharged at constant voltage. The same conversion is used to convert the storage max value between PE and IVQ variable space. The resulting storage end value function is shown in (39).

$$MC_e(e_T) = MC^{b,max}\left(1 - \frac{e_T}{E^{b,max}}\right) \tag{36}$$

$$\begin{aligned} C_e(e_T) &= \int_0^{e_T} MC_e(e)\ de \\ &= MC^{b,max}\left(e_T - \frac{{e_T}^2}{2E^{b,max}}\right) \end{aligned} \tag{37}$$

$$\begin{aligned} e_T &= V^{b,avg}\cdot N^b_{ser}\cdot N^b_{par}\cdot q_T \\ &= c_{eq}\cdot q_T \end{aligned} \tag{38}$$

$$C_q(q_T) = MC^{b,max}\cdot c_{eq}\left(q_T - \frac{{q_T}^2}{2\cdot Q^{b,max}}\right) \tag{39}$$

2.8. Model summary

The objective and constraints of the PE-model and the IVQ-model are summarized in Table 1.

Table 1
Summary of PE- and IVQ-model equations.

PE-model	
Objective	(20), (37) and (38)
Storage constraints	(25)
Other constraints	(2) (3) (4) (5), (6), (14), (15), (16), (17), (18) and (19)
IVQ-model	
Objective	(20) and (39)
Storage constraints	(27), (28) or (29)
Other constraints	(8), (9), (10), (11), (12), (13) and (15), (16), (17), (18), (19)

The PE-model formulation is quadratic and convex. Note that simultaneous charging and discharging is possible to create artificial losses. In these situations, an equally good solution will be to curtail the generation.

The IVQ-model is continuous and twice differentiable, but the constraints are non-linear and non-convex. Ipopt searches for the optimal solution in an iterative manner, hence the spline functions are only evaluated at their current point for each iteration. Binary variables are therefore not needed to decide which segment of the spline function is active. However, the optimal solution is only local and can not be guaranteed to be the global optimum.

3. Case study data

This section presents numerical values used to describe the BESS and the VSC in the optimization problem, and the procedure for converting the data points into spline functions. The resulting BESS and VSC efficiencies are presented as well as the total system efficiency. Other general numerical values are presented in Table 2. Case-specific numerical results are presented in Section 4.

3.1. Battery voltage splines

The battery voltage is given by experimental values from a Nissan Leaf battery cell [dataset][25]. The cell has been charged at around 15 A and discharged at 30, 60 and 90 A while the voltage has been monitored. To generate the spline functions, the voltage has been sampled with uniformly distributed sample points in the SOC variable space q and for four selected charge/discharge currents yielding the bi-variate spline function $f^b_v(q_t, i^b_t)$. Fig. 2shows the resulting splines compared to the original sampling points for different smoothing factors. In addition, voltage curves for 0 A and 30 A are shown to verify if the spline model predicts reasonable voltage values between and outside the sampling points. Fig. 2a shows that a low smoothing factor yields an accurate fit for the data points marked with black dots. However, the voltage at 0 A should be between the voltage at 15 A and -30 A which is not the case in Fig. 2a, hence is likely to be overfit. The intermediate smoothing factor in Fig. 2b fits quite well with the data point. The 0A voltage is also between the -30 A and the 15 A voltage, and the 30 A voltage seems to scale linearly compared to the other curves. However, the increasing slope for high SOC is not well captured for charging (positive current). The high

Table 2
Model numerical values.

Battery & VSC	
$V^{\min}/V^{\max}/V^{avg}$	3.20/4.15/3.90 V
$Q^{b,min}/Q^{b,max}/Q^{init}$	0/29/20 Ah
$I^{b,ch}/I^{b,dch}$	30/90 A
$VSC^{\max}$	25 kW
Market	
$P^{p,max}/P^{s,max}$	10/10 kW
c^p/c^s	10/9 € /kWh
$MC^{b,max}$	15 € /kWh

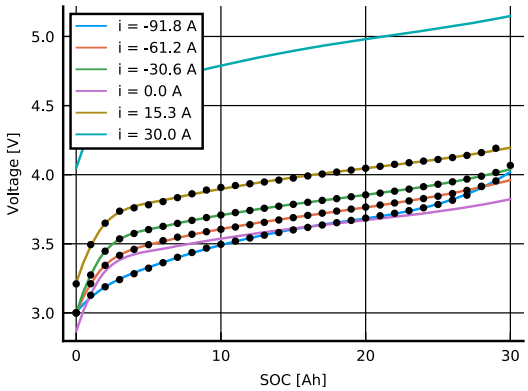

(a) Smoothing = 0.001

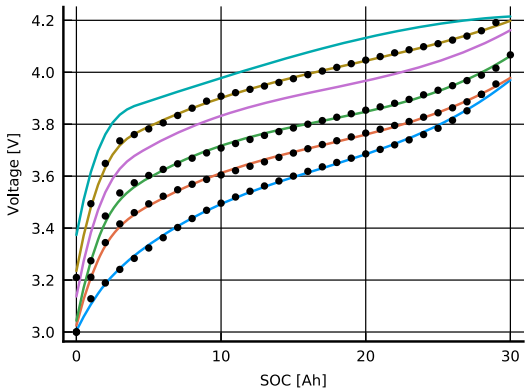

(b) Smoothing = 0.01

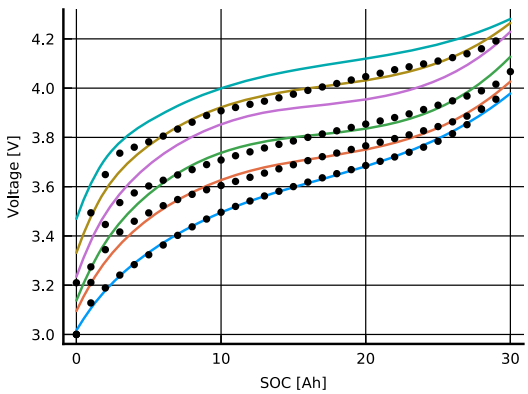

(c) Smoothing = 0.1

Fig. 2. Comparison of bi-variate spline curve and measured data for battery cell voltage for different smoothing factors.

smoothing factor in Fig. 2c captures the increasing slope for high SOC at the cost of accuracy, especially for low SOC where the deviation between the measured data points and the curves are significant. The intermediate smoothing factor 0.01 will be used further.

3.2. Battery modules and package

The Nissan Leaf 2013 battery package configuration consisting of 48 modules in series has been used. Each module has four cells, where two and two are in parallel. The experimental values in [25] has been obtained by cycling the battery cells between 3.0 V and 4.2 V. This configuration has $N^b_{ser} = 96$and $N^b_{par} = 2$yielding a voltage range from 288.0 to 403.2 V. Note that the examples in this paper use conservative voltage limits to illustrate the properties of the IVQ-model.

3.3. Voltage source converter loss curve

VSC loss values are obtained from [17] (SBS3.7–10), where the efficiency is given as function of AC side power. The efficiency is converted to absolute power loss as shown in (40), and the converted efficiency data points are used to generate the spline function $f^{VSC}_{loss}(p^{VSC,AC}_t)$. To adapt the size of the VSC for the different cases, the $p^{VSC,AC}_t$data points are scaled linearly with $P^{VSC,max}$ as the maximum value.

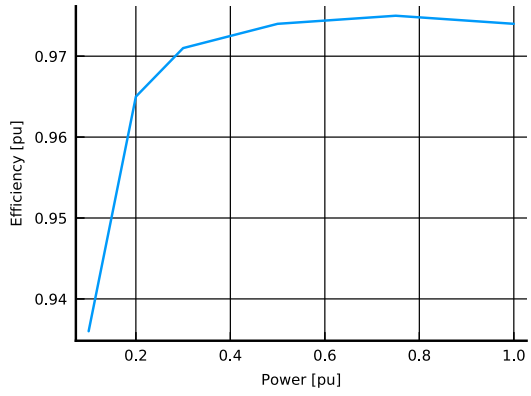

(a) Efficiency

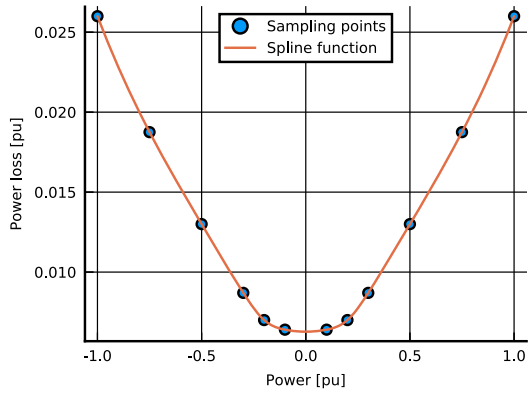

(b) Power loss

Fig. 3. VSC efficiency.

$$p_{loss}^{VSC}\left(p_t^{VSC,AC}\right) = \left(1 - \eta^{VSC}\left(p_t^{VSC,AC}\right)\right) \tag{40}$$

The VSC efficiency curve as function of per unit power is shown in Fig. 3a. This efficiency curve is for the nominal DC voltage 360 V. The VSC power loss sampling points and the resulting spline function are shown in Fig. 3b, where the solid line represents the spline function that is used in the optimization problem. The smoothing factor is 0.

The coefficients of the PE-model loss curve in (14) are fitted by evaluating the spline function for 0 and maximum power as shown in (41) and (42).

$$P_0^{VSC,loss} = f_{loss}^{VSC}(0) \tag{41}$$

$$P_2^{VSC,loss} = \frac{f_{loss}^{pu,VSC}\left(P^{VSC,max}\right) - P_0^{VSC,loss}}{\left(P^{VSC,max}\right)^2} \tag{42}$$

3.4. Battery and system efficiency

The battery round trip efficiency can be calculated based on the charge and discharge voltage. Assume the battery is charged at a constant current for a short optimization horizon, and then discharged with the same current. By neglecting the change in SOC due to the short time period, the battery round trip efficiency as a function of current and SOC can be found using (45). This has been mapped from the IVQ to the PE variable space, and the resulting numerical values are shown in Fig. 4a.

$$p^{b,dch} = f_v\left(q, i^b\right) \cdot i^b \tag{43}$$

$$p^{b,ch} = f_v\left(q, -i^b\right) \cdot i^b \tag{44}$$

$$\eta = \frac{p^{b,dch}}{p^{b,ch}} = \frac{f_v\left(q, i^b\right)}{f_v\left(q, -i^b\right)} \tag{45}$$

When storing energy in the battery, the energy can either come from surplus solar PV generation, or be purchased from the grid. Since PV generation is injected on the DC side, it does not have to pass VSC before it is discharged. However, when energy is purchased for storage, it is first converted to DC and then must be converted back later when consumed by the load. The system DC efficiency is the efficiency associated with storing solar PV energy for later use, and the VSC efficiency is multiplied with the BESS efficiency *once*. The AC efficiency is the efficiency when purchased energy is stored and consumed later, and the VSC efficiency is multiplied with the BESS efficiency *twice*. Both DC and AC efficiencies are shown in Fig. 4b and 4c respectively.

Both figures show that the system efficiency is highest for moderate power since the battery efficiency is highest for low power, while the VSC has a standby power consumption which shifts the system optimum. The efficiency decreases almost linearly when the SOC is around 50%, while the non-linearity is more pronounced for both high and low SOC.

4. Results and discussion

This section presents the implementation and solving method for the proposed models. Moreover, a simulation based validation method is proposed. Finally, the results from two examples are presented to demonstrate the capabilities of the IVQ optimization model. Both examples are built on the topology in Fig. 1 and the numerical values presented in Section 3, and solved using Ipopt in Julia/JuMP. The first example involves cycling of the battery, and demonstrates how the change in efficiency with respect to SOC influences the optimal solution. It also shows how the choice of step length and integration method can influence the accuracy of the numerical integration. The second case shows how the power delivery capability, due to voltage and current limits, is accounted for with an IVQ-model compared to a PE-model.

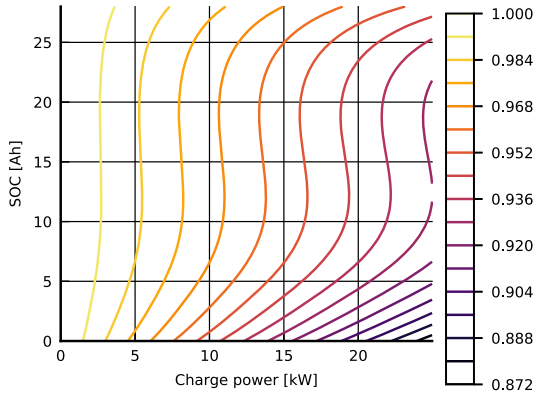

(a) Battery round trip efficiency

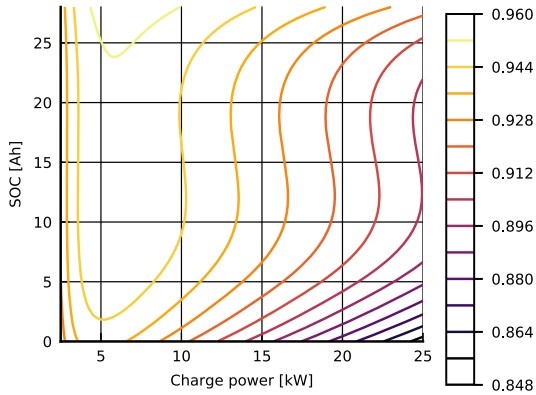

(b) Battery-VSC DC efficiency

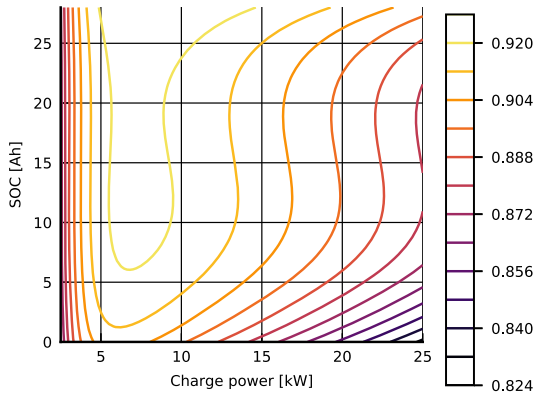

(c) Battery-VSC AC efficiency

Fig. 4. Battery and VSC efficiencies.

4.1. Implementation and solution method

The problem is solved using the optimization toolbox JuMP (0.21.2) [26] in the programming language Julia (1.2) and the non-linear interior point solver Ipopt (3.12.10) [27]. Ipopt finds a local solution to non-linear and non-convex optimization problems where the objective and the constraint functions are twice continuously differentiable.

Computation time of Ipopt depends on problem structure as well as the underlying linear equality solver. Both the default solver in Ipopt, i. e. MUMPS, as well as the large scale solver PARDISO (6.0) [19] have been tested in this paper. PARDISO generally performs well on large scale systems [28].

Moreover, the voltage function and the VSC loss function must also be twice continuously differentiable. A common continuous function for describing this voltage is given by [12]. However, this function will often give a significant stationary offset compared to the actual voltage curve.

JuMP supports automatic differentiation of user-defined non-linear functions [26]. Instead of using a rigorously defined polynomial, the voltage surface and the VSC loss are described with a cubic spline function. The cubic spline function is piece-wise polynomial, but has continuous derivatives up to order two, hence no integer variables are needed to solve the problem. Since the voltage is a function of both i and q, a bi-variate cubic spline function is used to approximate (8), and a uni-variate cubic spline function is used to describe the VSC losses in (15).

4.2. Validation

To verify feasibility of the proposed schedules from the optimization models, a simulation model is used. The simulation model is based on the IVQ-model with forward Euler, but the step length is shorter, only 1 second. The simulation will therefore give a more accurate update of SOC under the assumption that the IVQ-model is the true model.

The simulation model assumes the load, grid exchange, VSC AC power and battery discharge is given by the optimization, and simulates the battery current and voltage, VSC loss, PV curtailment and SOC. This comparison identifies how much the SOC in optimization will drift of from the simulation result due to the inaccuracy in numerical integration. Since the PE-model does not include voltage and current as variables, the simulation is also used to check for voltage and current limit violations in the model result. Note that the SOC from optimization is used in this case since the effect of SOC drift should be kept apart from other effects. This simulation method ensures that the load is always met, and will reveal if the proposed schedule causes violation of current, voltage or SOC limits.

4.3. Optimality and integration method

The system efficiency depends on SOC, hence the optimal strategy involves operating around the optimal SOC as well as hitting the optimal end value. The relation between charge-discharge power and SOC depends on the integration method. To demonstrate this, the net load (load minus generation) is set to a sine wave with period 2 hours and amplitude 10 kW. The system is optimized for 36 hours which involves 18 charge/discharge cycles, which is long enough to let the battery cycling stabilize around the optimal SOC. Other numerical values of this test case are shown in Table 3

The case is optimized with step length 30, 10 and 1 min, and Fig. 5 shows the resulting optimized SOC, the simulation result and the optimization error (difference between optimization and simulation) at 10-minute optimization step lengths. Fig. 5a shows how the forward Euler cycles at lower SOC than the other methods, which is not optimal based on the efficiency surface shown in Figs. 4b, and 4c. The voltage at the beginning of a time step is used for integrating the SOC, hence for discharging the voltage will be higher than the actual voltage. The losses

Table 3
Numerical values for sine wave case.

$P^{p,max}/P^{s,max}$	10.0/10.0 kW
c^p/c^s	10.0/9.0 €
$p^{VSC,max}$	25.0 € /kWh

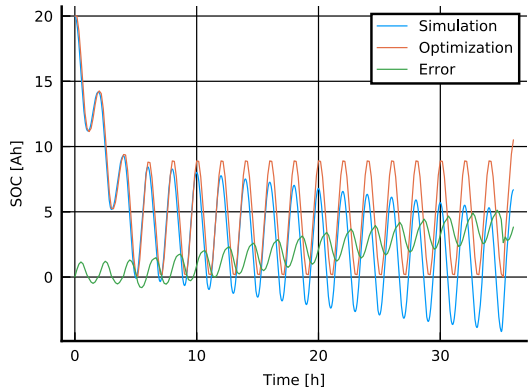

(a) Forward Euler

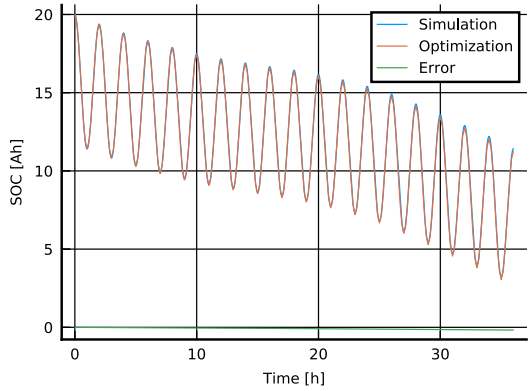

(b) Trapezoidal

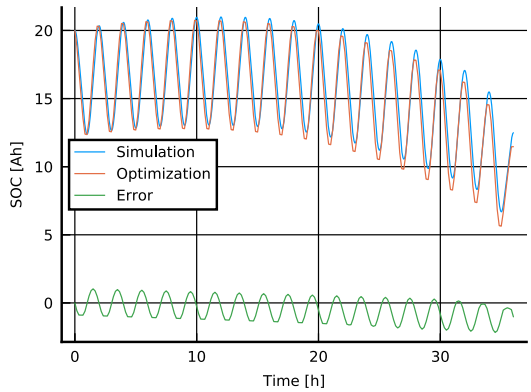

(c) Backward Euler

Fig. 5. Comparison of optimization and simulation results for battery cycling with different integration methods with step length 10 minutes.

and the discharge current will therefore be underestimated and promote high discharge power. When charging, the voltage will be lower than the actual voltage, hence the charge current will be overestimated. In total, Fig. 5a shows that the simulated value drifts off from the optimized value and the error in SOC accumulated up to the value shown in Table 4. When the step size is reduced, the error is reduced significantly.

Table 5 summarizes number of variables and constraints for the

Table 4
Accumulated optimization error SOC (Ah) for different integration methods and step length with sine wave net load.

Step length	30 min	10 min	1 min
Forward	24.13	3.856	0.1222
Trapezoidal	–1.172	–0.1670	–0.003733
Backward	–2.950	–1.125	–0.1215

Table 5
Optimization statistics for different integration methods and step length with sine wave net load.

Step length		30 min	10 min	1 min
#Variables		1024	3040	30,256
#Equality constraints		733	2173	21,613
#Inequality constraints		74	218	2162
#Iterations	Forward	119	132	44
	Trapezoidal	46	39	50
	Backward	49	38	39
Solve time (s)	Forward	2.9	6.1	16.5
	Trapezoidal	1.6	2.0	20.0
	Backward	2.0	2.1	15.3

problems solved, and the respective computation time and number of iterations. The default linear solver in Ipopt, MUMPS, took between four and eight minutes solving the cases with one minute step length, and several of the other cases did not converge to the desired tolerance. Therefore, the PARDISO [19] solver was used instead, which gave a significant reduction in computation time for the largest cases and improved convergence tolerance.

For longer step lengths, forward Euler showed convergence problems for small initial storage values, which is in accordance with its known properties. This is also confirmed by the higher number of iterations needed for these cases in Table 5.

Fig. 5b and 5c show similar comparison for the trapezoidal method and backward Euler respectively. The trapezoidal method has a smaller error compared to the other methods, which is as expected, since the integration is based on the average voltage value for the time step. Backward Euler has a smaller deviation than forward Euler for the long time steps, while the error magnitude is almost identical for small step length. Backward Euler uses the voltage at the end of the time step to calculate the current, hence it will underestimate the needed charging current and overestimate the discharge current.

4.4. Solar PV smoothing

The numerical values for solar PV generation are acquired from [29], where the overcast series from *Varennes* with *overcast* cloud cover has been used. The series have variable time resolution with step length $\leq$ 60*s*. This case demonstrates how the battery can be used to smooth the output from solar PV under the assumption that the system purchase/-sale only can be changed hourly. The PV generation is shown in Fig. 6 together with the system sale for both the IVQ- and the PE-model. Other numerical values specific for this case are shown in Table 6. It is noted that despite the differences, the dispatch curves are shaped similarly, suggesting that for the non-convex IVQ model the optimizer didn't converge to an obviously sub-optimal solution.

Table 6
Numerical values for PV smoothing case.

$P^{s,max}$	150.0 kW
c^{s}	10.0 € /kWh
$P^{VSC,max}$	150.0 kW

Fig. 7 shows the simulated SOC for the IVQ- and the PE-model, and the error between simulation and optimization. The result show that the PE-model violates the SOC lower bound (remark 1, indicated with a numbered red circle), and that the error increases when the battery is discharged at high power. The PE-model assumes constant battery efficiency, hence it does not capture the increasing loss for high discharge power causing the increase in error at remark 1.

The battery voltage is shown in Fig. 8a, and the both the upper and lower voltage is violated for the PE-model (remark 1–4). It would have been possible to adjust the power and energy limits such that they were not violated, but that would also put unnecessary conservative limits on the discharge power or SOC in other situations. Similar violations are observed for the current in Fig. 8b (remark 1).

Also note the difference is charging profile for the two models in Fig. 8c. Remark 1 and 2 shows how the charging is ramped down to avoid voltage limit violation, while at remark 3, the power is ramped up as the increasing battery voltage permits increasing charge power.

5. Conclusions

The IVQ optimization model enables operation closer to battery boundaries in terms of both voltage, current and SOC than a PE-model. Whereas a PE-model must implement conservative charge, discharge and SOC limits to ensure feasible solutions and battery life, the IVQ-model incorporates the voltage and current limits directly, allowing safe operation close to the battery limits. Moreover, the incorporation of the voltage surface and VSC efficiency with cubic splines enables the use of empirical data or updated measured data directly into the optimization model. The model can therefore be updated regularly through the battery lifetime providing optimal and feasible plans, even when the battery properties have changed due to degradation. Finally, the IVQ-model will ensure operation at the optimal SOC and charge/discharge

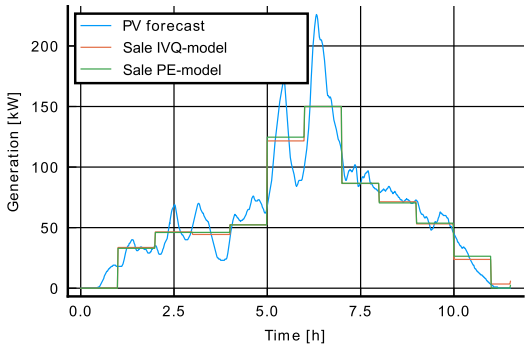

Fig. 6. PV generation and system output for PV smoothing case.

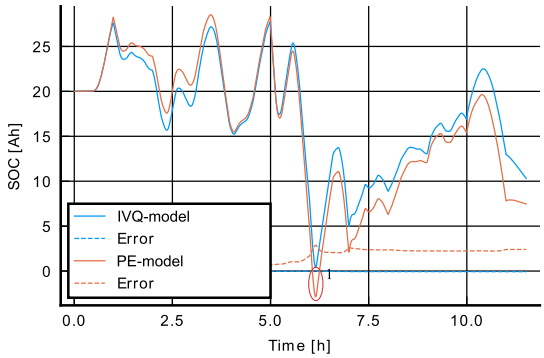

Fig. 7. Battery SOC for PV smoothing case.

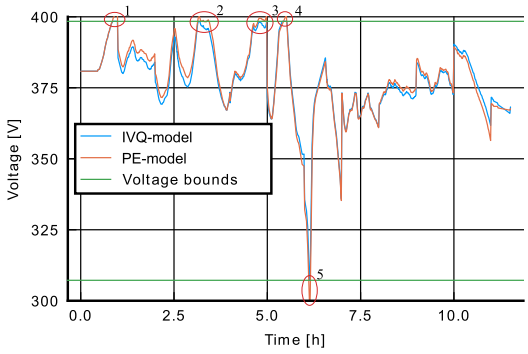

(a) Battery voltage

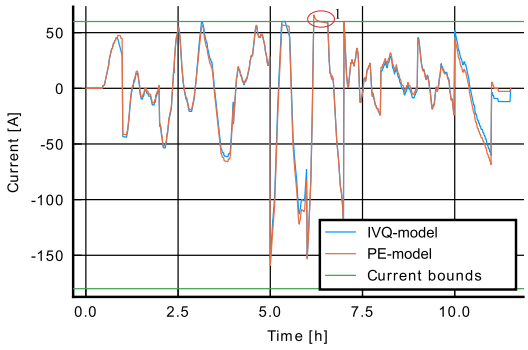

(b) Battery charging current

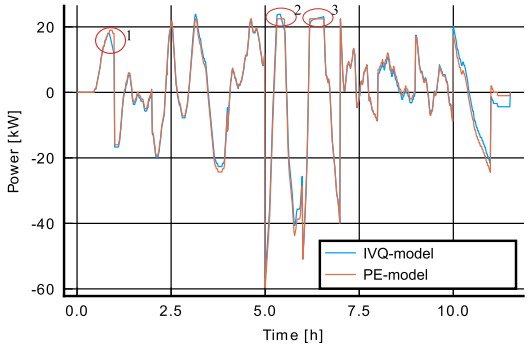

(c) Battery charging power

Fig. 8. Battery voltage, current and power for PV smoothing case.

power yielding highest efficiency whenever possible. However, the results are sensitive to choice of numerical integration method and step length. The trapezoidal integration method has similar scalability to problem size as forward and backward Euler, but significantly less error for similar step lengths.

5.1. Further work

A possible extension of this model is to incorporate degradation costs associated with operative variables such as SOC and charge/discharge power. The modelling principle may also be adapted to other types of storage technologies such as hydrogen or hydropower.

Renewable generation is subject to uncertainty, and the error from uncertainty is integrated over time when it comes to storage operation. Combining the proposed method with stochastic renewable generation and load is therefore also important further work.

Finally, the model may also be incorporated in an unbalanced OPF model using model predictive control to perform model-based congestion management through battery storage operation.

CRediT authorship contribution statement

Per Aaslid: Conceptualization, Methodology, Software, Formal analysis, Investigation, Visualization, Writing - original draft. **Frederik Geth:** Conceptualization, Methodology, Writing - review & editing. **Magnus Korpås:** Writing - review & editing. **Michael M Belsnes:** Writing - review & editing, Project administration. **Olav B Fosso:** Writing - review & editing, Supervision.

Declaration of Competing Interest

The authors declare that they have no known competing financial interests or personal relationships that could have appeared to influence the work reported in this paper.

Acknowlgedgments

This work has been funded by the Norwegian Research Council under grant number 272398.

References

[1] M. Müller, L. Viernstein, C.N. Truong, A. Eiting, H.C. Hesse, R. Witzmann, A. Jossen, Evaluation of grid-level adaptability for stationary battery energy storage system applications in Europe, Journal of Energy Storage 9 (2017) 1–11, https://doi.org/10.1016/j.est.2016.11.005.

[2] H.C. Hesse, M. Schimpe, D. Kucevic, A. Jossen, Lithium-ion battery storage for the grid - a review of stationary battery storage system design tailored for applications in modern power grids, Energies 10 (12) (2017) 2107, https://doi.org/10.3390/en10122107.

[3] O. Palizban, K. Kauhaniemi, Energy storage systems in modern grids-matrix of technologies and applications, Journal of Energy Storage 6 (2016) 248–259, https://doi.org/10.1016/j.est.2016.02.001.

[4] A. Castillo, D.F. Gayme, Grid-scale Energy Storage Applications in Renewable Energy Integration: A Survey, Energy Conversion and Management 87 (2014) 885–894, https://doi.org/10.1016/j.enconman.2014.07.063.

[5] A. Sani Hassan, L. Cipcigan, N. Jenkins, Optimal battery storage operation for PV systems with tariff incentives, Appl Energy 203 (2017) 422–441, https://doi.org/10.1016/j.apenergy.2017.06.043.

[6] B. Xu, A. Botterud, M. Korpas, Operational Valuation for Energy Storage Under Multi-stage Price Uncertainties, 2019.https://bolunxu.github.io/publication/xu_stochastic2019/http://arxiv.org/abs/1910.09149.

[7] J. Von Appen, T. Stetz, M. Braun, A. Schmiegel, Local voltage control strategies for PV storage systems in distribution grids, IEEE Trans Smart Grid 5 (2) (2014) 1002–1009, https://doi.org/10.1109/TSG.2013.2291116.

[8] M. Kazemi, H. Zareipour, N. Amjady, W.D. Rosehart, M. Ehsan, Operation scheduling of battery storage systems in joint energy and ancillary services markets, IEEE Trans. Sustainable Energy 8 (4) (2017) 1726–1735, https://doi.org/10.1109/TSTE.2017.2706563.

[9] X. Ai, Z. Wu, J. Hu, Y. Li, P. Hou, Robust operation strategy enabling a combined wind/battery power plant for providing energy and frequency ancillary services, International Journal of Electrical Power & Energy Systems 118 (2020) 105736, https://doi.org/10.1016/j.ijepes.2019.105736.

[10] S.M. Mousavi G., M. Nikdel, Various battery models for various simulation studies and applications, Renewable Sustainable Energy Rev. 32 (2014) 477–485, https://doi.org/10.1016/j.rser.2014.01.048.

[11] C.M. Shepherd, Design of primary and secondary cells - Part 2. An equation describing battery discharge. Journal of Electrochemical Society 112 (1965) 657–664.

[12] O. Tremblay, L.-A. Dessaint, A.-I. Dekkiche, A generic battery model for the dynamic simulation of hybrid electric vehicles. 2007 IEEE Vehicle Power and Propulsion Conference, IEEE, 2007, pp. 284–289, https://doi.org/10.1109/VPPC.2007.4544139.http://ieeexplore.ieee.org/document/4544139/.

[13] O. Tremblay, L.-A. Dessaint, Experimental Validation of a Battery Dynamic Model for EV Applications, World Electric Vehicle Journal 3 (2) (2009) 289–298, https://doi.org/10.3390/wevj3020289.http://www.mdpi.com/2032-6653/3/2/289.

[14] P. Fortenbacher, J.L. Mathieu, G. Andersson, Modeling and Optimal Operation of Distributed Battery Storage in Low Voltage Grids, IEEE Transactions on Power Systems 32 (6) (2017) 4340–4350, https://doi.org/10.1109/TPWRS.2017.2682339.http://ieeexplore.ieee.org/document/7879188/.

[15] J.M. Reniers, G. Mulder, S. Ober-Blöbaum, D.A. Howey, Improving optimal control of grid-connected lithium-ion batteries through more accurate battery and degradation modelling, Journal of Power Sources 379 (2018) 91–102, https://doi.org/10.1016/j.jpowsour.2018.01.004.https://www.sciencedirect.com/science/article/pii/S0378775318300041.

[16] H. Ergun, J. Dave, D. Van Hertem, F. Geth, Optimal power flow for AC-DC grids: formulation, convex relaxation, linear approximation, and implementation, IEEE Trans. Power Syst. 34 (4) (2019) 2980–2990, https://doi.org/10.1109/TPWRS.2019.2897835.

[17] SMA Solar Technology, Technical Information, Efficiency and Derating, Sunny Boy/Sunny Boy Storage/Sunny Tripower/Sunny Mini Central/Sunny Highpower, 2020.https://files.sma.de/dl/1348/WirkungDerat-TI-en-47.pdf.

[18] M. Schimpe, M. Naumann, N. Truong, H.C. Hesse, S. Santhanagopalan, A. Saxon, A. Jossen, Energy efficiency evaluation of a stationary lithium-ion battery container storage system via electro-thermal modeling and detailed component analysis, Appl Energy 210 (2018) 211–229, https://doi.org/10.1016/j.apenergy.2017.10.129.

[19] D. Kourounis, A. Fuchs, O. Schenk, Toward the next generation of multiperiod optimal power flow solvers, IEEE Trans. Power Syst. 33 (4) (2018) 4005–4014, https://doi.org/10.1109/TPWRS.2017.2789187.

[20] P. Dierckx, Curve and Surface Fitting with Splines., Oxford University Press, Inc., New York, 1995.https://books.google.com/books?hl=no&lr=&id=-RIQ3SR0sZMC&oi=fnd&pg=PR15&dq=Curve+and+Surface+Fitting+with+Splines&ots=IPSe_5k45a&sig=V9YUfX5SbtLVmGR8eb7Bak_bMG0.

[21] Yoshiki, S.C.V. Pauli, G. Ralf, O. Travis E., H. Matt, R. Tyler, C. David, B. Evgeni, P. Pearu, W. Warren, B. Jonathan, v.d.W. Stéfan J., B. Matthew, W. Joshua, M. K. Jarrod, M. Nikolay, SciPy 1.0: fundamental algorithms for scientific computing in Python, Nat. Methods 17 (3) (2020) 261–272, https://doi.org/10.1038/s41592-019-0686-2.

[22] O.B. Fosso, A. Gjelsvik, A. Haugstad, B. Mo, I. Wangensteen, Generation scheduling in a deregulated system. the norwegian case, IEEE Trans. Power Syst. 14 (1) (1999) 75–80, https://doi.org/10.1109/59.744487.

[23] O. Wolfgang, A. Haugstad, B. Mo, A. Gjelsvik, I. Wangensteen, G. Doorman, Hydro reservoir handling in Norway before and after deregulation, Energy 34 (10) (2009) 1642–1651, https://doi.org/10.1016/j.energy.2009.07.025.

[24] H.G. Svendsen, O.C. Spro, PowerGAMA: A new simplified modelling approach for analyses of large interconnected power systems, applied to a 2030 Western Mediterranean case study, Citation: J. Renewable Sustainable Energy 8 (2016) 55501, https://doi.org/10.1063/1.4962415.http://aip.scitation.org/toc/rse/8/5.

[25] G. Wiggins, S. Allu, H. Wang, Battery Cell Data from a 2013 Nissan Leaf, 2020, https://doi.org/10.5281/zenodo.2580327.

[26] I. Dunning, J. Huchette, M. Lubin, JuMP: A Modeling language for mathematical optimization, SIAM Rev. 59 (2) (2017) 295–320, https://doi.org/10.1137/15M1020575.

[27] A. Wächter, L.T. Biegler, On the implementation of an interior-point filter line-search algorithm for large-scale nonlinear programming, Math Program 106 (1) (2006) 25–57, https://doi.org/10.1007/s10107-004-0559-y.

[28] B. Tasseff, C. Coffrin, A. Wächter, C. Laird, Exploring Benefits of Linear Solver Parallelism on Modern Nonlinear Optimization Applications, 2019 arXiv:1909.08104.pdf.

[29] Natural Resources Canada, High-Resolution Solar Radiation Datasets, 2020.https://www.nrcan.gc.ca/energy/renewable-electricity/solar-photovoltaic/18409.

Paper III

The paper *"Pricing electricity in constrained networks dominated by stochastic renewable generation and electric energy storage"* is published by *Elsevier* in the journal *Electric Power Systems Research*. The final published paper is reprinted here without changes in compliance with the CC-BY 4.0 license [2] it is published under.

Cite as:

> P. Aaslid, M. Korpås, M. M. Belsnes, and O. B. Fosso, "Pricing electricity in constrained networks dominated by stochastic renewable generation and electric energy storage," *Electric Power Systems Research*, vol. 197, p. 107 169, Aug. 2021, ISSN: 03787796. DOI: 10.1016/j.epsr.2021.107169

[2] For license details, see: https://creativecommons.org/licenses/by/4.0/

Electric Power Systems Research 197 (2021) 107169

Contents lists available at ScienceDirect

Electric Power Systems Research

journal homepage: www.elsevier.com/locate/epsr

Pricing electricity in constrained networks dominated by stochastic renewable generation and electric energy storage

Per Aaslid [*,a,b], Magnus Korpås [b], Michael M Belsnes [a], Olav B Fosso [b]

[a] SINTEF Energy Research, Trondheim, Norway
[b] Norwegian University of Science and Technology, Department of Electric Power Engineering, Trondheim, Norway

ARTICLE INFO

Keywords:
Electricity price
Variable renewable energy
Electric energy storage
Stochastic dynamic programming
Multi-period optimal power flow
Splines
Infinite horizon

ABSTRACT

This paper studies the electricity price formation in a competitive market when introducing generation from variable renewable energy technologies with zero marginal cost and electric energy storage systems. A power system is analyzed with a stochastic optimization model combining multi-period optimal power flow with stochastic dynamic programming. The results illustrate how variable renewable energy, in this case solar photovoltaic generation, displaces some of the expensive thermal generation and reduces the price. Electric energy storage will reduce the price variations caused by the variable renewable generation and demand as the time with price cap and zero price is reduced. In systems with only variable renewable generation and energy storage, the price will be set by the probability of scarcity similar to the price formation in hydro power dominated systems. The price will indicated the future cost of scarcity as a stochastic expectation value. This paper assumes that the demand is inflexible. However, the resulting electricity prices will remunerate provision of flexibility, which in turn will contribute to securing the supply and reducing the price volatility.

1. Introduction

The share of Variable Renewable Energy (VRE) generation worldwide is increasing, and although most electricity markets still are dominated by thermal generation, projections show that VRE will be the dominant energy source by 2050 both in terms of electricity generation and and installed capacity [1]. Until now, the deployment of VRE has to a large extent been driven by subsidies, but the cost level of VRE has been decreasing rapidly and is now becoming lower than conventional generation, even without subsidies [2].

VRE has a marginal operating cost close to zero and will therefore displace some of the dispatchable generation due to the merit order effect, which has been extensively studied [3–8]. This in turn will reduce the profit of the conventional generation units, but also make large-scale deployment of competitive VRE more difficult due to the energy price reduction [9]. However, Helm and Mier [10] shows that VRE can be competitive in an energy-only market when the levelized cost of energy is sufficiently low. Moreover, Korpås and Botterud [11] show that there exists a market equilibrium including VRE in an energy-only market where all units recover their costs. The market price at the new equilibrium will be more volatile compared to a system without VRE. The new market equilibrium will also have a significant duration of zero price, a higher amount of energy not supplied, and there will be relatively more power stations with higher variable costs and lower fixed costs [12].

Electric Energy Storage (EES) can facilitate integration of VRE. The deployment of grid scale EES has seen a tremendous growth since 2013 [13], partly driven by decreasing EES costs [14]. The application of EES in combination with VRE has been extensively studied [15,16], either from a system optimization perspective [17,18], or from a price taker perspective [19,20] regardless of generating source. The EES profit in a wholesale market comes from arbitrage, hence accurate price forecasts capturing both the volatility as well as the uncertainty are important. Ward et al. [21] shows that current market models tend to underestimate the volatility, and suggests a more accurate description of the merit order to better capture the price volatility and to account for the implications on the market equilibrium caused by EES by solving the model iteratively. The implications EES have for the market equilibrium are studied more in detail in Korpås and Botterud [11] where they show how profit maximization for each generation and storage unit in a market based on marginal cost pricing and administrative scarcity pricing will have the same result as system cost minimization using traditional system optimality and cost recovery conditions from Stoft

* Corresponding author.
E-mail address: per.aaslid@sintef.no (P. Aaslid).

https://doi.org/10.1016/j.epsr.2021.107169
Received 12 November 2020; Received in revised form 9 February 2021; Accepted 11 March 2021
Available online 6 May 2021

Nomenclature

Sets and indices

$b \in \mathscr{B}$ Set of buses in network
$(i,k) \in \mathscr{L}$ Set of lines in network
$(i,k) \in \mathscr{L}_b$ Set of lines from bus b
$s \in \mathscr{S} = [1,S]$ Set of stages in optimization problem
$t \in \mathscr{T}_s = \left[\underline{t}_s, \bar{t}_s\right]$ Set of time steps at stage s
$n \in \mathscr{N} = [1,N]$ Set of discrete states at each stage
$\omega_s \in \Omega_s$ Noise in sample space at stage s
$m \in \mathscr{M}$ Set of discrete scenarios from noise probability distribution
$e \in \mathscr{E}_b$ Set of EES at bus b
$g \in \mathscr{G}_b$ Set of thermal generation units at bus b
$r \in \mathscr{R}_b$ Set of VRE generation units at bus b
$d \in \mathscr{D}_b$ Set of loads at bus b

Parameters

P_g^{max} Maximum active power for thermal generator g
$P_{r,t}^{max}$ Theoretical maximum generation solar power system r, time t
$\phi_{r,s}$ Clearness index solar power system r, stage s
ρ_m Noise probability scenario m
$PD_{d,t}$ Active power demand forecast load d, time t
B_{ik} Imaginary component of admittance matrix element ik
$\Theta_b^{min}/\Theta_b^{max}$ Minimum/maximum voltage angle at bus b
P_{ik}^{max} Maximum transmission capacity for line between bus i,k
C_g Generator g marginal operating cost
C_d Load d marginal shedding cost
X_n Discrete state n
ΔT_t Step length at time t
SOC_e^{min}/SOC_e^{max} Minimum/maximum SOC at storage e, time t
$PS_{e,t}^c/PS_{e,t}^d$ Maximum charge/discharge power at storage e, time t
$\beta_{q,s,n}$ Spline coefficient order q, discrete state n at stage s
η^c/η^d EES charge/discharge efficiency

Variables and Functions

x_s/x_s' Incoming/outgoing state variables at stage s
$\bar{x}_s$ Incoming state dummy variable at stage s
u_s Control variable at stage s
$U_s(x_s,\omega_s)$ Control variable feasibility set at stage s
$T_s(x_s,u_s,\omega_s)$ Stage-transition function between stage s and $s+1$
$C_s(x_s,u_s,\omega_s)$ Stage-objective function at stage s
$V_s(x_s,\omega_s)$ Future cost function at stage s
$\pi_s(x_s,\omega_s)$ Decision-rule function at stage s
$\lambda_{s,n}$ State variable dual value at stage s, discrete state n
$p_{b,t}$ Active power injection at bus b, time t
$p_{g,t}$ Active power thermal generator g, time t
$p_{r,t}$ Active power from solar power system r, time t
$p_{e,t}$ Active power withdrawn by storage e, time t
$ps_{e,t}$ Net power charged to storage e
$ps_{e,t}^c/ps_{e,t}^d$ Power charged to/discharge from storage e, time t
$soc_{e,t}$ Energy storage e SOC, time t
$p_{d,t}$ Active power withdrawn by load d, time t
$pls_{d,t}$ Shedding of load d, time t
$\theta_{b,t}$ Voltage angle at bus b, time t
$SEV_s(x_s)$ Storage end value function at stage s
$SMV_s(x_s)$ Storage marginal value function at stage s
sev_s Storage end value variable at stage s
$B_{q,s,n}(x_s)$ Spline order q, discrete state n at stage s
$\Pi_n(x_s)$ Spline activation function discrete state n

[22]. Since the approach is based on duration curves, the storage size limitations are not accounted for.

The similarities between the hydro power dominated electricity markets, such as the Nordic market, and markets with high penetration of VRE and EES, are interesting when studying the market equilibrium and the corresponding electricity prices. The marginal cost pricing principle is also used in these markets [23], and the marginal value for hydro power plants has been studied for decades [24]. In contrast to VRE and thermal generation, the marginal value for a hydro power plant is not given by its operational costs but the future opportunity value of saving the stored energy for later rather than using it now [25].

The marginal value of EES, hereby referred to as the Storage Marginal Value (SMV), is actually a function of both time, due to variations in generation and demand, and EES State-Of-Charge (SOC) as the capacity for avoiding expensive generation or load curtailment in the future depends on the current SOC. The SMV will therefore also be a function of the SOC of other EES' in the system [26] since the risk of scarcity depends on the total energy stored in the system and potential grid congestion associated with the EES locations. Although the proposed method supports multiple EES [27], this paper will study a single aggregated storage. Moreover, both generation from VRE and demand are subject to uncertainty. Seen from a system perspective, the future SOC depends on the realizations of the uncertainty and will therefore also influence the future electricity price. Since the operation strategy may be corrected multiple times as the uncertainty is revealed, the problem is tractable to formulate as a multi-stage stochastic model. Geske and Green [28] points out that if EES capacity replaces some generation capacity, the optimal EES strategy must balance arbitrage against the risk of not being able to meet the system demand. The electricity price can in this case be seen as an arbitrage against risk of extreme prices.

The implications on electricity prices caused by large-scale integration of VRE and EES have until now been studied for systems where dispatchable generation technologies are still the backbone of the electricity system. This paper goes one step further and analyses the implications on a power system when VRE is the dominating source of power generation, and the system relies on EES to secure the supply.

This paper presents a multi-stage stochastic optimization model of an electricity system with VRE and EES seen from a system perspective and solves it with Stochastic Dynamic Programming (SDP) [29]. The model formulation is based on Multi-Period Optimal Power Flow (MP-OPF) [30].

The solution of the model yields the SMV for all time steps as a function of SOC as a cubic spline function. The SMV indicates the operating strategy for that particular EES in a wholesale market. Moreover, by simulating several scenarios sampled from the probability distribution, a range of possible electricity prices can be generated yielding a probabilistic electricity price for all buses in the entire system. The resulting electricity price will be studied to illustrate the effect of introducing VRE and EES in a power system dominated by thermal generation, thus confirming the results from previous studies and the correctness of the proposed model. Finally, the electricity price in a system with only VRE and EES will be studied where the price is set by the risk of extreme prices caused by scarcity.

The contributions of this paper can be summarized as follows:

i) A novel SDP model for electricity system optimization including EES and uncertainty. The model embeds MP-OPF as stage-wise models, and connects them through cubic spline end value functions generated from the state variable dual values.

ii) The storage end value for the final stage is updated iteratively to simulate infinite horizon optimization.
iii) The electricity price is studied first for a traditional power system with thermal generation, followed by systems including VRE and EES. Finally, the price is studied for a system with only VRE and EES.
iv) The interpretation and usage of the storage marginal value function are discussed.

The remainder of this paper is organized as follows: Section 2 describes the optimization method used to find the SMV and Locational Marginal Price (LMP), Section 3 presents numerical data used to illustrate the energy price in a system dominated by thermal generation compared to VRE generation, Section 4 presents the results using the described method in combination with the presented numerical data, Section 5 discusses the implications of the presented results, and Section 6 draws the conclusions and presents possible directions for future work.

2. Method

This section presents a detailed description of the multi-stage stochastic optimization problem used to study the optimal operation and the corresponding electricity price in a constrained power system with VRE generation and EES under uncertainty, exemplified by the system in Fig. 1. The presented solution method combines SDP and MP-OPF.

2.1. Multi-stage stochastic programming

The goal with the proposed optimization problem is to find the optimal operation of generators, EES and loads, and to study the resulting LMP and SMV. The objective is to minimize operation costs. The ability to deliver and absorb energy from an EES depends on its SOC, and the SOC depends on the operation strategy and the realization of uncertain variables. The SOC and other variables coupled in time, hereby referred to as state x_s, will therefore require additional attention. Due to uncertainty in generation and load, the resulting operation strategy of a deterministic model formulation will often in practice be sub-optimal, and could even be infeasible due to the differences in the predicted and the actual generation and load. A more robust and realistic approach is to assume the uncertainty is revealed stage-wise as time elapses, and that the operation strategy also can be corrected stage-wise as more uncertainty becomes known. These assumptions makes the problem tractable to formulate as a multi-stage stochastic optimization problem.

The following stochastic programming terminology is based on Dowson [31]. Instead of solving the stochastic optimization problem as one large problem, it is broken down into a sequence of smaller stage-wise problems. Each stage $s \in \mathscr{S}$ represents a discrete moment in time where uncertainty is revealed and a decision is made. The stage objective represents the operation costs, such as generation and load shedding costs. The decision process for each stage is illustrated in Fig. 2, where the decision-rule $\pi_s(x_s, \omega_s)$ chooses a control u_s that respects the set of admissible controls such that $u_s \in U_s(x_s, \omega_s)$. The overall goal is to find a policy, a sequence of decision-rules $\pi = \{\pi_1, \cdots, \pi_S\}$, that minimizes the sum of all the stage objectives $C_s(x_s, u_s, \omega_s)$.

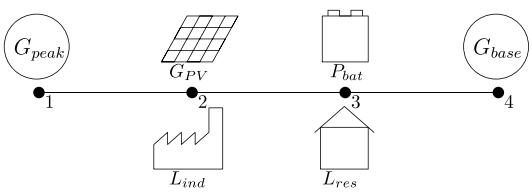

Fig. 1. Power system topology.

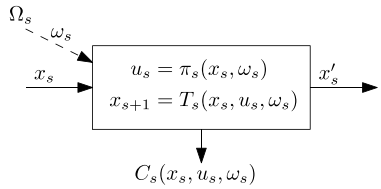

Fig. 2. Multi-stage stochastic optimization decision node [31]

The stages divide the full problem into smaller sub-problems in a similar manner as continuous time problems are divided into discrete time steps. The time between stages, the stage length, is a compromise between accuracy and computational burden but should also reflect how the system is operated. Hourly stages could be a good choice when operating in an hourly market, but the EES size and the noise variability are also important factors. At each stage, the noise $\omega_s \in \Omega_s$ is observed and assumed to be known for that stage. The noise represents the uncertainty in VRE generation, but may also include load uncertainty, and describes the possible variability in energy delivered by VRE due to uncertainty. The perfect foresight assumption for the current stage can be justified through accurate short-term forecasts and that the uncertainty has only a relatively small impact on the state for a single stage.

The noise in the model formulation should be stage-wise independent, signifying that the observed noise at a stage does not influence the noise in the next stage. In other words, if it is more sunny than expected at one stage such that the VRE generation is increased, it will not influence the probability of increased generation at the next stage. This assumption might be inaccurate and could be compensated for by including the VRE generation in the state with, for example, an autoregressive model [32,33].

For this particular system, the state is given by the EES SOC. The capability of delivering energy from the EES depends on sufficiently high SOC, and the capability of absorbing energy depends on sufficiently low SOC. In contrast, dispatchable generators can freely change the generation independent of generation in the previous stage (unless ramping limitations must be accounted for).

The control variable represents all the decisions made to balance generation and load, such as how much the different generators should deliver, and how much the EES should deliver or absorb. VRE generation curtailment and load shedding are also decisions in the control variable. All these decisions must be admissible $u_s \in U_s(x_s, \omega_s)$ such that that generation minimum and maximum limits, EES charge/discharge limits, load shedding limits and generation curtailment limits are respected, and the network is not overloaded.

The transition function $T_s(x_s, u_s, \omega_s)$ describes how the state evolves for a given control and observed noise, in this case how the EES SOC changes given the decisions for how to meet the load and the observed generation for the current stage. The stage-objective $C_s(x_s, u_s, \omega_s)$ represents the corresponding operation costs related to generation costs and load shedding.

2.2. Stochastic dynamic programming

According to Bellman's principle of optimality [29], the optimal policy can be found by solving the optimization problem recursive. By assuming the future optimal decisions are known, the optimal decision for the current stage can also be found. Moreover, the entire problem can then be solved with backward recursion. The resulting recursive optimization problem is shown in Eq. 1.

$$\begin{aligned} V_s(x_s, \omega_s) &= \min_{u_s} \left\{ C_s(x_s, u_s, \omega_s) + \mathop{\mathbb{E}}_{\omega_{s+1} \in \Omega_{s+1}} \left[V_{s+1}\left(x'_s, \omega_{s+1}\right) \right] \right\} \\ \text{s.t. } x'_s &= T_s(x_s, u_s, \omega_s) \\ u_s &\in U_s(x_s, \omega_s) \end{aligned} \tag{1}$$

This problem will be solved with a SDP method called the water value method from hydro power optimization [25]. The expectation of the future costs is replaced with the Storage End Value (SEV) as shown in Eq. 2.

$$\begin{aligned} &\min_{u_s}\{C_s(x_s,u_s,\omega_s) - sev_{s+1}\} \\ &\text{s.t. } x_s^{'} \;=\; T_s(x_s,u_s,\omega_s) \\ &sev_{s+1} \;\leq\; SEV_{s+1}\left(x_s^{'}\right) \\ &u_s \;\in\; U_s(x_s,\omega_s) \end{aligned} \tag{2}$$

The objective function of the presented optimization problem in Eq. 2 has a very interesting structure. The first term represents the operational costs of the current stage, often referred to as the immediate costs, while the second term represents the SEV and is a function of the outgoing state. Just like the generation marginal cost C_g is given by the derivative of the cost function with respect to the generation p_g Eq. 3, the marginal value of the state (here SOC) is given by the derivative of the SEV function with respect to the state Eq. 4. Numerical examples in Section 4 will provide a clearer understanding of the relation between SMV, generator marginal cost and their applications.

$$C_g = \frac{dC}{dp_g} \tag{3}$$

$$SMV_s(x_s) = \frac{dSEV_s(x_s)}{dx_s} \tag{4}$$

However, the marginal value of the state is a function of both state and stage. In other words, the marginal value of the EES depends on its SOC and stage due to the variability in future expected generation and load. Since it is difficult to solve the optimization problem with respect to a continuous state variable x, it is discretized into N discrete states. Each stage-wise optimization problem is solved for each discrete state $n \in \mathcal{N}$ and each scenario $\omega_s \in \Omega_s$. The solution of the optimization problems forms the basis for approximating the SEV function. This approximation is described in Section 2.3, and a procedure for finding the SEV for the final stage is described in Section 2.3.1. The SEV function $SEV_s(x_s)$ is convex if the sub-problem given by $C_s(.), T_s(.), U_s(.)$ is convex in x_s, ω_s and is therefore expressed as a convex relaxation in Eq. 2 (although SDP also permits non-linear sub-problems).

2.3. Storage end value function

The SEV function will be expressed as a cubic spline function yielding a smooth function, as illustrated in Fig. 3, demanding fewer discrete states than a piece-wise linear approximation [27]. A spline function is a piece-wise polynomial function composed of polynomials up to degree q with continuous derivatives up to the order $q-1$. A cubic spline will therefore have piece-wise cubic segments, and continuous derivatives up to the order of two. This makes it possible to embed the SEV function into a non-linear optimization problem where all the constraints and the objective must be twice continuously differentiable in order to solve the problem with interior point based methods.

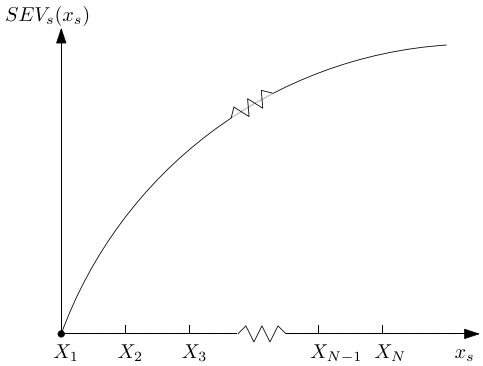

Fig. 3. Storage end value function.

The SEV function is approximated using the marginal value given by the dual value of the state x. The initial value of the SEV function can also be chosen arbitrarily and is set to zero such that the SEV of empty storage is zero. By adding the dummy variable $\overline{x}_s$ and the constraint Eq. 5 to the optimization problem in Eq. 2, the corresponding dual variable λ_s will represent the marginal value of SEV function with respect to the state x [34]. Let λ_{s,n,ω_s} denote the dual value at stage s for the discrete state n and the noise ω_s such that the expected dual value $\lambda_{s,n}$ for stage s and discrete state n is given by Eq. 6.

$$x_s = \overline{x}_s, \quad | \quad \lambda_s \tag{5}$$

$$\lambda_{s,n} = \mathop{\mathbb{E}}_{\omega_s \in \Omega_s}\left[\lambda_{s,n,\omega_s}\right] \tag{6}$$

The SEV function Eq. 7 is expressed as a sum of polynomials Eq. 8 multiplied with an activation function Eq. 9 defined such that the correct spline segment is activated.

$$SEV_s(x_s) = \sum_{n=1}^{N-1} B_{q,s,n}(x_s)\ \Pi_n(x_s), \tag{7}$$

$$B_{q,s,n}(x_s) = \sum_{\eta=0}^{q} \beta_{\eta,s,n}(x_s - X_n)^{\eta}, \tag{8}$$

$$\Pi_n(x_s) \;=\; \begin{cases} 1, & \text{if } X_n \leq x_s < X_{n+1} \\ 0, & \text{otherwise} \end{cases} \qquad s \in \mathcal{S}, n \in \mathcal{N}\backslash\{N\} \tag{9}$$

Each spline segment Eq. 8 of a cubic spline is uniquely defined by the four coefficients $\beta_{\eta,s,n} \mid \eta \in [0,q]$. If spline segment n is known, then the value and derivatives up to order two of segment $n+1$ are also given at the intersection between segment n and $n+1$. Therefore, segment $n+1$ has only one degree of freedom and can be fitted using the derivative at the next intersection. The initial value of the first segment and and the initial second order derivative is also assumed to be zero. The spline function can therefore be found by solving the set of equations in Eq. 10.

$$\begin{aligned} B_{3,s,1}(0) &= 0, \\ B_{3,s,1}^{''}(0) &= 0, \\ B_{3,s,n}^{'}(X_n) &= \lambda_{s,n} \\ B_{3,s,n}(X_{n+1}) &= B_{3,s,n+1}(X_n) \\ B_{3,s,n}^{'}(X_{n+1}) &= B_{3,s,n+1}^{'}(X_n) \\ B_{3,s,n}^{''}(X_{n+1}) &= B_{3,s,n+1}^{''}(X_n) \\ & s \in \mathcal{S},\ n \in \mathcal{N}\backslash\{N\} \end{aligned} \tag{10}$$

2.3.1. Storage end value boundary conditions

The presented storage optimization problem has in reality infinite horizon. Stage s in the SDP algorithm uses the SEV function generated in stage $s+1$ as the boundary condition for the stage-wise optimization problem. The final stage, which is optimized first due to the backward recursion, does not have any SEV function generated by the subsequent stage. If the SEV at the end of the final stage is not properly defined, the storage will typically be emptied. The end state can also be bounded by a fixed value [35–37]. However, this paper proposes an iterative SEV update procedure to approximate the SEV at the end of the final stage. The SEV function for the final stage is initially estimated by assuming that the slope equals the value of lost load for minimum SOC and the slope is zero for maximum SOC. The SEV function at the final stage is thereafter updated iteratively with the SEV function from the first stage until the solution converges. This is equivalent to solving the problem repeatedly such that the choice of final end value does not influence the

solution, and could be considered as equivalent with infinite horizon [25].

2.4. Multi-period optimal power flow

The stage-wise optimization problem Eq. 2 is given by a MP-OPF problem. The incoming state is given by the initial SOC and the outgoing state by the end SOC as shown in Eq. 11 and 12.

$$x_s = \left\{ soc_{e,\underline{t}_s} \right\} \tag{11}$$

$$\begin{aligned} x_s^{'} &= \left\{ soc_{e,\tilde{t}_s} \right\} \\ &\forall e \in \mathscr{E}_b, b \in \mathscr{B} \end{aligned} \tag{12}$$

All other variables are control variables, either given explicitly such as the generation, or implicitly like the bus voltage angle that follows from the other decisions as shown in Eq. 13. Moreover, the SOC variables not part of the state are included here and have therefore been assigned to a different subset of the time steps denoted $\tilde{t}$ in Eq. 13.

$$\begin{aligned} u_s = &\left\{ p_{b,t}, p_{g,t}, p_{r,t}, p_{e,t}, ps^c_{e,t}, ps^d_{e,t}, p_{d,t}, pls_{d,t}, soc_{e,t}, \theta_{b,t} \right\} \\ &\forall b \in \mathscr{B}, g \in \mathscr{G}_b, r \in \mathscr{R}_b, e \in \mathscr{E}_b, d \in \mathscr{D}_b, t \in \mathscr{T}_s, \tilde{t} \in \mathscr{T}_s \backslash \left\{ \underline{t}_s, \tilde{t}_s \right\} \end{aligned} \tag{13}$$

Finally, the noise of this model is the clearness index (CI) as shown in Eq. 14. The relation between CI and generation is described in Section 2.4.1, and a comprehensive introduction to CI is given in Section 2.5.1. The CI is sampled from a beta distribution, as described in Section 2.5.2.

$$\omega_s = \left\{ \phi_{r,s} \right\} \quad \forall r \in \mathscr{R}_b, b \in \mathscr{B} \tag{14}$$

2.4.1. Power flow

The power flow equations describe the relation between bus power injections and voltages at buses in a power system and form the key constraints for the Optimal Power Flow (OPF) optimization problem. All the power flow equations are included in the set of admissible control $U_s(x_s, \omega_s)$.

There exist many different OPF formulations, both exact models, approximations and relaxations, and they can be expressed in terms of bus injections or branch flows [38,39] either in rectangular or polar form [40]. The AC-OPF [41] provides an exact solution for the OPF problem, but due to the non-convex nature of the power flow equations, a global optimal solution cannot be guaranteed. The DC-OPF is linear, and derived by neglecting the line resistance and reactive power, assuming unity voltage magnitude and small voltage angles. The method is computationally efficient, easy to implement and widely used, but must be used carefully as it can deviate significantly from AC-OPF on constrained lines and therefore give inaccurate LMP [42].

To also account for the dynamic behavior of energy storage, the OPF formulation is repeated for each time step, and energy storage equations are included yielding the multi-period OPF.

This paper will use the DC MP-OPF, but the proposed method will work for any convex MP-OPF formulation. The DC power flow neglects the line resistance and assumes small voltage angles such that $\sin(\theta_i - \theta_k) \approx \theta_i - \theta_k$. The resulting bus power injections are given by Eq. 15, the line power is bounded by Eq. 16 and the voltage angle must stay within its limits Eq. 17.

$$p_{b,t} = \sum_{(i,k) \in \mathscr{L}_b} B_{ik} \left(\theta_{i,t} - \theta_{k,t} \right) \tag{15}$$

$$-P^{max}_{ik} \leq B_{ik} \left(\theta_{i,t} - \theta_{k,t} \right) \leq P^{max}_{ik} \tag{16}$$

$$\Theta^{min}_b \leq \theta_{b,t} \leq \Theta^{max}_b \tag{17}$$

To balance generation and load, the bus power injection is given by the sum of generation from both thermal and renewable generators minus loads and energy storage charging for all the units on the respective bus Eq. 18.

$$p_{b,t} = \sum_{g \in \mathscr{G}_b} p_{g,t} + \sum_{r \in \mathscr{R}_b} p_{r,t} - \sum_{e \in \mathscr{E}_b} p_{e,t} - \sum_{d \in \mathscr{D}_b} p_{d,t} \tag{18}$$

The thermal generation must not exceed its maximum generation and can be operated continuously from zero to maximum Eq. 19. The VRE generation is shown in Eq. 20. The maximum VRE generation is time dependent and is bounded by the theoretical maximum $P^{max}_{r,t}$ multiplied by a scale factor sampled from the uncertainty distribution and is further described in Section 2.5.1. Note that this representation of uncertainty is specific for solar PV generation. The load can be curtailed where the cost is given by the scarcity price Eq. 21.

$$0 \leq p_{g,t} \leq P^{max}_g \tag{19}$$

$$0 \leq p_{r,t} \leq \phi_{r,s} \cdot P^{max}_{r,t} \tag{20}$$

$$p_{d,t} = PD_{d,t} - pls_{d,t} \geq 0 \tag{21}$$

2.4.2. Electric energy storage

The EES SOC at a time step equals the SOC at the previous step plus the power charged $ps^c_{e,t}$ minus the power discharged $ps^d_{e,t}$ compensated for the efficiency losses η^c, η^d that includes both converter and battery losses Eq. 22. The power withdrawn from the bus equals the power charged minus the power discharged Eq. 23, and the energy storage upper and lower bounds are enforced by Eq. 24. The EES maximum charge and discharge power due to, for example, converter and battery limitations are enforced by Eq. 25 and 26.

$$soc_{e,t} = soc_{e,t-1} + \Delta T_t \left(\eta^c ps^c_{e,t} - \frac{ps^d_{e,t}}{\eta^d} \right), \forall t \in \mathscr{T}_s \backslash \left\{ \underline{t}_s \right\} \tag{22}$$

$$ps_{e,t} = ps^c_{e,t} - ps^d_{e,t} \tag{23}$$

$$SOC^{min}_e \leq soc_{e,t} \leq SOC^{max}_e \tag{24}$$

$$0 \leq ps^c_{e,t} \leq PS^c_{e,t} \tag{25}$$

$$0 \leq ps^d_{e,t} \leq PS^d_{e,t} \tag{26}$$

The state transition function $T_s(x_s, u_s, \omega_s)$ is given by the energy balance equation Eq. 22 when $t = \tilde{t}_s$. The energy balance for other values of t and the remaining constraints Eq. 23, 24, 25 and 26 are in the set of admissible controls $U_s(x_s, \omega_s)$.

2.4.3. Objective

A common OPF objective is minimizing the operating costs accounting for the constraints and losses in the grid. Recall that under perfect competition, the solution of global cost minimization equals profit maximization for each individual unit, and the dual values of the bus power balance from the OPF solution, also known as LMP, represents the electricity price for that bus. The objective in this case is to minimize the sum of generator operating costs and load shedding costs. The costs are given by constant marginal costs and must be summed for all generators and loads at all buses for all time steps as shown in Eq. 27, and define the stage-objective $C_s(x_s, u_s, \omega_s)$ in the SDP formulation in Eq. 2.

$$C_s(x_s, u_s, \omega_s) = \sum_{b \in \mathscr{B}} \sum_{t \in \mathscr{T}_s} \left(\sum_{g \in \mathscr{G}_b} C_g \; p_{g,t} + \sum_{d \in \mathscr{D}_b} C_d \; pls_{d,t} \right) \Delta T_t \tag{27}$$

2.5. Noise

This paper will study the effect of uncertainty from solar PV generation in combination with energy storage. Demand uncertainty will have similar implication on the result, but this has not been analyzed.

2.5.1. Solar PV forecasting

Solar PV forecasting can be grouped into statistical and physical methods, or a combination of these. The statistical methods exploit the properties of historical data, while the physical methods include Numerical Weather Prediction (NWP), sky imagery and satellite imaging. The forecasting technique for solar PV generation is highly dependent on forecasting horizon. Statistical methods are commonly used for short-term forecasts up to six hours, while NWP is used for forecasts up to 15 days ahead [43].

The maximum generation from solar PV depends on the PV panel's size, geographical location, direction and angle, and the time of day and year. Weather type also has a significant impact on the generation, and is commonly classified into different categories, such as *clear sky, partly clouded* and *overcast*. The weather type influences both the total daily generation as well as the generation variability [44]. A sunny day will, for example, provide stable high generation with low uncertainty, while the generation will fluctuate rapidly on partly clouded days due to the rapid changes in cloud cover.

The CI is the ratio between actual generation and the theoretical maximum at that time and location Eq. 28. The CI value is between 0 and 1 and quantifies how much the solar radiation passes through the clouds. It is commonly used for statistical analysis of the solar PV generation.

$$\phi_{r,s} = \frac{p_{r,t}}{P^{max}_{r,t}} \tag{28}$$

A probabilistic model for the CI will be used in this paper, where the expected value and variance are assumed to be known ahead. The CI is always between 0 and 1, which also applies for the beta distribution that is commonly used for solar PV CI [45–47]. The CI $\Phi_{r,s}$ is undefined for the hours where the theoretical maximum generation is zero due to zero division, but the resulting generation will of course be zero.

2.5.2. Beta distribution

The probability density function (PDF) of the beta distribution on standard form is shown in Eq. 29 where $B(1;\alpha,\beta)$ is a distribution specific constant given by the beta function Eq. 31 that ensures the distribution sums up to one. The cumulative distribution function is shown in Eq. 30.

$$f(x;\alpha,\beta) = \frac{1}{B(1;\alpha,\beta)} x^{\alpha-1}(1-x)^{\beta-1} \tag{29}$$

$$F(x;\alpha,\beta) = \frac{B(x;\alpha,\beta)}{B(1;\alpha,\beta)} \tag{30}$$

$$B(\alpha,\beta) = \int_0^x t^{\alpha-1}(1-t)^{\beta-1} dt \quad \alpha,\beta \geq 0,\ 0 \leq x \leq 1 \tag{31}$$

For a known expected value μ and variance σ^2, the beta distribution coefficients can be found from Eq. 32 and 33 [48].

$$\alpha = \frac{\mu^2(1-\mu)}{\sigma^2} - \mu \tag{32}$$

$$\beta = \left(\frac{\mu(1-\mu)}{\sigma^2} - 1\right)(1-\mu) \tag{33}$$

2.5.3. Uncertainty sampling

The noise in SDP must be stage-wise independent. However, dependencies in noise across stages can be respected by modelling the noise with state variables, but will also increase the dimensionality of the optimization problem and thus have not been accounted for in this paper.

The true continuous probability distribution must be represented with a discrete probability distribution with M discrete points ϕ_m and their corresponding probability ρ_m, where the probabilities sums up to one Eq. 34. By selecting initial probabilities $\widehat{\rho}_m$, the corresponding boundary values $\delta_1, \cdots, \delta_{M-1}$ where $0 = \delta_0 < \delta_1 < \cdots < \delta_{M-1} < \delta_M = 1$ can be found numerically from Eq. 35. Let $\widehat{\phi}_m$ represent an initial solution given by the expected value in the corresponding interval $[\delta_{m-1}, \delta_m]$ as shown in Eq. 36.

$$\sum_{m\in\mathscr{M}} \rho_m = 1 \tag{34}$$

$$\rho_m = \int_{\delta_{m-1}}^{\delta_m} f(\phi)\, d\phi,\ m \in \mathscr{M} \tag{35}$$

$$\widehat{\phi}_m = \frac{\int_{\delta_{m-1}}^{\delta_m} \phi f(\phi)\, d\phi}{\int_{\delta_{m-1}}^{\delta_m} f(\phi)\, d\phi},\ m \in \mathscr{M} \tag{36}$$

The discrete distribution given by $\widehat{\rho}_m, \widehat{\phi}_m$ will give the same expected value as the true distribution, but the variance will be lower. Let ρ_m, ϕ_m represent the improved discrete distribution for the boundary values δ_m. The improved discrete distribution can be found by minimizing the squared difference between the initial distribution points $\widehat{\phi}_m$ and ϕ_m, constrained such that expected value and variance from continuous distribution are conserved [49].

$$\begin{aligned} \min_{\rho,\phi} \quad & \sum_{m\in\mathscr{M}} \rho_m \left(\phi_m - \widehat{\phi}_m\right)^2 \\ \text{subject to} \quad & \sum_{m\in\mathscr{M}} \rho_m = 1 \\ & \sum_{m\in\mathscr{M}} \rho_m \phi_m = \mu \\ & \sum_{m\in\mathscr{M}} \rho_m {\phi_m}^2 = \mu^2 + \sigma^2 \end{aligned} \tag{37}$$

2.6. Simulation

A multi-stage stochastic optimization model provides a strategy for how to optimally operate at a given stage and state for a given realization of the noise. A simulation of multiple scenarios can give a probabilistic LMP and SMV. The scenarios are sampled from the noise distribution(s) and optimized with the stage-wise MP-OPF models beginning at the first stage and using the final state for each stage as the initial state for the next state. This procedure is similar to the one described in Fosso et al. [23] and is shown in Algorithm 1.

2.7. Model summary

The SDP optimization procedure is illustrated in Fig. 4, where stages are shown at the x-axis and the discrete states at the y-axis. Each stage-wise problem s is solved for each discrete state n and each scenario m, and a SEV-function is approximated using the expected gradients $\lambda_{s,n}$ for each discrete state n. The stage-wise problems are repeated extensively in Appendix A. Algorithm 2 summarizes the optimization procedure where ϵ is a convergence threshold.

3. Implementation and numerical values

This section presents implementation details, system topology and the numerical data that will be used to demonstrate the optimal operation and the corresponding prices in a power system with uncertain variable renewable generation and energy storage.

The optimization problem is implemented in the programming language Julia (1.4) using the JuMP modelling language (0.21.3) [50] with the non-linear solver Ipopt (0.6.2) [51]. The power flow equations have

Initialize x_1
for $s \in \mathcal{S}$ **do**
  Sample scenario $\omega_s \in \Omega_s$
  Solve (2) and (5)
  Save LMP (dual value of (18))
  Save SMV (dual value of (23))
  Save EES SOC ($soc_{e,t}$ from (23))
  Initialize incoming state for the next stage with outgoing state of current stage: $x_{s+1} \leftarrow x'_s$
end for

Algorithm 1. Simulation algorithm.

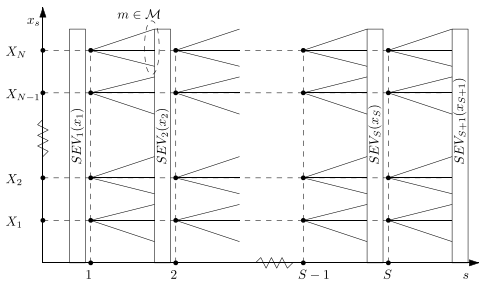

Fig. 4. Stochastic dynamic programming solution procedure.

been implemented using PowerModels (0.17.1) [52] with the multi-period description from [53].

3.1. System topology

Fig. 1 shows the system topology, where bus 1 has an expensive peak generator, bus 2 industrial loads and VRE generation in terms of solar PV, bus 3 has residential loads and battery storage, and bus 4 has a cheaper base generator. The base generator typically represents combined cycle gas turbines (CCGT), where the investment cost is high, and the marginal operating cost is low. The peak generator typically represents open cycle gas turbines (OCGT) where the investment cost is lower and the marginal operating cost is higher. The base generator demands a relatively higher duration compared to the peak generator in order to be profitable. Thermal plants also have limitations in start-up time, ramping rates, minimum generation limits and marginal operating cost varying with generation [54], which have not been modelled in this paper. Section 3.6 presents the combination of generation capacities that will be analyzed in Section 4.

3.2. Time steps and stages

The time step length in the MP-OPF problems is one hour, and there are three time steps between each stage. That means perfect foresight three hours ahead at a stage, and that the uncertainty in the next stage is revealed every three hours. The planned operation will also be adjusted every three hours.

3.3. Solar PV clearness index

The CI expected value and variance are assumed to be known ahead based on forecasts. Three different weather types are used: sunny, partly clouded and overcast. Both the continuous and discrete probability distributions are shown in Fig. 5 as well as the expected value and standard deviation, and assumes a similar pattern as described in [44]. The discrete probability distribution has been obtained using the method described in Section 2.5.3 with probability intervals 5%, 20%, 50%, 20% and 5%. Table 1 shows the sequence of weather types for the respective days used in the simulations. The probability distribution and the maximum PV generation are shown in Fig. 6.

The SDP algorithm does not propose a single solution to the problem, but an operation strategy for all state combinations at any time. To verify the strategy, different scenarios are sampled using the continuous probability distribution, and simulated based on the SDP strategy.

For real-time operation, the ideal solution is to update the CI forecast, and the corresponding operation strategy as often as possible. It is

Initialize $SEV_{S+1}(x_{S+1})$
repeat
  for $s \in reverse(\mathcal{S})$ **do**
    for $n \in \mathcal{N}$ **do**
      for $\omega_s \in \Omega_s$ **do**
        Solve (2) and (5) for $x_s = X_n$ and ω_s
      end for
      Find $\lambda_{s,n}$(6)
    end for
    Approximate $SEV_s(x)$, equation (7) to (10)
  end for
  $SEV_{S+1}(x) \leftarrow SEV_1(x)$
until Terminate when final end value function has converged: $\left|SEV_{S+1}(X_n) - SEV_1(X_n)\right| < \epsilon,\ \forall\, n \in \mathcal{N}$

Algorithm 2. SDP algorithm.

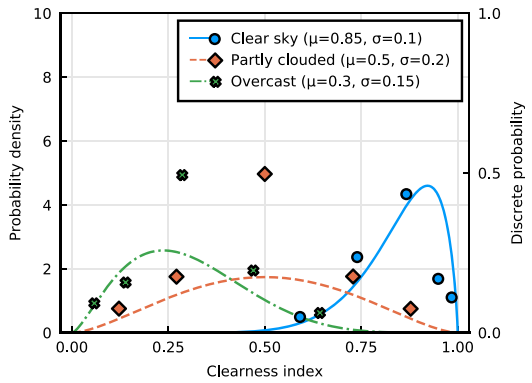

Fig. 5. Continuous and discrete probability distributions of clearness index for different weather types with 5 samples per distribution.

Table 1
Expected value and standard deviation of clearness index beta distribution for the simulated days.

Day	Weather type
1	Partly clouded
2	Partly clouded
3	Sunny
4	Overcast
5	Overcast
6	Sunny
7	Overcast

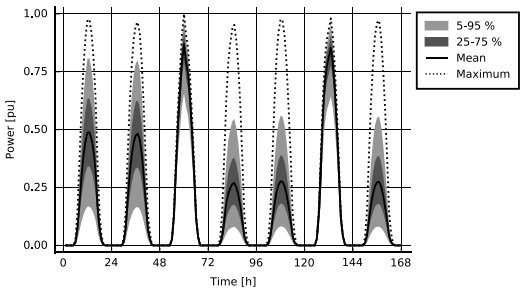

Fig. 6. Solar PV one week probabilistic profile.

also possible to use a combination of different forecasting techniques to cover the different time horizons as accurately as possible. In this paper, the prices and operation are only studied from one point in time.

3.4. Load forecast time series

The system load is typically subject to uncertainty, often represented as a Gaussian distribution. There is also often a correlation between load and VRE generation since they both depend on weather. Neither the load uncertainty nor the correlation between load and generation are not modelled in this paper such that the impact of generation uncertainty is clearer. The system has two loads, as shown in Fig. 1, an industrial and a residential load where the profiles for the loads are shown in Fig. 7, where the profiles have been generated using the FASIT model developed by SINTEF Energy Research [55]. Note that the weekday profiles

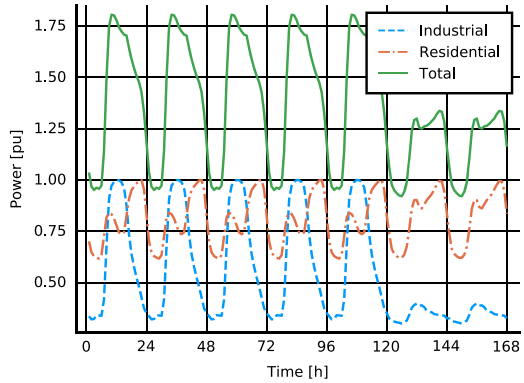

Fig. 7. Industrial and residential weekly load profile.

differ from the weekends. The time series shows the one week profile.

3.5. Generation and storage capacities and cost

The base generator has a marginal operating cost of 20 € /MWh and the peak generator 30 € /MWh, and start and stop costs are neglected. The solar PV generation and storage have zero marginal cost. The scarcity price in the system is 100 € /MWh for both loads. The storage duration is 4 hours, meaning that it takes 4 hours to empty a full battery at maximum discharge. The storage efficiency is 95% for both charging and discharging. The maximum charge and discharge power are equal.

3.6. Test cases

The price making will be studied for four different cases with different combinations of generation and storage capacities as shown in Table 2. The first case includes only thermal generation to illustrate how the price is set by the marginal unit at the respective nodes. Moreover, the next case will show how the introduction of solar PV and storage will change the price. Finally, the last case will show a system with no thermal generation to set the price. The transmission capacity between bus 2 and 3 is limited in all cases, but the maximum capacity is increased when introducing VRE.

4. Results

This section presents the numerical results of the cases outlined in Section 3. Both optimal dispatch, LMP and SMV based on the resulting marginal values will be studied.

For the examples involving stochastic solar PV generation and energy storage, the SMV is presented as a function of time and state of charge. The interpretation of the SMV will also be discussed. Optimal generation and storage operation, and energy prices are presented as percentiles based on multiple simulations using the continuous distribution of the uncertain variable.

Table 2
Test case generation, EES and transmission capacities.

Case name	Base	Peak	PV	Storage	Line 2-3 limit
Only thermal (Section 4.1)	1.5	0.5	0.0	0.0	0.7
Thermal & PV (Section 4.2)	1.5	0.5	4.0	0.0	0.7
Thermal, PV & EES (Section 4.3)	1.0	1.0	4.0	0.8	0.8
PV & EES (Section 4.4)	0.0	0.0	9.5	10.0	5.0

4.1. Only thermal generation

In a system with only thermal power generation and fixed demand, the price is set by the marginal producing unit if the capacity is higher than the load. For a congested grid, the price will also vary between the different nodes, as illustrated in this simple 4-bus system with two thermal generators and two loads.

Fig. 8a shows the two system loads and generators over the first 24 hours, and Fig. 8b shows the corresponding LMPs. The price is 20 € /MWh when the base generator can meet the entire load, and 30 € /MWh when the peak generator also must contribute. From hour 12, the LMPs are different between the nodes since the transmission line between bus 2 and 3 has reached its limit, hence the peak generation must replace some of the base generation to prevent overloading of the line. In this situation, the base generator will be the marginal unit for the residential load since it is not able to generate at maximum capacity so the two nodes get different prices.

4.2. Variable renewable generation

As explained earlier, introduction of variable renewable generation with zero marginal cost will reduce the prices when the existing generation capacities are unchanged due to the merit order effect. Solar PV generation is installed at bus 2.

The resulting generation and price are shown in Fig. 9a and b respectively. Note that the base generator gets a high ramp rate due to the high solar PV generation in the middle of the day, and the shape of the curve is often referred to as the "duck curve" [56]. The solar PV generation makes the peak generation redundant and reduces the price at both buses compared to the previous case. At the middle of the day, the transmission capacity between node 2 and 3 is insufficient to meet the demand with solar PV generation, thus the price is set by the base generator for the residential load. However, the industrial load can meet all its demand with solar PV generation that becomes the marginal generation unit at this bus, thus the price becomes zero.

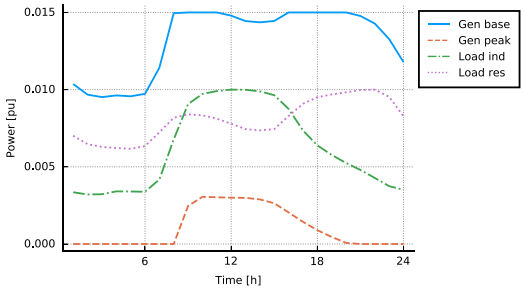

(a) Load and generation.

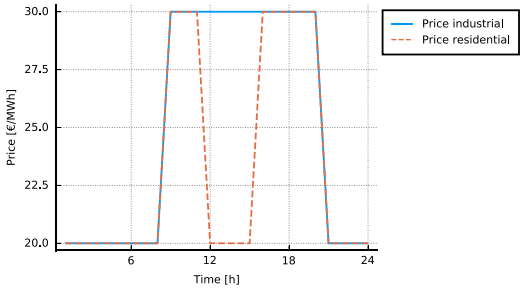

(b) System LMP.

Fig. 8. Simulation of case with only thermal generation.

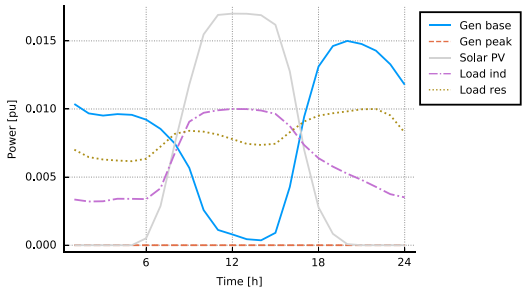

(a) Load and generation.

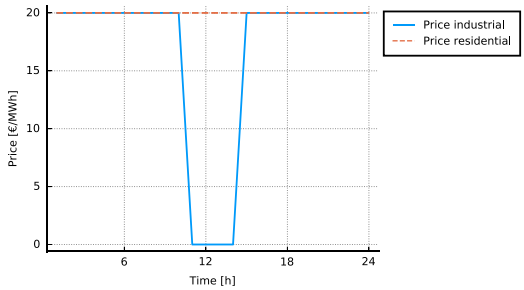

(b) System LMP.

Fig. 9. Simulation of case with thermal and solar PV generation.

4.3. Energy storage

In the previous cases, the optimal generation and energy price were only dependent on the present load and PV generation. When energy storage is introduced, the optimal strategy and the corresponding energy price also depend on the state of charge of the energy storage. Moreover, the state depends on previous decisions, which in turn are influenced by uncertainty. The stochastic result will therefore be studied for this case and the following cases.

In a competitive market, the VRE will typically displace some of the base generation that depends on a high duration to recover its costs. Some of the base capacity has therefore been replaced with peak capacity in the case setup.

Fig. 10a shows the SMV as a function of time and storage SOC. As emphasized earlier, the SMV represents the marginal future value by storing an additional unit of energy. The SMV has several interesting interpretations. Under perfect competition, the individual energy storage profit is maximized by bidding the SMV, and the solution of individual profit maximization for all units equals the system optimal solution. The SMV will therefore set the LMP when the storage is the marginal unit at that node. Since the marginal value has been found using SDP, it also captures uncertainty, hence the value represents a weighted probability of the prices of the units in the system at any time and SOC taking into account the probabilistic forecast of PV.

The optimal usage of the storage in this case involves charging from the cheap generators such that the storage can discharge later in order to avoid using the expensive generators or load shedding.

The SMV is close to zero for maximum SOC around mid-day all the days (hours 12, 36 and 60). This occurs when the solar PV generation is high, and it is likely that the battery can be charged to maximum before the solar PV generation reduces. It also indicates that the energy from the EES should be used rather than the thermal generation since the SMV is less than the marginal cost of both thermal units. The SMV is higher in the evening (hours 18, 42 and 66), when there is no or very low solar PV generation and a relatively high load. For very low SOC, the SMV is close

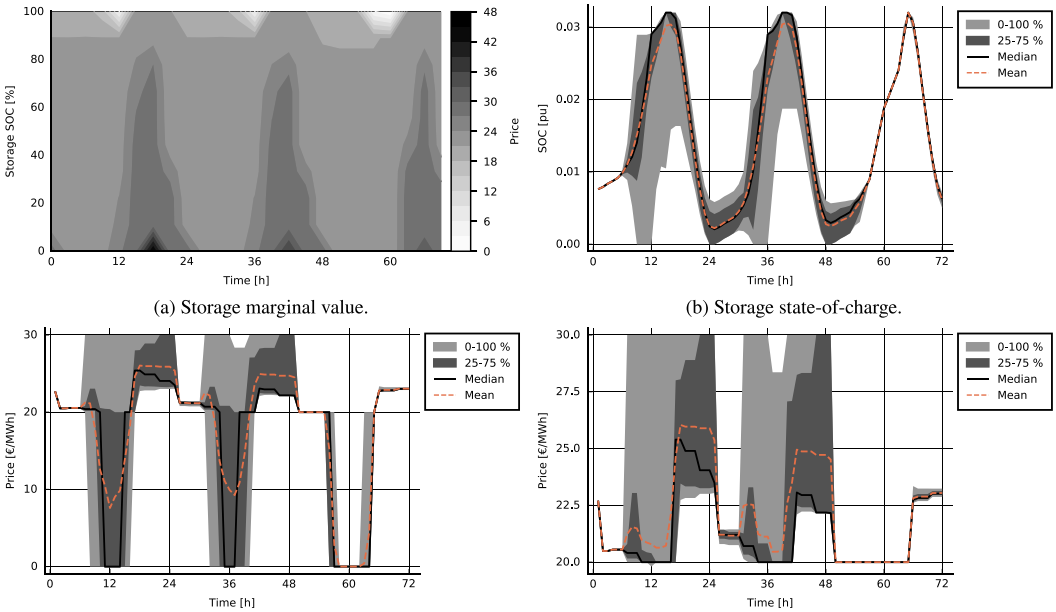

(a) Storage marginal value.

(b) Storage state-of-charge.

(c) LMP at industrial bus.

(d) LMP at residential bus.

Fig. 10. Multiple simulations of case with thermal and solar PV generation and energy storage.

to 50 and higher than the marginal cost of both thermal generators. This indicates that the thermal generators should be used rather than the EES unless the thermal generators are insufficient to prevent load shedding. The scarcity price is 100 € /MWh, and a SMV at 50 indicates a significant probability of scarcity price in this situation. Finally, observe that the SMV is between 20 and 30 in most situations. That is when the EES is used to balance the probability of being able to meet the demand with base generation versus peak generation for the different combinations of time and SOC taking into account the probabilistic forecast of PV.

Fig. 10c and d show the price percentiles for 50 simulations sampled from the continuous probability distribution of the solar PV generation at the bus with industrial loads and residential loads respectively. The price will often be zero at the industrial node around mid-day as the storage does not have capacity to store the surplus generation. At the same time, the residential node will not get zero price as the transmission capacity between the nodes is at the maximum limit. Uncertainty plays an important role in the price making for the system as the spread for both nodes is quite significant.

The resulting SOC in Fig. 10b shows that almost the entire storage capacity is utilized to minimize the generation costs.

4.4. Only renewable generation and energy storage

In the final case, the thermal units are removed completely, and the solar PV generation and EES capacity are sized up considerably. The EES must be large enough to meet all the demand through the evening and night when the solar PV is not generating. Moreover, the solar PV must be sized such that it provides enough generation for both the current demand as well as the evening/night demand - even for a day with relatively low generation. An important assumption to avoid imperfect competition is that the EES actually represents multiple aggregated EES with different operators. Otherwise, the EES operator could maximize its profit by bidding the scarcity price.

The price will now be set solely by the scarcity price, and future foresight is even more important for the electricity price. The optimization model is therefore using a one-week generation forecast.

Fig. 11a shows the SMV for all states and the corresponding expected solar PV generations are shown in Fig. 6. As observed earlier, the SMV follows the pattern from the solar PV generation. High generation reduces the marginal value of stored energy and vice versa. Another interesting observation is that due to expected low generation from hour 72, the marginal value of the storage increases upfront, indicating it is important to increase the SOC before entering the days with expected low generation. Likewise, the SMV decreases towards hour 120 as the expected generation the next day is high.

The corresponding LMPs are shown in Fig. 11c and d. The price is on average low until the end of day 3 (around hour 66), where the SOC has been built up to meet the expected low generation the next two days. However, the spread in price is high due to the high variability in generation. Then the price increases instantaneously and the further development has a high spread and high expected value. Finally, the price reduces at the end as the expected further generation is equal to the generation in the beginning.

Note that the price change is no longer dominated by the solar PV generation pattern as in previous cases, but rather the future probability of scarcity. This market price will be attractive for suppliers of flexibility capable of shifting energy over several days by utilizing the price variations. They will also get paid for reducing the risk of scarcity rather than getting paid only if scarcity occurs.

The differences between the LMP for the industrial and residential nodes occur when some of the solar PV generation is curtailed due to insufficient load and transmission capacity. The development in SOC in Fig. 11b clearly shows how the SOC is built up ahead of the period with low generation and emptied towards the period with high generation.

5. Discussion

VRE and EES play a key role in the future fully renewable energy system, and they will also have significant implications on the market equilibrium and electricity prices. As already emphasized in previous

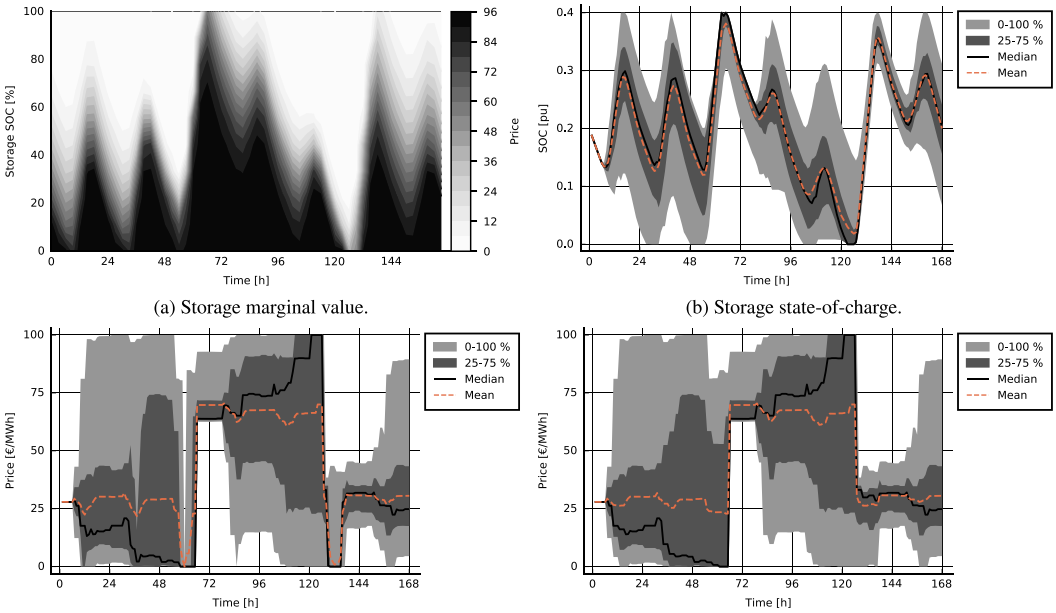

(a) Storage marginal value.

(b) Storage state-of-charge.

(c) LMP at industrial bus.

(d) LMP at residential bus.

Fig. 11. Multiple simulations of case with only solar PV generation and EES.

literature, the short-term consequence of increasing VRE generation is a reduction in electricity price due to the merit order effect as shown in Section, but also increased volatility. However, the price volatility can be reduced by EES. When uncertainty is accounted for, the combination of VRE and EES will result in a probabilistic price spanning between the price of the most and the least expensive unit.

While previous studies primarily focus on the electricity price in systems combining VRE with thermal generation, this paper also focuses on the price formation when most of the generation is supplied by VRE sources. If EES replaces some of the dispatchable capacity such that the system depends on EES to meet peak demand, scarcity may occur and load shedding can be considered as the most expensive unit. The electricity price can then be seen as an arbitrage against the risk of scarcity. An interesting consequence of this is that the scarcity price becomes effective without scarcity necessarily occurring, and the price can be seen as a precaution against scarcity.

The weighted scarcity price creates possibilities for flexible loads with marginal price below the scarcity price to enter the market. A flexible load can in its simplest form be modelled as a dispatchable negative generator, meaning that the load can be curtailed at a predetermined cost with no need of delivering the lost load at a later stage. A flexible load can also represent shifting of load, and can be modelled as an EES where a penalty applies when deviating from the ideal SOC.

Flexible loads will in general contribute to reducing the high prices by reducing the risk of scarcity. The scarcity price has a practical implication although the electricity price rarely reaches the full scarcity price. With sufficient flexibility in the system to fully eliminate the risk of scarcity, the maximum price will be set by the most costly flexible unit. Likewise, the flexible loads will also increase the low prices by reducing the risk of generation curtailment.

5.1. Future work

Possible steps towards a more practical applicable model could involve modelling of flexible demand, and also other uncertainties such as demand and generation from wind. Uncertainties are often correlated, with both auto-correlation and correlation between uncertainties. Both handling correlated uncertainty and additional EES will require new state variables, which scale poorly with SDP although the scalability can be improved using splines [27]. A more common method for handling increasing number of state variables is using Stochastic Dual Dynamic Programming (SDDP) [57], where the model formulation must be convex. The infinite horizon method suggested in this paper is not feasible to implement in SDDP, but cyclic graphs and discount factors provides an interesting alternative to infinite horizon optimization in SDDP [31].

Multi-stage stochastic models are in general computationally intensive to solve, and scalability often goes hand in hand with convexity and linearity such as for SDDP. Real-life power systems are neither linear nor convex. Thermal generators as well as hydro power plants have discontinuous production functions due to rigorous minimum generation limits, and the power flow equations are both non-linear and non-convex. Convexification and linearization must therefore be performed cautiously since the result could easily deviate from the true optimal solution. However, recent research has proposed methods to handle integer variables in the SDDP framework [58].

In a competitive market where each individual unit seeks to maximize its profit and where the price is given exogenously, it is important to also recall that the price is set by the VRE generation and demand. Additionally, there will be a strong correlation between the generation and demand uncertainty, and the price uncertainty. Managing uncertainty in price yields a non-linear optimization problem that can be handled in several ways [59,60].

EES is subject to degradation caused by its operational pattern, and Aaslid et al. [32] indicate that EES degradation could be an important factor in combination with generation uncertainty.

The proposed model will also provide storage end value functions for all stages. The end value function can be used as boundary conditions for a more detailed finite horizon storage model [61]. This principle has been described for hydro power in [62] and combines detailed storage

modelling and stochastic modelling with long foresight while still keeping the computational burden modest.

Flexibility has traditionally been provided by centralized generation units, but has to a greater extent been decentralized through flexible demand. A preferred approach is to solve operational challenges in the electricity system as close as possible to their origin. Until now, power markets have been driven by development and limitations on transmission level. However, solving problems locally demands local price signals reflecting the local challenges. A good starting point for this is to study the LMP in these systems as it can give valuable insight into how to design and operate future electricity systems with more distributed resources.

6. Conclusions

The road towards a zero emission electricity system calls for massive integration of VRE and flexibility to ensure a secure and efficient supply. These major changes will influence the price-making process in competitive markets. While capacity inadequacy is the main driver for high prices in markets dominated by thermal generation, energy inadequacy is the main driver for high price in markets dominated by VRE and EES. Managing uncertainty is crucial to balance optimal operation by reducing generation curtailment while keeping the risk of scarcity sufficient low.

This paper presents a multi-stage stochastic electricity market model including grid constraints, EES and VRE. The model uses SDP to solve a multi-stage MP-OPF problem under uncertain VRE generation, EES and administrative scarcity pricing, both with and without dispatchable generation. The stage-wise problems are interconnected with SEV functions describing the marginal value of stored energy both in time and with respect to SOC represented as cubic spline functions. The results shows how the LMP can be seen as an arbitrage between the marginal cost of the units in the system, where load shedding is the most expensive unit through the scarcity price. The SMV depends on the state of all EES in the system as well as expected future VRE generation and can be used to determine the optimal operation of EES, and will set the price when EES is the marginal generating unit.

CRediT authorship contribution statement

Per Aaslid: Conceptualization, Methodology, Software, Formal analysis, Investigation, Visualization, Writing - original draft. **Magnus Korpås:** Conceptualization, Writing - review & editing. **Michael M Belsnes:** Writing - review & editing, Project administration. **Olav B Fosso:** Writing - review & editing, Supervision.

Declaration of Competing Interest

The authors declare that they have no known competing financial interests or personal relationships that could have appeared to influence the work reported in this paper.

Acknowledgements

This work has been funded by the Norwegian Research Council under grant number 272398. The authors are grateful to the reviewers and the editor for their critical and constructive feedback. The authors would also like to thank Siri Gulaker Mathisen, SINTEF Energy Research, for constructive comments regarding the paper structure and intelligibility.

Appendix A. Summary of optimization problem

A1. Stage-wise optimization problem

$$\begin{aligned}
&\min_{u_s}\{C_s(x_s,u_s,\omega_s) - sev_{s+1}\}\\
&\text{s.t. } x_s^{'} = T_s(x_s,u_s,\omega_s)\\
&sev_{s+1} \leq SEV_{s+1}\left(x_s^{'}\right)\\
&u_s \in U_s(x_s,\omega_s)
\end{aligned}$$

A2. State variables

Incoming state is given by the initial SOC and outgoing state by the end SOC of the stage-wise problem.

$$\begin{aligned}
x_s &= \left\{soc_{e,\underline{t}_s}\right\}\\
x_s^{'} &= \left\{soc_{e,\bar{t}_s}\right\}\\
&\forall e \in \mathscr{E}_b, b \in \mathscr{B}
\end{aligned}$$

A3. Control variables

All variables except the state variables are considered control variables and are set either explicit or implicit.

$$\begin{aligned}
&u_s = \left\{p_{b,t}, p_{g,t}, p_{r,t}, p_{e,t}, ps_{e,t}^{c}, ps_{e,t}^{d}, p_{d,t}, pls_{d,t}, soc_{e,\tilde{t}}, \theta_{b,t}\right\}\\
&\forall b \in \mathscr{B}, g \in \mathscr{G}_b, r \in \mathscr{R}_b, e \in \mathscr{E}_b, d \in \mathscr{D}_b, t \in \mathscr{T}_s, \tilde{t} \in \mathscr{T}_s \setminus \left\{\underline{t}_s, \bar{t}_s\right\}
\end{aligned}$$

A4. Noise

$$\omega_s = \{\phi_{r,s}\} \quad \forall r \in \mathscr{R}_b, b \in \mathscr{B}$$

A5. Stage-objective

$$C_s(x_s, u_s, \omega_s) = \sum_{b\in\mathscr{B}}\sum_{t\in\mathscr{T}_s}\left(\sum_{g\in\mathscr{G}_b} C_g\ p_{g,t} + \sum_{d\in\mathscr{D}_b} C_d\ pls_{d,t}\right)\Delta T_t$$

A6. State-transition

The state transition is given by the energy balance for the final time step in current stage. The incoming state x_s is connected implicitly with the outgoing state $x_s^{'}$ through the admissible controls $u_s \in U_s(x_s, \omega_s)$.

$$soc_{e,\tilde{t}_s} = soc_{e,\tilde{t}_{s-1}} + \Delta T_t\left(\eta^c ps^c_{e,\tilde{t}_s} - \frac{ps^d_{e,\tilde{t}_s}}{\eta^d}\right)$$

A7. Admissible controls

The admissible controls include all constraints except the state transition:

$$U_s(x_s, u_s, \omega_s) = u_s : \left\{ \begin{array}{rcl} p_{b,t} & = & \sum\limits_{(i,k)\in\mathscr{L}_b} B_{ik}\left(\theta_{i,t} - \theta_{k,t}\right) - P^{max}_{ik} \le B_{ik}\left(\theta_{i,t} - \theta_{k,t}\right) \le P^{max}_{ik} \\ \Theta^{min}_b & \le & \theta_{b,t} \le \Theta^{max}_b \\ p_{b,t} & = & \sum\limits_{g\in\mathscr{G}_b} p_{g,t} + \sum\limits_{r\in\mathscr{R}_b} p_{r,t} - \sum\limits_{e\in\mathscr{E}_b} p_{e,t} - \sum\limits_{d\in\mathscr{D}_b} p_{d,t} \\ 0 & \le & p_{g,t} \le P^{max}_g \\ 0 & \le & p_{r,t} \le \phi_{r,s}\cdot P^{max}_{r,t} \\ p_{d,t} & = & PD_{d,t} - pls_{d,t} \ge 0 \\ ps_{e,t} & = & ps^c_{e,t} - ps^d_{e,t} \\ SOC^{min}_e & \le & soc_{e,t} \le SOC^{max}_e \\ 0 & \le & ps^c_{e,t} \le PS^c_{e,t} \\ 0 & \le & ps^d_{e,t} \le PS^d_{e,t} \\ \widetilde{soc}_{e,t} & = & \widetilde{soc}_{e,t-1} + \Delta\widetilde{T}_t\left(\eta^c \widetilde{ps}^c_{e,t} - \frac{\widetilde{ps}^d_{e,t}}{\eta^d}\right) \\ & & \forall b \in \mathscr{B}, g \in \mathscr{G}_b, r \in \mathscr{R}_b, e \in \mathscr{E}_b, d \in \mathscr{D}_b, t \in \mathscr{T}_s, \widetilde{t} \in \mathscr{T}_s \backslash \left\{\tilde{t}_s\right\} \end{array} \right\}$$

References

[1] International Renewable Energy Agency, Global energy transformation: a roadmap to 2050 (2019 edition). Technical Report, IRENA, 2019.978-92-9260-121-8

[2] C. Kost, S. Shammugam, V. Jülch, H.-T. Nguyen, T. Schlegl, Levelized cost of electricity renewable energy technologies. Technical Report, Fraunhofer institute for solar energy systems ise, 2018.

[3] F. Sensfuß, M. Ragwitz, M. Genoese, The merit-order effect: a detailed analysis of the price effect of renewable electricity generation on spot market prices in Germany, Energy Policy 36 (8) (2008) 3086–3094, https://doi.org/10.1016/j.enpol.2008.03.035.

[4] J.C. Ketterer, The impact of wind power generation on the electricity price in Germany, Energy Econ. 44 (2014) 270–280, https://doi.org/10.1016/j.eneco.2014.04.003.

[5] S. Djørup, J.Z. Thellufsen, P. Sorknæs, The electricity market in a renewable energy system, Energy 162 (2018) 148–157, https://doi.org/10.1016/j.energy.2018.07.100.

[6] C.K. Woo, J. Moore, B. Schneiderman, T. Ho, A. Olson, L. Alagappan, K. Chawla, N. Toyama, J. Zarnikau, Merit-order effects of renewable energy and price divergence in California's day-ahead and real-time electricity markets, Energy Policy 92 (2016) 299–312, https://doi.org/10.1016/j.enpol.2016.02.023.

[7] D. Azofra, E. Jiménez, E. Martínez, J. Blanco, J.C. Saenz-Díez, Wind power merit-order and feed-in-tariffs effect: A variability analysis of the Spanish electricity market, Energy Conver. Manag. 83 (2014) 19–27, https://doi.org/10.1016/j.enconman.2014.03.057.

[8] J. Cludius, H. Hermann, F.C. Matthes, V. Graichen, The merit order effect of wind and photovoltaic electricity generation in Germany 2008-2016 estimation and distributional implications, Energy Econ. 44 (2014) 302–313, https://doi.org/10.1016/j.eneco.2014.04.020.

[9] L. Hirth, The market value of variable renewables. The effect of solar wind power variability on their relative price, Energy Econ. 38 (2013) 218–236, https://doi.org/10.1016/j.eneco.2013.02.004.

[10] C. Helm, M. Mier, Efficient diffusion of renewable energies: a roller-coaster ride. Technical Report, University of Oldenburg, Department of Economics, 2016.

[11] M. Korpås, A. Botterud, Optimality conditions and cost recovery in electricity markets with variable renewable energy and energy storage, 2020.

[12] R. Green, N.V. Vasilakos, The long-term impact of wind power on electricity prices and generating power, SSRN Electron. J. (2012), https://doi.org/10.2139/ssrn.1851311.

[13] IEA, Energy Storage. Technical Report, International Energy Agency, Paris, 2020.

[14] W. Cole, A. Frazier, Cost projections for utility-scale battery storage: 2020 update. Technical Report, National Renewable Energy Laboratory (NREL), Golden, CO (United States), 2020, https://doi.org/10.2172/1665769.

[15] F. Díaz-González, A. Sumper, O. Gomis-Bellmunt, R. Villafáfila-Robles, A review of energy storage technologies for wind power applications, Renewable and sustainable energy reviews 16 (4) (2012) 2154–2171, https://doi.org/10.1016/j.rser.2012.01.029.

[16] H. Zhao, Q. Wu, S. Hu, H. Xu, C.N. Rasmussen, Review of energy storage system for wind power integration support, Appl. Energy 137 (2015) 545–553, https://doi.org/10.1016/j.apenergy.2014.04.103.

[17] N. Li, C. Uckun, E.M. Constantinescu, J.R. Birge, K.W. Hedman, A. Botterud, Flexible operation of batteries in power system scheduling with renewable energy, IEEE Trans. Sustain. Energy 7 (2) (2016) 685–696, https://doi.org/10.1109/TSTE.2015.2497470.

[18] M. Arbabzadeh, R. Sioshansi, J.X. Johnson, G.A. Keoleian, The role of energy storage in deep decarbonization of electricity production, Nature Commun. 10 (1) (2019) 1–11, https://doi.org/10.1038/s41467-019-11161-5.

[19] D. Krishnamurthy, C. Uckun, Z. Zhou, P.R. Thimmapuram, A. Botterud, Energy storage arbitrage under day-ahead and real-time price uncertainty, IEEE Trans. Power Syst. 33 (1) (2017) 84–93, https://doi.org/10.1109/tpwrs.2017.2685347.

[20] R. Sioshansi, P. Denholm, T. Jenkin, J. Weiss, Estimating the value of electricity storage in PJM: arbitrage and some welfare effects, Energy Econ. 31 (2) (2009) 269–277, https://doi.org/10.1016/j.eneco.2008.10.005.

[21] K.R. Ward, R. Green, I. Staffell, Getting prices right in structural electricity market models, Energy Policy 129 (2019) 1190–1206, https://doi.org/10.1016/j.enpol.2019.01.077.

[22] S. Stoft, Power system economics: designing markets for electricity, IEEE Press, 2002, https://doi.org/10.1109/MPAE.2003.1180363.

[23] O.B. Fosso, A. Gjelsvik, A. Haugstad, B. Mo, I. Wangensteen, Generation scheduling in a deregulated system. the norwegian case, IEEE Trans. Power Syst. 14 (1) (1999) 75–80, https://doi.org/10.1109/59.744487.

[24] S. Stage, Y. Larsson, Incremental cost of water power, Trans. Am. Inst. Electric. Eng. Part III: Power Apparat. Syst. 80 (3) (1961) 361–364, https://doi.org/10.1109/AIEEPAS.1961.4501045.

[25] O. Wolfgang, A. Haugstad, B. Mo, A. Gjelsvik, I. Wangensteen, G. Doorman, Hydro reservoir handling in Norway before and after deregulation, Energy 34 (10) (2009) 1642–1651, https://doi.org/10.1016/j.energy.2009.07.025.

[26] M.V. Pereira, L.M. Pinto, Stochastic optimization of a multireservoir hydroelectric system: a decomposition approach, Water Resour. Res. 21 (6) (1985) 779–792, https://doi.org/10.1029/WR021i006p00779.

[27] S.A. Johnson, J.R. Stedinger, C.A. Shoemaker, Y. Li, J.A. Tejada-Guibert, Numerical solution of continuous-state dynamic programs using linear and spline interpolation, Oper. Res. 41 (3) (1993) 484–500, https://doi.org/10.1287/opre.41.3.484.

[28] J. Geske, R. Green, Optimal storage, investment and management under uncertainty: it is costly to avoid outages!, Energy J. 41 (2) (2020), https://doi.org/10.5547/01956574.41.2.jges.

[29] R. Bellman, Dynamic Programming, 1, Princeton University Press, 1957.

[30] K.M. Chandy, S.H. Low, U. Topcu, H. Xu, A simple optimal power flow model with energy storage. 49th IEEE Conference on Decision and Control (CDC), IEEE, 2010, pp. 1051–1057, https://doi.org/10.1109/CDC.2010.5718193.

[31] O. Dowson, The policy graph decomposition of multistage stochastic optimization problems, Networks 76 (1) (2020) 3–23, https://doi.org/10.1002/net.21932.

[32] P. Aaslid, M.M. Belsnes, O.B. Fosso, Optimal microgrid operation considering battery degradation using stochastic dual dynamic programming. SEST 2019 - 2nd International Conference on Smart Energy Systems and Technologies, Institute of Electrical and Electronics Engineers (IEEE), 2019, pp. 1–6, https://doi.org/10.1109/SEST.2019.8849150.

[33] A. Papavasiliou, Y. Mou, L. Cambier, D. Scieur, Application of stochastic dual dynamic programming to the real-time dispatch of storage under renewable supply uncertainty, IEEE Trans. Sustain. Energy 9 (2) (2018) 547–558, https://doi.org/10.1109/TSTE.2017.2748463.

[34] P. Girardeau, V. Leclere, A.B. Philpott, On the convergence of decomposition methods for multistage stochastic convex programs, Math. Oper. Res. 40 (1) (2015) 130–145, https://doi.org/10.1287/moor.2014.0664.

[35] A. Gabash, P. Li, Active-reactive optimal power flow in distribution networks with embedded generation and battery storage, IEEE Trans. Power Syst. 27 (4) (2012) 2026–2035, https://doi.org/10.1109/TPWRS.2012.2187315.

[36] G. Carpinelli, G. Celli, S. Mocci, F. Mottola, F. Pilo, D. Proto, Optimal integration of distributed energy storage devices in smart grids, IEEE Trans. Smart Grid 4 (2) (2013) 985–995, https://doi.org/10.1109/TSG.2012.2231100.

[37] D. Kourounis, A. Fuchs, O. Schenk, Toward the next generation of Multiperiod optimal power flow solvers, IEEE Trans. Power Syst. 33 (4) (2018) 4005–4014, https://doi.org/10.1109/TPWRS.2017.2789187.

[38] M.E. Baran, F.F. Wu, Optimal sizing of capacitors placed on a radial distribution system, IEEE Trans. Power Del. 4 (1) (1989) 735–743, https://doi.org/10.1109/61.19266.

[39] M.E. Baran, F.F. Wu, Optimal capacitor placement on radial distribution systems, IEEE Trans. Power Del. 4 (1) (1989) 725–734, https://doi.org/10.1109/61.19265.

[40] D.K. Molzahn, I.A. Hiskens, A survey of relaxations and approximations of the power flow equations, Now Publishers, 2019.

[41] J. Carpentier, Contribution á létude du dispatching économique, Bulletin de la Société Française des Électriciens 3 (8) (1962) 431–447.

[42] B. Stott, J. Jardim, O. Alsaç, DC power flow revisited, IEEE Trans. Power Syst. 24 (3) (2009) 1290–1300, https://doi.org/10.1109/TPWRS.2009.2021235.

[43] M.N. Akhter, S. Mekhilef, H. Mokhlis, N.M. Shah, Review on forecasting of photovoltaic power generation based on machine learning and metaheuristic techniques, IET Renewable Power Generation 13 (7) (2019) 1009–1023, https://doi.org/10.1049/iet-rpg.2018.5649.

[44] S. Alimohammadi, D. He, Multi-stage algorithm for uncertainty analysis of solar power forecasting. IEEE Power and Energy Society General Meeting 2016-Novem, IEEE Computer Society, 2016, pp. 1–5, https://doi.org/10.1109/PESGM.2016.7741199.

[45] A.R. Jordehi, How to deal with uncertainties in electric power systems? A review, Renewable and sustainable energy reviews 96 (2018) 145–155, https://doi.org/10.1016/j.rser.2018.07.056.

[46] A. Soroudi, M. Aien, M. Ehsan, A probabilistic modeling of photo voltaic modules and wind power generation impact on distribution networks, IEEE Syst. J. 6 (2) (2012) 254–259, https://doi.org/10.1109/JSYST.2011.2162994.

[47] Y.M. Atwa, E.F. El-Saadany, M.M. Salama, R. Seethapathy, Optimal renewable resources mix for distribution system energy loss minimization, IEEE Trans. Power Syst. 25 (1) (2010) 360–370, https://doi.org/10.1109/TPWRS.2009.2030276.

[48] N.L. Johnson, S. Kotz, N. Balakrishnan, Continuous Univariate Distributions, 2nd, Wiley & Sons, 1994.

[49] Z. Drezner, D. Zerom, A simple and effective discretization of a continuous random variable, Commun. Stat. - Simulat. Comput. 45 (10) (2016) 3798–3810, https://doi.org/10.1080/03610918.2015.1071389.

[50] I. Dunning, J. Huchette, M. Lubin, JuMP: a modeling language for mathematical optimization, SIAM Rev. 59 (2) (2017) 295–320, https://doi.org/10.1137/15M1020575.

[51] L.T. Wächter Andreas;Biegler, On the implementation of an interior-point filter line-search algorithm for large-scale nonlinear programming, Math. Program. 106 (1) (2006) 25–57, https://doi.org/10.1007/s10107-004-0559-y.

[52] C. Coffrin, R. Bent, K. Sundar, Y. Ng, M. Lubin, PowerModels.jl: an Open-source framework for exploring power flow formulations. 20th Power Systems Computation Conference, PSCC 2018, Institute of Electrical and Electronics Engineers Inc., 2018, pp. 1–8, https://doi.org/10.23919/PSCC.2018.8442948.

[53] F. Geth, C. Coffrin, D.M. Fobes, A flexible storage model for power network optimization, e-Energy 2020 - Proceedings of the 11th ACM International Conference on Future Energy Systems (2020) 503–508.

[54] M.K. Mohammed, O.I. Awad, M.M. Rahman, G. Najafi, F. Basrawi, Abd Alla, R. Mamat, The optimum performance of the combined cycle power plant: A comprehensive review, Renewable and Sustainable Energy Reviews 79 (2017) 459–474, https://doi.org/10.1016/j.rser.2017.05.060.

[55] A.O. Eggen, H. Vefsenmo, FASIT kravspesifikasjon - Versjon 2019. Technical Report, SINTEF Energy Research, 2018.

[56] P. Denholm, M. O'Connell, G. Brinkman, J. Jorgenson, Overgeneration from Solar Energy in California. A Field Guide to the Duck Chart. Technical Report, National Renewable Energy Laboratory (NREL), Golden, CO (United States), 2015, https://doi.org/10.2172/1226167.

[57] M.V.F. Pereira, L.M.V.G. Pinto, Multi-stage stochastic optimization applied to energy planning, Math. Program. 52 (1-3) (1991) 359–375, https://doi.org/10.1007/BF01582895.

[58] J. Zou, S. Ahmed, X.A. Sun, Stochastic dual dynamic integer programming, Math. Program. (2018) 1–42, https://doi.org/10.1007/s10107-018-1249-5.

[59] A. Gjelsvik, M.M. Belsnes, A. Haugstad, An algorithm for stochastic medium-term hydrothermal scheduling under spot price uncertainty. Proc. 13th Power System Computation Conference, Trondheim, Norway, 1999, pp. 1079–1085.

[60] A. Downward, O. Dowson, R. Baucke, Stochastic dual dynamic programming with stagewise dependent objective uncertainty, Optim. Online (2018).

[61] P. Aaslid, F. Geth, M. Korpås, M.M. Belsnes, O.B. Fosso, Non-linear charge-based battery storage optimization model with bi-variate cubic spline constraints, J. Energy Storage 32 (2020) 101979, https://doi.org/10.1016/j.est.2020.101979.

[62] O.B. Fosso, M.M. Belsnes, Short-term hydro scheduling in a liberalized power system. 2004 International Conference on Power System Technology PowerCon 2004 2, 2004, pp. 1321–1326, https://doi.org/10.1109/ICPST.2004.1460206.

Paper IV

Cite as:

> P. Aaslid, M. Korpas, M. M. Belsnes, and O. Fosso, "Stochastic Optimization of Microgrid Operation With Renewable Generation and Energy Storages," *IEEE Transactions on Sustainable Energy*, pp. 1–1, 2022, ISSN: 1949-3029. DOI: 10.1109/TSTE.2022.3156069. [Online]. Available: https://ieeexplore.ieee.org/document/9727092/

This is the accepted version of an article published in IEEE Transactions on Sustainable Energy
https://doi.org/10.1109/TSTE.2022.3156069

Stochastic Optimization of Microgrid Operation With Renewable Generation and Energy Storages

Per Aaslid, *Member, IEEE,* Magnus Korpås, *Member, IEEE,* Michael M Belsnes, *Member, IEEE,* and Olav B Fosso, *Senior Member, IEEE*

***Abstract*—The operation of energy storage systems (ESSs) in power systems where variable renewable energy sources (VRESs) and ESSs must contribute to securing the supply, can be considered as an arbitrage against scarcity. The value of using stored energy instantly must be balanced against its potential future value and future risk of scarcity. This paper proposes a multi-stage stochastic programming model for the operation of microgrids with VRESs, ESSs and thermal generators that is divided into a short- and a long-term model. The short-term model utilizes information from forecasts updated every six hours, while the long-term model considers the value of stored energy beyond the forecast horizon. The model is solved using stochastic dual dynamic programming and Markov chains, and the results show that the significance of accounting for short- and long-term uncertainty increases for systems with a high degree of variable renewable generation and ESSs and limited dispatchable generation capacity.**

***Index Terms*—Energy Management, Variable Renewable Energy Sources, Energy Storage Systems, Stochastic Dual Dynamic Programming, Markov Chains, Quantile Regression**

NOMENCLATURE

Sets and indices

i, j	Markov node indices
i^+	Children of Markov node i
$\omega_i \in \Omega_i$	Set of scenarios at Markov node i
$k \in K$	SDDP iteration index
$n \in \{1, \dots, N\}$	Scenario node sequence number
R	Markov chain root node
$g \in \mathcal{G}$	Set of dispatchable generators
$r \in \mathcal{R}$	Set of renewable generators
$d \in \mathcal{D}$	Set of loads
$e \in \mathcal{E}$	Set of EES
$m \in \mathcal{M}$	Set of markets
$t \in \mathcal{T}_i$	Set of timesteps in node i
$\underline{t}_i, \bar{t}_i$	First and last time step in $\mathcal{T}_i$

Parameters

ϕ_{ij}	Transition probability from Markov node i to j
ΔT_i	Time step length at time t
CG_g	Generation cost of generator g
CP_m/CS_m	Purchase/sale price in market m
CD_d	Load shedding cost of demand d
CE_e	Fixed SMV of EES e
PG_g^{max}	Maximum power generation generator g
$PR_{r,i}^{max}$	Renewable generator r power forecast at time t
PM_m^p/PM_m^s	Maximum purchase/sale power at market m
$PD_{d,i}$	Active power demand (before load shedding) by load d at time t
$PS_{e,t}^c/PS_{e,t}^d$	Maximum charge/discharge power of EES e at time t
SOC_e^{min}/SOC_e^{max}	Minimum/maximum SOC of EES e
η_e^c/η_e^d	Charge/discharge efficiency of EES e

Variables and functions

x_i/x_i'	Incoming/outgoing state variables at Markov node i
$\bar{x}_i$	Incoming state dummy variable at Markov node i
u_i	Control variable at Markov node i
ω_i	Random variable at Markov node i
λ_i	State dual variable of solution at Markov node i
θ_i	SDDP cut variable at Markov node i
α_i^k, β_i^k	SDDP cut coefficients at Markov node i, iteration k
$U_i(x_i, \omega_i)$	Control variable feasibility set at Markov node i
$T_i(x_i, u_i, \omega_i)$	Stage-transition function at Markov node i
$C_i(x_i, u_i, \omega_i)$	Stage-objective function at Markov node i
$V_i(x_i, \omega_i)$	Value function at node i
$SEV_i(x_i)$	Storage end value at node i for state x_i
$SMV_i(x_i)$	Storage marginal value at node i for state x_i
$p_{g,t}$	Power from dispatchable generator g at time t
$p_{r,t}$	Power from renewable generator r at time t
$p_{m,t}^p/p_{m,t}^s$	Power purchase/sale from/to market m at time t
$p_{d,t}$	Power withdrawn by load d at time t
$pls_{d,t}$	Load shedding by load d at time t
$ps_{e,t}^c/ps_{e,t}^d$	Active power charge/discharge to/from EES e at time t
$ps_{e,t}$	Net active power charge to EES e at time t
$soc_{e,t}$	State-of-charge of storage e at time t

P. Aaslid is a PhD student at the Norwegian University of Science and Technology and SINTEF Energy Research. M. M. Belsnes is with SINTEF Energy Research. M. Korpås and O. B. Fosso are with Norwegian University of Science and Technology.

I. INTRODUCTION

VARIABLE renewable energy sources (VRESs), primarily solar photovoltaic (PV) and wind, are expected to be the main electricity sources in the future. The levelized cost of energy (LCOE) of solar PV and onshore wind has been reduced by 77% and 30% respectively in less than ten years [1],

This is the accepted version of an article published in IEEE Transactions on Sustainable Energy
https://doi.org/10.1109/TSTE.2022.3156069

and VRESs stand out as a clean and competitive alternative in the electricity market [2]. Despite their relatively low LCOE, large-scale integration of VRESs impose new challenges in balancing the supply and demand. Energy storage system (ESS) technologies have taken large steps both in terms of technological improvements and cost reduction, and ESSs will probably play an important role in balancing the electricity system.

Traditionally, the electricity system have been organized hierarchically with a relatively small number of centralized dispatchable generators operating to meet an almost inflexible demand. In contrast, VRESs are to great extent distributed, weather-driven and uncertain. Moreover, the market price in today's system is often set for large geographical areas and does not capture the challenges related to distributed generation [3]. With the increasing share of distributed energy resources (DERs), a viable option is to move towards decentralized control [4] to manage the system complexity. Microgrids (MGs) offer a possible way of integrating distributed VRESs and ESSs into the power system [5]–[7]. MGs are capable of operating disconnected from the main grid for a limited time or permanently [8], and remote areas may also be organized as MGs to avoid expensive grid expansions.

In energy-constrained systems, where the capacity of VRESs is high and ESSs replace some of the dispatchable capacity, the ESSs must contribute to secure the supply in periods with low generation from VRESs. The operation of these systems can be considered as balancing dispatchable generation costs against the risk of scarcity [9]. The system's ESSs must be operated to have sufficient high state-of-charge (SOC) for periods with high demand, and they should also have sufficient low SOC upfront periods with high generation from VRESs to minimize generation curtailment. These decisions must account for both the daily variations and uncertainty in demand and solar PV generation, as well as the variations and uncertainty in wind power generation over several days.

Power and energy limitations as well as efficiencies also vary for different ESS technologies. Lithium-ion batteries can deliver and absorb high power with low losses, but for a limited time due to energy limitations. A key factor for large scale integration of VRESs is long-duration energy storage with sufficient low storage capacity cost, and hydrogen stands out as one of the most viable options [10]. For hydrogen ESSs (electrolyzer and fuel cell), the size of the hydrogen tank can be scaled up at modest cost, while the electrolyzer and the fuel cell are expensive to scale up and have poor round-trip efficiency compared to lithium-ion batteries [11]. The combination of power and energy limitations, efficiency losses, and uncertain generation and demand makes the operation optimization problem highly complex, and the long-duration storage necessitates scheduling several days ahead.

Rule-based energy management has been successfully applied for managing DERs, both for experimental systems [12]–[14] and virtual systems [15], [16]. These rule-based methods charge/discharge the respective ESSs based on fixed SOC thresholds and predefined priorities, and their computational performance makes them well suited for integration in a real-time environment. However, they do not utilize knowledge about expected future generation and demand from forecasts.

Information from forecasts can improve the operation strategy by formulating dynamic optimization problems with either deterministic or stochastic generation and load forecasts. The resulting power dispatch or SOC can be used as a reference to a real-time control system where the system is re-optimized using rolling horizon each time where either the forecast or observed state are updated [17]–[19].

Stochastic dynamic programming (SDP) approaches [20] also account for how the uncertainty is revealed stage-wise, and the operation strategy can be adjusted stage-wise as more uncertainty is revealed. Instead of providing an optimal control, it provides an optimal policy which is a set of decision rules on how to respond to a given state at a given time. The storage marginal value (SMV) obtained from the SDP solution also has a useful interpretation with respect to deciding when to use the different ESSs compared to generators using constant marginal cost principles [21]. However, SDP approaches require stage-wise independent noise and the auto-correlation of the scenarios are lost. Uncertainty from VRESs is naturally auto-correlated [22]. Therefore, forecast errors tends to sustain and must be accounted for to prevent the security of supply from worsening.

The operation of ESSs is in reality an infinite horizon optimization problem, and this is particularly important when studying systems where ESSs must be used to prevent extreme prices from, for example, periods of scarcity. A common approach to prevent emptying the ESSs at the end of the optimization period, is to apply a bound on the end SOC, typically for daily planning [23]–[25]. However, this approach is unnecessarily inflexible and prevents utilization of the flexibility beyond the optimization horizon [26]. Solar PV and wind power both have distinct seasonal variation, hence the operation method should also be verified through a whole year as in [15], [16], but these only consider rule-based approaches.

Existing literature often studies ESSs' capabilities to minimize thermal power generation and reduce CO_2 emissions, but very few papers consider how ESSs should be operated if they must contribute to prevent extreme prices and scarcity. The valuation of stored energy beyond the optimization period has therefore gained little attention. However, research on large-scale hydropower has paid more attention to infinite horizon optimization both with SDP [27] and stochastic dual dynamic programming (SDDP) [28].

This paper presents a multi-stage stochastic programming (MSSP) energy management model that is solved using a combination of SDP and SDDP [28], [29]. Unlike most previous studies, we address energy-constrained systems where the ESSs are decisive to prevent scarcity. While previous approaches consider forecast uncertainty [17], [19], our model also accounts for the uncertainty beyond the forecast horizon with a separate stochastic long-term model. Moreover, we do not enforce rigorous state end value constraints [23]–[25], but approximate state and time dependent storage end value functions. The storage end value functions are updated monthly to account for seasonal variations and represents infinite horizon similar to approaches applied for hydropower

This is the accepted version of an article published in IEEE Transactions on Sustainable Energy
https://doi.org/10.1109/TSTE.2022.3156069

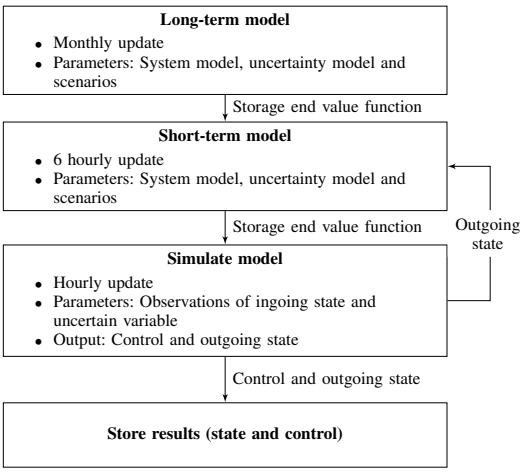

Fig. 1. Summary of stochastic optimization method

scheduling [27]. To overcome the limitations of using stage-wise independent noise, we address the auto-correlation in wind uncertainty to maintain adequate security of supply.

Moreover, we bridge the gap between rule-based [12]–[16] and optimization-based [17]–[19] operation by showing how the solution of the stage-wise optimization problems can be translated into a set of time and state dependent rules, and investigate how these adaptive rules perform compared to static rules for the operation of an actual MG over almost a full year. Stochastic scenarios are generated using gradient boosting quantile regression.

The remainder of this paper is organized as follows: Section II describes the method, section III presents and discusses the results from the application of the method, while section IV provides the conclusions.

II. Method

The proposed method divides the decision process into multiple stages where the stages within the look-ahead of the forecasts are categorized as the short-term model and the stages beyond the forecast horizon as the long-term model. The short-term model stage length follow the frequency of the weather forecast updates, while the long-term model stage length is one day and repeated cyclically.

As illustrated in Fig. 1, the long-term model is solved first. It considers typical seasonal weather, in this case for the present month. Therefore, it is only re-optimized every month as decribed in section II-D. Thereafter, the short-term model is solved using scenarios based on the most recent weather forecast that are updated six-hourly as described in section II-E. Based on the short-term strategy, the optimal control is obtained for the observed state, generation and demand. Finally, the results are saved. The stages and models are connected using the storage end value (SEV) functions as described mathematically in section II-A and interpreted in section II-C.

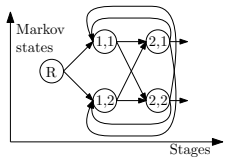

Fig. 2. Example of policy graph as a Markov chain.

A. Stochastic dual dynamic programming

MSSP represents the stage-wise decision process where new uncertainty is revealed and control decisions are taken stage-wise. The solution of an MSSP model is therefore not a sequence of controls, but rather a sequence of decision-rules, often referred to as policies, on how to respond to a given state and for the revealed uncertainty. This is an important difference from the classical two-stage stochastic model [30] where the optimal control is obtained by assuming all uncertainty is revealed at once.

The MSSP model variables are classified into state x_t, control u_t and random variable ω_t where the objective is to find a set of admissible controls (1c) that minimizes the expected stage-wise operating costs for all stages (1a). The state transitions function (1b) describes how the state changes for a given scenario ω_t and control u_t, representing decisions taken both explicitly and implicitly.

$$\min_{u_t}\left\{C_1(x_1,u_1,\omega_1)+\mathop{\mathbb{E}}_{\omega_2|\omega_1}\left[\min_{u_2}\Big(C_2(x_2,u_2,\omega_2)+\ldots + \mathop{\mathbb{E}}_{\omega_T|\omega_{T-1},\ldots,\omega_2}\Big[\min_{u_T}\big(C_T(x_T,u_T,\omega_T)\big)\Big]\Big)\right]\right\} \quad (1a)$$

$$\text{s.t.}\quad x_{t+1}=T_t(x_t,u_t,\omega_t) \quad (1b)$$

$$u_t\in U_t(x_t,\omega_t) \quad (1c)$$

$$\forall t\in\mathcal{T}$$

The MSSP formulation is an optimization problem with nested expected values of optimization problems, and where the random variable at each stage depends on all previous random variables. The size of the extensive problem becomes too large to solve even for problems of modest size. MSSP models are therefore commonly solved with dynamic programming, where the full problem is decomposed into a sequence of stage-wise problems.

This paper considers SDDP [31] for solving the proposed MSSP problem. SDDP requires a convex problem formulation [32] and stage-wise independent random variables. Similar to SDP [33], SDDP divides the full problem into smaller stage-wise problems, and approximates the future cost for each stage using backward recursion. Whereas SDP discretizes the state space, SDDP utilizes the convex problem formulation and approximates the future cost iteratively using multiple linear hyperplanes which serve as lower bounds for the future cost.

A common approach for managing the stage-wise dependent random variables, are to model them as state variables using an auto-regressive model [34]. These can be both additive

This is the accepted version of an article published in IEEE Transactions on Sustainable Energy
https://doi.org/10.1109/TSTE.2022.3156069

and multiplicative [35] depending on the random variable properties, but require a linear model formulation. However, this paper uses a combination of SDDP and SDP with Markov chains [29]. The sequence of stages and the corresponding Markov states can be described with a policy graph [28] as illustrated in Fig. 2: Each node is associated with a stage representing a discrete moment in time, and a Markov state which captures discrete states not included in the state variable x_i. Each node i has a set of children i^+ representing the next stage for the different Markov states. The transition probability between nodes ϕ_{ij} is positive if j is a child of i and otherwise zero.

Given that all future decisions are optimal from a given node and onward, the optimal decision for a previous node can be found with backward recursion using Bellman's principle of optimality [33] by reformulating the model in (1a) to (1c) as shown in (2a) to (2d).

$$V_i(x_i, \omega_i) = \min_{u_i} \Big\{ C_i(x_i, u_i, \omega_i) - SEV_i(x_i') \Big\} \tag{2a}$$

$$SEV_i(x_i') = - \mathop{\mathbb{E}}_{j \in i^+,\ \omega_j \in \Omega_j} \big[V_j\left(x_i', \omega_j\right) \big] \tag{2b}$$

$$\text{s.t.} \quad x_i' = T_i(x_i, u_i, \omega_i) \tag{2c}$$

$$u_i \in U_i(x_i, \omega_i) \tag{2d}$$

The recursive formulation can be solved with SDDP and the algorithm can be divided into two phases: forward and backward pass. In the forward pass, a random sequence of nodes $i^1, \ldots, i^N$ is sampled from the Markov model, and a random scenario $\omega_i \in \Omega_i$ is sampled for each node. The Markov model can also be cyclic to represent infinite horizon where the probability of entering a cycle must be less than one to ensure that the future value produces a finite sum. For the example illustrated in Fig. 2, the outgoing edges from node (2,1) and (2,2) will each sum up to the cycling discount factor [28]. The algorithm also enforces a maximum number of subsequent nodes. For the randomly sampled sequence of nodes and scenarios, the optimization problem (3a) to (3e) is solved sequentially using the outgoing state of previous node as the ingoing state to the next node. When a random scenario has been solved through all stages, the backward pass can start. For each node i and state x_i in the sequence $i^1, \ldots, i^N$, (3a) to (3e) is solved for all outgoing nodes $j \in i^+$ and all scenarios $\omega_j \in \Omega_j$. The resulting objectives $V_j^K(\hat{x}, \omega_j)$ and dual values λ_j are used to calculate a linear hyperplane (3e) for the current node i. The whole procedure is repeated until enough hyperplanes have been added to represent the future cost functions sufficiently accurate. Detailed algorithms are provided in reference [28].

$$V_i^K(\bar{x}_i, \omega_i) = \min_{u_i, x_i, x_i', \theta_i} C_i(x_i, u_i, \omega_i) + \theta_i \tag{3a}$$

$$\text{s.t. } x_i = \bar{x}_i, \quad [\lambda_i] \tag{3b}$$

$$x_i' = T_i(x_i, u_i, \omega_i) \tag{3c}$$

$$u_i \in U_i(x_i, \omega_i) \tag{3d}$$

$$\theta_i \geq \alpha_i^k + \beta_i^k x_i', \quad k \in \{1, 2, \ldots, K\} \tag{3e}$$

Unlike SDP, where the entire state space is explored, SDDP explores the most interesting states based on sampling from the uncertainty distribution.

B. Mathematical description

The detailed mathematical description below is repeated for each node i. Incoming state x_i is the initial SOC $soc_{e,t-1}$ for the first time step in each node, and the outgoing state x_i' is the SOC $soc_{e,t}$ for the final step in each node. The random variable ω_i includes the maximum generation from VRESs (5), such that they can be freely curtailed at no cost, and the demand (6). The admissible controls includes all the remaining constraints.

Dispatchable generators can adjust the generation between zero and maximum generation continuously (4), while the VRES generators have time dependent upper bounds given by weather conditions (5). The demand is also variable in time and load shedding can be applied if the system has insufficient capacity (6). Power can be injected and withdrawn from the ESSs at constant efficiency (7a), but the SOC limits must be respected (7b) and the charge and discharge power must stay within their limits (7c) and (7d). The change in SOC and power limits due to degradation are relatively small for the studied interval and has not been considered. The operation costs due to lifetime reduction for ESSs has neither been considered, but has been addressed for future work. In grid-connected mode, the system can exchange power with an external market within the transmission limits (8a) and (8b). The power injected and withdrawn must be balanced at all time (9). The objective is to minimize the cost of dispatchable generation, net import and load shedding (10).

$$0 \leq p_{g,t} \leq PG_g^{max}, \quad \forall g \in \mathcal{G}, t \in \mathcal{T}_i \tag{4}$$

$$0 \leq p_{r,t} \leq PR_{r,t}^{max}(\omega_t), \quad \forall r \in \mathcal{R}, t \in \mathcal{T}_i \tag{5}$$

$$p_{d,t} = PD_{d,t}(\omega_t) - pls_{d,t} \geq 0, \quad \forall d \in \mathcal{D}, t \in \mathcal{T}_i \tag{6}$$

$$soc_{e,t} = soc_{e,t-1} + \Delta T_t \left(\eta^c ps_{e,t}^c - \frac{ps_{e,t}^d}{\eta^d} \right) \tag{7a}$$

$$SOC_e^{min} \leq soc_{e,t} \leq SOC_e^{max} \tag{7b}$$

$$0 \leq ps_{e,t}^c \leq PS_{e,t}^c \tag{7c}$$

$$0 \leq ps_{e,t}^d \leq PS_{e,t}^d \tag{7d}$$

$$\forall e \in \mathcal{E}, t \in \mathcal{T}_i$$

$$0 \leq p_{m,t}^p \leq PM_m^p \tag{8a}$$

$$0 \leq p_{m,t}^s \leq PM_m^s \tag{8b}$$

$$\forall m \in \mathcal{M}, t \in \mathcal{T}_i$$

$$\sum_{g \in \mathcal{G}} p_{g,t} + \sum_{r \in \mathcal{R}} p_{r,t} + \sum_{m \in \mathcal{M}} p_{m,t}^p + \sum_{e \in \mathcal{E}} ps_{e,t}^d = \sum_{d \in \mathcal{D}} p_{d,t} + \sum_{m \in \mathcal{M}} p_{m,t}^s + \sum_{e \in \mathcal{E}} ps_{e,t}^c, \ t \in \mathcal{T}_i \tag{9}$$

This is the accepted version of an article published in IEEE Transactions on Sustainable Energy
https://doi.org/10.1109/TSTE.2022.3156069

$$\min \sum_{t\in\mathcal{T}_i}\left\{\sum_{g\in\mathcal{G}} CG_g\ p_{g,t} + \sum_{d\in\mathcal{D}} CD_d\ pls_{d,t} + \sum_{m\in\mathcal{M}}\left[CP_m\ p^p_{m,t} - CS_m\ p^s_{m,t}\right]\right\} \quad (10)$$

C. Model interpretation

The optimal energy management of a small-scale power system can be considered as the decision process of meeting the energy demand using the available resources with the lowest marginal operating cost. The marginal cost of dispatchable generators is mainly given by the fuel and emission costs, while VRESs have marginal operating costs close to zero. The value of lost load (VOLL) represents the cost of not being able to meet the demand, and is normally assigned a high value [36]. Since the ESSs neither consume nor deliver energy, but shift energy in time, the marginal cost/value can be considered as the future opportunity cost/value given they are dispatched perfectly in the future. Therefore, they will vary between zero and the VOLL since the energy charged to an ESS can originate from VRESs, and the discharged energy can prevent loss of load [21].

The objective in (2a) has two terms: the stage-objective and the SEV function. The stage-objective is a function of the control variable, while the SEV function is a function of the state. The marginal operating cost of dispatchable generators, demand, purchase and sale are all time and state independent (11), and the optimal dispatch can easily be obtained by picking the unit with the lowest marginal cost first.

$$\begin{aligned}\frac{\partial C_i(x_i,u_i,\omega_i)}{\partial p_{g,t}} &= CG_g, \quad \frac{\partial C_i(x_i,u_i,\omega_i)}{\partial pls_{d,t}} = CD_d\\ \frac{\partial C_i(x_i,u_i,\omega_i)}{\partial p^p_{m,t}} &= CP_m, \quad \frac{\partial C_i(x_i,u_i,\omega_i)}{\partial p^s_{m,t}} = -CS_m\end{aligned} \quad (11)$$

The marginal charge and discharge cost of an ESS is both time and state dependent and can be expressed as a function of the SMV, the marginal value of the SEV function with respect to state (12), as shown in (13) and (14).

$$\frac{\partial SEV_i(x_i)}{\partial x_i} = SMV_i(x_i) \quad (12)$$

$$\frac{\partial SEV_i(x'_i)}{\partial ps^c_{e,t}} = \frac{\partial SEV_i(x'_i)}{\partial x'_i}\frac{\partial x'_i}{\partial ps^c_{e,t}} = SMV_i(x'_i)\cdot\eta^c \quad (13)$$

$$\frac{\partial SEV_i(x'_i)}{\partial ps^d_{e,t}} = \frac{\partial SEV_i(x'_i)}{\partial x'_i}\frac{\partial x'_i}{\partial ps^d_{e,t}} = -SMV_i(x'_i)\cdot\frac{1}{\eta^d} \quad (14)$$

When the SMV function is known, the operation strategy of both generators, loads and ESSs can be translated into a set of time and state dependent decision-rules where the resources with the lowest marginal operating costs are chosen similar to the rule-based approaches in references [12]–[16]. However, the proposed rules based on SMV are both time and state dependent and will therefore consider the future generation and demand under uncertainty.

D. Long-term model

The long-term model uses 24-hour scenarios which are representative for the time of day and year, in this case the respective month, to represent the expectation beyond the forecast horizon. The SDDP algorithm is typically run from a known initial state. In this case, the outgoing state of the short-term model which is the incoming state of the planning is not known ahead, hence the initial Markov state and state variable value are randomized to ensure the model to be sufficiently explored by the algorithm. Since the problem is, in reality, an infinite horizon problem, a cyclic Markov model is used [28]. The cyclic Markov model permits transition from the nodes representing the final stage back to nodes representing previous stages, in this case 24 hours back, with probability 0.8. This will represent an infinite horizon with a discount and prevents the ESSs from emptying after 24 hours. This decomposition permits updating the long-term strategy monthly instead of six-hourly.

1) Wind power: The main purpose of the long-term model is to predict net power balance over several days. Wind power is the dominant energy source and has an evident auto-correlation. The long-term model assumes constant daily wind power generation using five scenarios represented as individual Markov states. The scenarios are generated based on the 24-hourly mean values of historical wind power observations which are sorted and divided into intervals of relative size $0.1, 0.2, 0.4, 0.2, 0.1$. The mean value of each interval represents the scenario. The transition probabilities between the scenarios are obtained using the method described in section II-J.

2) Solar PV power: Clearness index (CI) is a number between zero and one and gives the ratio between solar PV power generation and the clear sky generation at that particular time. The CIs are calculated for the historical observations where hours with zero generation are neglected to avoid zero division. The mean daily CIs are sorted and divided into three equally sized intervals. The mean value for each interval is used as the CI for the long-term model scenarios. The auto-correlation has not been considered to keep the number of Markov states sufficiently low, and since wind is the dominant power source.

3) Demand power: The demand scenarios are generated using quantile regression with the hour of day and the month of year as explanatory variables. The scenarios are given by the $0.1, 0.5, 0.9$ quantiles with probability $0.2, 0.6, 0.2$. The quantile regression method is further described in section II-J.

E. Short-term model

The short-term model stage length is equal to the weather forecast update frequency, six hours, and the forecasts have 60 hours look-ahead yielding ten stages.

1) Wind power: The ratio between wind speed and power generation is non-convex [37] and has increasing variability with increasing wind speed [35]. Wind power scenarios are generated using the $0.1, 0.3, 0.5, 0.7, 0.9$ quantiles, each with 0.2 probability, where each scenario represents a Markov state. The quantile regression model is fitted using the following explanatory variables: wind power forecast at turbine height, wind speed forecast, wind direction forecast, look-ahead hours and last observed power before the forecast period.

This is the accepted version of an article published in IEEE Transactions on Sustainable Energy
https://doi.org/10.1109/TSTE.2022.3156069

The wind speed v_{ref} is forecasted at a reference height h_{ref} which usually differs from the turbine height $h_{turbine}$. Therefore, the turbine wind speed $v_{turbine}$ is scaled using the power law profile [38] shown in (15).

$$v_{turbine} = v_{ref} \left(\frac{h_{turbine}}{h_{ref}} \right)^{k} \tag{15}$$

The roughness factor k is an empirical value for the roughness of the terrain around the wind turbine. Transition probabilities are obtained as described in section II-J.

2) Solar PV power: Solar power explanatory variables are: cloud area fraction forecast, normalized maximum solar power, initial solar power and look-ahead hours. The normalized maximum solar power represents the theoretical maximum generation for that time of day and year as a number between zero and one. There are theoretical methods for determining this value given the geographical location, and the panel direction and tilt. Since panel angle and direction as well as seasonal configurations are unknown for the case in this paper, the normalized maximum solar power has been approximated using historically observed generation by assuming the normalized maximum solar power is given by the maximum observed value at that day and hour plus/minus nine days for all observed years.

3) Demand power: The demand will use the same regression model as the long-term model described in section II-D3.

F. Simulation

To verify the value of the different optimization strategies, historical observations are simulated with rolling horizon. For each observed value, the corresponding node i is identified based on the Markov state and stage, and the optimal control is found by solving (3a) to (3e). The optimal control and the resulting state are saved, and the procedure is repeated for the next stage using the previous outgoing state as the incoming state. The short- and long-term models are updated as shown in Fig. 1.

G. Reference models

1) Perfect foresight: The perfect foresight model uses the mathematical model description from section II-B but optimizes the whole period at once with the actual historical generations and demand instead of using forecasts. The SEV at the end of the optimization is set using the fixed SMV described in section II-G3. The perfect foresight model can be considered as a theoretical absolute lower bound of the operating costs.

2) Deterministic model: The deterministic model formulation uses the same mathematical model description presented in section II-B as the stochastic model, but with least square point forecasts for generation from VRESs and demand instead of multiple scenarios, stages and Markov states. The deterministic model only considers the short-term model horizon and is similar to references [17], [18].

3) Rule-based model: Rule-based models [12]–[14] use a fixed priority for generators and ESSs to decide where to withdraw lacking or inject surplus energy. Given an arbitrary ESS e with charge/discharge efficiency η_e^c/η_e^d and SMV CE_e, then the cost of discharging one unit will be $\frac{CE_e}{\eta_e^d}$, hereby referred as discharge cost. The corresponding value of charging one unit, the charge value, will be $CE_e\eta_e^c$. If the SMV is chosen such that the discharge cost is less than the diesel generation cost, the ESS will be used to meet the demand before the diesel generator. Likewise, diesel will not be used to charge the ESS as long the charge value is less than the diesel cost, and the ESS with highest charge value will be charged first when there are surplus generation from VRESs.

The cases with fixed end value will use SMV $80\ €/MWh$ for both ESSs. Since the charge value is less than the marginal cost of the diesel generator, both of the ESSs will only be charged when there are surplus generation from VRESs. The discharge value of the battery is less than the diesel generator marginal cost or the grid purchase price, hence it will displace diesel generation or import whenever possible. However, the discharge value of hydrogen is higher. Consequently, it will only be used to prevent load shedding.

H. Implementation

The proposed method has been implemented in the programming language Julia (1.4.2) using the toolbox SDDP.jl (0.3.14) [39] and Gurobi (9.1) for solving the stage-wise linear optimization models. The long-term models were trained with 1000 iterations, and the short-term models with 100 iterations. To simulate the proposed case, 1350 short-term models were trained and simulated in 4-5 hours while the training time for 12 months of the long-term model was around 1.5 hours on a laptop with Intel i7-8650U CPU and 16 GB RAM.

I. Case study

Rye microgrid is located in Central Norway near Trondheim and is partly funded by the Horizon 2020 project REMOTE [40]. The MG comprises a farm and a few residential houses, and the electricity is supplied by solar PV panels and a wind turbine [41]. The turbine height and the reference height are 30 and 10 meters respectively, and the terrain roughness factor is set to 0.3 considering the wind turbine is partially surrounded by forest [42]. There is also a lithium-ion battery and a hydrogen storage unit with an electrolyzer and a fuel cell to balance the load and generation. A diesel generator serves as backup when the VRE generation is persistently low. The generation capacities are 86 and 135 kW for solar PV and wind respectively. The import price and diesel generator operating cost are both 100 €/MWh, while the sale price is 50 €/MWh. The VOLL is 5000 €/MWh. The numerical values of the ESSs are presented in Table I. Diesel and wind power generation capacities in this study have been reduced from the original system to increase the probability of scarcity. This choice is made to study the impact of ESS operation strategies in critical periods of the year where ESSs are needed to prevent load shedding. Time series for historical observed generation and

This is the accepted version of an article published in IEEE Transactions on Sustainable Energy
https://doi.org/10.1109/TSTE.2022.3156069

TABLE I
NUMERICAL VALUES FOR MICROGRID ENERGY STORAGE SYSTEMS.

Description	Unit	Lithium-ion	Hydrogen
Charge power	[kW]	500	55
Discharge power	[kW]	500	100
Size	[kWh]	500	3300
Charge efficiency	[%]	96	64
Discharge efficiency	[%]	96	50

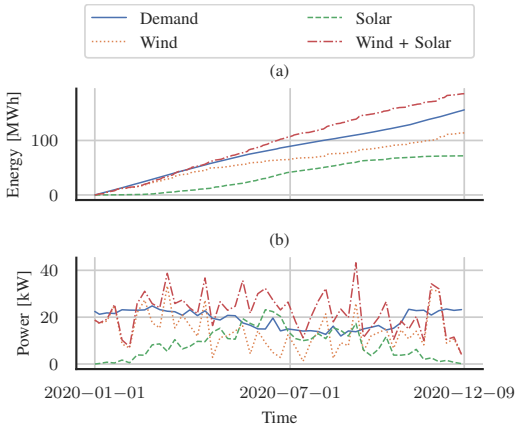

Fig. 3. Accumulated generation and load (a) and weekly average generation and load (b) for the entire studied period.

load, and historical weather forecasts can be downloaded from [43].

The system has sufficient power generation from VRESs in the long run, as shown in Fig. 3a. However, Fig. 3b shows a significant weekly variability, especially for the wind power, that must be balanced with ESSs. For an average daily load above 20 kW, a fully charged lithium-ion battery can meet the load for maximum 24 hours, while a full hydrogen tank can meet the demand for around 80 hours. If the dispatchable generation capacity is low, sufficient stored energy in the ESSs is crucial to prevent load shedding. The analysis period is between 2020-01-01 and 2020-12-09.

J. Quantile regression and transition probability

Generation forecasts for the short-term model are determined based on meteorological weather forecasts from the Norwegian Meteorological Institute with a 60-hour foresight updated every sixth hour. Let $\psi_{t+k|t}$ denote the weather forecast for time $t+k$ issued at time t. The goal is to find a set of scenarios $\Omega_{t+k} = f(\omega_{t-i}, \psi_{t+k|t}, k)$ given previous observations and forecast variables. Unfortunately, it is difficult to include the look-ahead as an explanatory variable in a linear model as the product of two variables is not allowed. Linear models will therefore require a separate regression model for each look-ahead value k [44]. Gradient boosting (GB) is a machine learning technique that can be used for regression by forming an ensemble of weak decision trees [45], [46]. Moreover, GB is not limited to linear combinations, hence the look-ahead can be used directly as an explanatory variable. All training data can therefore be used to fit one model instead of an individual models for each k. This approach will therefore be less dependent on having a large training data set compared to linear regression. The regression has been performed with MLJ.jl (0.16.2) [47] and ScikitLearn (0.24.0) [48] with regularization constant 1.0 and interior-point solver. Deterministic point forecasts are generated using a least square regressor, while scenarios are generated using quantile regression.

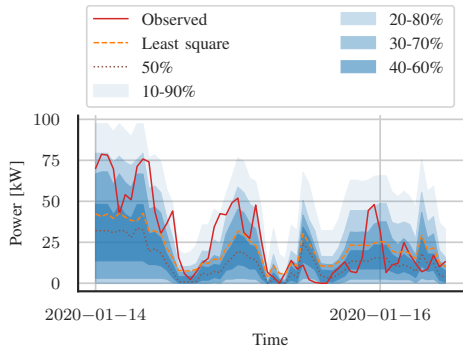

Fig. 4. Example of wind power percentile forecasts (blue) compared to least square forecast and observed power for a 60 hours interval. Percentile median values are used as wind power scenarios for the stochastic optimization. Least square forecast is used for the deterministic optimization.

Let ω_i^α denote the α quantile of a random variable at node i, and $\hat{\omega}_i$ an observed value, then $P(\omega_i^\alpha \geq \hat{\omega}_i) = \alpha$. Moreover, let $\mathbb{E}[\omega_i^\alpha]$ and $\mathbb{E}[\hat{\omega}_i]$ denote the mean value of the respective quantiles and the observed values over time. The observed values at the node i are then in the j'th quantile interval if $\mathbb{E}[\omega_i^{\alpha_{j-1}}] \leq \mathbb{E}[\hat{\omega}_i] < \mathbb{E}[\omega_i^{\alpha_j}]$ where $\alpha = [\alpha_0, \ldots, \alpha_n]$.

The quantile regression model is trained using historical weather forecasts as explanatory variables and the actual generation as the outcome variable. For each historical forecast, the outcome variable is classified into quantile interval and the number of transitions between the quantile intervals is counted. Let the matrix Φ denote the transition counts such that Φ_{ij} denotes the number of transitions between quantile interval i and j, then the resulting transition probability matrix ϕ is given by $\phi_{ij} = \frac{\Phi_{ij}}{\sum_{k=1}^{n} \Phi_{ik}}$. The resulting quantile intervals compared to the point forecast and observed wind power are shown for a random interval in Fig. 4.

III. RESULTS AND DISCUSSION

A. Long-term strategy

As explained in section II-C, generation from VRESs with zero marginal cost is always preferred if available, while the priorities between the dispatchable generation, import, export and ESS charge and discharge varies and are given by the SMV. Fig. 5 illustrates the resulting long-term operation strategy for the ESSs based on the SMVs as a function of both battery SOC (x-axis) and hydrogen SOC (y-axis). The SMV

This is the accepted version of an article published in IEEE Transactions on Sustainable Energy
https://doi.org/10.1109/TSTE.2022.3156069

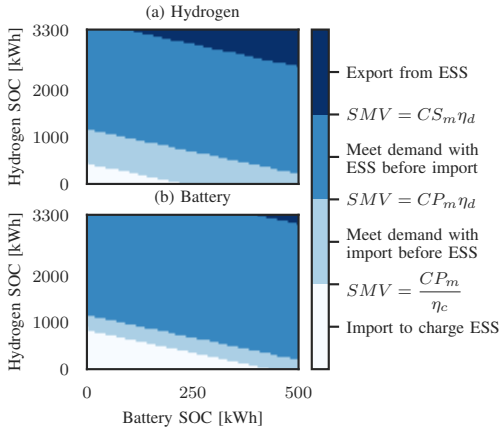

Fig. 5. Long-term model strategy for ESS dispatch based on SMV as a function of battery and hydrogen SOC for the system with $15kW$ import/export capacity in May with intermediate wind speeds (Markov state 3 of 5) for (a) hydrogen and (b) battery. The storage marginal value in the transition between the different areas are shown in the legend and the numerical values are shown in Table I and section II-I.

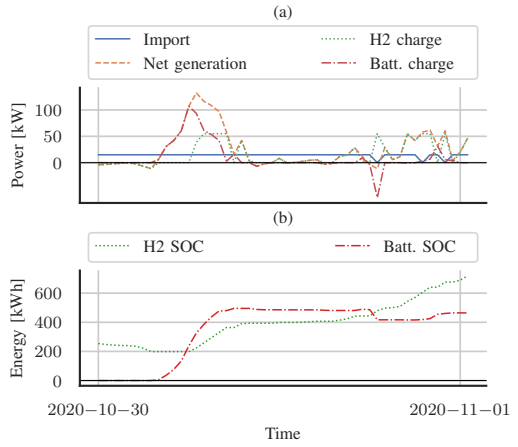

Fig. 6. Snapshot from case 21 where power is imported due to low SOC despite of positive net generation.

boundaries are based on the charge/discharge cost derived in (13) and (14).

Fig. 5 shows that it is optimal to use available import capacity to charge the ESSs when the SOC is sufficiently low. For slightly higher SOC, the optimal strategy is to import instead of using stored energy such that the stored energy is saved for potential future situations with risk of scarcity. When the SOC is sufficiently high, the stored energy should be used to meet the demand instead of import, while when the SOC is close to maximum, the energy should be exported to prevent potential generation curtailment.

A similar strategy can be extracted from the short-term strategy giving even more accurate rules which also considers the short-term generation and load forecasts. Additionally, this makes the proposed method suitable for integration towards real-time systems.

B. Simulation of historical observations

The optimal operation of almost a full year with historical data is summarized in Table II for three conditions of the system: high dispatchable capacity (75 kW), low dispatchable capacity (15 kW) and weakly grid connected system (15 kW import/export capacity). Each condition has been analysed with seven different methods. The first method (cases 1,8 and 15) shows the results with perfect foresight which can be considered as an absolute lower bound of the costs. The remaining methods are different combinations of short- and long-term models, where the stochastic model is our proposed model. The outgoing SOC is shown in Table II, but the value of it is not included in the costs.

The dispatchable generation capacity of $75kW$ of the cases 1-7 is always sufficient to meet the peak demand. Therefore, the load shedding is always zero and the difference in operating cost between the different methods originates from the diesel consumption. The fixed end value (rule-based) of the cases 2-4 is conservative and prioritizes hydrogen for load shedding prevention, which results in a poor utilization of VRE compared to the cut end values from the stochastic long-term model. By also considering the forecast uncertainty in case 4, the utilization of VRESs increase considerably. The stochastic cuts of cases 5-7 adapt the strategy both with respect to SOC, wind state and time of the day and seasonal variations, and position the SOC such that surplus generation can be absorbed efficiently.

Given perfect information (case 8), it is also possible to fully prevent load shedding with a $15kW$ diesel generator through early activation upfront periods with low generation from VRESs to ensure sufficient energy in the system's ESSs. The operating costs are actually slightly less than for case 1 due to lower final hydrogen SOC. The rule-based long-term strategy (cases 9-11), where only surplus generation from VRESs is stored, causes significant load shedding. In contrast, the stochastic long-term model (cases 12-14) almost eliminates load shedding. A key difference is that the stochastic long-term model provides a state dependent valuation of the stored energy, while the rule-based method represents fixed valuation. Therefore, the stochastic long-term model is very thrifty with the stored energy when the SOC is low, which is essential to prevent load shedding. Moreover, the use of weather forecasts (cases 10-11), and in particular with stochastic modeling (cases 13-14), is important to keep both load shedding and diesel generation low. Also note that case 12 has a high utilization of wind and solar compared to 14, but still higher operating costs. The lack of forecast imposes rapid cycling of the hydrogen storage resulting in high efficiency losses, while the stochastic model has less frequent cycling of the hydrogen storage and less losses.

By replacing the diesel generator with a grid connection with equal capacity, the surplus generation can be exported (cases 15-21). The export price is set to half of the import

This is the accepted version of an article published in IEEE Transactions on Sustainable Energy
https://doi.org/10.1109/TSTE.2022.3156069

TABLE II
SUMMARY OF OPERATING COSTS, LOAD SHEDDING, IMPORT, EXPORT, GENERATION AND FINAL EES SOC FOR ALL CASES AND ALL OPTIMIZATION METHODS. NUMBERS IN PARENTHESIS SHOWS PERCENTAGE OF VRES THAT HAS BEEN UTILIZED.

				[€]	Energy $[MWh]$							
	Case	Short-term model	Long-term model	Cost	Load shedding	Diesel	Import	Export	Wind generation	Solar generation	H2 end SOC	Batt. end SOC
Diesel capacity: 75 kW	1	Perfect	-	1957	0.00	19.6	-	-	109.0 (57%)	55.8 (78%)	3.30	0.00
	2	None	Rule-based	2917	0.00	29.2	-	-	83.6 (44%)	50.6 (70%)	3.30	0.00
	3	Deterministic	Rule-based	2988	0.00	29.9	-	-	88.6 (47%)	52.6 (73%)	3.29	0.00
	4	Stochastic	Rule-based	2219	0.00	22.2	-	-	102.4 (54%)	58.6 (82%)	0.58	0.00
	5	None	Stochastic	2341	0.00	23.4	-	-	107.6 (57%)	59.8 (83%)	0.00	0.00
	6	Deterministic	Stochastic	2055	0.00	20.5	-	-	108.3 (57%)	59.3 (83%)	0.00	0.00
	7	Stochastic	Stochastic	1929	0.00	19.3	-	-	105.4 (56%)	56.9 (79%)	0.00	0.00
Diesel capacity: 15 kW	8	Perfect	-	1954	0.00	19.5	-	-	108.9 (57%)	55.6 (77%)	3.15	0.00
	9	None	Rule-based	9267	1.42	21.6	-	-	96.0 (51%)	52.3 (73%)	0.10	0.00
	10	Deterministic	Rule-based	5563	0.61	25.3	-	-	95.6 (50%)	53.5 (74%)	1.33	0.00
	11	Stochastic	Rule-based	3424	0.24	22.2	-	-	104.1 (55%)	58.6 (82%)	0.08	0.00
	12	None	Stochastic	3288	0.00	32.9	-	-	107.6 (57%)	61.5 (86%)	1.73	0.13
	13	Deterministic	Stochastic	2746	0.07	23.9	-	-	106.7 (56%)	55.8 (78%)	1.41	0.00
	14	Stochastic	Stochastic	2354	0.00	23.5	-	-	103.0 (54%)	55.3 (77%)	1.99	0.00
Import/export capacity: 15 kW	15	Perfect	-	632	0.00	-	24.7	36.8	120.2 (63%)	65.2 (91%)	3.15	0.00
	16	None	Rule-based	8610	1.42	-	21.6	13.1	104.3 (55%)	57.1 (79%)	0.10	0.00
	17	Deterministic	Rule-based	4023	0.54	-	26.0	25.2	107.1 (56%)	61.7 (86%)	1.33	0.00
	18	Stochastic	Rule-based	2260	0.27	-	26.5	34.5	117.8 (62%)	64.8 (90%)	0.10	0.00
	19	None	Stochastic	3302	0.11	-	41.9	28.5	115.5 (61%)	64.1 (89%)	1.63	0.13
	20	Deterministic	Stochastic	1918	0.13	-	28.6	32.3	117.5 (62%)	64.8 (90%)	1.13	0.00
	21	Stochastic	Stochastic	1185	0.00	-	28.2	32.9	117.8 (62%)	64.8 (90%)	2.05	0.00

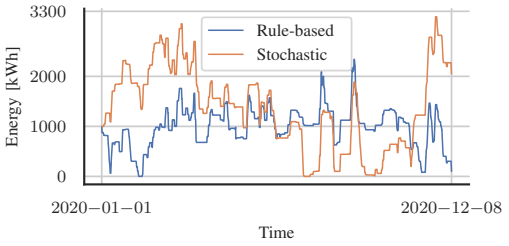

Fig. 7. Comparison of hydrogen SOC for rule-based (case 18) and stochastic long-term model (case 21) with stochastic short-term model through the entire optimization period for the weakly grid connected system.

price, for example due to grid tariffs. The trends are similar to previous cases (8-14), but the differences are even more pronounced. The stochastic short-term models (cases 18 and 21) have both the lowest load shedding and the highest export compared to the equivalent deterministic and no-forecast short-term models. Cases 19 and 21 also have higher outgoing SOC than the corresponding fixed end value cases (16 and 18) making them better prepared to prevent future scarcity.

The snapshot from case 21 in Fig. 6 shows positive import although the net generation (generation from VRESs minus demand) is positive. If the SOC is sufficiently low, it is important to increase the SOC to prevent potential future load shedding. This is also reflected by the brightest area in the long-term strategy shown in Fig. 5.

Fig. 7 shows how the stochastic long-term strategy adapts to seasonal variations compared to the rule-based method. The risk of scarcity is higher through the winter due to higher load and increased probability of sustained low generation from wind compared to solar power. Therefore, the SOC is higher in the beginning and the end of the year for the stochastic long-term model compared to the rule-based long-term model. The stochastic long-term model also permits lower SOC through the summer to enable buffering surplus generation.

Although the results originate from a small-scale power system, they are also relevant to large-scale power systems. To reach net zero emissions towards 2050, 63% of the energy will originate from VRESs with 74% of the total generation capacity [49]. The high share of variable and uncertain generation makes prevention of scarcity and extreme prices increasingly important. The stored hydro-dominated Nordic power system which has been operated as a competitive market where the price has been influenced by the risk of scarcity since the early 1990s [50] shows that this is a feasible direction.

IV. CONCLUSIONS

The work presented in this paper shows the importance of accounting for uncertainty in power systems when more of the dispatchable generation capacity in autonomous systems is replaced by VRESs and ESSs. The proposed multi-stage stochastic programming model has demonstrated a reduction in the operational costs associated with import, export and thermal generation while at the same time increasing the security of supply for the presented isolated microgrid compared to a deterministic point-forecast model and a no-forecast model. The results show a 70% cost reduction when using the stochastic model compared to a deterministic point-forecast model with fixed storage end value for the weakly grid connected system, where 95% of the improvement originates from reduction in load shedding. The model is also able to export excess energy while keeping the risk of load shedding low.

This is the accepted version of an article published in IEEE Transactions on Sustainable Energy
https://doi.org/10.1109/TSTE.2022.3156069

The benefits of the proposed model were most significant for weakly connected systems and systems with low dispatchable generation capacity.

Managing generation and load uncertainty is particularly important in MGs where stored energy is the limiting factor rather than installed capacity. Realistic and robust scheduling models are a key component in the efficient and secure operation of systems with a high share of VRESs and ESSs.

A. Future work

Possible steps towards a more applicable model could be to add more details such as: generation cost curves and efficiency as a function of charge/discharge for ESSs, ESS degradation costs, start/stop costs for generators and ESSs, as well as power flow equations. The proposed improvements will impose new challenges with respect to convexity which can be handled both with convex relaxations and integer variables, and by using stochastic dual dynamic integer programming as solution method [51].

Although SDDP is capable of handling several hundred state variables [52], the use of discrete Markov states to represent uncertainty has clear limitations with respect to dimensionality. Moreover, adding new types of random variables, such as new generation or demand, increases the number of scenarios rapidly. Therefore, random variables must be chosen carefully and can be managed with principal component analysis to reduce the dimensionality, and by using a linear model formulation of the random variables to enable the method to also scale up for larger systems.

ACKNOWLEDGMENT

This work has been funded by the Norwegian Research Council under grant number 272398. The authors would like to thank TrønderEnergi Kraft AS for sharing data from Rye Microgrid.

REFERENCES

[1] International Renewable Energy Agency, *Global energy transformation: A roadmap to 2050 (2019 edition)*, Abu Dhabi, 2019. ISBN 978-92-9260-121-8

[2] C. Kost, S. Shammugam, V. Jülch, H.-T. Nguyen, and T. Schlegl, "Levelized cost of electricity renewable energy technologies," 2018. [Online]. Available: https://www.ise.fraunhofer.de/content/dam/ise/en/documents/publications/studies/EN2018_Fraunhofer-ISE_LCOE_Renewable_Energy_Technologies.pdf (Accessed 2020-09-03).

[3] E. Mengelkamp, J. Gärttner, K. Rock, S. Kessler, L. Orsini, and C. Weinhardt, "Designing microgrid energy markets: A case study: The Brooklyn Microgrid," *Applied Energy*, vol. 210, pp. 870–880, 1 2018.

[4] W. Tushar, C. Yuen, T. K. Saha, T. Morstyn, A. C. Chapman, M. J. E. Alam, S. Hanif, and H. V. Poor, "Peer-to-peer energy systems for connected communities: A review of recent advances and emerging challenges," *Applied Energy*, vol. 282, p. 116131, 1 2021.

[5] M. Yan, M. Shahidehpour, A. Paaso, L. Zhang, A. Alabdulwahab, and A. Abusorrah, "Distribution Network-Constrained Optimization of Peer-to-Peer Transactive Energy Trading among Multi-Microgrids," *IEEE Transactions on Smart Grid*, vol. 12, no. 2, pp. 1033–1047, 3 2021.

[6] H. Karimi and S. Jadid, "Optimal energy management for multi-microgrid considering demand response programs: A stochastic multi-objective framework," *Energy*, vol. 195, p. 116992, 3 2020.

[7] A. Hasankhani and S. M. Hakimi, "Stochastic energy management of smart microgrid with intermittent renewable energy resources in electricity market," *Energy*, vol. 219, p. 119668, 3 2021.

[8] N. Hatziargyriou, H. Asano, R. Iravani, and C. Marnay, "Microgrids," *IEEE Power and Energy Magazine*, vol. 5, no. 4, pp. 78–94, 7 2007.

[9] J. Geske and R. Green, "Optimal Storage, Investment and Management under Uncertainty: It is Costly to Avoid Outages!" *The Energy Journal*, vol. 41, no. 2, 4 2020.

[10] N. A. Sepulveda, J. D. Jenkins, A. Edington, D. S. Mallapragada, and R. K. Lester, "The design space for long-duration energy storage in decarbonized power systems," *Nature Energy 2021 6:5*, vol. 6, no. 5, pp. 506–516, 3 2021.

[11] M. A. Pellow, C. J. Emmott, C. J. Barnhart, and S. M. Benson, "Hydrogen or batteries for grid storage? A net energy analysis," *Energy and Environmental Science*, vol. 8, no. 7, pp. 1938–1952, 7 2015.

[12] L. Valverde, F. Rosa, and C. Bordons, "Design, planning and management of a hydrogen-based microgrid," *IEEE Transactions on Industrial Informatics*, vol. 9, no. 3, pp. 1398–1404, 2013.

[13] Y. Han, G. Zhang, Q. Li, Z. You, W. Chen, and H. Liu, "Hierarchical energy management for PV/hydrogen/battery island DC microgrid," *International Journal of Hydrogen Energy*, vol. 44, no. 11, pp. 5507–5516, 2 2019.

[14] H. Yang, Q. Li, S. Zhao, W. Chen, and H. Liu, "A Hierarchical Self-Regulation Control for Economic Operation of AC/DC Hybrid Microgrid with Hydrogen Energy Storage System," *IEEE Access*, vol. 7, pp. 89 330–89 341, 2019.

[15] A. Kafetzis, C. Ziogou, K. D. Panopoulos, S. Papadopoulou, P. Seferlis, and S. Voutetakis, "Energy management strategies based on hybrid automata for islanded microgrids with renewable sources, batteries and hydrogen," *Renewable and Sustainable Energy Reviews*, vol. 134, p. 110118, 12 2020.

[16] A. Monforti Ferrario, F. Vivas, F. Segura Manzano, J. Andújar, E. Bocci, and L. Martirano, "Hydrogen vs. Battery in the Long-term Operation. A Comparative Between Energy Management Strategies for Hybrid Renewable Microgrids," *Electronics*, vol. 9, no. 4, p. 698, 4 2020.

[17] R. Palma-Behnke, C. Benavides, F. Lanas, B. Severino, L. Reyes, J. Llanos, and D. Saez, "A microgrid energy management system based on the rolling horizon strategy," *IEEE Transactions on Smart Grid*, vol. 4, no. 2, pp. 996–1006, 2013.

[18] M. Elkazaz, M. Sumner, and D. Thomas, "Energy management system for hybrid PV-wind-battery microgrid using convex programming, model predictive and rolling horizon predictive control with experimental validation," *International Journal of Electrical Power and Energy Systems*, vol. 115, p. 105483, 2 2020.

[19] M. Petrollese, L. Valverde, D. Cocco, G. Cau, and J. Guerra, "Real-time integration of optimal generation scheduling with MPC for the energy management of a renewable hydrogen-based microgrid," *Applied Energy*, vol. 166, pp. 96–106, 3 2016.

[20] A. G. Bakirtzis and E. S. Gavanidou, "Optimum operation of a small autonomous system with unconventional energy sources," *Electric Power Systems Research*, vol. 23, no. 2, pp. 93–102, 3 1992.

[21] P. Aaslid, M. Korpås, M. M. Belsnes, and O. B. Fosso, "Pricing electricity in constrained networks dominated by stochastic renewable generation and electric energy storage," *Electric Power Systems Research*, vol. 197, p. 107169, 8 2021.

[22] A. Michiorri, J. Lugaro, N. Siebert, R. Girard, and G. Kariniotakis, "Storage sizing for grid connected hybrid wind and storage power plants taking into account forecast errors autocorrelation," *Renewable Energy*, vol. 117, pp. 380–392, 3 2018.

[23] H. Shuai, J. Fang, X. Ai, Y. Tang, J. Wen, and H. He, "Stochastic optimization of economic dispatch for microgrid based on approximate dynamic programming," *IEEE Transactions on Smart Grid*, vol. 10, no. 3, pp. 2440–2452, 5 2019.

[24] M. Sedighizadeh, M. Esmaili, A. Jamshidi, and M. H. Ghaderi, "Stochastic multi-objective economic-environmental energy and reserve scheduling of microgrids considering battery energy storage system," *International Journal of Electrical Power and Energy Systems*, vol. 106, pp. 1–16, 3 2019.

[25] H. Moradi, M. Esfahanian, A. Abtahi, and A. Zilouchian, "Optimization and energy management of a standalone hybrid microgrid in the presence of battery storage system," *Energy*, vol. 147, pp. 226–238, 3 2018.

[26] I. Sperstad and M. Korpås, "Energy Storage Scheduling in Distribution Systems Considering Wind and Photovoltaic Generation Uncertainties," *Energies*, vol. 12, no. 7, p. 1231, 3 2019.

[27] O. Wolfgang, A. Haugstad, B. Mo, A. Gjelsvik, I. Wangensteen, and G. Doorman, "Hydro reservoir handling in Norway before and after deregulation," *Energy*, vol. 34, no. 10, pp. 1642–1651, 10 2009.

[28] O. Dowson, "The policy graph decomposition of multistage stochastic optimization problems," *Networks*, vol. 76, no. 1, pp. 3–23, 2020.

This is the accepted version of an article published in IEEE Transactions on Sustainable Energy
https://doi.org/10.1109/TSTE.2022.3156069

[29] A. Gjelsvik, M. M. Belsnes, and A. Haugstad, "An algorithm for stochastic medium-term hydrothermal scheduling under spot price uncertainty," in *Proc. 13th Power System Computation Conference*, Trondheim, Norway, 1999, pp. 1079–1085.
[30] J. R. Birge and F. Louveaux, *Introduction to Stochastic Programming*, 2nd ed., ser. Springer Series in Operations Research and Financial Engineering. New York, NY: Springer New York, 2011. ISBN 978-1-4614-0236-7
[31] M. V. F. Pereira and L. M. V. G. Pinto, "Multi-stage stochastic optimization applied to energy planning," *Mathematical Programming*, vol. 52, no. 1-3, pp. 359–375, 5 1991.
[32] P. Girardeau, V. Leclere, and A. B. Philpott, "On the convergence of decomposition methods for multistage stochastic convex programs," *Mathematics of Operations Research*, vol. 40, no. 1, pp. 130–145, 2 2015.
[33] R. E. Bellman, *Dynamic Programming*. Dover Publications, 2003. ISBN 9780486428093
[34] A. Shapiro, "Analysis of stochastic dual dynamic programming method," *European Journal of Operational Research*, 2011.
[35] A. Papavasiliou, Y. Mou, L. Cambier, and D. Scieur, "Application of Stochastic Dual Dynamic Programming to the Real-Time Dispatch of Storage under Renewable Supply Uncertainty," *IEEE Transactions on Sustainable Energy*, vol. 9, no. 2, pp. 547–558, 4 2018.
[36] S. Stoft, *Power System Economics: Designing Markets for Electricity*. IEEE Press, 2002. ISBN 9780470545584
[37] "Vestas V27." [Online]. Available: https://en.wind-turbine-models.com/turbines/9-vestas-v27 (Accessed 2021-06-18).
[38] J. F. Manwell, J. G. McGowan, and A. L. Rogers, *Wind energy explained: theory, design and application.* John Wiley & Sons, 2010. ISBN 978-0-470-01500-1
[39] O. Dowson and L. Kapelevich, "SDDP.jl: A julia package for stochastic dual dynamic programming," *INFORMS Journal on Computing*, vol. 33, no. 1, pp. 27–33, 12 2021.
[40] "Remote EU project," 2021. [Online]. Available: https://www.remote-euproject.eu/remote-project/ (Accessed 2021-06-17).
[41] P. Marocco, D. Ferrero, M. Gandiglio, and M. Santarelli, "Remote area Energy supply with Multiple Options for integrated hydrogen-based TEchnologies - Deliverable number 2.2," 2018. [Online]. Available: https://www.remote-euproject.eu/remote18/rem18-cont/uploads/2019/03/REMOTE-D2.2.pdf (Accessed 2021-06-17).
[42] World Meteorological Organization, "Guide to Meteorological Instruments and Methods of Observation," 2008. [Online]. Available: https://www.weather.gov/media/epz/mesonet/CWOP-WMO8.pdf (Accessed 2021-04-12).
[43] P. Aaslid, "Rye microgrid load and generation data, and meteorological forecasts." 2021. [Online]. Available: https://doi.org/10.5281/zenodo.4448894 (Accessed 2021-06-21).
[44] P. Pinson, H. Madsen, H. A. Nielsen, G. Papaefthymiou, and B. Klöckl, "From probabilistic forecasts to statistical scenarios of short-term wind power production," *Wind Energy*, vol. 12, no. 1, pp. 51–62, 1 2009.
[45] G. Ridgeway, "Generalized Boosted Models: A guide to the gbm package," 2020. [Online]. Available: https://cran.r-project.org/web/packages/gbm/vignettes/gbm.pdf (Accessed 2021-06-17).
[46] J. H. Friedman, "Greedy Function Approximation: A Gradient Boosting Machine," *The Annals of Statistics*, vol. 29, no. 5, pp. 1189–1232, 6 2001.
[47] A. D. Blaom, F. Kiraly, Y. Simillides, D. Arenas, T. Lienart, and S. J. Vollmer, "MLJ: A Julia package for composable machine learning," *The Journal of Open Source Software*, vol. 5, no. 55, p. 2704, 7 2020.
[48] F. Pedregosa, G. Varoquaux, A. Gramfort, V. Michel, B. Thirion, O. Grisel, M. Blondel, P. Prettenhofer, R. Weiss, V. Dubourg, J. Vanderplas, A. Passos, D. Cournapeau, M. Brucher, M. Perrot, and E. Duchesnay, "Scikit-learn: Machine Learning in Python," *Journal of Machine Learning Research*, vol. 12, pp. 2825–2830, 2011.
[49] International Renewable Energy Agency, *WORLD ENERGY TRANSITIONS OUTLOOK 1.5° C PATHWAY*, 2021. ISBN 978-92-9260-334-2
[50] O. B. Fosso, A. Gjelsvik, A. Haugstad, B. Mo, and I. Wangensteen, "Generation scheduling in a deregulated system. the norwegian case," *IEEE Transactions on Power Systems*, vol. 14, no. 1, pp. 75–80, 1999.
[51] J. Zou, S. Ahmed, and X. A. Sun, "Stochastic dual dynamic integer programming," *Mathematical Programming*, pp. 1–42, 3 2018.
[52] K. S. Gjerden, A. Helseth, B. Mo, and G. Warland, "Hydrothermal scheduling in Norway using stochastic dual dynamic programming; a large-scale case study," in *2015 IEEE Eindhoven PowerTech*. IEEE, 6 2015. doi: 10.1109/PTC.2015.7232278. ISBN 978-1-4799-7693-5 pp. 1–6.

Per Aaslid received the M.Sc. degree in engineering cybernetics in 2009 from Norwegian University of Science and Technology (NTNU), Trondheim, Norway. He is a research scientist at SINTEF Energy Research and is currently pursuing the Ph.D. degree with the Department of Electrical Power Engineering (NTNU). His research interests include stochastic optimization, operation of distributed energy storages and hydropower optimization.

Magnus Korpås received his Ph.D. degree from the Norwegian University of Science and Technology (NTNU), Norway, in 2004 on the topic of optimizing the use of energy storage for distributed wind energy in the power market. He is currently working as Professor at the Department of Electric Power Engineering, NTNU, where he also leads the Electricity Markets and Energy System Planning research group. He is a leader and active participant in several large energy research projects at national and European levels. He is a former Research Director of the Department of Energy Systems at SINTEF Energy Research, Norway. He was a visiting researcher in the MIT Laboratory for Information & Decision Systems (LIDS) in 2018-2019. He is also the leader of the scientific committee and the leader of the work package on flexible resources in the power system in the Centre for Intelligent Electricity Distribution (CINELDI).

Michael M Belsnes has a M.Sc. from Technical University of Denmark 1995 and received his PhD degree from NTNU in 2008 on the topic "Optimal Utilization of the Norwegian Hydropower System". In SINTEF Energy Research where he was employed from 1995, he has worked with power system modelling and hydropower scheduling both as researcher and research manager. He is currently managing development and deployment of the scheduling tools deployed by: power producers, the Norwegian regulator, and Nordic TSOs. He is active as sub-program manager in EERA JP HydroPower and JP e3s.

Olav B Fosso is Professor at the Department of Electric Power Engineering of the Norwegian University of Science and Technology (NTNU). He has previously held positions as Scientific Advisor and Senior Research Scientist at SINTEF Energy Research, and Director of NTNUs Strategic Thematic Area Energy from September 2014 - September 2016. He has been Chairman of CIGRE SC C5 Electricity Markets and Regulation and Member of CIGRE Technical Committee (2008 – 2014). He has been expert evaluator in Horizon2020 and in a number of science foundation internationally. His research activities involve hydro scheduling, market integration of intermittent generation and signal analysis for study of power system's dynamics and stability.

Paper V

The paper Stochastic Operation of Energy Constrained Microgrids Considering Battery Degradation has been accepted for Power Systems Computation Conference (PSCC) 2022.

Stochastic Operation of Energy Constrained Microgrids Considering Battery Degradation

Per Aaslid*†, Magnus Korpås†, Michael M Belsnes* and Olav B Fosso†
*Department of Energy Systems, SINTEF Energy Research, Trondheim, Norway
†Department of Electrical Power Engineering, Norwegian University of Science and Technology, Trondheim, Norway

***Abstract*—Power systems with high penetration of variable renewable generation are vulnerable to periods with low generation. An alternative to retain high dispatchable generation capacity is electric energy storage that enables utilization of surplus power, where the electric energy storage contributes to the security of supply. Such systems can be considered as energy-constrained, and the operation of the electric energy storage must balance the minimization of the current operating costs against the risk of not being able to meet the future demand. Safe and efficient operation requires stochastic methods with sufficient foresight. Operation dependent storage degradation is a complicating factor. This paper proposes a linear approximation of battery state-of-charge degradation and implements it in a stochastic dual dynamic programming based energy-management model in combination with cycling degradation. The long-term implications of degradation modelling in the daily operation are studied for a small Norwegian microgrid with variable renewable power generation and limited dispatchable generation capacity as well as battery and hydrogen storage to balance supply and demand. Our results show that the proposed strategy can prolong the expected battery lifetime by more than four years compared to the naive stochastic strategy but may cause increased degradation for other system resources.**

***Index Terms*—Energy Management, Electric Energy Storage, Multi-Stage Stochastic Programming, Battery Degradation**

I. Introduction

Electricity systems with high penetration of variable renewable energy sources (VRESs) rely on sufficient dispatchable generation capacity to meet the peak demand in periods with low VRES generation. An alternative to dispatchable thermal generation capacity is to utilize electric energy storage (EES) flexibility. A challenge with EES is that the current decision also affects the energy content and the capability of providing capacity in the future. The decisions here and now must be taken while accounting for future power generation and load under uncertainty, and needs to balance the risk of generation curtailment versus the risk of not being able to meet the demand. The operation of EES in these situations can be seen as a precaution or arbitrage against extreme prices [1], [2]. Moreover, these systems require significant VRES overcapacity and will also be exposed to lasting periods with excess energy resulting in generation curtailment [3]. The EESs must be operated to balance short-term variations in generation and demand, and also store energy for potential future energy deficit.

Different EES technologies have complementary properties with respect to power and energy scalability. Lithium-ion batteries have gained high attention both in the research community as well as for power system applications due to their ability to deliver and absorb very high power almost instantaneously with very high efficiency. They also have a relatively high energy to weight ratio compared to similar battery technologies. A key factor of large scale VRES integration is long-duration energy storage [4]. Batteries are expensive to scale up with respect to energy compared to hydrogen, which can be stored in large tanks and scaled up at a relatively low cost. However, the cost of fuel cells and electrolyzers are still very high, and the round-trip efficiency is poor compared to batteries [5].

Unlike traditional thermal power generators where the marginal operating cost is well defined based on fuel and emission costs, VRESs have marginal operating cost close to zero. However, the expected lifetime of the power system components, such as the EESs, are influenced by their operational pattern. Degradation characteristics differ for batteries and hydrogen systems. The aging of hydrogen fuel cells are largely affected by start, stop and rapid ramping. However, the degradation has often been studied for vehicles that exhibit several cycles each hour [6], while a grid connected fuel cell will operate with less frequent cycling. Moreover, degradation of fuel cells can also be related to dry membranes caused by limited operation, and modest operation can extend the expected lifetime compared to low operation [7]. The degradation cost of the hydrogen system has therefore been neglected.

The degradation of lithium-ion batteries is closely related to operating conditions like charge/discharge power, depth-of-discharge (DOD), state-of-charge (SOC), temperature, and ampere throughput [8]. Energy management of VRES typically involves daily cycles, and the battery will rarely operate close to its maximum power capabilities. Moreover, the battery temperature will be controlled to ensure optimal operating conditions and minimal degradation. Whereas balancing the short-term fluctuation causes degradation due to DOD, long-term storage increases the SOC degradation. This paper will therefore consider degradation caused by DOD and SOC.

The aging is therefore influenced by the operational pattern, and the optimal power dispatch largely depends on the battery's aging model [9]. Previous studies of microgrid

This work has been funded by the Norwegian Research Council under grant number 272398.

(MG) economic dispatch often neglect the cost associated with degradation [10], [11]. Single factor models, considering degradation either as a function of power, SOC, DOD, or ampere hour throughput, are also widely adopted [9]. For example, references [12]–[15] assume the degradation is proportional with energy throughput. More sophisticated models capture non-linear effects, either as a single factor model [16] or combined models [17], [18].

However, previous studies mainly focus on daily battery cycling under variable photovoltaic (PV) generation with deterministic models [9], [16], [17]. This paper also considers the effect of lasting generation surplus and deficit with respect to how the battery and hydrogen storage are operated. To account for the uncertainty in generation from VRES, which is crucial for energy constrained systems [19], a multi-stage stochastic formulation is implemented. Moreover, the expected implication on the battery lifetime is considered using actual data for a real MG over a whole year.

Non-linear models are often computationally intensive, especially for large-scale systems and stochastic problems. Convex and linear problem formulations reduce the computational burden, and enable utilization of decomposition techniques such as dual decomposition. Reference [20] proposes a piecewise linear relaxation of the the non-linear DOD degradation, and shows that a cost reduction can be achieved by considering the cyclic degradation in the market clearing of a battery. However, linear approximation of the non-linear SOC degradation has gained less attention.

This paper proposes a piece-wise linear approximation of the battery SOC degradation effect, and demonstrates it in combination with linear DOD degradation [20] on a real MG from the EU project REMOTE [21], [22]. The system is operating islanded, and is energy constrained since the backup generator is too small to cover the peak demand and the EES must be operated to prevent load shedding in extreme situations. The optimal operation is considered using rolling horizon [23] and stochastic dual dynamic programming (SDDP) [24]. The system is simulated for a whole year with rolling horizon using real observations from the MG and scenarios generated from historical weather forecasts. Infinite horizon is embedded using cyclic Markov chains [25], and the implication of including battery degradation will be studied with respect to the costs, VRES and EES utilization as well as expected battery lifetime.

The contributions of this paper can be summarized as: *i)* a linear battery SOC degradation formulation, *ii)* a multi-stage stochastic energy management formulation including both battery DOD and SOC degradation, and *iii)* an analysis of a full year operation of an actual MG using the proposed formulation to valuate the importance of considering battery degradation in a life cycle perspective.

The remainder of the paper is organized as follows: section II describes the rolling horizon simulation method as well as the SDDP algorithm, and derives the linear power system model including the SOC degradation model; section III presents how the proposed method is implemented and the numerical values of the cases; section IV shows and discusses the results; and section V draws the conclusions and suggests future work.

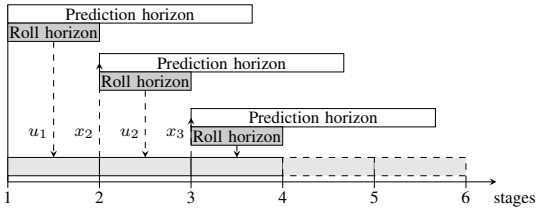

Fig. 1. Rolling horizon optimization.

II. Method

This section presents the rolling horizon stochastic energy-management model where the goal is to find the optimal stage-wise control decisions u_s at each stage s for the in-going state x_s and the stage-wise uncertainty ω_s.

A. Rolling horizon simulation

Generation forecasts are based on weather forecasts issued with fixed intervals, and the stochastic model is trained each time a new forecast is available for the prediction horizon as illustrated in Fig. 1. The actual generation and demand is observed and evaluated for the roll horizon interval using the trained stochastic model yielding the optimal control u_s that is implemented. Finally, the optimization horizon is moved forward and the procedure is repeated using the end state x_{s+1} from previous optimization as the initial value.

B. Multi-stage stochastic programming

This paper considers multi-stage stochastic programming (MSSP) for solving the proposed energy management problem. MSSP captures that energy management is a sequential decision making process and recognizes that decisions can be updated stage-wise as uncertainty is revealed. The MSSP formulation in (1a) to (1c) is divided into several stages s, each representing a discrete moment in time. The goal is to minimize the current and future operating costs. State variables x_s represent variables connected across stages, such as EES SOC. Control variables u_s are decisions, both implicit and explicit, and must be within the technical limitations of the system given by the set of admissible controls (1c). The state transition function (1b) describes the relation between the state variables across stages. The random variable ω_s represents the uncertainty in demand and VRES generation.

$$\min_{u_t} \Bigg\{ C_1(x_1,u_1,\omega_1) + \mathop{\mathbb{E}}_{\omega_2|\omega_1} \Bigg[\min_{u_2} \Big(C_2(x_2,u_2,\omega_2) + \dots + \mathop{\mathbb{E}}_{\omega_S|\omega_{S-1},\dots,\omega_2} \Big[\min_{u_S} \big(C_S(x_S,u_S,\omega_S) \big) \Big] \Big) \Bigg] \Bigg\} \quad \text{(1a)}$$

$$\text{s.t.} \quad x_{s+1} = T_s(x_s, u_s, \omega_s) \tag{1b}$$
$$u_s \in U_s(x_s, \omega_s) \tag{1c}$$

Generation from solar and wind power are correlated and has significant auto-correlation. However, the auto-correlation is partially captured by the stage-wise scenarios that can span several hours. By assuming the random variable is stage-wise independent and has a discrete set of realizations for each stage, the problem can be formulated on extended form. Instead of solving the intractable extended problem, SDDP [24] decomposes the problem into sub-problems for each stage $s \in S$ and realization of the random variable $\omega_s \in \Omega_s$ as shown in (2a) to (2e). The algorithm is divided into two phases: forward pass and backward recursion. The forward pass samples a random variable for each stage and solves the sequence of sub-problems using the outgoing state of stage s as the in-going state to stage $s+1$. When the final stage is reached, the backward recursion starts by solving the final stage for all the random variables. From convexity, the dual variables λ_s of the state variable x_s (2b) can be used to generate a linear cutting plane (2e) that acts as a lower bound for the previous stage problem, and the procedure is repeated all the way back to the first stage. The whole procedure is repeated, adding new cuts for each iteration k, until the convergence criteria is met [24], [25] and it has been shown that the algorithm under certain conditions will converge [26].

$$\min_{u_s, x_s, x_{s+1}, \theta_s} C_s(x_s, u_s, \omega_s) + \theta_s \tag{2a}$$
$$\text{s.t. } x_s = \bar{x_s}, \quad [\lambda_s] \tag{2b}$$
$$x_{s+1} = T_s(x_s, u_s, \omega_s) \tag{2c}$$
$$u_s \in U_s(x_s, \omega_s) \tag{2d}$$
$$\theta_s \geq \alpha_s^k + \beta_s^k x_{s+1}, \quad k \in \{1, 2, \ldots, K\} \tag{2e}$$

C. Power system model

Each stage-wise problem in (1a) to (1c) comprises a power system model with multiple timesteps t. The power system model including the battery degradation model will be expressed using the following sets and indices:

- $t \in \mathcal{T}_s$: Time index t and the set of time steps $\mathcal{T}_s$ from stage s.
- $g \in \mathcal{G}$: Generator g and the set of dispatchable generators $\mathcal{G}$.
- $r \in \mathcal{R}$: VRES r and the set of VRESs $\mathcal{R}$.
- $d \in \mathcal{D}$: Consumer d and the set of consumers $\mathcal{D}$.
- $e \in \mathcal{E}$: EES e and the set of EESs $\mathcal{E}$.
- $k_\delta \in \mathcal{K}_\delta$: Battery cycling segment k_δ in the set of segments $\mathcal{K}_\delta$.
- $k_\sigma^{up} \in \mathcal{K}_\sigma^{up}/k_\sigma^{dn} \in \mathcal{K}_\sigma^{up}$: Battery SOC segment $k_\sigma^{up}/k_\sigma^{dn}$ direction up/down in the set of segments $\mathcal{K}_\sigma^{up}/\mathcal{K}_\sigma^{up}$ respectively.

The following parameters have been used:

- ΔT_t: Timestep t step length.
- PG_g^{max}: Generator g maximum power dispatch.
- C_g: Generator g marginal operating cost.
- $PR_{r,t}^{max}$: VRES r maximum power at time t.
- $PD_{d,t}$: Demand of consumer d at time t.
- C_d: Consumer d marginal load shedding cost.
- SOC_e^{min}/SOC_e^{max}: EES e minimum and maximum SOC.
- PS_e^c/PS_e^d: EES e maximum charge/discharge power.
- C_{e,k_δ}: EES e DOD marginal degradation cost segment k.
- SOC_e^{ref}: EES e SOC degradation reference value.
- $C_{e,k_\sigma}^{up}/C_{e,k_\sigma}^{dn}$: EES e SOC marginal degradation cost up/down segment $k_\sigma^{up}/k_\sigma^{dn}$.
- η_e^c/η_e^d: EES e charge/discharge efficiency.
- R: Battery replacement cost.

The functions and variables are:

- $p_{g,t}$: Generator g power dispatch at time t.
- $p_{g,t}$: VRES r power dispatch at time t.
- $p_{d,t}$: Consumer d demand at time t.
- $pls_{d,t}$: Consumer d load shedding at time t.
- $ps_{e,t(,k_\delta)}^c/ps_{e,t(,k_\delta)}^d$: EES e power charge/discharge DOD (segment k_δ) at time t.
- soc_{e,t,k_δ}: EES e SOC DOD segment k_δ at time t.
- $soc_{e,t,k_\sigma}^{up}/soc_{e,t,k_\sigma}^{dn}$: EES e SOC degradation segment $k_\sigma^{up}/k_\sigma^{dn}$ above/below reference value at time t.
- δ_t: Unitless EES cycle depth at time t.
- σ_t: Unitless EES SOC at time t.
- σ^{ref}: Unitless EES reference SOC.
- $f_\delta(\delta_t)$: Incremental battery fade as a function of cycle depth δ_t at time t.
- $f_\sigma(\sigma_t)$: Incremental battery fade as a function of SOC σ_t at time t.

The resulting model is summarized in (3) to (13). The objective is to minimize the dispatchable generation costs, load shedding, and EES degradation associated with both DOD and SOC (3). The total power injections and withdrawals must balance at all time steps (4). The generation, both dispatchable and VRES, must respect the maximum generation (5) and (6). Demand that can not be met, causes load shedding (7). The battery charge/discharge must respect the maximum limits, both per segment (8) and (9) and the sum of the segments (10) and (11). The EES energy balance is expressed per segment (12), where the segments are divided into equal sizes (13).

$$\min \sum_{t \in \mathcal{T}} \left[\sum_{g \in \mathcal{G}} C_g p_{g,t} + \sum_{d \in \mathcal{D}} C_d pls_{d,t} + \sum_{e \in \mathcal{E}} \sum_{j \in \mathcal{J}} C_{e,k_\delta} ps_{e,t,k_\delta}^d + \sum_{e \in \mathcal{E}} \left(\sum_{k_\sigma \in \mathcal{K}_\sigma^{up}} C_{e,k_\sigma}^{up} soc_{e,t,k_\sigma}^{up} + \sum_{k_\sigma \in \mathcal{K}_\sigma^{dn}} C_{e,k_\sigma}^{dn} soc_{e,t,k_\sigma}^{dn} \right) \right] \tag{3}$$

subject to

$$\sum_{g \in \mathcal{G}} p_{g,t} + \sum_{r \in \mathcal{R}} p_{r,t} + \sum_{e \in \mathcal{E}} ps_{e,t}^d = \sum_{d \in \mathcal{D}} p_{d,t} + \sum_{e \in \mathcal{E}} ps_{e,t}^c \tag{4}$$

$$0 \leq p_{g,t} \leq PG_g^{max} \tag{5}$$
$$0 \leq p_{r,t} \leq PR_{r,t}^{max} \tag{6}$$
$$p_{d,t} = PD_{d,t} - pls_{d,t} \tag{7}$$
$$0 \leq ps_{e,t,k_\delta}^c \leq PS_e^c \tag{8}$$
$$0 \leq ps_{e,t,k_\delta}^d \leq PS_e^d \tag{9}$$
$$ps_{e,t}^c = \sum_{j \in \mathcal{J}} ps_{e,t,k_\delta}^c \leq PS_e^c \tag{10}$$
$$ps_{e,t}^d = \sum_{j \in \mathcal{J}} ps_{e,t,k_\delta}^d \leq PS_e^d \tag{11}$$

$$soc_{e,t,k_\delta} = soc_{e,t-1,k_\delta} + \Delta T_t \left(\eta_e^c ps_{e,t,k_\delta}^c - \frac{1}{\eta_e^d} ps_{e,t,k_\delta}^d \right) \tag{12}$$
$$0 \leq soc_{e,t,k_\delta} \leq \frac{1}{|\mathcal{K}_\delta|} (SOC_e^{max} - SOC_e^{min}) \tag{13}$$

Note that restrictions to prevent simultaneous charging and discharging have not been included since it requires integer variables or non-linear modeling. This assumption implies that dumping of energy from the battery is accepted. This is not a problem when the VRES generation can be curtailed at no cost. However, by introducing SOC degradation cost, situations where dumping of energy is beneficial might arise. Moreover, minimum power for the thermal generator and the hydrogen system has not been considered since it would require binary variables that is not supported by standard SDDP. As a consequence, the flexibility of the diesel generator and the hydrogen system is overestimated and the battery cycling need might be underestimated. This limitation can be overcome by using SDDiP [27], but would increase the computational burden significantly.

The state x_s comprises the initial SOC variable soc_{e,t,k_δ} at each stage, and the final SOC variable at the outgoing state x_{s+1}. The random variable ω comprises the renewable generation $PR_{r,t}^{max}$ and the demand $PD_{d,t}$ for all the steps in the stage. The remaining variables are decisions u_s, either explicit or implicit.

D. EES degradation model

Experimental results show that the degradation rate of lithium-ion batteries increases with increasing DOD. Moreover, the degradation rate is also higher for high SOC [28], [29], but very low SOC will also cause high degradation [30]–[33].

The proposed model assumes the degradation due to DOD and SOC are decoupled. For an arbitrary convex DOD capacity fade function $f_\delta(\delta_t)$, the EES SOC is divided into equally sized segments K_δ yielding cost coefficients $C_{\delta k}$ (14) [20].

$$C_{\delta k} = \frac{R}{\eta^d SOC^{max}} |\mathcal{K}_\delta| \left[f_\delta \left(\frac{k}{|\mathcal{K}_\delta|} \right) - f_\delta \left(\frac{k-1}{|\mathcal{K}_\delta|} \right) \right], k \in \mathcal{K}_\delta \tag{14}$$

Each energy level soc_t and charge/discharge ps_t^c/ps_t^d is divided into K_δ segments. Since the marginal cost curve is convex, the cheapest available segment will always be discharged, and the suggested method will therefore count cycles in a similar manner as the Rainflow counting algorithm [34].

The same principle can be used for modelling the SOC degradation. For an arbitrary convex SOC capacity fade function $f_\sigma(\sigma)$, as illustrated in Fig. 3, σ^{ref} represents the SOC level where the SOC degradation is lowest as shown in (15).

$$\sigma^{ref} = \underset{\sigma}{\operatorname{argmin}} f_\sigma(\sigma) \tag{15}$$

The incremental capacity fade as a function of SOC can be found by taking the derivative of $f_\sigma(\sigma)$ with respect to soc_t.

$$\frac{\partial f_\sigma(\sigma_t)}{\partial soc_t} = \frac{df_\sigma(\sigma_t)}{d\sigma_t} \frac{\partial \sigma_t}{\partial soc_t} = \frac{1}{SOC^{max}} \frac{df_\sigma(\sigma_t)}{d\sigma_t} \tag{16}$$

The $soc_{e,t}$ variable is divided into K_σ^{up} and K_σ^{dn} equally sized segments $soc_{e,t,k}^{up}$ and $soc_{e,t,k}^{dn}$ for up and down direction as illustrated by the orange and green segments in Fig. 3 respectively, and shown in (17) to (20). Therefore, $soc_{e,t,k}^{up}$ and $soc_{e,t,k}^{dn}$ represent the distance from the reference value in both directions.

$$\sum_{k \in \mathcal{K}_\sigma^{up}} soc_{e,t,k}^{up} \geq soc_{e,t} - SOC_e^{ref} \tag{17}$$
$$\sum_{k \in \mathcal{K}_\sigma^{dn}} soc_{e,t,k}^{dn} \geq SOC_e^{ref} - soc_{e,t} \tag{18}$$
$$0 \leq soc_{e,t,k}^{up} \leq \frac{1}{|\mathcal{K}_\sigma^{up}|} \left(SOC^{max} - SOC_e^{ref} \right) \tag{19}$$
$$0 \leq soc_{e,t,k}^{dn} \leq \frac{1}{|\mathcal{K}_\sigma^{dn}|} SOC_e^{ref} \tag{20}$$

Let $C_{\sigma,k}^{up}$ and $C_{\sigma,k}^{dn}$ denote the incremental aging cost with respect to each segment in either direction $soc_{e,t,k}^{up}$ and $soc_{e,t,k}^{dn}$, which can be interpreted as the segment slopes in Fig. 3. The resulting cost coefficients are expressed in (21) and (22).

$$C_{\sigma k}^{up} = \frac{R}{SOC^{max}} |\mathcal{K}_\sigma^{up}| \left[f_\sigma \left(\sigma^{ref} + \frac{k}{|\mathcal{K}_\sigma^{up}|} (1 - \sigma^{ref}) \right) - f_\sigma \left(\sigma^{ref} + \frac{k-1}{|\mathcal{K}_\sigma^{up}|} (1 - \sigma^{ref}) \right) \right], k \in \mathcal{K}_\sigma^{up} \tag{21}$$

$$C_{\sigma k}^{dn} = \frac{R}{SOC^{max}} |\mathcal{K}_\sigma^{dn}| \left[f_\sigma \left(\sigma^{ref} - \frac{k}{|\mathcal{K}_\sigma^{dn}|} \sigma^{ref} \right) - f_\sigma \left(\sigma^{ref} - \frac{k-1}{|\mathcal{K}_\sigma^{dn}|} \sigma^{ref} \right) \right], k \in \mathcal{K}_\sigma^{dn} \tag{22}$$

The cheapest segments will always be used first, and the correct segment will be used given a convex cost function. Non-convex cost functions should consider convex relaxation or mixed-integer programming to ensure global optimality but has not been considered in this paper.

III. Implementation and Numerical Values

The proposed method is implemented in Julia (1.4.2) with SDDP.jl (0.3.14) [35] and Gurobi (9.1). The models were trained with 50 SDDP iterations.

TABLE I
MICROGRID NUMERICAL VALUES

Description	Unit	Value
Wind turbine capacity	[kW]	135
Solar PV capacity	[kW]	86
Diesel generator capcity	[kW]	25 / 75
Diesel generation cost	[€/MWh]	100
Load shedding cost	[€/MWh]	5000

TABLE II
NUMERICAL VALUES FOR MICROGRID EES.

Description	Unit	Lithium-ion	Hydrogen
Charge power	[kW]	500	55
Discharge power	[kW]	500	100
Size	[kWh]	500 / 1000	3300 / -
Charge efficiency	[%]	96	64
Discharge efficiency	[%]	96	50
Replacement cost	[€/kWh]	100	NA

A. Microgrid

The model has been tested on the Rye microgrid in central Norway that is partly funded by the Horizon 2020 project REMOTE [21]. The MG comprises a few farms and houses, and is supplied by a wind turbine, solar PV, and a diesel generator that serves as backup in case of insufficient VRES generation. The system is equipped with battery and hydrogen storage to balance supply and demand [22]. Load shedding costs occur if the supply is unable to meet the demand. Numerical values for the MG are shown in Table I, and the EES in Table II. Note that the wind and diesel generator sizes in this case differs from the actual system. Fig. 2 shows the four day average VRES generation and demand for the whole period.

B. Battery degradation

This paper uses a quadratic DOD capacity fade function (23) [17], [33]. The upper range of the SOC stress function (24) is exponential [36], while the lower part is defined to capture the potential collapse associated with operating at very low SOC

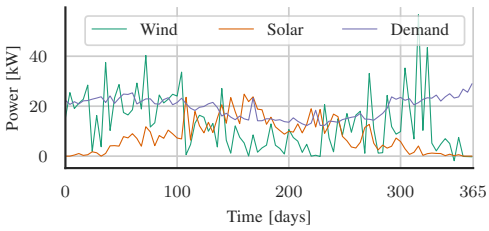

Fig. 2. Four day average generation and demand for the optimization period.

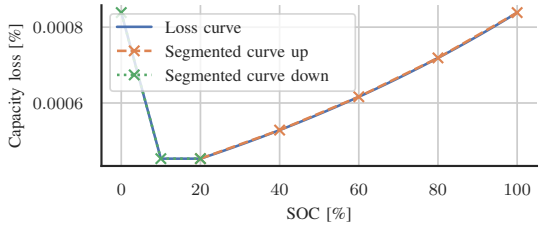

Fig. 3. Continuous and linearized SOC capacity loss functions.

[18], [32]. Note that any convex fade function can be used.

$$f_\delta(\delta) = k_\delta \ \delta^2 \tag{23}$$

$$f_\sigma(\sigma) = \begin{cases} k_{\sigma 1} e^{k_{\sigma 2}(\sigma - \sigma^{ref})} & 0.2 \leq \sigma \leq 1 \\ f_\sigma(1.0) + \frac{\sigma}{0.1}(f_\sigma(0.2) - f_\sigma(1.0)) & 0 \leq \sigma < 0.1 \\ f_\sigma(0.2) & 0.1 \leq \sigma < 0.2 \end{cases} \tag{24}$$

Assuming the battery fade is 85% higher at 90% compared to 10% SOC [37], yields $k_{\sigma 2} = 0.769$. The battery is assumed to reach end of life after 10 years with 3,000 cycles at 80% DOD with 50% average SOC and after 20 years with no cycling at 50% SOC. These assumptions yield $k_\delta = 3.092\text{e}{-4}$ and $k_{\sigma 1} = 5.708\text{e}{-6}$, respectively. The resulting SOC loss function and the corresponding linearized segments are shown in Fig. 3. The SOC loss curve is assumed to be flat between 10 and 20%, and the SOC degradation is equal at 0 and 100% SOC to also capture capacity fade at low SOC.

C. Scenarios and stages

The time-series for wind and solar PV power and demand are based on actual values from the Rye MG through year 2020 and is available online [38]. The wind power has been scaled down to 60% of the original size. Wind, solar PV and demand have each been forecasted with a low, medium, and high scenario with probability 20, 60 and 20% respectively, based on the 0.2, 0.5, and 0.8 quantiles, yielding a combination of 27 scenarios. These have been ordered based on accumulated net production and reduced by selecting the median scenario of the percentiles 0-10, 10-30, 30-70, 70-90, and 90-100 with the corresponding probabilities 0.1, 0.2, 0.4, 0.2, and 0.1. More sophisticated scenario generation methods could have been used but are outside the scope of this paper. The individual percentiles are published online [39]. The interval between the four first stages are 6 hours each, the next is 24 hours, while the final is 72 hours and repeated cyclicly with discount factor 0.7 as described in reference [25]. The final stage is beyond the meterological forecast, and historical daily mean values are applied as scenarios using the same quantiles as previous stages.

D. Cases

The model has been simulated with three different variants of the system with respect to generator and EES sizes as

TABLE III
OVERVIEW OF CASES THE PROPOSED MODEL HAS BEEN TESTED ON.

Case	Diesel generator [kW]	Battery [kWh]	Hydrogen [kWh]
1.	25	500	3300
2.	75	500	3300
3.	25	1000	-

TABLE IV
OVERVIEW OF METHODS THE PROPOSED CASES HAVE BEEN ANALYZED WITH.

Method	Forecast	DOD	SOC
a.	Perfect	X	X
b.	Deterministic		
c.	Stochastic		
d.	Stochastic	X	
e.	Stochastic		X
f.	Stochastic	X	X

shown in Table III. The systems in cases *1* and *3* are energy constrained since the diesel generator is too small to meet the peak demand, hence load shedding depends on how the EESs are scheduled. However, the diesel generator in case *2* is large enough to always meet the peak demand, hence there is never a risk of scarcity unless the generator fails.

Each case will be analyzed with perfect forecast, deterministic forecast, and stochastic optimization, both with and without degradation in the optimization model as shown in Table IV.

IV. RESULTS AND DISCUSSION

The main objective is to always meet the demand in the most cost effective way by using as much VRES generation as possible, and only using diesel if necessary to avoid load shedding. EES must also be utilized to maximize the VRES utilization and to minimize the diesel consumption and the load shedding. However, the battery degradation is a complicating element. Although cycling the battery is less expensive than generating power from the diesel generator, even for deep cycles, it is difficult due to the uncertainty in determining if the power charged now is needed later or if it can be consumed directly from VRES generation. It is therefore necessary to balance the cost of cycling the battery toward the expected diesel generation reduction. Additionally, there is an increasing cost associated with staying at high SOC. It can therefore be cost effective to keep the SOC low in periods with a stable high VRES generation to extend the battery's lifetime.

The results in Table V show that accounting for DOD and SOC degradation increases the load shedding in the cases *1* and *3*, and the diesel cost for all cases. However, the reduction in degradation surpasses the increase in diesel and load shedding costs and indicates an increase in expected battery life time of more than four years for all the cases when comparing methods *c* and *f*. A very common way to reduce battery degradation is to apply fixed operating limits, such as enforcing a permanent operating range between 10 and 90%. However, in situations where the only alternative is load shedding, it is optimal to utilize the full battery range since the cost reduction associated with reducing load shedding outperforms the cost accrued by degradation.

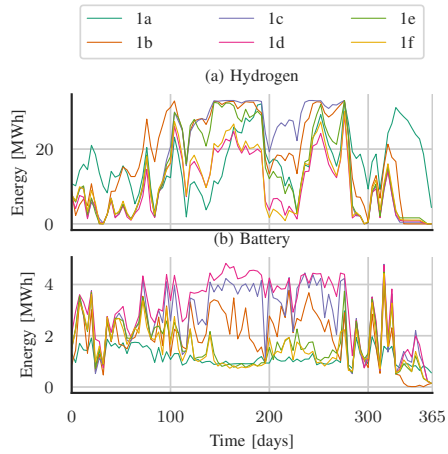

Fig. 4. Four day average SOC for case *1*.

The energy balance in the cases *1* and *2* show that the hydrogen system replaces some of the battery cycling from method *c* to *f*, since it has no degradation costs. However, case *3*, which has no hydrogen in the system, also shows a significant cost reduction associated with battery degradation when hydrogen is taken out of the system. SOC degradation without DOD degradation (method *e*) causes significant cycling and energy dumping through simultaneous charging and discharging of the battery, hence the DOD degradation reduces the occurrence of simultaneous charging and discharging caused by SOC degradation as indicated in method *f*.

Fig. 4a shows that the hydrogen SOC on average is lower when including the DOD degradation in methods *d* and *f*. The wind turbine peak capacity is 135 kW while the electrolyzer charge capacity is only 55 kW. In periods with very high wind power, the battery can act as a buffer for the hydrogen system that is unable to absorb the wind power peaks. However, DOD degradation makes this less profitable, resulting in lower hydrogen filling.

Fig. 4b shows that the battery SOC for methods *e* and *f*, where SOC degradation is included, is stable low in mid-year when the demand is low. These periods require relatively low stored energy to secure the supply, especially when the solar PV is delivering substantial energy due to many hours of sunlight through the summer. However, SOC degradation will, in general, lower the battery SOC, and DOD degradation will lower the hydrogen SOC, which in turn increases the risk of scarcity. The results in Table V shows a modest increase in both load shedding and diesel consumption when accounting for battery degradation.

TABLE V
OVERVIEW OF OPERATING COSTS, DEGRADATION COSTS, BATTERY EXPECTED LIFETIME, VRES GENERATION AND EES CHARGE/DISCHARGE FOR CASES IN TABLE III AND METHODS IN TABLE IV.

		Operating cost $[e]$			Degradation cost $[e]$			$[year]$	Energy $[MWh]$		
Case	Method	Total	Load shedding	Diesel	DOD	SOC up	SOC down	Lifetime	VRES	H2 ch/dch	Batt ch/dch
1	a	3719.7	0.00	3076	514	117	12	21.68	185.03	61.52 / 20.19	39.83 / 36.90
1	b	8541.1	4054.93	2840	1041	435	171	17.81	171.41	40.74 / 13.54	49.34 / 45.67
1	c	6011.1	968.94	2860	1328	731	123	16.26	166.73	32.87 / 11.02	52.67 / 48.73
1	d	5579.5	1086.00	2934	627	882	50	18.09	181.56	57.16 / 18.79	40.84 / 37.83
1	e	5804.1	1108.53	2861	1488	310	37	17.23	181.25	53.03 / 17.47	63.36 / 58.58
1	f	5256.8	1414.40	2964	582	268	29	20.62	183.48	60.64 / 19.90	39.71 / 36.79
2	a	3719.7	0.00	3076	514	117	12	21.68	185.03	61.52 / 20.19	39.83 / 36.90
2	b	4508.7	0.00	2917	998	445	149	17.98	171.41	40.86 / 13.58	47.87 / 44.31
2	c	5093.3	0.00	2864	1285	723	220	16.13	166.46	32.50 / 10.90	50.46 / 46.69
2	d	4575.3	0.00	2892	650	848	185	17.69	181.75	56.55 / 18.60	40.43 / 37.45
2	e	4704.9	0.00	2883	1494	313	16	17.27	181.26	53.10 / 17.49	62.37 / 57.63
2	f	3814.1	0.00	3000	556	253	6	20.90	183.46	60.79 / 19.95	38.50 / 35.63
3	a	4631.9	0.00	3459	771	348	53	19.45	141.21	- / -	56.93 / 52.66
3	b	9718.3	3822.67	3071	1228	1258	338	14.72	143.96	- / -	63.49 / 58.71
3	c	7202.8	775.38	3064	1436	1741	186	13.64	143.42	- / -	59.47 / 55.00
3	d	6968.8	1061.56	3091	885	1745	186	14.74	143.05	- / -	59.03 / 54.59
3	e	8467.5	1107.20	3215	3133	945	67	12.32	161.68	- / -	181.47 / 167.43
3	f	6188.1	1236.83	3321	776	789	66	17.86	140.56	- / -	56.43 / 52.20

V. CONCLUSIONS

Battery degradation is strongly connected to the operational pattern. In this study, the expected battery lifetime was prolonged by more than four years by properly accounting for degradation effects caused by DOD and SOC. Moreover, the total operating costs were reduced by up to 25% compared to the naive stochastic model without representation of degradation. However, battery degradation minimization also influences the operational pattern for the remaining resources in the system. The operational costs for generators and other EES technologies can, in the worst case scenario, increase even more than the savings for battery degradation. Degradation costs and inefficiencies associated with the operational pattern should therefore be considered for the whole system.

Dedicated battery degradation minimization can be contradictory to maximizing the security of supply, and the risk of scarcity must be balanced against the potential reduction in degradation. Realistic uncertainty models are therefore highly important.

The optimal operation of the future power system will to a greater extent be influenced by technology prices rather than fuel price, and energy adequacy rather than power adequacy. Future research should therefore give more attention to both the degradation of all the flexible resources in the system as well as precise uncertainty modeling to capture the future risk of scarcity accurately.

REFERENCES

[1] J. Geske and R. Green, "Optimal Storage, Investment and Management under Uncertainty: It is Costly to Avoid Outages!" *The Energy Journal*, vol. 41, no. 2, 4 2020.

[2] P. Aaslid, M. Korpås, M. M. Belsnes, and O. B. Fosso, "Pricing electricity in constrained networks dominated by stochastic renewable generation and electric energy storage," *Electric Power Systems Research*, vol. 197, p. 107169, 8 2021.

[3] H. Klinge Jacobsen and S. T. Schröder, "Curtailment of renewable generation: Economic optimality and incentives," *Energy Policy*, vol. 49, pp. 663–675, 10 2012.

[4] N. A. Sepulveda, J. D. Jenkins, A. Edington, D. S. Mallapragada, and R. K. Lester, "The design space for long-duration energy storage in decarbonized power systems," *Nature Energy 2021 6:5*, vol. 6, no. 5, pp. 506–516, 3 2021.

[5] M. A. Pellow, C. J. Emmott, C. J. Barnhart, and S. M. Benson, "Hydrogen or batteries for grid storage? A net energy analysis," *Energy and Environmental Science*, vol. 8, no. 7, pp. 1938–1952, 7 2015.

[6] P. Ahmadi, S. H. Torabi, H. Afsaneh, Y. Sadegheih, H. Ganjehsarabi, and M. Ashjaee, "The effects of driving patterns and PEM fuel cell degradation on the lifecycle assessment of hydrogen fuel cell vehicles," *International Journal of Hydrogen Energy*, vol. 45, no. 5, pp. 3595–3608, 1 2020.

[7] B. Bidoggia and S. K. Kær, "Estimation of membrane hydration status for standby proton exchange membrane fuel cell systems by complex impedance measurement: Constant temperature stack characterization," *International Journal of Hydrogen Energy*, vol. 38, no. 10, pp. 4054–4066, 4 2013.

[8] J. Wang, H. Zhong, W. Tang, R. Rajagopal, Q. Xia, C. Kang, and Y. Wang, "Optimal bidding strategy for microgrids in joint energy and ancillary service markets considering flexible ramping products," *Applied Energy*, vol. 205, pp. 294–303, 11 2017.

[9] S. Wang, D. Guo, X. Han, L. Lu, K. Sun, W. Li, D. U. Sauer, and M. Ouyang, "Impact of battery degradation models on energy management of a grid-connected DC microgrid," *Energy*, vol. 207, p. 118228, 9 2020.

[10] H. Shuai, J. Fang, X. Ai, Y. Tang, J. Wen, and H. He, "Stochastic optimization of economic dispatch for microgrid based on approximate dynamic programming," *IEEE Transactions on Smart Grid*, vol. 10, no. 3, pp. 2440–2452, 5 2019.

[11] W. Gil-González, O. D. Montoya, E. Holguín, A. Garces, and L. F. Grisales-Noreña, "Economic dispatch of energy storage systems in dc microgrids employing a semidefinite programming model," *Journal of Energy Storage*, vol. 21, pp. 1–8, 2 2019.

[12] M. Elkazaz, M. Sumner, and D. Thomas, "Energy management system for hybrid PV-wind-battery microgrid using convex programming, model predictive and rolling horizon predictive control with experimental validation," *International Journal of Electrical Power and Energy Systems*, vol. 115, p. 105483, 2 2020.

[13] T. A. Nguyen and M. L. Crow, "Stochastic Optimization of Renewable-Based Microgrid Operation Incorporating Battery Operating Cost," *IEEE Transactions on Power Systems*, vol. 31, no. 3, pp. 2289–2296, 5 2016.

[14] D. Fioriti, D. Poli, P. Duenas-Martinez, and I. Perez-Arriaga, "Multi-year stochastic planning of off-grid microgrids subject to significant load growth uncertainty: overcoming single-year methodologies," *Electric Power Systems Research*, vol. 194, p. 107053, 5 2021.

[15] W. Su, J. Wang, and J. Roh, "Stochastic energy scheduling in microgrids with intermittent renewable energy resources," *IEEE Transactions on Smart Grid*, vol. 5, no. 4, pp. 1876–1883, 7 2014.

[16] C. Ju, P. Wang, L. Goel, and Y. Xu, "A two-layer energy management system for microgrids with hybrid energy storage considering degradation costs," *IEEE Transactions on Smart Grid*, vol. 9, no. 6, pp. 6047–6057, 11 2018.

[17] M. Koller, T. Borsche, A. Ulbig, and G. Andersson, "Defining a degradation cost function for optimal control of a battery energy storage system," *2013 IEEE Grenoble Conference PowerTech, POWERTECH 2013*, 2013.

[18] B. Xu, A. Oudalov, A. Ulbig, G. Andersson, and D. S. Kirschen, "Modeling of lithium-ion battery degradation for cell life assessment," *IEEE Transactions on Smart Grid*, vol. 9, no. 2, pp. 1131–1140, 3 2018.

[19] P. Aaslid, M. Korpas, M. M. Belsnes, and O. Fosso, "Stochastic Optimization of Microgrid Operation With Renewable Generation and Energy Storages," *IEEE Transactions on Sustainable Energy*, pp. 1–1, 2022. [Online]. Available: https://ieeexplore.ieee.org/document/9727092/

[20] B. Xu, J. Zhao, T. Zheng, E. Litvinov, and D. S. Kirschen, "Factoring the Cycle Aging Cost of Batteries Participating in Electricity Markets," *IEEE Transactions on Power Systems*, vol. 33, no. 2, pp. 2248–2259, 3 2018.

[21] "Remote EU project," 2021. [Online]. Available: https://www.remote-euproject.eu/remote-project/

[22] P. Marocco, D. Ferrero, M. Gandiglio, and M. Santarelli, "Remote area Energy supply with Multiple Options for integrated hydrogen-based TEchnologies - Deliverable number 2.2," 2018. [Online]. Available: https://www.remote-euproject.eu/remote18/rem18-cont/uploads/2019/03/REMOTE-D2.2.pdf

[23] J. M. Maciejowski, *Predictive Control with Constraints*. Pearson education, 2002.

[24] M. V. F. Pereira and L. M. V. G. Pinto, "Multi-stage stochastic optimization applied to energy planning," *Mathematical Programming*, vol. 52, no. 1-3, pp. 359–375, 5 1991.

[25] O. Dowson, "The policy graph decomposition of multistage stochastic optimization problems," *Networks*, vol. 76, no. 1, pp. 3–23, 2020.

[26] K. Linowsky and A. B. Philpott, "On the Convergence of Sampling-Based Decomposition Algorithms for Multistage Stochastic Programs," *Journal of Optimization Theory and Applications 2005 125:2*, vol. 125, no. 2, pp. 349–366, 5 2005. [Online]. Available: https://link.springer.com/article/10.1007/s10957-004-1842-z

[27] J. Zou, S. Ahmed, and X. A. Sun, "Stochastic dual dynamic integer programming," *Mathematical Programming*, pp. 1–42, 3 2018.

[28] P. Keil, S. F. Schuster, J. Wilhelm, J. Travi, A. Hauser, R. C. Karl, and A. Jossen, "Calendar Aging of Lithium-Ion Batteries," *Journal of The Electrochemical Society*, vol. 163, no. 9, p. A1872, 7 2016.

[29] K. Liu, T. R. Ashwin, X. Hu, M. Lucu, and W. D. Widanage, "An evaluation study of different modelling techniques for calendar ageing prediction of lithium-ion batteries," *Renewable and Sustainable Energy Reviews*, vol. 131, p. 110017, 10 2020.

[30] J. Vetter, P. Novák, M. R. Wagner, C. Veit, K. C. Möller, J. O. Besenhard, M. Winter, M. Wohlfahrt-Mehrens, C. Vogler, and A. Hammouche, "Ageing mechanisms in lithium-ion batteries," *Journal of Power Sources*, vol. 147, no. 1-2, pp. 269–281, 9 2005.

[31] Y. Gao, J. Jiang, C. Zhang, W. Zhang, and Y. Jiang, "Aging mechanisms under different state-of-charge ranges and the multi-indicators system of state-of-health for lithium-ion battery with Li(NiMnCo)O2 cathode," *Journal of Power Sources*, vol. 400, pp. 641–651, 10 2018.

[32] J. Zhu, M. Knapp, D. R. Sørensen, M. Heere, M. S. Darma, M. Müller, L. Mereacre, H. Dai, A. Senyshyn, X. Wei, and H. Ehrenberg, "Investigation of capacity fade for 18650-type lithium-ion batteries cycled in different state of charge (SoC) ranges," *Journal of Power Sources*, vol. 489, p. 229422, 3 2021.

[33] I. Laresgoiti, S. Käbitz, M. Ecker, and D. U. Sauer, "Modeling mechanical degradation in lithium ion batteries during cycling: Solid electrolyte interphase fracture," *Journal of Power Sources*, vol. 300, pp. 112–122, 12 2015.

[34] C. Amzallag, J. P. Gerey, J. L. Robert, and J. Bahuaud, "Standardization of the rainflow counting method for fatigue analysis," *International Journal of Fatigue*, vol. 16, no. 4, pp. 287–293, 6 1994.

[35] O. Dowson and L. Kapelevich, "SDDP.jl: A julia package for stochastic dual dynamic programming," *INFORMS Journal on Computing*, vol. 33, no. 1, pp. 27–33, 12 2021.

[36] A. Millner, "Modeling lithium ion battery degradation in electric vehicles," *2010 IEEE Conference on Innovative Technologies for an Efficient and Reliable Electricity Supply, CITRES 2010*, pp. 349–356, 2010.

[37] D. I. Stroe, M. Swierczynski, A. I. Stroe, R. Teodorescu, R. Laerke, and P. C. Kjaer, "Degradation behaviour of Lithium-ion batteries based on field measured frequency regulation mission profile," *2015 IEEE Energy Conversion Congress and Exposition, ECCE 2015*, pp. 14–21, 10 2015.

[38] TrønderEnergi, "AI Hackathon Challenge - Optimal Control of Microgrid," 2021. [Online]. Available: http://doi.org/10.5281/zenodo.5500209

[39] P. Aaslid, "Rye microgrid historical weather forecasts and stochastic scenarios [Data set]," 2021. [Online]. Available: https://doi.org/10.5281/zenodo.5526241

ISBN 978-82-326-5308-9 (printed ver.)
ISBN 978-82-326-5536-6 (electronic ver.)
ISSN 1503-8181 (printed ver.)
ISSN 2703-8084 (online ver.)

NTNU

Norwegian University of
Science and Technology